Calendar Aging and Lifetimes of $LiFePO_4$ Batteries and Considerations for Repurposing

by

John Catton

A thesis

presented to the University of Waterloo

in fulfillment of the

thesis requirement for the degree of

Master of Applied Science

in

Chemical Engineering

Waterloo, Ontario, Canada, 2017

Author’s Declaration

This thesis consists of material all of which I authored or co-authored: see Statement of Contributions included in the thesis. This is a true copy of the thesis, including any required final revisions, as accepted by my examiners.

I understand that my thesis may be made electronically available to the public.

Statement of Contributions

This thesis contains material, primarily in Chapter 6, based on a co-authored article to be published in the 5th annual IEEE International Conference on Smart Energy Grid Engineering [SEGE] 2017. I am the lead author of the article, joined by co-authors: Sean B. Walker, Paul McInnis, Michael Fowler, Roydon Fraser, Steven B. Young, and Ben Gaffney. Chapter 7 contains the methods, results, discussion, and conclusion sections of the article.

Abstract

In response to rising petroleum prices, the demand for lower emissions standards for vehicles, and better vehicle fuel economy, the market for hybrid and electric vehicles is expanding. These systems incorporate advanced battery systems which store and provide energy in the vehicle. Over time, though, cells degrade and lose capacity in accordance with two different aging phenomena: cycling and calendar aging. It is imperative to understand how these degradation phenomena occur as the loss in capacity results in a loss in vehicle range. Through understanding how these phenomena occur, mitigation efforts can be designed to prevent or lessen their effects.

This thesis will focus primarily on studying the effects of calendar aging on commercial $LiFePO_4$ cells. Cells are aged at varying temperatures and states of charge (SOC) to determine the extent of capacity fade and degradation. Additional testing methods are then utilized to attempt to determine which aging phenomena are promoting the losses within the cell.

Capacity loss in cells stored at high temperature and fully charged conditions resulted in faster degradation rates. Temperature had the most significant role in the degradation of the cell and then the cell's SOC. Comparing capacity losses between cells stored at the same temperature, but with different SOCs, found that the cells with higher SOC experienced increased rates of degradation in comparison to their fully discharged counterparts. In addition, storage at high SOC and high temperatures promoted such severe losses that the cells in question were unable to recapture capacity that they had lost reversibly.

The primary degradation mode for the cells was the loss of cyclable lithium, and was found to occur under all of the storage conditions. Cells stored at much more severe conditions, though, also demonstrated a loss of active material at the anode. The extent of the loss of the active material was largely predicated on whether or not the cell was stored at fully charged or discharged conditions. Storage of lithium-ion batteries at high temperatures has a dramatic effect on the continual usage of the cells after storage conditions have changed. Despite shifting temperatures or states-of-charge to a lower value, the initial storage conditions leads to increased degradation rates throughout the cell life. Thus, the history of storage for the cell must be also be taken into account when considering losses in capacity.

Utilizing the collected degradation data from the calendar aging experiments and manufacturer's cycling data a lifetime degradation model was produced to simulate the extent of aging from different geographic locations and to compare which degradation mode had the most influence over a ten year lifespan. The model was validated using additional data not included in the non-linear degradation model and the results tabulated using real-world temperature and drive cycle data. According to the simulations, calendar aging plays a significant role in the loss of capacity within the battery pack, due to the battery pack not being utilized on a constant basis in the vehicle. Incorporating it into the simulation resulted in the battery pack reaching its EOL much sooner than the targeted consumer requirement of ten years.

Finally, to conclude the findings on the research of degradation of lithium-ion batteries, a final study was completed on the examination of how electric vehicle batteries can be repurposed. A design process for a repurposed battery pack is proposed, taking into account design steps from initial market predictions to installation of the assembly at a residence, as well as an analysis of the potential risks. This work established an understanding of the limitations of repurposing, as well as the current codes and standards that affect repurposed battery pack designs. Utilizing these requirements, a bench test setup was designed, built, and tested to determine feasibility. This work also identified a number of risks still evident in the design of a repurposed system as the relevant codes and legislation have not been written and supply chain and testing of repurposed packs is currently unknown. More research needs to be completed on the establishment of state-of-health for battery packs and proper guidelines on installation need to be refined.

Acknowledgements

I would like to thank all of those who contributed to this work and my other research. Thank you to Dr. Michael Fowler especially for your continued support and guidance over the past two years. I would also like to thank Mohammad Farkhondeh and Manoj Matthew for helping me to gather, analyse, and prepare the necessary information to complete this work. I would not have been able to complete this if it was not for them and I am very thankful to have worked with such amazing people.

Many thanks go out to the UWAFT team for providing additional support. Dr. Fraser was a great support to be able to work under on the UWAFT team. To all of those on the team who I have worked and interacted with, I am eternally grateful to have worked with you. It was truly an amazing experience.

Finally, to my parents, I can only hope I made you proud. Thanks for always being there for me.

Table of Contents

Author's Declaration ii
Statement of Contributions iii
Abstract iv
Acknowledgements vi
Nomenclature xv
1 Introduction 1
2 Background 4
2.1 Batteries 4
2.2 Lithium-ion Batteries 5
2.3 Vehicle-grade Batteries 7
2.4 Pouch cells 8
2.5 Battery Pack Construction 9
2.6 Regulations and tests 11
2.7 Battery Failure Modes 12
2.7.1 Assessment of Battery Failure Modes Using DFMEA 13
2.7.2 Battery Safety Precautions 14
2.8 Modelling Battery Degradation 17
2.8.1 Electrochemical Modelling 17
2.8.2 Electrical-based Modelling 18
2.8.3 Empirical Modelling 20
2.9 Drive Cycles 21
2.10 Degradation Mechanisms for Lithium Ion Batteries 23
2.10.1 Calendar Aging: 24
2.10.2 Cycling Aging 27
2.11 Battery Testing 35
2.11.1 State of Charge Estimations 35
2.11.2 C-Rate 36
2.11.3 Reversible Capacity Determination, Self-Discharge Test 37
2.11.4 Rate-Capability Tests 37
3 Experimental Procedures 38

3.1 Calendar Aging Studies of LFP Cells 38
3.1.1 Non-destructive Testing 41
3.1.2 Post-Mortem Analysis (Destructive Testing) 41
4 Results of Calendar Aging Studies 44
4.1 Degradation of Cells 44
4.2 Analyzing cells stored at 100% SOC at different temperatures 44
4.2.1 Capacity Fade: 45
4.2.2 Comparison of capacity between cycles of battery tests 53
4.2.3 Incremental Voltage Analysis, Differential Voltage Capacity Curves: 59
4.3 Analyzing cells stored at 0% SOC at different temperatures 65
4.3.1 Capacity Fade: 65
4.3.2 Incremental Voltage Analysis, Differential Voltage Capacity Curves: 69
4.4 Post-Mortem Analysis 74
4.4.1 Qualitative Analysis of Electrode Material 74
4.4.2 Scanning Electron Microscopy (SEM) 75
4.4.3 EDX Results 82
4.4.4 Optical Microscopy 85
4.4.5 Inductively coupled plasma (ICP) Analyses: 86
4.4.6 Profilometry 89
4.4.7 4 Point Conductivity Measurement 90
4.5 Summary of Calendar Aging of $LiFePO_4$ Cells 91
4.6 Failure of $LiFePO_4$ Cells due to Cycling and Calendar aging conditions 93
4.6.1 Failure of cells stored under OCP conditions 93
4.6.2 Case study of Safety of cycling $LiFePO_4$ Cells at high and low temperatures 97
4.6.3 Thermal Runaway Conditions 99
4.6.4 Preventative Measures 100
4.6.5 Summary of Degradation Case Study 101
4.7 Battery Pack Design for EcoCar 3 Competition 102
4.7.1 UWAFT Procedure for Developing a Battery Pack Design: 103
4.7.2 Construction and Design Criteria 105
4.7.3 Additional Requirements 114

5 Warranty Simulation Lifespan Analysis of a $LiFePO_4$ Battery Pack 118
5.1 Modeling degradation 118
5.2 Calendar Aging 118
5.3 Cycling Aging 118
5.4 Model Parameters' Identification Method 119
5.5 Simulation Assumptions 119
5.6 Vehicle Model 120
5.6.1 Proposed Architecture: 120
5.7 Fitting the Data and Model Verification 121
5.7.1 Model Verification 122
5.8 Battery Control System of Simulation 122
5.9 Simulation Results 123
5.10 Temperature: 124
5.11 Daily Cycling Schedule 126
5.12 Capacity Fade Results after 1 year duration 127
5.14 Summary of Lifetime Prediction Modelling 131
6 Second-Use of Vehicle Batteries 133
6.1 Canada's Energy Market and the Need for Repurposed Batteries 134
6.2 Controlling Battery Degradation in Electric Vehicles 136
6.3 Barriers to Adoption 138
6.3.1 Insurance Codes and Liability Standards 138
6.3.2 Lack of data on degradation of battery packs 139
6.3.3 Availability and Variability 140
6.3.4 Installation into Residences 142
6.4 Current Applicable Design Codes 142
6.5 Failure Analysis 145
6.5.1 Severity 146
6.5.2 Occurrence 146
6.5.3 Detection 147
6.5.4 Results of Analysis 147
6.5.5 Fault Tree Analysis 148

6.6 Degradation Classification 149
6.7 Summary of Second-Use of Vehicle Grade Battery Packs 150
7 Conclusions and Recommendations 151
7.1 Conclusions 151
7.2 Recommendations 153
8 References 155
Appendix A: Regulation Test Criteria 168
Appendix B: Images of post-mortem analysis of $LiFePO_4$ cells 169
Appendix C: Optical Microscopy Images 173
Appendix D: Vehicle Technical Specifications 181

List of Figures

Figure 1: Ragone plot of various ESSs 6
Figure 2: (a) Cylindrical, (b) prismatic, (c) coin, and (d) pouch packaging for LiBs 8
Figure 3: Cross-Section of De-Constructed A123 Battery Pack 9
Figure 4: Equivalent Circuit Model Example 19
Figure 5: R_{INT} Model Equivalent Circuit 19
Figure 6: Thevenin Model Equivalent Circuit 20
Figure 7: Drive Cycle Federal Test Procedure (FTP) 22
Figure 8: Highway Fuel Economy Test Procedure 22
Figure 9: Cathode Degradative Processes 32
Figure 10: Commercial 20Ah LiFePO4/graphite prismatic battery manufactured by A123 38
Figure 11: MACCOR 4200 Series multichannel battery tester 40
Figure 12: Battery Cycler Test Bench 40
Figure 13: Climate Chamber 40
Figure 14: High Voltage Routing for A123 Battery Modules in a 6x15S3P Arrangement 104
Figure 15: End-of-Life points for tested cells 44
Figure 16: Charge and discharge curves for cells stored at 100% SOC and 35°C, and 60°C 46
Figure 17: Charge and discharge curves over aging period for cells stored at 100% SOC 47
Figure 18: Charge and discharge curves for cells stored at 100% SOC and50°C 48
Figure 19: Capacity fades over time for different cell conditions 49
Figure 20: Irreversible capacity loss of cells 51
Figure 21: Irreversible capacity loss of cells 53
Figure 22: Loss of recapture of reversible capacity loss of cells stored at 60°C and 100% SOC 54
Figure 23: Gain of reversible capacity, for cells stored at 35°C and 100% SOC 55
Figure 24: Gain of reversible capacity, for cells stored at 50°C and 100% SOC 56
Figure 25: Decrease in recapture of reversible capacity loss 57
Figure 26: Loss of recapture of reversible capacity 58
Figure 27: Discharge dV/dQ curve at a rate of C/20 for cells stored at 35°C and 100% SOC 60
Figure 28: Discharge dV/dQ curve at a rate of C/20 for cells stored at 60°C and 100% SOC 61
Figure 29: Discharge dV/dQ curve at a rate of C/20 for cells stored at 50°C and 100% SOC 62
Figure 30: Discharge dV/dQ curve (stored at 60°C/100% SOC shifted to 35°C/100% SOC) 63
Figure 31: Discharge dV/dQ curve (stored at 35°C/100% SOC shifted to 50°C/100% SOC) 64
Figure 32: Charge and discharge curves for discharged cells over aging period 65
Figure 33: Percent remaining capacity of cells stored at 60°C and 0% SOC 66
Figure 34: Percent remaining capacity (stored at 60°C/100% SOC shifted to 60°C/0% SOC) 67
Figure 35: Percent remaining capacity (stored at 60°C/0% SOC shifted to 35°C/100% SOC) 67

Figure 36: Remaining capacity of cells stored 50°C and 0% SOC 68
Figure 37: Discharge dV/dQ curve at a rate of C/20 for cells stored at 60°C and 0% SOC 69
Figure 38: Discharge dV/dQ curve at a rate of C/20 for cells stored at 50°C and 0% SOC 71
Figure 39: Discharge dV/dQ curve (stored at 60°C/100% SOC shifted to 60°C/0% SOC 72
Figure 40: Discharge dV/dQ curve (stored at 60°C/0% SOC shifted to 35°C/100% SOC) 73
Figure 41: SEM micrographs of unaged graphite electrode 75
Figure 42: SEM micrographs of aged graphite electrode (60°C and 0% SOC) 76
Figure 43: Back-scattering SEM micrographs of aged graphite electrode (60°C and 0% SOC) . 76
Figure 44: SEM micrographs of aged graphite electrode (60°C and 100% SOC) 77
Figure 45: Back-scattering SEM micrographs of aged graphite electrode (60°C/100% SOC) 78
Figure 46: SEM micrographs of aged graphite electrode (35°C and 100% SOC) 78
Figure 47: SEM micrographs of unaged LFP electrode 79
Figure 48: SEM micrographs of aged LFP electrode (60°C and 0% SOC) 80
Figure 49: SEM micrographs of aged LFP (60°C and 100% SOC) 81
Figure 50: SEM micrographs of aged LFP (35°C and 100% SOC) 82
Figure 51: SEM micrographs of particulate matter for graphite stored at 60°C and 0% SOC 84
Figure 52: SEM micrographs of particulate matter for graphite stored at 60°C and 100% SOC . 84
Figure 53: Extent of swelling of aged cell compared to fresh cell 94
Figure 54: Swelling Observed between Aged cells stored at 0% SOC and 100% SOC 95
Figure 55: $LiFePO_4$ cell thermal runaway aftermath 98
Figure 56: Post-mortem analysis first assessment of thermal runaway 98
Figure 57: Extent of damage to anodes and cathodes 99
Figure 58: Module Design 1 106
Figure 59: Module Design 2 106
Figure 60: Module Design 3 106
Figure 61: Meshing of lower battery mount 108
Figure 62: Meshing of upper battery mount 109
Figure 63: Load and constraint location for upper battery frame 109
Figure 64: Load and constraint location for upper battery frame 110
Figure 65: Upper frame design von Mises stress contour for 20g longitudinal load case 110
Figure 66: Upper battery frame design von Mises stress contour for 20g lateral load case 111
Figure 67: Upper battery frame design von Mises stress contour for 8g vertical load case 111
Figure 68: Lower frame von Mises stress contour plot for 20g longitudinal load case 112
Figure 69: Lower frame von Mises stress contour plot for 20g lateral load case 113
Figure 70: Lower frame von Mises stress contour plot for 8g vertical load case 113
Figure 71: Upper mounting Structure of ESS 114
Figure 72: Lower Mounting Section of ESS 114

Figure 73: High Voltage Schematic for UWAFT Team 115
Figure 74: Battery Pack Vent 116
Figure 75: Vehicle Architecture 120
Figure 76: Current profile of drive cycle for battery pack 124
Figure 77: Temperature samples for a random day in the Waterloo data for winter and spring 124
Figure 78: Temperature samples for a random day in the Waterloo data for summer and fall .. 125
Figure 79: Temperature samples for a random day in the Tampa area for winter and spring 125
Figure 80: Temperature samples for a random day in the Tampa area for summer and fall 125
Figure 81: Capacity profile of vehicle given as SOC change over 1 day of usage 126
Figure 82: Total, Calendar, and Cycling aging losses after 1 year Waterloo area 127
Figure 83: Total, Calendar, and Cycling aging losses after 1 year in Tampa area 128
Figure 84: Actual capacity fade of battery pack over one year 129
Figure 85: Capacity fade from calendar and cycling aging in the Waterloo area 129
Figure 86: Capacity fade from calendar and cycling aging in the Tampa area 130
Figure 87: Vehicle Battery Life Cycle 134
Figure 88: Average Household Annual Energy Usage 2009 135
Figure 89: Canada's Energy Mix for Electricity Generation 2014 135
Figure 90:EV sales in Canada over the past four years 141
Figure 91: Fault Tree Analysis Example for Burns/Explosions 149
Figure 92: Graphite electrode aged 60^{o}C 100% SOC 169
Figure 93: LFP electrode aged 60^{o}C 100% SOC 169
Figure 94: Graphite electrode aged 60^{o}C 0% SOC 170
Figure 95: LFP electrode aged 60^{o}C 0% SOC 170
Figure 96: Graphite electrode aged 35^{o}C 100% SOC 171
Figure 97: LFP electrode aged 35^{o}C 100% SOC 171
Figure 98: Fresh Graphite electrode 172
Figure 99: Fresh LFP electrode 172
Figure 100: Fresh LFP 173
Figure 101: LFP aged 60^{o}C and 0% SOC 174
Figure 102: LFP aged 35^{o}C and 100% SOC 175
Figure 103: LFP aged 60^{o}C and 100% SOC 176
Figure 104: Fresh graphtite 177
Figure 105: Graphite aged 60^{o}C and 0% SOC 178
Figure 106: Graphite aged 35^{o}C and 100% SOC 179
Figure 107: Graphite aged 60^{o}C and 100% SOC 180

List of Tables

Table 1: List of vehicle manufacturers and the battery chemistries used in each EV model 5
Table 2: Comparison of Battery Pack in Electrified Vehicles 10
Table 3: Examples of Failure Modes of Lithium-Ion Batteries 12
Table 4: Safety modification for lithium-ion cells 15
Table 5: US EPA Drive Cycle Characteristics 22
Table 6: Cells stored at constant temperature and constant state of charge (SOC) 39
Table 7: Cells that underwent a shift in temperature of state of charge conditions 39
Table 8: EDX Results of Graphite Electrode samples 83
Table 9: EDX Results of LFP Electrode samples 83
Table 10: EDX analysis of particulate matter 85
Table 11: ICP Results of Metallic Species 87
Table 12: Percentage increase or decrease of metallic species 88
Table 13: Profilometry measurements of electrodes 89
Table 14: Electric conductivity of LFP samples 91
Table 15: Battery pack options for EcoCAR3 competition 103
Table 16: Upper Battery Frame FEA Results 112
Table 17: Lower Battery Frame FEA Results 114
Table 18: Fitted parameters of calendar aging model 121
Table 19: List of Battery Types and Designs 141
Table 20: Applicable Codes for Repurposed Li-ion Battery Packs in a Stationary Application 143
Table 21: Applicable Codes for the Repurposed Battery Pack Assembly 143
Table 22: Applicable Codes for Repurposed Li-ion Battery Canadian Electrical Codes 144
Table 23: Severity RPN Ranking 146
Table 24: Occurrence RPN Ranking 146
Table 25: Detection RPN Ranking 147
Table 26: Highest Risks of Design 147
Table 27: Repurposed Battery Pack Classification 149
Table 28: Regulation Testing Criteria 168
Table 29: Vehicle Technical Specifications 181

Nomenclature

15s3p. *15 cells in series and 3 parallel strings*
A. *Ampere*
Ah. *Ampere-hours*
Al. *Aluminum*

ANN. *Artificial Neural Network*
ANSI. *American National Standards Institute*
AVTC. *Advanced vehicle technology competition*

BEV. *Battery Electric Vehicle*
BMS. *Battery Management System*

BOL. *Beginning of Life*
c_a. *Aging fitting parameter*

CAFE. *Corporate Average Fuel Economy*
CAN. *Controller Area Network*
CC. *Constant Current*
CCCV. *Constant Current Constant Voltage*
CID. *Circuit Interrupt Device*
C_{nom}. *Nominal capacity*
c_T. *Temperature fitting parameter*
c_V. *Voltage fitting parameter*
DEC. *Diethyl carbonate*
DET. *Detection*

DFMEA. *Design Failure modes and effects analysis*
DIS. *Diffusion-induced stresses*
DMC. *Dimethyl carbonate*
DOD. *Depth-of-discharge*

EA. *Ethyl Acetate*
EC. *Ethylene carbonate*
EDV. *Electric drive vehicle*
EDX. *Energy dispersive X-ray*

EIS. *Electrochemical Impedance Spectroscopy*
EMC. *Ethyl Methyl Carbonate*
EOL. *End of Life*
EPA. *Environmental Protection Agency*
ESS. *Energy Storage Source*

ESS. *Energy Storage Systems*
EV. *Electric vehicle*
FCEV. *Fuel Cell Electric Vehicle*
FEA. *Finite Element Analysis*
FMEA. *Failure modes and effects analysis*
FTA. *Fault Tree Analysis*
FTP. *Federal Test Procedure*

GHG. *Greenhouse Gas*
GUI. *Graphical User Interface*
HEV. *Hybrid Electric Vehicle*
HPPC. *Hybrid Power Pulse Characterization*
HTB. *Hybrid Test Bench*
HV. *High Voltage*
HVIL. *High Voltage Interlock Loop*
HWFET. *Highway Fuel Economy Test*
I. *Current*
ICE. *Internal combustion engine*
ICP. *Inductively coupled plasma*
ICP-AES. *Inductively coupled plasma atomic emission spectroscopy*
IEC. *International Electrotechnical Commission*
ISO. *International Organization for Standardization*
kWh. *kilowatt-hour*
LCA – Life cycle analysis

LCO. *Lithium Cobalt Oxide*
LFP. *Lithium Iron Phosphate*
LiB

LiB. *Lithium Ion Battery*
$LiCoO_2$. *Lithium Cobalt Oxide*

Li-ion. *Lithium-ion*
$LiMn_2O_4$.*Lithium Manganese Oxide*
$LiPF_6$. *Lithium hexafluorphosphate*

LMO. *Lithium Manganese Oxide*
LUT. *Look Up Table*
MA. *Methyl Acetate*
MBD. *Model Based Design*
mg/kg. *Milligram per kilogram*

MPC. *Methyl Propyl Carbonate*
MPG. *Mile Per Gallon*
MPG_e. *Mile Per Gallon Equivalent*
MSD. *Manual Service Disconnect*

NCA. Nickel Cobalt Aluminum
NiMH. *Nickel Metal Hydride*

NMC. *Nickel Manganese Cobalt*
NMP. *1-methyl-2-pyrolidinone*
NRTL. *Nationally Recognized Testing Laboratory*

OBD. *On Board Diagnosis*
OCC. *Occurrence*
OCP. *Open Circuit Potential*

OEM. *Original Equipment Manufacturers*
P2D. *Pseudo Two Dimensional*
PC. *Propylene Carbonate*
PHEV. *Plug-in Hybrid Electric Vehicle*
PM. *Palmgren Miner*
Q. *Capacity*
RC. *Rate capability*

RC. *Resistor Capacitor*
RC. *Resistor-capacitor*
Redox. *Reduction reaction*
RPN. *Risk Priority Number*

RPT. *Reference Performance Test*
SAE. *Society of Automotive Engineers*
SD. *Self-discharge*

SEI. *Solid Electrolyte Interface*
SEM. *Scanning Electron Microscopy*
SEV. *Severity*
Sm. *Siemen-meters*

SOC. *State of Charge*
SOH. *State of Health*
SP. *Single Particle*
UDDS. *Urban Dynamometer Driving Schedule*

UDDS. *Urban Dynamometer Driving Schedule*
UL. *UL*
UN. *United Nations*
USABC. *United States Advanced Battery Consortium*

UWAFT. *University of Waterloo Alternative Fuels Team*
VC. *Vinyl Carbonate*
VEC. *Vinyl ethyl carbonate*

VSSD. *Variable Solid State Diffusivity*
VTS. *Vehicle Technical Specifications*
Wh/kg. *Watt-hours per kilogram*
µm. *Micrometer*

1 Introduction

Credit of the first internal combustion engine car is given to Jean Joseph Étienne Lenoir who invented and patented a double-acting, electric spark-ignition internal combustion engine fueled by coal gas in 1860. [1] Since then, improvements have been made upon this first primitive vehicle to increase fuel efficiency, length of travel, and overall comfort, which have led to the creation of present day vehicles. In relation to this, though, internal combustion engines (ICEs) have remained the primary engine to be used to generate power for said vehicles and have caused humanity to become reliant on fossil fuels in the process.

In 1901 Ferdinand Porsche developed the first gasoline-electric hybrid vehicle. [1] It was not until 1997, though, that the hybrid-electric vehicle became widely available with the release of the Toyota Prius in Japan. [2] With increasing fuel prices, the need to decrease emissions, and consumer's desire to have increased fuel economies for their vehicles, vehicle manufacturers have begun to design, market, and sell more electrified vehicles, with a variety of architectures. [3] There are several varieties available to consumers including: Battery Electric Vehicles (BEVs), Hybrid Electric Vehicles (HEVs), and Plug-in Hybrid Electric Vehicles (PHEVs), in addition to conventional vehicles. [4] Conventional vehicles are still the most prevalent type of vehicles used by consumers, but the introduction of electric-drive vehicles (EDVs) to the consumer vehicle market offers the potential to reduce reliance on fossil fuels and by extension reduce emissions. In order to achieve this EDVs have to accomplish significant market penetration. [3]

In EDVs the batteries are often the most expensive component. [5] Both hybrid and full-electric vehicles use large batteries to provide storage of onboard electrical energy. As such, extensive research and innovation is being completed in order to further reduce battery cost, weight, and overall volume, while extending range and reliability. This is required in order to make the vehicles more attractive in the marketplace. Based on the literature, the fundamental requirement for HEVs and PHEVs, and BEVs, to attain consumer approval, is that they must sustain performance capabilities for approximately 10 to 15 years, or between 20000 to 30000 cycles. [6]

EDVs need to meet consumer requirements in order to gain significant market penetration and to become more economically viable, however, over time, battery performance decreases. The decrease in performance is a result of the degradation of the battery. Battery degradation phenomenon is instigated by two different sources [7] [8] [9]:

- Operating conditions, which is influenced by a variety of parameters,
- And engine-off storage conditions with the main parameters to monitor being calendar life performance, time, and temperature.

With continual usage, throughout the day, cycling the cells will have a more dominant impact on the degradation of the battery, but generally, a vehicle is not used on a constant basis throughout the day. [8]

On a typical day a vehicle is only used for the express purpose of getting the consumer to and from their place of business. In 2011, the most common mode of transportation to work for Canadians was car, truck or van (74.0% of commuters, or 11.4 million workers), with an average commute time of 25.4 minutes (note that 17.2% of commuters experience commute times of more than 45 minutes). [10] The vehicle can then be considered to be under engine-off storage conditions from the point the vehicle is shut down to when the consumer comes back and uses his or her vehicle again for the commute home, approximately 8 or more hours later. It is estimated that a personal car will spend about 95% of its life in parking mode making battery life during storage seems particularly relevant. [8] As said previously, under engine-off storage conditions the system is undergoing degradation with respect to processes related to calendar aging, which are affected by temperature and state-of-charge (SOC). Thus, as the vehicle usage increases and the battery pack ages, the all-electric range will begin to diminish. [8] [11] [8]

In order to understand, how a battery pack will age over time and usage, lifetime assessment models are designed to depict the degradation and determine how long the battery pack will sustain life. The end-of-life point for a battery as declared by the United States Advanced Battery Consortium (USABC) is when the battery capacity delivered to the powertrain is less than 80% of the rated capacity, or if the battery's peak power is less than 80% of the rated power at 80% depth-of-discharge (DOD). [12] The rate at which a battery degrades with time is crucial in determining available SOC in the battery. Thus it is very important to develop accurate battery

models that utilize degradation relationships to model the available capacity in the battery at a given time. [11]

The most fundamental assessment method, and the one used herein, is to utilize a semi-empirical based model of the battery from experimental data. Battery testing is conducted to understand how the cells will degrade at different conditions and collect the necessary data to fit the model parameters. After the model is validated, simulations on various load profiles can be run to predict battery performance and degradation. Integrating the battery degradation model into a vehicle model combines a real world simulation of driving to predict battery performance and degradation on any drive cycle. In other words, battery performance and degradation over its lifetime can be determined by implementing different driving profiles for various drivers.

In order to be able to perform such an analysis in this work, an A123 AMP20 pouch battery of $LiFePO_4$ chemistry will be tested, modeled, and simulated to predict lifetime performance and degradation according to the Environmental Protection Agency (EPA) drive cycles. Physical experiments will be performed on commercial cells to determine the degradation pathways occurring within the cells, thereby improving the modelling of the battery pack. In doing so, the extent of degradation due to operating conditions versus aging due to length of storage can be compared and the factors affecting battery degradation will be determined to create more effective control strategies or preventative measures to reduce battery pack degradation. Finally, an assessment of potential secondary uses of depleted batteries will be conducted to analyse the potential for repurposing depleted electric vehicle battery packs in a stationary storage application.

2 Background

2.1 Batteries

Batteries are devices that convert stored chemical energy into electrical energy via an oxidation-reduction (redox) reaction. [13] [14] [15] As the process is electrochemical, it is not subject to the limitations of the Carnot cycle (internal combustion engines restricted by this law), and higher energy conversion efficiencies can be achieved. [16]

Batteries can be classified as primary batteries, secondary (rechargeable) batteries, and flow batteries. [16] Primary batteries can only be discharged once, but are composed of materials that can attain high energy densities. Secondary batteries are used as energy storage devices as they are capable of recharging, by connecting a power supply to the battery, and then subsequently delivering the energy to a load on demand. [16] [17] Finally, a flow battery can be considered similar to both a fuel cell and an electrochemical accumulator. It utilizes chemical energy outside of the battery in a fluid state. The fluid is passed through the battery, reacting electrochemically to produce electrical energy. [16] [17] Depending on their design flow batteries can be used as primary batteries, with the fluid acting as a fuel that is spent to produce electrical energy, or as secondary batteries, with the reversal of the electrochemical process to store chemical energy in the fluid once again. [16] To further develop and provide innovations to the automotive industry, it is necessary to understand how these batteries work to determine their applicability.

Secondary batteries have been typically utilized to power small portable devices such as tools, toys, lighting, and consumer electronic devices. [16] [18] As the fuel economy and emissions requirements of vehicles has increased in the past few decades, though, renewed interest has been given to the potential of electrifying vehicles by introducing secondary batteries as a power source. [16] The automotive industry has taken advantage of this by applying secondary batteries in one of two scenarios [17]:

1. The secondary battery is used as an energy storage device. The battery is charged by a prime energy source and then provides power only when demanded.
2. The battery is discharged and then recharged after use, allowing for convenience and overall cost savings as, opposed to primary batteries, the battery can be recharged rather than replaced.

The range that a user is able to drive over a single charge is greatly influenced by the choice of battery. Thus, vast amounts of research have been completed on determining the battery chemistry with the best energy density, to extend distance and lower battery weight. In Table 1, a list of the batteries used by different vehicle manufacturers for their different vehicles is given.

Table 1: List of vehicle manufacturers and the battery chemistries used in each electric vehicle [2] [19] [20] [21]

Company	Vehicle Model	Battery Technology
GM	Chevy-Volt	Li-ion
	Saturn Vue Hybrid	NiMH
Ford	Escape, Fusion, MKZ HEV	NiMH
	Escape PHEV	Li-ion
Toyota	Prius, Lexus	NiMH
BMW	Mini E	Li-ion
Nissan	Leaf EV	Li-ion
Tesla	Roadster	Li-ion

2.2 Lithium-ion Batteries

There are a variety of secondary batteries to be used for electric vehicle applications. The Toyota Prius uses a Nickel Metal Hydride (NiMH) battery as an energy storage source (ESS) and the Tesla EVs use lithium-ion cells for their battery packs. [19] When these batteries are compared in Figure 1, the Li-ion cells are found to be able to attain higher specific energies as well as higher specific powers. As a result, lithium-ion batteries have achieved significant market penetration in the electric vehicle market as the most viable secondary battery for hybrid and battery electric vehicle applications. [8] [9]

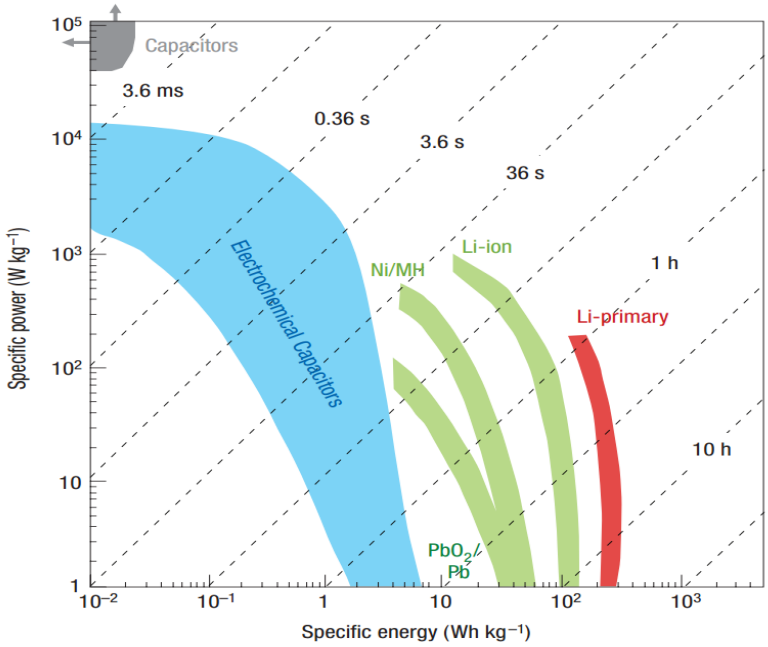

Figure 1: Ragone plot of various ESSs with time constants obtained through the division of energy density with power density [22]

Lithium-ion (Li-ion) batteries utilize cells whose chemistries employ lithium intercalation compounds in both the positive and negative electrodes. [6] [23] During operation (cycling), lithium ions are exchanged between the two electrodes, which have resulted in these batteries being designated as “rocking-chair” batteries. [16] [19]

Lithium ion batteries come in many different varieties and are classified based on their cell chemistries and electrode composition. A typical lithium-ion battery is composed of three parts: an anode (negative electrode), a cathode (positive material), and an electrolyte with a specialised chemistry to mitigate the transfer of ions from anode to cathode and vice-versa. [16] [19] In terms of electrode material the positive electrodes are typically composed of a metal oxide with a layered structure ($LiCoO_2$) or a material with a tunneled structure ($LiMn_2O_4$) on a current collector of aluminum foil. [16] [19] [24] As for the negative electrodes, they are typically composed of graphitic carbon adhered on a copper current collector. [16] [19] [24] Graphite is the most widely used material for anodes because of its availability, cycling performance, and its safety compared to lithium. [18] [24]

During discharging, the lithium ions de-intercalate from the negative electrode providing free electrons to power a load, according to **Equation 2.1**. [16] [19]

$$Li_xC \rightarrow C + xLi^+ + xe^- \quad \text{Equation 2.1}$$

The lithium ions are transported through the electrolyte to meet the electrons at the positive electrode and intercalate into the metal oxide active material, according to Equation 2.2. [16] [19]

$$Li_{1-x}MO_2 + xLi^+ + xe^- \rightarrow Li_xMO_2 \quad \text{Equation 2.2}$$

2.3 Vehicle-grade Batteries

In order to meet the requirements for operation, vehicle-grade batteries are designed and built to maintain the highest standards, for both safety and function. With time, though, the battery will degrade to the point that it reaches its end-of-life (EOL) and must be retired from its vehicle application. [9] [25] This EOL point is typically when the battery pack has reached 70 to 80% of its original energy storage capacity (loss of ~20 to 30% of its range). [26] Due to the possibility of unexpected increased rates of degradation, vehicle manufacturers will oversize the battery in order to account for this. In doing so, it increases the range of the vehicle to aid in decreasing consumer's range anxiety. [17] The downside of this, though, is that the price and mass of the battery pack in the vehicle increases.

Battery size is an important parameter of the vehicle as the battery is one of the heaviest components, with the amount that the battery is oversized by being dependent on the unpredictability of the degradation effects. [27] By being able to accurately determine the battery degradation the extent to which the battery is oversized can be decreased as controls can be put in place to reduce the rates of degradation for various aging phenomena. [5] Battery size reduction will create significant financial benefits due to the high cost of the battery and need for other structural components.

Battery size, also, greatly affects the range of the vehicle and is dependent on the energy density of the cells being used in the pack (in addition to the size of the battery pack). [26] The range the vehicle is capable of travelling on a single battery charge is a very important parameter for the consumer as it will dictate how far he or she can travel on a daily basis. When designing batteries for vehicle applications, one must consider the performance requirements and their impact on

battery degradation. [9] [28] Over time the degradation of the lithium ion battery will impact the drivable range of the vehicle, limiting the range that the vehicle can travel. Thus, it becomes an optimization problem for vehicle manufacturers to select an appropriate battery chemistry to maximize range while limiting the size of the battery pack in the vehicle to decrease cost and overall weight.

2.4 Pouch cells

Battery packs are composed of battery cells linked together in a series or parallel arrangement, or some combination of the two. Combining cells in series and parallel allows manufacturers to generate higher voltages and/or currents for operation. [17] Battery cells come in a variety of configurations, including: button, cylindrical, prismatic and soft-pouch. [16] [29] The various cell configurations are displayed in Figure 2.

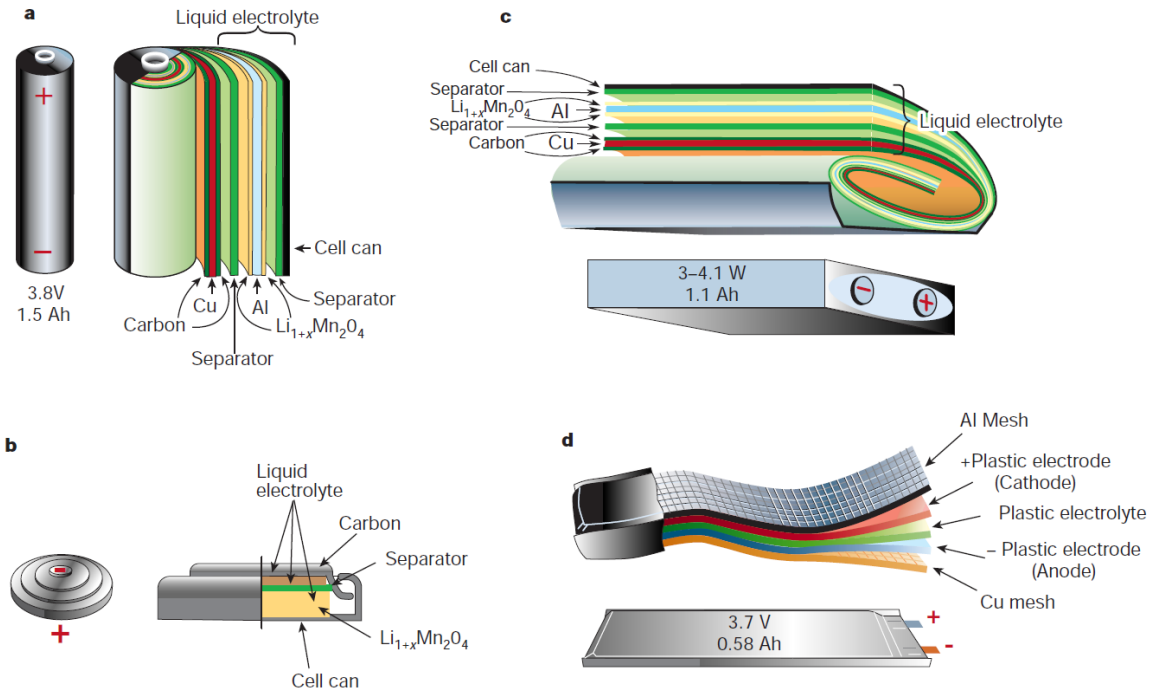

Figure 2: (a) Cylindrical, (b) prismatic, (c) coin, and (d) pouch packaging for lithium ion batteries [29]

Of the four cell configurations, the soft pouch-cell, also commonly referred to as pouch, polymer, or Li-Po cells, is the configuration that is most predominantly utilized for electric vehicles. [30] The major difference between the pouch cell and its other battery cell counterparts is that fabrication of a pouch cell does not require a rigid metal enclosure, reducing the weight. Instead a pouch cell enclosure can be made from polymer-coated aluminum foil. The pouch cell

makes the most efficient use of space, due to its slender design, and achieves a 90 to 95 percent packaging efficiency, the highest among battery packs. [31] Despite these major benefits, though, this form of the lithium-ion battery has a lower energy density and is less durable than its cylindrical counterpart. Also, if the pouch becomes polarized it will likely corrode and result in cell leakage and swelling. [31] [32] Swelling is caused from the gases generated within the cell during charge and discharge and it poses a dramatic concern for battery safety. [31] [32] Since pouches offer limited mechanical protection to cell electrodes, protection of the cells must be accomplished by surrounding materials that enclose the cells.

2.5 Battery Pack Construction

Battery pack construction must take into account a variety of parameters including: the voltage and runtime requirements, the loading conditions, and the size and weight limitations. [33] In order to better meet the pack requirements, the design of the battery pack must utilize the space provided effectively. Thus, the selection of the type of cell to be used within the pack will decide its overall packing capability. With higher packing capability, a greater number of cells will fit into the battery pack, extending vehicle range, especially if the cell has high energy densities. The A123 battery pack is composed of AMP20 Prismatic Cells (lithium iron phosphate cell chemistry) that are tightly packed together, as indicated in Figure 3.

Figure 3: Cross-Section of De-Constructed A123 Battery Pack

Although, extending range with higher packing is an advantage of this battery pack design, the system does suffer overheating problems due to a lack of space to promote proper cooling. Thus, despite the cylindrical cell not being ideal, due to having lower packing capability compared to

the pouch cell, the empty spaces it creates in a multi-cell configuration allows for better dissipation of heat. [34] The battery pack designed by Tesla for their S85 EV uses over 7,000 18650 cells (modified Panasonic cells with nickel-cobalt-aluminum cathodes of the 18650 format). [35] This battery pack configuration, also, allows for more flexibility in terms of losses to the pack. For instance, if a cell in series was to open, there is minimal total power loss and if one in parallel shorts the integrated fuse protection will remove (isolate) the cell from the circuit. [34] [36]

EV manufacturers are certainly not limited in their choices to one particular cell type for battery pack design, but there is a tendency to migrate towards packs composed of larger cells. [35] Using larger cells will reduce the need for supportive electronics, which typically adds up to 20–25 percent to the finished pack. [35] These electronic components, though, become more expensive as they have to endure higher current handling. Thus, despite the drop in complexity the increase in price can greatly affect the pack design's market acceptance. Table 2 lists the prices of the battery packs for different EVs and HEVs.

Table 2: Comparison of Battery Pack in Electrified Vehicles

Make and Model	Cell Type	Cost Per kWh	Specific Energy (Wh/kg)
Chevrolet Bolt, 60 kWh (2016) [21]	Prismatic/Pouch	$145/kWh	138 Wh/kg
Tesla S 85, 90kWh (2015) [35]	18650	$260/kWh	250 Wh/kg
Best practices DoE/AABC [35]	Pouch/prismatic	$350/kWh	150–180 Wh/kg
Nissan Leaf, 30kWh (2016) [35]	Pouch/prismatic	$455/kWh	80–96 Wh/kg

In terms of cost per kWh, Chevrolet's Bolt battery pack has the least cost/kWh and they, along with many other battery manufacturers are pursuing a cost per kWh of less than $100. In pursuing this goal, though, all battery manufacturers must first provide the necessary safety design features to ensure consumers will be protected from the possible failure modes that can occur at the cell or pack level. A variety of tests and regulations must be strictly performed and adhered to before a cell or battery pack can be used by a consumer.

2.6 Regulations and tests

In order to ensure the safety risks associated with the use of lithium-ion batteries are decreased (or eliminated), a number of standards and testing protocols have been developed. These standards aid in providing manufacturers with guidance on the safe construction and use of lithium-ion batteries. [37] The subsequent tests ensure that the cells will be able to effectively function in the potential environment that they are placed in or fail safely. Safety tests for lithium-ion batteries are typically intended to assess specific risks from electrical, mechanical and environmental conditions. [37]

The completed battery must be tested and registered to assure correct assembly and compliance with safety standards. [37] As set by the United Nations, the Recommendations on the Transport of Dangerous Goods on lithium-ion batteries outline the necessary test requirements that must be fulfilled in order to transport a completed battery. [35] These verification and validation tests fall under UN 38.3, which includes [35] [37]:

- T1 – Altitude Simulation (Primary and Secondary Cells and Batteries)
- T2 – Thermal Test (Primary and Secondary Cells and Batteries)
- T3 – Vibration (Primary and Secondary Cells and Batteries)
- T4 – Shock (Primary and Secondary Cells and Batteries)
- T5 – External Short Circuit (Primary and Secondary Cells and Batteries)
- T6 – Impact (Primary and Secondary Cells)
- T7 – Overcharge (Secondary Batteries)
- T8 – Forced Discharge (Primary and Secondary Cells)

Additional testing expectations for vehicle-grade batteries have been created by a number of standards organisations, including: SAE, ISO, ANSI, IEC, UN, and UL. [37] All of the tests developed are meant to assess the battery's ability to withstand different forms of abuse and are designed to ensure that the products fulfill all of the necessary safety protocols. A list of these tests is provided in Appendix A: Regulation Test Criteria in Table 28. In order to have battery packs, or simply the cells themselves, enter into the consumer market they must be able to pass all of the safety requirements. [37] If they do not pass the requirements the cells cannot be utilized and will have to be destroyed.

2.7 Battery Failure Modes

Despite the great advantages electrification will bring to creating a future for the electric vehicle market, it should be kept in mind that the materials being used to create these energy storage systems are hazardous to consumers. Should a battery fail it can do so in an uncontrolled manner. [32] The destructive potential of LiBs has increased public awareness for battery safety, especially since the 2013 incident of the full grounding of the entire Boeing 787 fleet. [38] This was a result of many incidents of the planes' lithium-ion batteries undergoing thermal runaway and catching fire during operation. Governments have responded to the changing energy climate with new policy, such as Natural Resources Canada project for Developing Electrical Safety Standards to Introduce Electric Vehicles into Canada [39], and companies have further refined the development of safety systems on their batteries.

Table 3 describes some examples of the potential failure modes of LiBs as defined by Hendricks et al. [32]

Table 3: Examples of Failure Modes of Lithium-Ion Batteries

Battery Component	Failure Mode	Failure Cause	Failure Effects
Anode (active material)	Thickening of SEI layer	Chemical side reactions between lithium, electrode, and solvent	Increased charge transfer resistance, reduction of capacity, reduction of power
Cathode (active material)	Particle fracture	Mechanical stress from intercalation of lithium ions	Reduction of capacity, reduction of power
Separator	Hole in separator	Dendrite formation, external crushing of cell	Perforation of separators in cell causes electrolyte to leak making contact with other cell components.
Organic solvents	Gas generation and bloating of cell casing	High external temperature, overcharging of the cell	Increased diffusion resistance, and may lead to thermal runaway.

Any of the battery failure modes determined through Failure Modes and Effect Analyses (FMEAs) can result in the failure of the entire battery. Some failure modes, though, are less severe and unavoidable. [32] [40] For instance, the capacity fade occurring within the cell is a progressive failure mode and cannot be avoided. Other failure modes, though, can be potentially disastrous and require mitigation strategies. [32]

The failures described in Table 3 are presented from the view of the cell under operation. The cell failures can be potentially caused by a number of other factors including: poor cell design (electrochemical or mechanical), cell manufacturing flaws, external abuse of cells (thermal, mechanical, or electrical), poor battery pack design or manufacture, poor protection electronics design or manufacture, and poor charger or system design or manufacture. [36] [40]

2.7.1 Assessment of Battery Failure Modes Using DFMEA

Design Failure Modes and Effects Analysis (DFMEA) is a method to assess potential failure modes and identify the resultant effects on system operations in the design. [32] These assessments can be performed at the system, subsystem, assembly, subassembly or part level and are, therefore, an essential assessment method for determining methods of failure for systems in the workplace. [41] These can then be mitigated by determining controls, detection methods, and action plans to alleviate the risk of failure. Establishing these mitigation actions help the systems and the vehicle, in general, to be safer to use and operate on.

In order to complete a DFMEA on the battery pack and its associated components, one must become acquainted with all of the respective parts to determine how they may potentially fail. A significant amount of research is required to better understand the failure modes associated with each component and operation.

After establishing each part and how they function within the system, each function and the associated risk are assigned a number from 1-10 for the following three categories:

Severity (SEV): Defined as the extent to how damaging a failure can be

Risk of Occurrence (OCC): Defined as the probability of an incident occurring

Probability of Detection (DET): the extent to which a failure mode can be determined

The Risk Priority Number (RPN) can then be calculated by using Equation 2.3. The higher the RPN, the higher the risk of the failure mode occurring.

$$RPN = \begin{pmatrix} Severity \\ Rating \end{pmatrix} * \begin{pmatrix} Occurrence \\ Rating \end{pmatrix} * \begin{pmatrix} Detection \\ Rating \end{pmatrix} \qquad \text{Equation 2.3}$$

Based on the calculated RPN, a person can determine the highest risks to the battery pack. By targeting the greatest risks, more attention can be given to these potential failure modes during

the design phase. Thus, appropriate mitigation techniques and processes can be implemented to prevent the failure from even occurring.

2.7.2 Battery Safety Precautions

In order to ensure safe operation for the consumer, a variety of safety precautions have to be implemented at both the chemistry level and in the design of completed modules. By having proper cell and pack design features in place, manufacturers ensure that any potential faults encountered during operation, can be mitigated, whether they be at the cell, pack, or vehicle level. [42] It is also required to have many safety redundancy layers. [34] [42] Should one of the layers fail the additional layers of safety will ensure that, if a potential fault occurs, the fault condition for the battery pack or cell can still be safely and effectively mitigated. [34]

2.7.2.1 Battery Pack Level

At the battery pack level there are a number of advanced safety systems that work in tandem. It is important to have three levels of safety integrated into the design of the pack: electronic controls, electrical disconnects (also referred to as contactors) and electrical fuses. [42] Should one of the safety features of the pack fail to function properly, the other safety measures will be able to identify and address any potential faults in the battery pack. For instance, at the electronic controls level, the Battery Management System (BMS) continuously monitors the voltage of every cell, the temperature of numerous points in the pack and current at the pack level. If the safety algorithms determine that a particular operating condition is out of range, which could result in a hazard occurring, a fault code is recorded and transferred to the supervisory controller. [15] [33] The supervisory controller will initiate some form of mitigation to prevent the hazard from occurring, or if the system does not respond to the fault within an appropriate amount of time, the BMS can open the contactors to disconnect the battery from the vehicle. [33] Should the BMS fail, though, the pack also has a hardwired safety protection circuit with three layers of fuses: one at the individual cell, module and overall pack level. [33]

In addition to electrical systems being able to provide mitigation of various faults occurring in the battery pack, the overall material construction of the battery pack needs to be selected based on a criterion of providing safety. [36] Choice of material must be done based on the requirement of avoiding conditions that could lead to a path for low level current leakage (current that flows through the protective ground conductor to ground) or direct short circuiting. To achieve this, the

proper insulating materials must be utilized that possess high insulation resistance. In addition, the chosen materials surrounding the cells have to be strong and durable in order to sustain abrasions or puncturing. [41]

2.7.2.2 Cell Level

At the cell level, battery manufacturers can affect a number of factors within the cell chemistry and overall cell construction to increase its safety. A list of some of these factors, along with their descriptions of what is affected is provided in Table 4.

Table 4: Safety modification for lithium-ion cells [36] [37]

Battery Component	Description of Safety Modification
Cell chemistry	Using a less reactive chemistry, or by introducing some form of chemical retardant. Example: substituting Lithium Cobalt oxide cells for Lithium Manganese oxides or Lithium phosphate cells.
Electrolytes	Electrolyte chemistry modified to include chemical inhibitors. They make the system self-extinguishing or flame retarding, if cell is abused.
Cell Construction	Design cells to remove excess heat, else localised hot spots can develop.
Separators	A cell overheating can cause the separators to distort or melt, leading to a short circuit between the electrodes. External circuits cannot protect against internal short circuits, but better separators can be used including: • Rigid separators that do not distort even under extreme temperature conditions. • Flexible ceramic powder coated plastic: prevents contact between the electrodes, resists penetration by impurities, reduces shrinkage at high temperatures and impedes the propagation of a short circuit across the separator. • Shut down separators: melting plastic closes up the pores avoiding a short circuit, but it is irreversible. Cell will no longer function. Once an internal short occurs, though, the occurrence can be detected by a drop in cell voltage, triggering isolation of the battery from charger or load. This will not prevent the short, but the mitigation will prevent further damage to neighbouring cells and the pack.
Circuit Interrupt Device (CID)	Should a cell reach an internal gas pressure that exceeds its manufacturing specifications, the CID will interrupts the flow of current.
Safety Vents	Side reactions can produce gases and the active materials will also expand due to the temperature rise. This expansion and gas build-up will lead to a pressure increase inside the cell that may rupture the case or cause the cell to explode. Safety vents are installed on each cell to release pressure. To prevent external air being absorbed into the cell, automatic release guard vents allow controlled release of excess internal pressure. This avoids the potential for leakage and prevents uncontrolled rupture of the cell case.

The above safety precautions are only beneficial if the quality of the battery manufacturing process is maintained throughout production, otherwise they will be useless. Burrs on the electrodes, misaligned or out of tolerance components, and contaminated electrode coatings or electrolytes can all cause short circuits or penetration of the separator. [36] [37] These conditions may result in the thermal runaway of the cell. Thus, the entire manufacturing process needs to be well maintained and continually monitored. [36] [37]

2.7.2.3 Battery Management Systems

To re-iterate the discussion on safety systems provided in the previous section, protecting the consumer from the battery pack undergoing a potentially catastrophic failure is of the utmost importance. As a result, there have been vast developments in the area of battery management systems (BMS) to increase consumer safety. [43] [44] These systems are used to manage rechargeable batteries, in order to prevent them from operating outside of their safe operating limits. Overcharging the lithium-ion battery can have very damaging effects on the cell, so a BMS system is required for any battery pack to monitor each individual cell. [15] [32] The BMS will monitor the state of the cells with time, using the collected data as parameters to make calculations to determine if it is outside of its threshold. If this occurs then the BMS will take steps to control the system and, also, communicate the results to a higher level controller through CAN-bus signals. [17] [43]

Depending upon the specifications, a BMS may monitor many different parameters in a battery pack, including [15]:

- Voltage: measuring total voltage, as well as the voltages of individual cells;
- Temperature: be it the average temperature, coolant input and output temperatures, or, once again the temperatures of individual cells;
- Capacity: to measure the remaining capacity within the battery, or cells, to calculate state of charge (SOC) or depth of discharge (DOD);
- State of health (SOH): the overall condition of the battery;
- Coolant flow; and
- Current: current in or out of the battery.

By being able to monitor these parameters, the BMS can determine if a problem will arise in the battery and apply the necessary controls to mitigate the issue.

Despite being able to analyze all of these parameters, though, Battery Management Systems still do not possess an accurate and dependable method for determining the SOC. [15] In comparison to its counterpart, the internal combustion engine, attempting to determine the remaining energy in a battery is much more complex than reading the level of liquid fuel in a gas tank and the rate at which it is being transferred to the engine. The most prominent problem is trying to assess the flow in and out of coulombs as the battery ages, in order to assess the State of Health (SOH) and capacity fade of the battery. [45] BMS systems do have the capacity to provide information on the SOH of the battery but, in order to remain computationally efficient they have lost accuracy in their assessments. [44]

2.8 Modelling Battery Degradation

As described previously, a battery will degrade over time via a variety of different processes. [9] [24] Being able to understand and quantify these different processes is paramount to determining the state of health of a battery over its lifetime. [15] Thus, lifetime prediction models are developed in order to better understand the design and operational consequences on performance degradation of Li-ion batteries. [11] [46] With these models, predictions are made regarding specific properties of the battery as it ages, such as its resistance, capacity, or power. The degradation model developed for the application can be: empirical, chemistry/physics-based, or some combination of both. This has led to the creation to a wide variety of model forms. [11] The specific form that the model takes will, most likely, depend on the particular technology that is used and the set of stress factors that are being monitored for degradation analysis. [47] [48]

2.8.1 Electrochemical Modelling

Electrochemical models are used to optimize the physical aspects of batteries and characterize power, voltage and current parameters. [49] The models are based on the chemical processes that occur within the cell using a combination of electrical and physical properties. The goal of these types of models is to capture all key behaviours within a cell, including characterizing power, voltage and current parameters [49]. The models utilize equations that are based on the chemical processes that occur within the cell using a combination of electrical and physical properties. These equations include: Fick's and Ohm's laws, and the Butler-Volmer and Tafel equations.

The models are highly accurate and can describe the cell parameters in an enormous amount of detail [50].

Although highly descriptive, the level of detail that is incorporated into these models results in them being very complex and difficult to configure requiring significant memory and computation [49] [50]. In terms of time to reach a solution, the solver may take hours to solve the non-linear differential equations with a large number of unknown parameters [49].

Furthermore, another issue arises when attempting to measure the physical parameters over time and use, as the battery usage and the battery aging causes them to change. [50] Thus, it is difficult to obtain an accurate model and apply it to vehicle applications. As a simplifying measure to decrease the experimental and computational costs, a single source of degradation is assumed limiting the number of dimensions involved in the equations and, in doing so, the general complexity. [49] [50] This will help limit the calculation time, which is very important.

In battery management systems for vehicles, PDE-based electrochemical models are not desirable and are mostly only used in research settings. As these models are too computationally intensive to run for a long duration simulation, it would not be advantageous to pursue modelling the battery pack from the electrochemical scheme [49].

2.8.2 Electrical-based Modelling

Electrical based models utilize equivalent circuit components to predict the terminal characteristics of the batteries (i.e. current and voltage). [50] An equivalent circuit for a battery represents it as an electrical circuit containing components that capture the various phenomena within the battery during operation. [26] For instance, based on Figure 4, the R_0 represents the internal resistance of the cell while the resistor-capacitor (RC) components represent the impedance from each electrode. These models can then be extended and become more complex by including more electrical components with different circuit architectures [49]

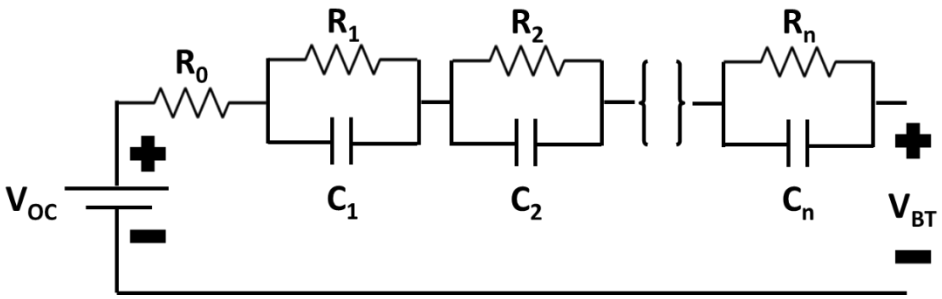

Figure 4: Equivalent Circuit Model Example [48]

The equivalent circuit parameters change with operating conditions (i.e. temperature, SOC, current) and as the battery ages. [49] [50] Thus, when performing both performance and aging analyses for batteries, an HPPC test is required to define how they change under different operating conditions and their degradation trends. [49] [50] Predictions, through extrapolation of the degradation trends, can then be made in regards to which battery components (electrolyte, anode, cathode, etc.) are degrading and the rate of degradation. Using these pieces of information the lifespan of the battery can be predicted. As extrapolation attempts to predict the future health of the battery, the model is inherently inaccurate as it is unknown what possible degradation events may occur.

2.8.2.1 R_{INT} Model

The R_{INT} model is the simplest equivalent circuit, using a resistor to model the internal resistance of the battery. [51] The parameters in this model vary with SOC, temperature, and the direction of current flow (dependent on whether the battery is charging or discharging). Figure 5 displays the equivalent circuit of the R_{INT} model.

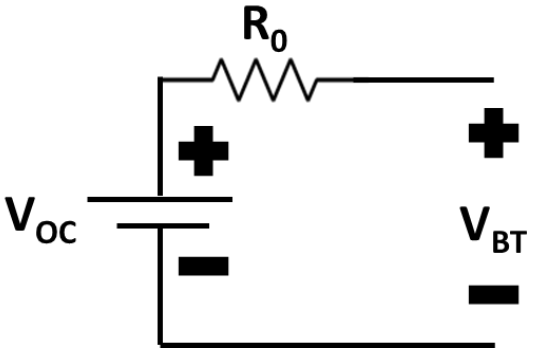

Figure 5: R_{INT} Model Equivalent Circuit [51]

2.8.2.2 Thevenin Model

The Thevenin Model is an extension of the Rint model, which connects a parallel RC network in series with the resistor from the Rint model. [51] By having the additional equivalent circuit components, the model is capable of describing the dynamic characteristics of the battery. [51] The new equivalent circuit is displayed in Figure 6.

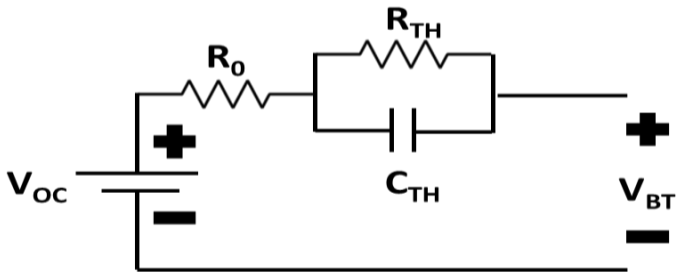

Figure 6: Thevenin Model Equivalent Circuit [51]

2.8.3 Empirical Modelling

As opposed to electrochemical models, empirical models use experimental data from cells to interpret the battery degradation over a testing period for specific operating conditions [49]. With the fitted model, future behavior can be extrapolated without the consideration of physicochemical principles that would require large computing requirements. Their simplicity allows empirical models to be able to perform fast computations and be able to look at much larger aging timespans. [26] Unfortunately, since the models are based on fitting experimental data for only a small subset of potential operating conditions, predictions can be very poor for other battery conditions [52]. This is a fatal flaw for empirical models attempting to predict battery degradation on-board HEVs, PHEVs, and BEVs, because operating conditions are constantly in flux [49]. In addition extrapolating data, from 1 year of aging experiments, all the way to 10 or even 15 years of operation, can be quite risky as the aging phenomena can change over time [49] [52].

To alleviate some of the problems from using empirical models, a semi-empirical approach can be taken to describe the aging phenomena occurring within cells. In some cases, this approach relies on combining some of the physiochemical aspects of cells with simple neuronal network models (an aspect of empirical models) to create the combined model [11]. Ecker et al. used this

particular approach to develop a semi-empirical model to describe the calendar aging process within $LiFePO_4$ cells.

Based on the research completed by Ecker et al., they were able to develop a semi-empirical model for the calendar aging of lithium-ion batteries, utilizing the parameters of: temperature, aging period, and potential which is related to the SOC of the cell. [11] The following equations can be derived to fit the measured calendric aging data:

$$\frac{C}{C_{nom}} = 1 + B(T,V) * F(t) \qquad \text{Equation 2.4}$$

Where C is the new capacity of the cell following degradation, C_{nom} is the nominal capacity, B is a function of temperature and potential, and F is a function of aging time. [11]

These functions B and F can be described by the following equations:

$$B(T,V) = \left(c_T^{\frac{T-T_0}{\Delta T}}\right)\left(c_V^{\frac{V-V_0}{\Delta V}}\right) \qquad \text{Equation 2.5}$$

$$F(t) = c_a t^{\beta} \qquad \text{Equation 2.6}$$

Where c_a, c_T, and c_V are fitting parameters determined through a regression analysis. T_0 and V_0 are a reference temperature and voltage and ΔT and ΔV are unit parameters for the system. The collected calendar aging data for the cells is then used to fit the parameters (c_T, c_A, and c_V) and develop an aging equation.

2.9 Drive Cycles

A drive cycle is a series of data points of vehicle speed versus time that resembles actual driving. [53] It is produced in order to assess the performance of vehicles, especially in regards to fuel consumption and release of emissions. The driving cycle is performed on a chassis dynamometer, where tailpipes emissions of the vehicle are collected and analyzed to assess the emissions rates. The Environmental Protection Agency (EPA) utilizes a variety of different drive cycle series for investigating each vehicle. Table 5 describes the characteristics of some of the drive cycles run by the US EPA. [53] [54]

Table 5: US EPA Drive Cycle Characteristics

Drive cycle	UDDS	HWEFT	US06
Description	City driving conditions	Highway driving conditions	High acceleration aggressive driving schedule
Duration (s)	1369	765	596
Distance (mile)	7.45	10.26	8.01
Average Speed (mph)	19.59	48.3	48.37

Two of the drive cycles most frequently used for testing is: the Federal Test Procedure (FTP) cycle, and the Highway Fuel Economy Test (HWFET). [53] [54] The FTP cycle represents a commuting cycle. Contained within the cycle are periods of urban driving, frequent stops, and a part of highway driving. This cycle utilizes the Urban Dynamometer Driving Schedule (UDDS) cycle followed by the first 505 seconds of the same cycle. [53] Figure 7 depicts the FTP cycle.

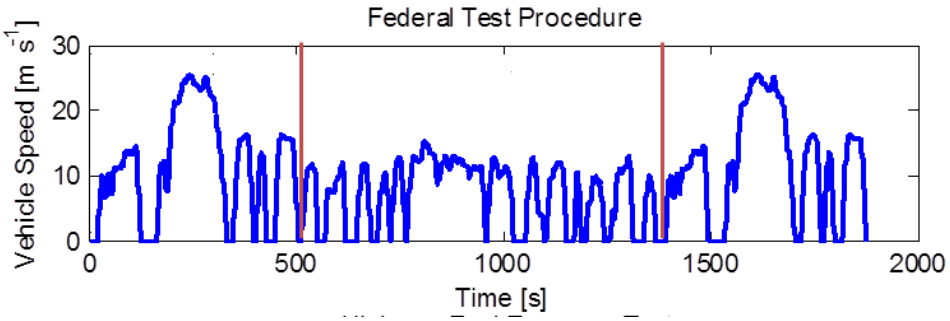

Figure 7: Drive Cycle Federal Test Procedure (FTP) [53]

The HWFET is used to assess fuel economy over highway driving cycle. The speed of the vehicle is less than sixty miles per hour for the entire cycle. [53] [54] Figure 8 depicts the highway fuel economy test drive cycle.

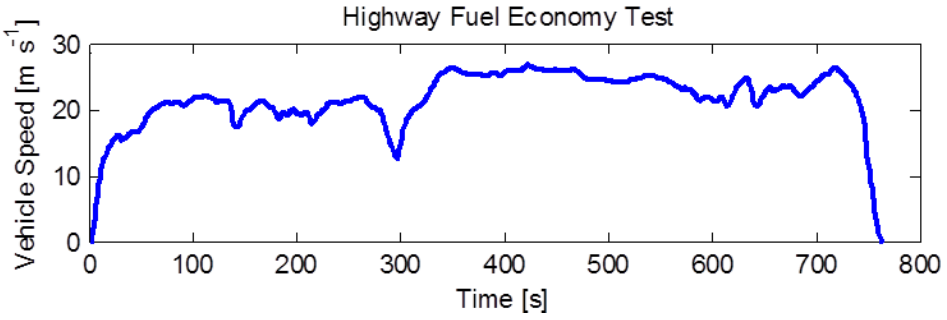

Figure 8: Highway Fuel Economy Test Procedure [53]

Drive cycles are also used is in vehicle simulations. Utilizing a series of drive cycles, an annual schedule can be developed to simulate vehicle operation and determine information on the diagnostics of the vehicle over a year or for even longer durations. In the case of this work, simulations will be run over the course of ten years (the consumer required lifespan of a battery [6]) to determine information on the degradation of the battery.

2.10 Degradation Mechanisms for Lithium Ion Batteries

Li-ion batteries provide one of the best energy-to-weight ratios, exhibit no memory effect, and have low self-discharge when not in use. [16] These aspects have spurred the adoption of lithium ion batteries as the main power source for most electronic devices, and by consequence they have also aided in spurring the development of hybrid and battery electric vehicles. [55]. In order to make an impact on the existing vehicle market, largely composed of internal combustion engine (ICE) vehicles, these battery powered vehicles have to satisfy existing performance requirements and last long enough for consumer acceptability. [6] Due to these requirements, rigorous research has been completed in determining and quantifying the processes by which the battery will degrade. [9] [24] [49] Limiting these degradative processes will increase battery life and thereby increase consumer acceptability.

Battery lifetime is the measure of battery performance and longevity. The value can be quantified in several ways: as run time on a full charge (estimated by a manufacturer in milliampere-hours or ampere-hours) or as the number of charge cycles until it degrades irreversibly and cannot hold a useful charge. [56] For vehicle-grade batteries the End-of-Life (EOL) point has been defined as the point in the life in the battery that it has degraded to 80% of its original SOC. [12]

It was found that the performance loss of these batteries is caused by various mechanisms, and depends on the electrode materials. [9] The aging mechanisms within batteries are often difficult to identify and quantify due to the many different and complex reactions and physical changes that are taking place within them. [6] The capacity fade and impedance increase are distinct and vary depending on the conditions at which the battery is stored at, cycled at, and what materials make-up the batteries. [6]

2.10.1 Calendar Aging:

The aging mechanisms can be classified as one of two types: cycling and calendar aging. Calendar aging is the degradation of the battery over time with the battery being stored under Open Circuit Potential (OCP) conditions. [8] [13] [23] With time lithium-ion cells will lose capacity, even when it is not being utilized. Calendar aging losses are smaller than those experienced by cycling aging losses in the cell, but a personal vehicle is in park (OCP conditions) for most of its service life. [8] While parked the battery pack is undergoing calendar aging.

The largest capacity loss within lithium-ion cells, due to calendar aging, occurs early in the life of the battery (when lithium concentration in battery is at its highest) and then they continue to lose capacity at a much more gradual rate from that point on. [23] The loss of capacity can be quite detrimental for the lifespan of the battery and its overall effectiveness. Within a cell there are two sets of processes that result in capacity loss in the cell with time (calendar aging). They are reversible and irreversible capacity loss. [24]

2.10.1.1 Reversible Capacity Loss

Reversible capacity loss in lithium-ion cells is the result of the spontaneous re-intercalation of the lithium-ions from the electrolyte into the framework of the unstable de-lithiated cathode, and electrochemical processes. [8] [57] This phenomenon occurs when the cell is fully charged. This is due to the high potential of Li-ion batteries at a completely charged state increasing the likelihood for the lithiated graphite negative and de-lithiated positive electrode to be oxidized or reduced by the electrolyte, respectively. [14] The lithium-ions that are exposed to the electrolyte can de-intercalate from the graphite electrode and be shuttled to the positive electrode (same species at both electrodes). [14] This process is the result of a diffusion-limited transfer of lithium across the two-phase interface that increases with increasing current density. [58] The side reactions at both electrodes occur simultaneously with equal amounts of cyclable-lithium ions being exchanged between the electrodes and electrolyte at both electrodes. [14]

Identification of what species is shuttling the lithium-ions has been difficult to determine. Some researchers have suggested that the reaction of acidic impurities generated at the cathode with the SEI is an example of a shuttle mechanism. [59] Sloop et al. proposed that the $LiPF_6$ salt within

EC-containing electrolytes acts as a Lewis acid generating transesterification products, PEO polymers and CO_2. The CO_2 produced becomes reduced at the anode to form oxalate or CO. The oxalate moves through the electrolyte to the cathode where it is re-oxidized back to CO_2. [14]

Safari and Delacourt found that the main contributor to the reversible capacity loss of the cell (resulting in a decrease of the OCP) was mainly due to the LFP electrode. The LFP electrode is very sensitive to small variations of lithium content at a completely charged state. [14] Even though there is only a minor uptake of lithium ions from a side reaction of the cell, there is a substantial contribution to the OCP decrease. In order for this to happen though, there must be another side reaction at the graphite electrode to release the lithium. [14] Thus, the cell is balanced.

In lithium-ion cells the reversible capacity loss is typically very low [60], however, lithium-ion cells are not capable of enduring overcharging [60]. Thus, they are not able to bear extra battery recharge that is typically used to balance the self-discharge losses in the cells, unless some form of charge control is in place. [60] Also, when a number of cells are connected in series to form a battery, recharge of each cell to the desired voltage level cannot be done unless the cells remain perfectly matched in voltage and capacity, or unless some form of charge control is provided. [60] The amount of self-discharge experienced by the cell under OCP conditions is directly related to the temperature and SOC at which the cell is stored at. These two variables have a direct influence on irreversible losses but, Safari and Delacourt found that the temperature has less effect than the SOC on reversible losses. [14]

2.10.1.2 Irreversible Capacity Loss

The other set of processes are irreversible as they are chemical in nature and the losses in capacity cannot be reclaimed. The irreversible process is caused from side reactions occurring within the cell. [24] [49] The predominant mode of decomposition is due to side reactions occurring at the negative and positive electrodes and is governed by the electronic conductivity of the SEI layer, with a larger extent of side reaction at the graphite negative electrode. [9] [24] [49] Electrolyte decomposition decreases the available lithium concentration in the electrolyte that can be utilized the cell and the extent of degradation is influenced by a variety of factors, such as: purity of the active material or electrolyte, the specific surface area of the electrodes, conductors, binders or separators. [60]

Research completed by M. Kassem et al. found that cells aged under stored conditions experienced increases in impedance resulting in cutoff potentials being reached sooner for the individual cells. In addition, the cells experienced a decline in rate capability. [9] The main factors affecting capacity fade and impedance increase in cells under OCP conditions is the temperature at which they are stored at, the SOC at which the cells are stored, and the length of storage.

2.10.1.2.1 Effect of Temperature

The most predominant cause of degradation under OCP is the storage temperature of the cell. When the temperature is high, secondary reactions such as corrosion proliferate causing losses of the cyclable lithium. [6] M. Kassem et al. determined through rate capability, impedance and PITT tests that the loss of cyclable lithium is the main source of aging [7]. In research performed by Grolleau et al., 15 Ah Li-ion cells aged at three different storage temperatures resulted in the following capacity fades: cells stored at 30^{o}C experienced less than 10% capacity loss after 450 days of storage whereas, at 45^{o}C, capacity fade was 20% for fully charged cells [8]. In comparison, fully charged cells stored at 60^{o}C, reached a 20% capacity loss within only 60 days [8].

To counteract this manufacturers store the cells at low temperature conditions to limit the development of these phenomena but even storage at these conditions can cause other problems for the cells due to the loss of material diffusion and the altering of the battery chemistry [6].

2.10.1.2.2 Effect of State of Charge (SOC)

Testing of various cells at different SOCs but under the same temperature storage conditions has led to the determination that SOC plays a major role in cell degradation. From Ohue et al. results of cells stored at equal temperatures but for different SOCs were found to not age in the same manner [61]. The cells stored at elevated SOCs experienced increased battery degradation compared to those stored at lower SOCs [61]. SOC represents the proportion of ions present on either electrode, thus, for high SOC there is a significant number of lithium-ions available at the graphite electrode to partake in potential side reactions with the electrolyte.

2.10.1.2.3 Morphology of Electrodes

In order to determine the impact of aging on the electrodes Scanning Electron Microscopy (SEM) can be used to find possible changes of the electrode morphology after storage. Based on the research done by Kassem and Deleacourt, aging leads to the appearance of round-shape particles that vary in size depending on the temperature of storage. [13] The particles were found to be rich in fluorine, and that the atomic percentage of fluorine within these particles becomes larger with the severity of the storage condition. [13] In terms of aging at the positive electrode under OCP conditions, Koltypin et al. [62] found that the cells experienced decreased performance, increases in the electrode resistance, as well as the Fe dissolution at elevated temperatures. [62]

Kassem and Delacourt also analyzed the graphite electrode using SEM. Storage temperature influenced the electrode by causing a change of the electrode color. At 60^{o}C it was found that the dark brown colour becomes bluish, but for cells aged at 45^{o}C or less there were no changes in colour. [13] The colour of the graphite electrode plays a big role in understanding the degree of lithiation. Graphite electrode colour depends on the lithium content. [13] [63] Despite being fully discharged the graphite electrodes sampled were found to still be lithiated. Also, the SEM studies found that aging leads to some roughening of the particle facets, likely related to the growth of the SEI film (becomes fluffy as it increases). [13]

Analysis of the SEM found that there is no change in particle-size distribution, however, the researchers did find that the atomic percentage of oxygen in aged electrodes is relatively larger than those of the fresh electrode. Kassem and Delacourt believed that it was related to the presence of SEI compounds, such as Li_2CO_3 or lithium alkylcarbonates, at the particle surface that are O-rich. [7]

2.10.2 Cycling Aging

The term cycling aging refers to aging mechanisms that occur within the cell while the cell is in operation (cycled under load). The losses that occur under these conditions are typically irreversible and are attributed to a number of processes. [7] These include: (i) loss of capacity in the formation of the Solid Electrolyte Interface (SEI) layer when cell is first formed and continually throughout its lifespan (occurring at both electrodes), (ii) loss of active materials due to: material dissolution, structural degradation, particle isolation, and electrode delamination, as

well as, (iii) impedance increase from the formation of the SEI layer that passivates the active particle surface. [7]

As previously described, aging can occur at both electrodes, but many researchers have determined that the most prominent loss of available capacity occurs at the anode. [14] Negative electrodes of LIBs are typically composed of graphite, carbon, titanate, or silicone. Of these materials, though, graphite is the most commonly used anode material in lithium-ion batteries, thus, many degradation models are based off of graphite-based cells. [18] Experimental data from the literature is difficult to analyze as each lithium-ion cell system has its own chemistry and many aging effects are influenced by the nature of the cell components. To simplify equations, this study will therefore focus on only the dominant aging mechanisms of graphite anodes.

There are a variety of mechanisms which result in the degradation of the carbonaceous material, many of them considered to be the primary components in lithium-ion battery degradation. [64] [23]These aging mechanisms can predominantly be attributed to changes of the electrode and electrolyte occurring at the interface between the two. [23]

2.10.2.1 Aging of Negative Electrode:

Negative electrodes of LIBs are typically composed of graphite, carbon, titanate, or silicone. Of these materials, though, graphite is the most commonly used anode material in lithium-ion batteries, thus, many degradation models are based off of graphite-based cells. [18] Experimental data from the literature is difficult to analyze as each lithium-ion cell system has its own chemistry and many aging effects are influenced by the nature of the cell components. To simplify equations, this study will therefore focus on only the dominant aging mechanisms of graphite anodes.

There are a variety of mechanisms which result in the degradation of the carbonaceous material, many of them considered to be the primary components in lithium-ion battery degradation. As explained previously there are two forms of aging, cycling and calendar aging. For the electrode, calendar aging in the cell is primarily caused by parasitic reactions occurring at the electrode/electrolyte interface that develops an irreversible passivation film on the surface (solid

electrolyte interface (SEI)). Cyclic aging is the result of several degradation processes caused from mechanical stresses and continual SEI formation.

2.10.2.1.1 Degradation of Electrode due to Solid Electrolyte Interface Formation

The formation of the solid electrolyte interface is the primary source of aging at the anode. The reduction of compounds in the electrolyte leads to formation of this solid film on the negative electrode. The interphase has the role of acting as a barrier between the electrolyte solution and the electrode, preventing solvent decomposition and graphite exfoliation, and facilitates the movement of lithium ions from electrolyte to electrode surface (and vice versa). From a safety point of view, the SEI limits the reactivity of the cell by decreasing the dendritic nature of the lithium that could potentially cause an internal short circuit. This safety feature aids in promoting lithium ion batteries for use in consumer applications.

As the cell is cycled, though, the SEI continues to increase. The electrode can potentially become damaged during cycling, as it exposes the graphite to the electrolyte resulting in the utilization of more lithium to form an SEI layer over the exposed surface. Thus, there is both a loss of cyclable lithium from the cell and an increase in resistance on the electrode from the increase of thickness of the SEI, leading to capacity fade (from the loss of lithium) and power fade (from SEI thickness increase).

Throughout the life of the cell, the resistance of the electrode continues to rise resulting in significant power fading. The increase in resistance is caused from thickening of the SEI and continual chemical changes of the SEI. The growth of the SEI creates resistance to lithium ion flow as it reduces the number of active sites available for intercalation and de-intercalation to occur. Also, with the growth of the SEI, the number of available lithium ions in the electrolyte decreases resulting in reduced capacity.

Formation of various SEI components is characterized by the following reactions [23]:

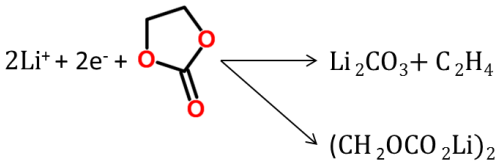

Equation 2.7

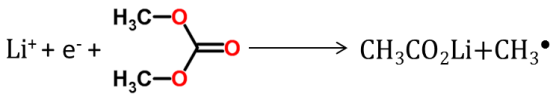

Equation 2.8

$$Li^+ + e^- + Trace\ H_2O \rightarrow LiOH + \frac{1}{2}H_2$$ Equation 2.9

$$LiOH + e^- + Li^+ \rightarrow Li_2O + \frac{1}{2}H_2$$ Equation 2.10

$$2Li^+ + 2e^- + 2CO_2 \rightarrow LiCO_3 + CO$$ Equation 2.11

$$nLi^+ + ne^- + PF_6^- \rightarrow LiF + Li_xPOF_y$$ Equation 2.12

In addition to the lithium ions and electrolyte components, mechanisms at the cathode, also occurs resulting in the dissolution of the cathode electrode metal from the lattice [23]. The metals are subsequently incorporated into the SEI.

2.10.2.1.2 Anode Mechanical Failure

As intercalation, and subsequently de-intercalation, of the lithium ions occurs during the charging and the discharging of the battery, there is the potential for the anode to fracture. This is due to the fact that a large volume change occurs during the process, referred to as diffusion-induced stresses (DISs). [23] Cycling the battery at high C-rate and high state of charge (SOC) will induce higher mechanical strain on the graphite lattice of the anode electrode due to the steep gradient of lithium ions.

In addition to the mechanical stresses placed on the anode caused from the intercalation process, electrolyte reduction and gas evolution inside the graphite also causes a rapid decay of the electrode. Gas evolution inside the cell has been known to have a large influence on cell operation, resulting in accelerated aging through degradation of active materials. [23]

2.10.2.1.3 Degradation from Lithium Plating

Under the right conditions, lithium can become plated onto the active material of the anode, instead moving into the carbon intercalation sites. The graphite electrode materials are susceptible to lithium plating and lithium dendrite growth because of the close proximity of its reversible potential to that of Li^+/Li. [23] This leads to loss of capacity from the loss of lithium ions and increases the potential for a short circuit to occur due to accumulation of conductive metal in the separator, while also changing cell compression. [65]

This form of deposition can be caused by a number of factors. When fully charged, lithium ions are unable to intercalate any further as the graphene layers are filled. If the system becomes overcharged, further lithium deposition will result in lithium plating. In electrified vehicles, overcharging can occur when charging current is very high, as might occur during regenerative braking. [23] [65] Lithium plating is also promoted when the cell is operating at low temperatures because the normal intercalation kinetics (diffusion of lithium within the SEI and graphite) into the graphite electrode becomes too slow and Li plating becomes the dominant process. [23] The depositing of metallic lithium can continue to grow within the cell forming dendrites between the polymer separator and the anode. This will lead to an internal short circuit occurring, which then can lead to thermal runway and battery failure. [23]

2.10.2.2 Aging of Positive Electrode

Selection of the cathode materials will have a significant impact on determining the performance of lithium-ion batteries, but also their calendar and cycle lives. [23] The aging mechanisms occurring at the cathode will differ when assessing different electrode chemistries as the physical nature of the cathode is dependent on its composition and structure. As is the case with the negative electrode, there are a variety of mechanisms that can cause aging in the battery via the positive electrode. Results from Bourlot et al. found that the positive electrode went through the following degradative changes after accelerated cycle life: less active lithium in the material, and some binder or conductive carbon dissolution. [66] Figure 9 from J. Vetter et al. is a schematic diagram that displays the different aging phenomenon for cathode materials.

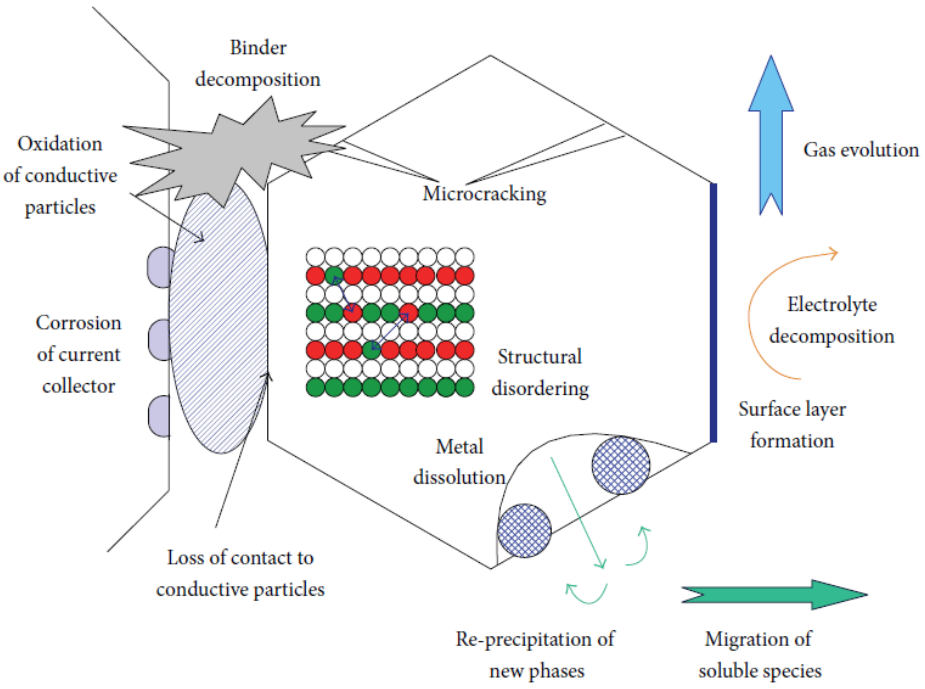

Figure 9: Cathode Degradative Processes [18]

Several of the degradation mechanisms are similar between the two electrodes. As the batteries tested were composed of $LiFePO_4$ active material, the aging mechanisms being discussed will focus on degradation of this type of electrode.

2.10.2.2.1 Structural Factors

The cathode, much like the anode, is susceptible to damage when the cell is operating. The intercalation and de-intercalation of lithium ions from the cathode material causes changes in the molar volume. These changes result in mechanical stress and strain on the metallic oxide particles that form the crystal lattice structure. In addition, when cell operation takes place at elevated temperatures and voltages, dissolution of oxide particles into the electrolyte is promoted, which as previously stated can become incorporated within the SEI. [23] [6]

Loss of the metal in the cathode and its subsequent incorporation increases cell impedance. In addition, the loss in active material causes a reduction in the cell capacity. The most significant of issues, though, is the phase change will cause even higher mechanical stresses on the cathode, and if the stress is too great for the cathode material to handle micro-fractures will begin to

occur. In comparison to the anode, though, the aging rate of the cathode material is much lower, depending on the chosen material [6].

As depicted in Figure 9, the materials that make up the cathode are: the current collector, cathode material, and a chemical binder. Changes at the surface of the cathode material can become severe enough that there can be a loss of contact between binder and material and/or current collector and binder. The loss of contact between the binder and the current collector can be caused from the binder degrading through decomposition.

2.10.2.2.2 Solid Electrolyte Interface (SEI) Formation

An SEI layer can also build-up along the cathode, formed from the decomposition of the electrolyte. This SEI is formed from oxidation of compounds in the electrolyte and contaminants in the electrolyte that catalyze polymerization reactions. It is also, susceptible to damage from gaseous products also produced by the contaminants [19]. Gases can also cause damage to the active material. Again as with the anode, the formation and overall stability of the SEI is dependent temperature, SOC, and voltage. As only a thin SEI film is formed, very few lithium ions are consumed, thus the overall effect on the battery degradation is marginal. The SEI film products can, also, affect ionic motion due to pore plugging, or could contribute to resistive electrical paths to parts of the cathode structure.

2.10.2.3 Aging due to Degradation of the Electrolyte

The electrolyte, within the cell, provides the medium by which lithium ions can be shuttled from the anode to the cathode during discharge (and vice-versa during charging). The most widely used salt in the electrolyte is $LiPF_6$ dissolved in a mixture of several liquid organic solvents, including: EC (ethylene carbonate), also a widely used compound, PC (propylene carbonate), DEC (diethyl carbonate) and DMC (dimethyl carbonate). [64] The basis for why $LiPF_6$ and EC are so widely used is because:

(i) $LiPF_6$ passivates and protects Al (used as the current collector for the cathode);
(ii) EC has high dielectric constant to supply high ionic conductivity; and
(iii) Their presence favors the formation of a stable SEI layer on the graphite anode [64].

In addition to these compounds, VC (vinyl carbonate) or VEC (vinyl ethyl carbonate) will sometimes be used, as additives, to increase the life of the battery.

Although these compounds are necessary for ensuring the proper flow of electrical charge between the cathode and anode, they have the capacity to react, undesirably, in the cell at relatively low voltages. The partial reduction of many compounds within the electrolyte can result in the production of gaseous and/or insoluble species. For instance, at elevated temperatures and high SOC, oxidation of the electrolyte components can occur at the positive electrode interface resulting in the production of CO_2 and ethylene gas. This is demonstrated in the following reaction equations, Equation 2.13 and Equation 2.14. [67]

$$EC + 2e^- + 2Li^+ \rightarrow (CH_2OCO_2Li)_2 + CH_2 = CH_2(g) \quad \text{Equation 2.13}$$

$$(CH_2OCO_2Li)_2 + H_2O \rightarrow Li_2CO_3 + (CH_2OH)_2 + CO_2(g) \quad \text{Equation 2.14}$$

Equation 2.13 and Equation 2.14 is not the only method by which carbon dioxide can be produced in the cell. CO_2 can also be produced from reactions caused from: the presence of traces of HF (with the presence of Lithium Carbonate as well), by the thermally driven decomposition of the SEI, by deterioration of the $LiPF_6$ salt, or oxidation of EC. These reactions are described in Equation 2.15 through Equation 2.21. [67]

$$(CH_2OCO_2Li)_2 \overset{\Delta H}{\rightarrow} Li_2CO_3 + CH_2 = CH_2(g) + CO_2(g) + \frac{1}{2}O_2(g) \quad \text{Equation 2.15}$$

$$ROCO_2Li + HF \rightarrow ROH + CO_2 + LiF \quad \text{Equation 2.16}$$

$$Li_2CO_3 + 2HF \overset{\Delta H}{\rightarrow} 2LiF + CO_2 + H_2O \quad \text{Equation 2.17}$$

$$LiPF_6 \rightarrow LiF + PF_5 \quad \text{Equation 2.18}$$

$$PF_5 + ROH \rightarrow HF + RF + POF_3 \quad \text{Equation 2.19}$$

$$POF_3 + solvent \rightarrow CO_2 + phosphate \quad \text{Equation 2.20}$$

$$EC + \frac{5}{2}O_2 \overset{\Delta H}{\rightarrow} 3CO_2 + 2H_2O \quad \text{Equation 2.21}$$

There can also be the presence of CH_4, C_2H_6, C_3H_6, and C_3H_8 in the cell. Additional hydrocarbon species, except for C_2H_4, are produced from the reduction of DMC, EMC, or EDC, and radical reactions. This side reaction is also referred to as ester exchange. The reactions to produce these gases are described in Equation 2.22 through Equation 2.25, from K. Kumai et al. [68]

$$ROCO_2R + Li^+ + e^- \rightarrow ROCO_2Li + R\cdot \quad \text{Equation 2.22}$$

$$ROCO_2Li + Li^+ + e^- \rightarrow Li_2CO_3 + R\cdot \quad \text{Equation 2.23}$$

$$R\cdot + \frac{1}{2}H_2(g) \rightarrow Alykl \quad \text{Equation 2.24}$$

$$R\cdot + R\cdot \rightarrow R - R \quad \text{Equation 2.25}$$

The products of these reactions can have very damaging effects on the cells. They can cause obstruction of the electrode and separator pores and cause the reduction of available lithium ions. [64] With fewer lithium ions available for electrochemical reactions to take place, there is a decrease in the capacity of the cell.

The production of gaseous species in the cell will, also, increase the internal pressure of the cell and cause it to swell outwards. [34] Cell swelling may force electrodes apart, effectively curtailing the transfer of ions and interrupting charging, or internal pressures can reach values that may lead to the triggering circuit-interrupt-devices (CIDs). [32] [69] Triggering the CID will permanently disable operation of the cell within the module (or battery pack) and the pressure exerted by the cell will cause damage to the battery pack enclosure. The most dangerous hazard mode is that the swelling of the cell can result in enhanced cell leakage rates, with gaseous and liquid species venting and seeping out, respectively, and potentially igniting. [69]

2.11 Battery Testing

2.11.1 State of Charge Estimations

State of charge (SOC) is the measure of available capacity, in percent, of the battery that is available for operation of a device. SOC is equivalent to a fuel gauge for a battery pack system in electric-drive vehicles. The units of SOC are given as percentage points (0% = empty; 100% = full). Unfortunately, there is no way to directly measure SOC, and therefore must be estimated using other quantities.

Coulomb counting is most commonly used, in which the total number of coulombs entering and exiting the battery over a given period are summated. [70] This then leads to the given expression of:

$$N_c = \int_{t_0}^{t} I dt \qquad \text{Equation 2.26}$$

Where *I* is the current, in coulombs per second, which is then integrated over the time period *t*, in order to provide the total number of coulombs, N_c. The total number of coulombs can also be expressed as a capacity, *Q*. Using this relation, the SOC can be estimated. Given an initial SOC for the battery system, SOC_o, and the capacity processed during the period of usage, defined as a percentage of the maximum battery capacity, Q_{max}.

$$SOC = SOC_0 - \frac{Q}{Q_{max}} * 100\% \qquad \text{Equation 2.27}$$

Unfortunately this expression has an unfortunate drawback in that there may possibly be a lack of information as to the initial SOC at a given point in time. [15] The SOC measurement, though, is an effective quantity for controlling battery-powered systems especially for Li-ion batteries. It is also a useful measurement for dynamic power management and battery scheduling. [26]

With this expression, for accurate SOC measurements, it needs to be taken into account that the releasable charge from a battery pack will always be less than the stored charge in a charging/discharging cycle. This is due to the cycling losses that occur during charging and discharging, as well as the calendar losses. These losses can cause accumulating errors to the SOC estimate, thus in order to accurately quantify SOC, modifications have to be made to the method used to account for said losses. [70]

2.11.2 C-Rate

C-rate is a measure of the current that the battery is being charged or discharged at. For instance, if a battery is charged, or discharged, at 1C and it has a capacity of 1,000mAh, then the current required at this rate is 1,000 mA and the duration of time needed to carry it out is one hour. The capacity, or Ah rating, is typically marked on the battery.

$$C_{rate} = \frac{I}{Q_{max}} \qquad \text{Equation 2.28}$$

2.11.3 Reversible Capacity Determination, Self-Discharge Test

In order to measure the percentage self-discharge of the battery, a self-discharge test is completed. The self-discharge test consists of cycling the battery for five consecutive cycles at a constant current at $1C_{nom}$ rate (this is the nominal C-rate of the battery when first discharged). The first initial discharge provides the amount of capacity remaining in the cell after the storage period. Several cycles over the 0-100% state-of-charge range can then be used to detect permanent cell capacity loss. [60]

The test procedure consists of a constant current discharge at 1 C_{nom} down to 2 V with a decrease in current until the system reaches 1A, followed by a 1 hour rest, and a constant current constant voltage (CCCV) charge ($1C_{nom}$) up to 3.65V and potential hold at 3.65V until a cut-off current ($|I|=C_{nom}/20$), and another 30 min rest period. This continues for four more cycles to pre-condition the battery for the subsequent rate capability test.

2.11.4 Rate-Capability Tests

A rate-capability test cycles the cell at varying C-rates in order to generate rate capability curves. [7] As the cell ages, impedance increases resulting in cutoff potentials to be reached much sooner for the cell. Also, the rate capability of the cell declines. [7] Thus, over time, the rate-capability curves are expected to show a change in slope as a result of the current dependence on the polarization effects within the cell. [7] After performing a "Self-Discharge" test, the rate capability test is performed, cycling the battery at various C-rates ranging from $C_{nom}/20$ to $3C_{nom}$, for a total of 8 charge/discharge cycles.

3 Experimental Procedures

Experimental studies were performed on graphite/$LiFePO_4$ cells produced by A123 Systems which are designed for power-type applications (depicted in Figure 10). [71] These cells consist of C–$LiFePO_4$ cathode and graphite anode with a nominal capacity of 20 Ah and cell dimensions of 227mm long, 160mm wide, and 7.25mm high, with a mass of 496 g, on average. LFP has a theoretical capacity of 170mAhg^{-1} and a redox potential around 3.43 V versus Li electrode. [71] The reason LFP is used as a cathode material in industry is because it has a high thermal stability making it a safe choice, and has a low toxicity and a low cost compared to cathodes such as $LiCoO_2$. [9] The salt used for the electrolyte is $LiPF_6$, but the solvent solution was not determined.

Figure 10: Commercial 20Ah LiFePO4/graphite prismatic battery manufactured by A123 Systems [71]

3.1 Calendar Aging Studies of LFP Cells

The cells were stored at varying conditions over their lifecycles. There are three different temperatures in which the batteries were stored at: 35◦C, 50◦C, and 60◦C, and at two different states of charge (SOCs): 0% and 100%. For each set of experimental conditions selected for the respective cells, at least two cells were stored at the same conditions in order to have reproducibility between the results. Table 6 and Table 7 depict the storage conditions of each cell tested.

Table 6: Cells stored at constant temperature and constant state of charge (SOC)

	State of Charge (SOC)	
Temperature	**0% SOC**	**100 % SOC**
35ºC	-	P37, P38
50ºC	P05, P06	P45, P46
60ºC	P09, P11, P12, P13, P14, P19, P23, P25, P26, P30, P31, P32, P35	P27, P28

Table 7: Cells that underwent a shift in temperature of state of charge conditions

Cell	Initial Conditions (Storage Period)	Modified Storage Conditions
P36	60ºC/0% SOC (7 months)	35ºC/100% SOC
P07, P08, P16, P17	60ºC/100% SOC (3 months)	60ºC/0% SOC
P21, P22	60ºC/100% SOC (3 months)	35ºC/100% SOC
P33, P34	35ºC/100% SOC (15 months)	50ºC/100% SOC
P18, P39	35ºC/100% SOC (13 months)	50ºC/0% SOC

In total, 32 A123 20AH cells underwent calendar aging tests. Cells would be periodically removed from their storage conditions after a period of time to determine the effects of the aging on the cells. The length of storage was at first done on a monthly basis, with the cells being removed to reach ambient temperature conditions before cycling. As time progressed, however, the length of storage increased to analyze the effect of longer storage times for cells stored at less arduous conditions.

All the experiments were conducted using a MACCOR 4200 Series multichannel battery tester. Aging of the cells was achieved in a temperature-controlled environment; climatic chambers (VWR 1410, Cincinnati Sub-Zero micro Climate, and VWR 1305U) were used for this purpose. The bench set-up of the test station and aging chamber is displayed in Figure 11 through to Figure 13.

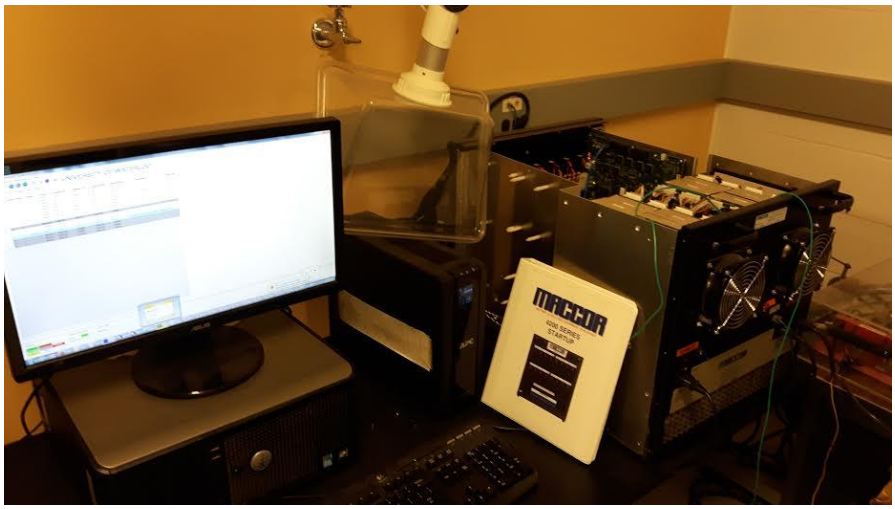

Figure 11: MACCOR 4200 Series multichannel battery tester

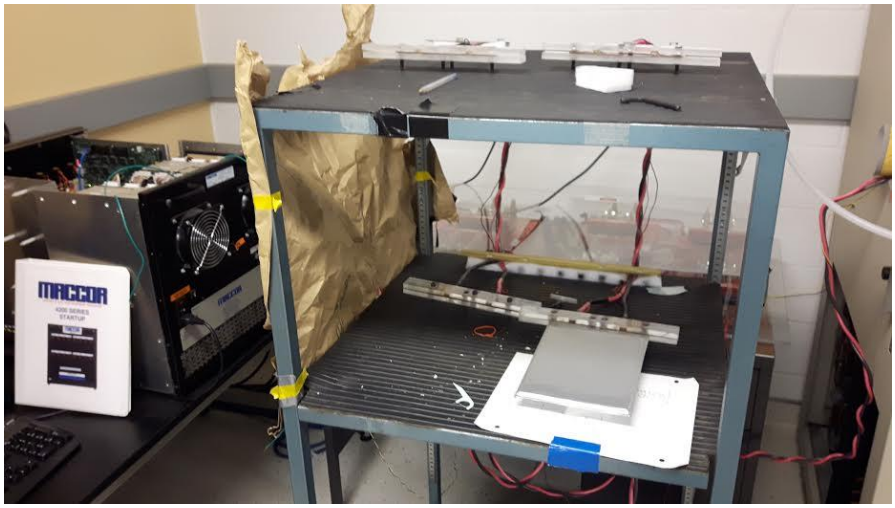

Figure 12: Battery Cycler Test Bench

Figure 13: Climate Chamber

3.1.1 Non-destructive Testing

Before performing the rate capability tests, a self-discharge test was run (refer to Section 2.11.3 Self-Discharge (SD) Test for procedure) to precondition the cells. Running this test allows for the removal of possible outliers and establishes the degree of reversible capacity loss the cell underwent while being stored.

After completing the SD test, a rate capability test was run on the cell with varying C-rates between cycles (refer to Section 2.11.4 Rate Capability (RC) Test for procedure). The test aids in determining the impact of storing the battery at various conditions. A variety of analyses can be completed by utilizing the data from the RC curves, including: determining irreversible capacity fade, differential voltage-capacity curves, resistance of batteries, and capacity between cycles.

Once the cell had completed the necessary cycling tests, the electrode leads were enclosed in insulating tape to prevent short-circuiting and placed back in the appropriate oven for further storage. This process of aging and monitoring, with scheduled testing was completed until the cells reached their respective EOL points, whether it be by the capacity of the cell dropping below 80% of its nominal capacity, the cell short-circuiting, or by the cell swelling. After the cells have degraded to their end-of-life point, they can no longer be cycled and cease being stored under higher temperature conditions.

3.1.2 Post-Mortem Analysis (Destructive Testing)

Opening of each pouch cell needs to be completed under controlled conditions in a glovebox filled with Argon gas. Exposure of the lithium to the water vapour in the air can cause a highly exothermic reaction to occur and result in damage to equipment and personnel, thus the glovebox must be purged of all water vapour and oxygen gas. [36] [72] Before opening the cells the fresh and calendar-aged cells were fully discharged under constant current/constant voltage (CCCV) conditions down to the lower cutoff potential of the cell (2.0V) at a current of 1C, which is then followed by a potential hold at 2V with discharge occurring at a decreasing current until the values reaches a C-rate of approximately C/20.

When opened, the electrodes within the cell can be analyzed using a variety of techniques to quantify, and qualitatively analyze, the extent of degradation within the aged and fresh cells.

3.1.2.1.1 Optical Microscopy

Optical microscopy is a technique used to analyze materials at the micron and sub-micron level. [73] For this experiment the technique was used to analyze the aged electrode materials to determine the extent of degradation and the presence of crack formation. The scale of the images is shown in the lower right corner of each of the images.

During post-mortem analysis, samples of the degraded electrodes were taken and placed under a microscope to determine from optical microscopy defects in the electrode from the aging effects. These optical micrographs were taken with an MA 200 Nikon Eclipse microscope.

3.1.2.1.2 Scanning Electron Microscope (SEM):

Scanning electron Microscopy (SEM) is an experimental tool used to view the surface of materials of interest at the nanometer range. [74] [75] The procedure utilizes a focused electron beam to interact with electrons at the surface of the material and delivers information about morphology. The scanning electron microscope used for the experiments is a Zeiss Leo 1530 unit. The voltage for the experiments was set to 10 kV. The machine was equipped with an energy-dispersive X-ray (EDX) analyzer to perform atomic composition analysis of the surface of the electrode samples. [74] [75] [76]

The lateral resolution can be in the nanometer range while different detectors can be used including the secondary electron and back-scattering detector. [74] Secondary electrons are electrons from the material itself which were excited by the incident electron beam giving different intensity depending on the tilt of the measured surface. Backscattering electrons originate from elastic scattering of the beam electrons on the surface of the material and travel back to a detector. [74] [76] They contain often more information of the material composition since they interact with the material directly. Additionally, they can often deliver a more topographic image of the surface when they are measuring from the side of the sample. [76]

In general, the material needs to be conducting. Otherwise, local charging can occur creating an electric field thus decreasing the resolution drastically. Conductive additives like carbon or gold sputtering onto insulating materials can help to overcome this challenge. [75]

3.1.2.1.3 Energy Dispersive X-ray Spectroscopy

Energy Dispersive X-ray Spectroscopy is an analytical technique used to perform an elemental analysis or chemical characterization of a sample. [77] The technique relies on principle that each element has a unique atomic structure. When stimulated using a high energy beam of charged particles, such as electrons, protons, or x-rays, a sample will release x-rays that are characteristic of the elements in the sample. The x-rays emitted produce a unique set of peaks on an electromagnetic emission spectrum for each of the elements. [77] [74]

The process by which these characteristic x-rays are released from the atoms is as follows. When at rest, an atom in the sample contains unexcited electrons that are at discrete energy states, also referred to as electron shells. [77] [74] The focused beam can excite an electron in an inner shell to rise to a higher energy state (higher electron shell) creating a "hole". An electron at a higher energy state can then drop down to a lower energy state to fill the opening created. [74] In the process of moving from a higher to a lower state, the difference in energy may be released in the form of an x-ray. To measure the number and energy of the x-rays an energy-dispersive spectrometer is utilized. [77]

4 Results of Calendar Aging Studies

4.1 Degradation of Cells

Batteries stored under the conditions described in Section 3.1, experienced varying degrees of capacity fade, resulting in either fast or slow degradation to their EOL point. Figure 14 describes cells that have degraded to their EOL point, the length of time in months, and the conditions that the cells were stored at.

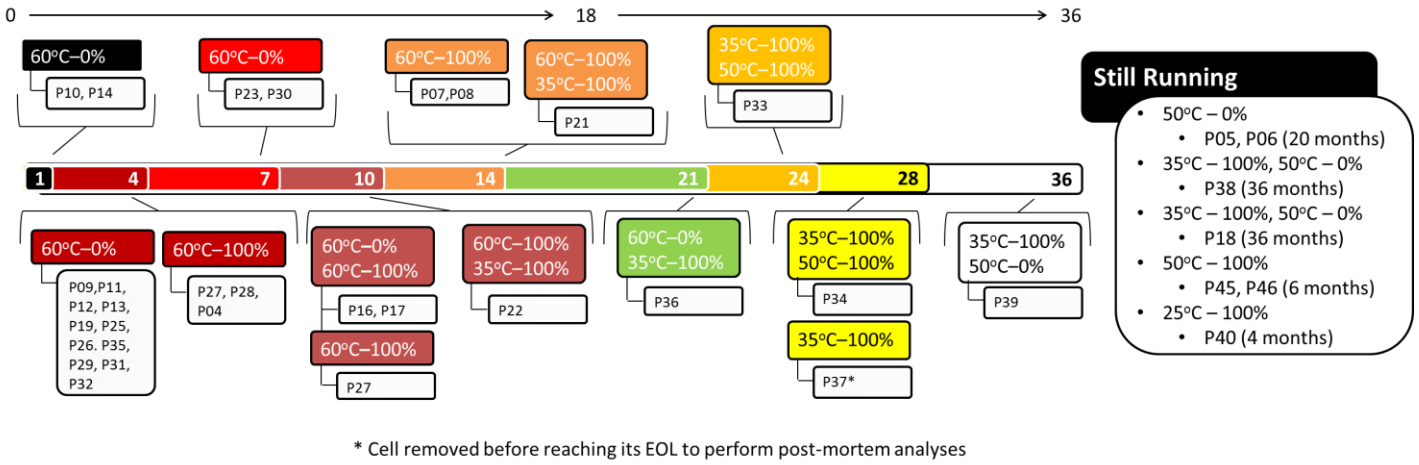

Figure 14: End-of-Life points (measured in months) for tested cells

Cells stored at 60°C regardless of their SOC, reached their EOL very prematurely, only being able to sustain aging in the storage conditions for a maximum of 4 months. Cells tested at 50°C displayed a much slower rate of decline in capacity, and those stored at 35°C showed only a marginal decrease, even despite being stored at high SOC. After 28 months of storage a cell stored at 35°C and 100% SOC was only removed in order to perform post-mortem analysis for comparison with other cells.

4.2 Analyzing cells stored at 100% SOC at different temperatures

The two variables that most affect degradation within Li-ion cells under OCP conditions are temperature and SOC. [9] The most predominant cause of degradation under OCP is the storage temperature of the cell. When the storage temperature for the cell is high, secondary reactions proliferate causing accelerated losses of the cyclable lithium (the main source of losses within the cell). [6] Testing of various cells at different SOCs but under the same temperature storage

conditions has, also, led to the determination that SOC plays a major role in cell degradation. [14] Cells stored at elevated SOCs experienced increased battery degradation compared to those stored at lower SOCs [61]. SOC represents the proportion of ions present on either electrode, thus, for high SOC there is a significant number of lithium-ions available at the graphite electrode to partake in potential side reactions with the electrolyte.

In addition to the irreversible capacity losses that can occur at high SOC, the degree to which reversible capacity will occur is also affected. In comparison to the irreversible losses that can occur within the cell, reversible losses were found by Safari and Delacourt to be more affected by SOC than by temperature. [14] Li-ion batteries do experience the lowest reversible capacity losses, but that can be heavily influenced by the storage temperature (if all cells are stored at the same SOC).

Cells kept at 100% SOC during storage were separated into three chambers at three different temperatures: 35^{o}C, 50^{o}C, and 60^{o}C. Many different metrics were calculated from the captured results to understand the extent to which the cells degraded and the various different degradation phenomena that would occur for cells stored at these conditions.

4.2.1 Capacity Fade:

Capacity losses occurring within the cells were tracked over their storage. Figure 15 and Figure 16 shows the charge and discharge curves for 4 different cells at different storage periods at a fully charged state (SOC equal to 100%) and at temperatures (a) 35^{o}C, (b) 60^{o}C, (c) 60^{o}C shifted to 35^{o}C, and (d) 35^{o}C shifted to 50^{o}C. The charge/discharge curves depicted in the figures in this section were achieved by cycling the cell at a C-rate of C_{nom}/20 and T = 25^{o}C.

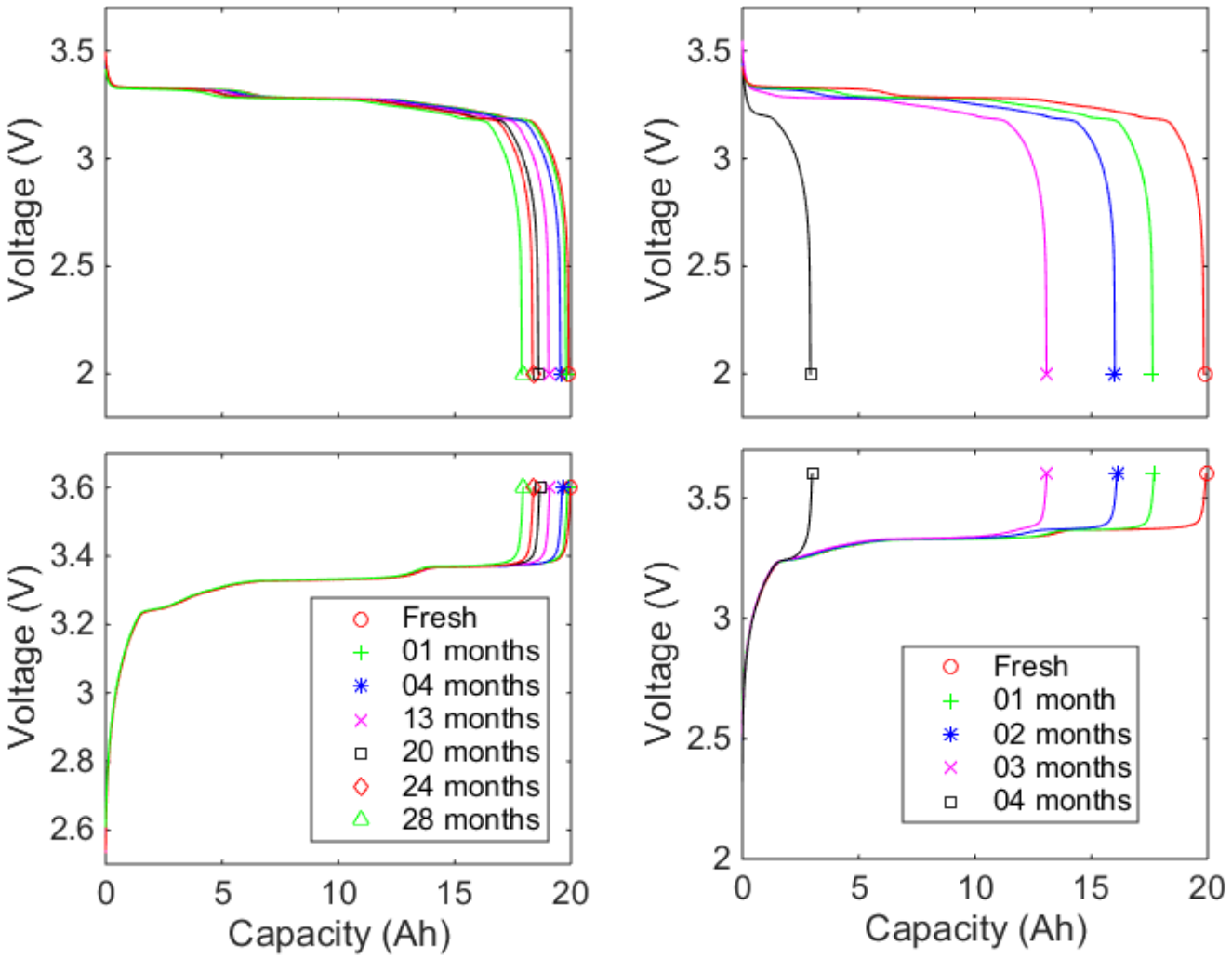

Figure 15: Charge and discharge curves over aging period for cells stored at 100% SOC and 35ºC (left), and 60ºC (right)

The profiles generated for the cells stored at 60ºC demonstrate the severe capacity loss occurring. After only a small period of storage the cells had reached their EOL and could no longer be cycled safely. Storage at this severe condition causes the cells to reach their discharge limits much more rapidly due to the critical decline in capacity. Cells stored 35ºC, though, do not reveal a major decrease in capacity. Despite the long duration of storage, the capacity charge and discharge voltage curves only showed a small decrease in capacity.

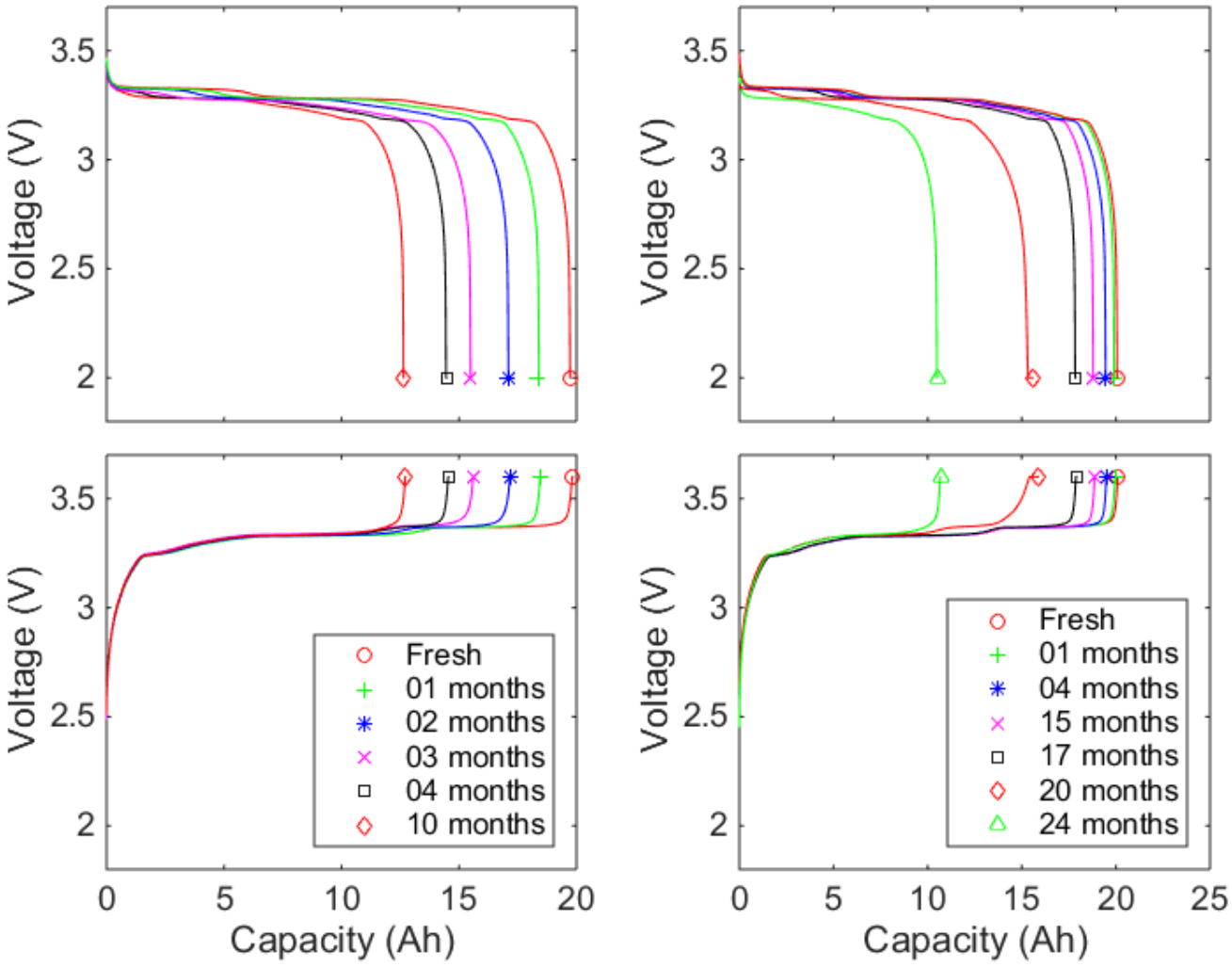

Figure 16: Charge and discharge curves over aging period for cells stored at 100% SOC and 60ºC, shifted to 35ºC after three months of storage (left), and cells stored at 100% SOC 35ºC, shifted to 50ºC after 15 months (right)

In order to determine the impact that storage has on cell degradation certain cells were shifted between storage temperatures. Cells initially stored at the most severe condition of 60ºC, were shifted to 35ºC, and cells initially stored at 35ºC were shifted to the 50ºC storage chamber. The reason the cells were shifted to a slightly lower temperature than 60ºC, was due to the fact that it was already known what would happen at that temperature so the goal of the test was to see if the same phenomena would occur at a slightly lower temperature condition.

The charge/discharge curves yielded results that cells, initially stored at harsher temperature conditions, can have their cell life extended by shifting them to a lower temperature condition. The severity of the degradation occurring under the initial storage conditions within the cells, though, leads to continued decline of the cell capacity and the cell reaching its EOL prematurely.

In response to the high degradation being observed at the 60ºC condition, a third temperature condition was established for testing. Cells were stored at 50ºC and 100 SOC to see if a similar phenomenon would be observed. Figure 17 displays the charge and discharge curves of a cell stored at these conditions for 6 months.

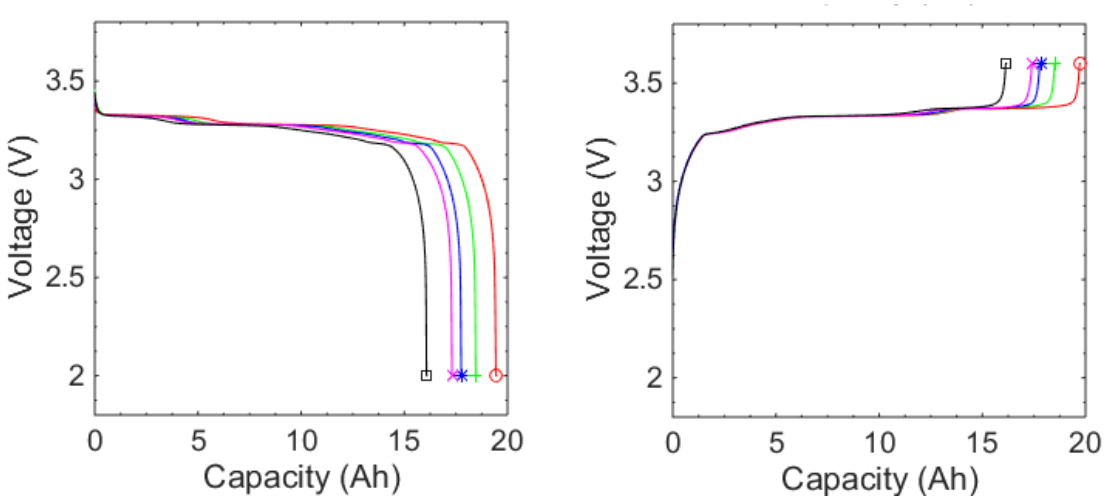

Figure 17: Charge and discharge curves over aging period for cells stored at 100% SOC and 50ºC

After 6 months of storage at this condition the cell had reached approximately 16 Ah. The degradation was not as severe as the 60ºC storage condition and the loss in capacity appears to be fairly similar between storage periods.

Cells initially stored at a lower temperature that are then shifted to a higher storage temperature (after a period of time) will experience an increased rate of degradation. This is to be expected, as the cells stored at 50ºC and 60ºC experienced higher degradation rates.

4.2.1.1 Remaining Capacity

In terms of percent capacity loss Figure 18 depicts the actual calculated capacity loss for the cells at each of the conditions. The capacity loss is given as a percentage of the remaining capacity of

the cell from its initial measured capacity. Capacity loss is calculated from using the rate capability test data for the discharge C-rate of C/20.

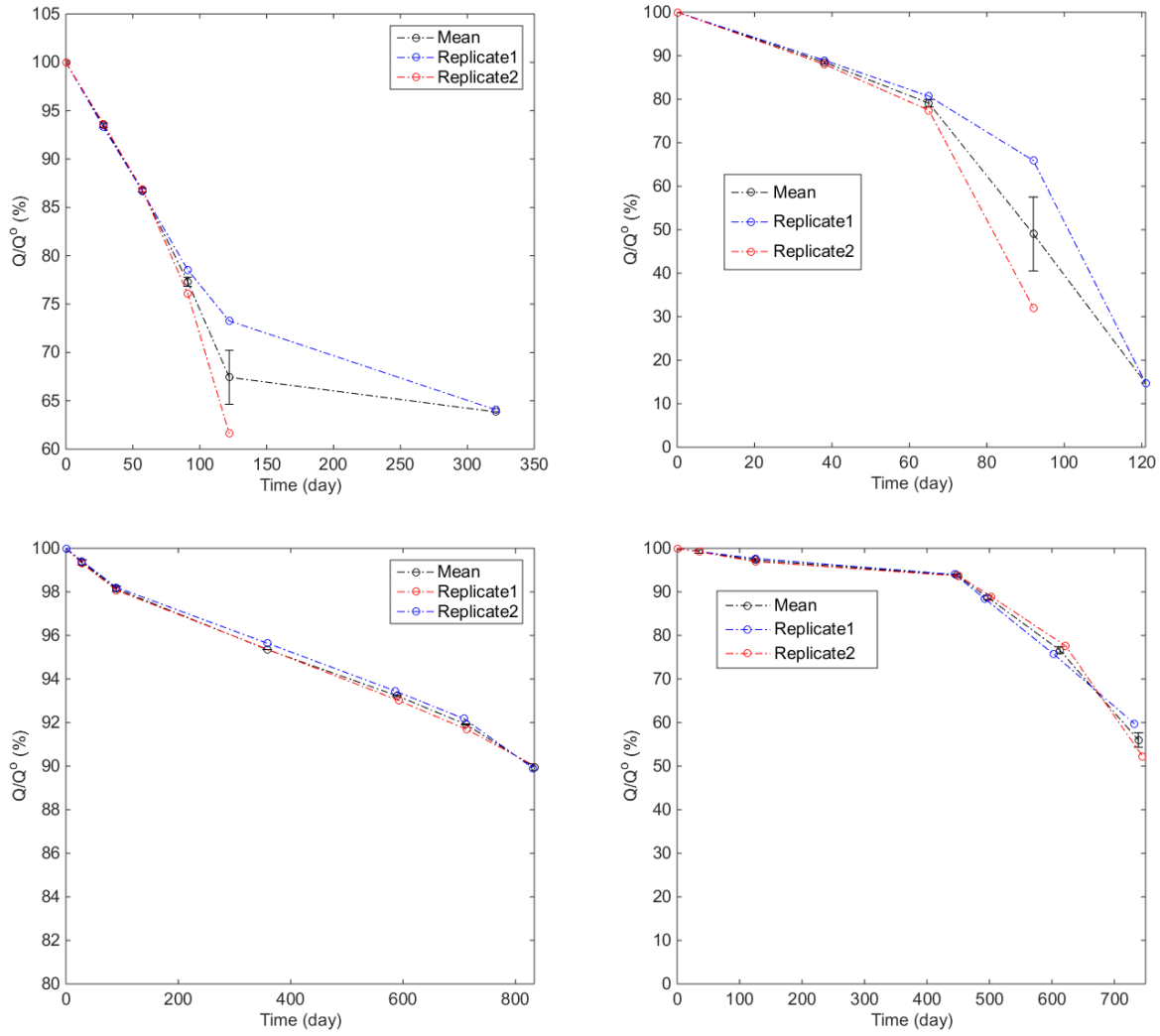

Figure 18: Capacity fades over time for different cell conditions; top left 60ºC 100%SOC shifted to 35ºC 100%SOC, top right 60ºC 100%SOC, bottom left 35ºC 100% SOC, and bottom right 35ºC 100% SOC shifted to 50ºC 100% SOC

Cells stored at higher temperature conditions experienced severe degradation, resulting in the end-of-life point for the cells to be reached prematurely. Cells stored at 60ºC and 100% SOC experienced almost 90% loss in capacity after only four months of storage, whereas cells stored at 35ºC only experienced just over 10% loss in capacity despite being stored for over two years.

Shifting the storage temperature conditions for the cells played an interesting role in cell degradation. Cells initially stored at 60ºC and then shifted to 35ºC experienced a decreased

degradation rate after the shift, increasing the longevity of the battery, but it was unsustainable. Storage of the cell at the initial high temperature condition caused irreversible and damaging degradation within the cells that resulted in much higher rates of capacity fade throughout its life than if the cells were simply stored at 35^{o}C. This makes understanding the history of storage for a cell important when considering its capacity fade.

Finally, the cells that underwent a shift to a higher storage temperature condition experienced higher capacity fade and the cells reach their EOL point faster than if they had been kept at the initial conditions.

4.2.1.2 Loss of Capacity due to Reversible and Irreversible reactions:

Under OCP conditions lithium-ion batteries will experience a reduction in state-of-charge due to the transfer of cyclable lithium ions from the anode to the cathode, or loss of them from side reactions occurring within the cell. The former process is a reversible one with the lost capacity being able to be recovered after subsequent cycling, the latter, however, is permanent and the capacity cannot be recovered from further cycling of the cell.

In order to determine the reversible and irreversible capacity loss, at each storage point, the following protocol was put into place to establish how each should be calculated. Using the data from the self-discharge test, the capacity at the end of the CC-CV discharge for both the first and second test cycles were subtracted from each other to obtain the reversible capacity loss. Irreversible capacity loss was obtained from the rate-capability tests, utilizing the ending capacity (CC-CV) at the C-rate of C/20 for the current storage point and the capacity for the previous storage point. Subtracting the two values yields the irreversible capacity loss. Using this protocol, the two variables can be tracked over the storage period to determine the effect of storage conditions on the capacity losses.

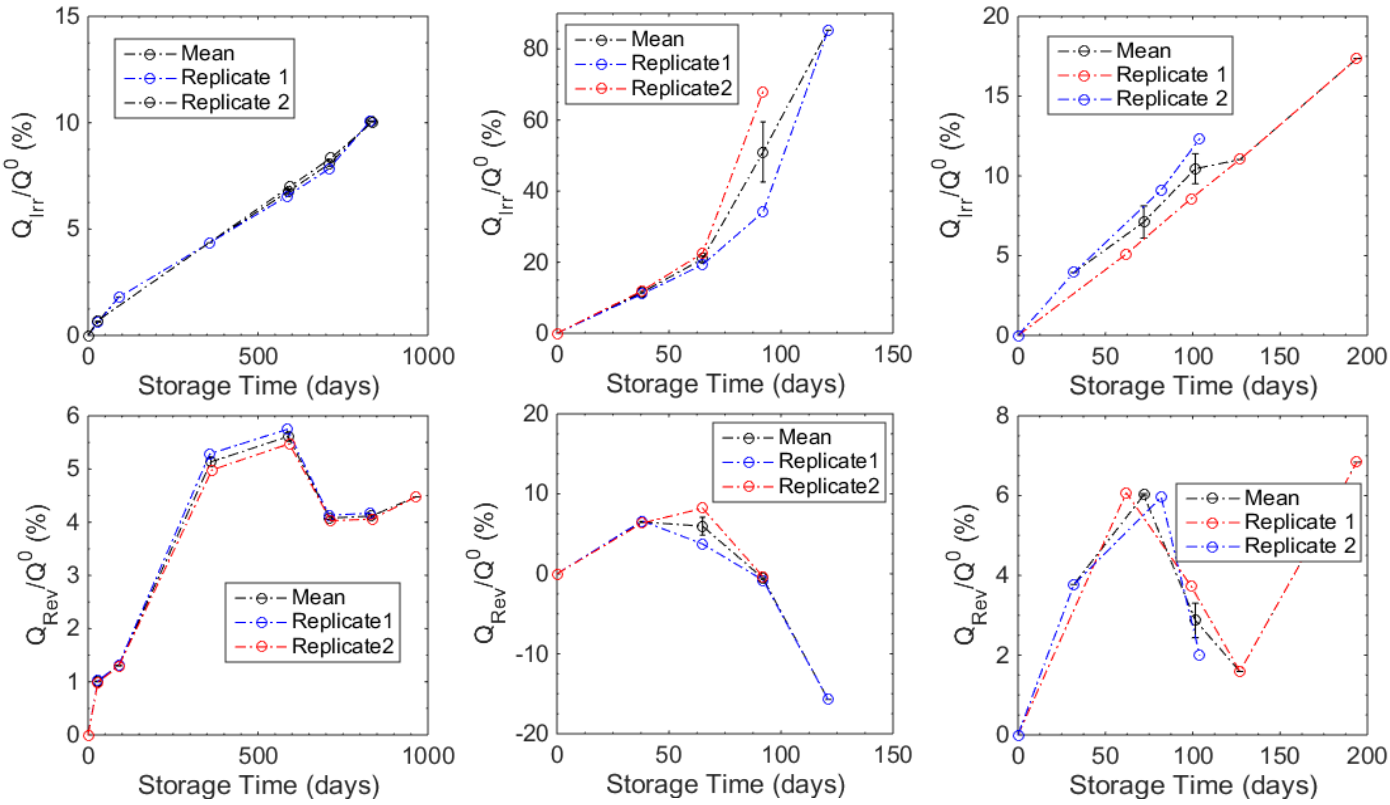

Figure 19: Irreversible capacity loss of cells stored at 35ºC and 100% SOC (top left), reversible capacity loss of cells stored at 35ºC and 100% SOC (bottom left), irreversible capacity loss of cells stored at 60ºC and 100% SOC (top center), reversible capacity loss of cells stored at 60ºC and 100% SOC (bottom center), and irreversible capacity loss of cells stored at 50ºC and 100% SOC (top right), reversible capacity loss of cells stored at 50ºC and 100% SOC (bottom right)

The graphs depicted in Figure 19 show the reversible and irreversible capacity losses for cells stored at 35ºC, 60ºC, and 50ºC respectively. The cells stored at the higher temperature conditions experienced much higher capacity losses in a much shorter period of time. This is to be expected as increased temperatures at high SOC will promote irreversible degradation reactions to occur at a faster rate.

The increased temperature storage condition, also, promoted the increase in the reversible capacity losses within the cell. After only one month of storage the reversible capacity losses for cells stored at 60ºC and 50ºC were approximately 7.5% and 6% respectively. Comparing to cells stored at 35ºC, they experienced a reversible capacity loss of only 1% (maximum reversible capacity loss for this condition only ended up being 5.5%). For cells stored at 35ºC and 50ºC the

reversible capacity losses occurring went through increases and decreases over the storage period, but remained positive. For cells stored at 60ºC, though, this was not the case.

In addition to the increase in the reversible capacity loss first experienced by the cells in the first month of storage, another interesting phenomenon that occurred was that the reversible capacity loss reached a maximum peak and then started to fall. Eventually the reversible capacity observed ended up going from a positive recapture of capacity to a negative irreversible loss. Storage of the cells at this condition caused such drastic degradation that after three months of storage, the cells no longer gained back capacity during the cycling test, but simply lost capacity.

The graphs depicted in Figure 20 show the reversible and irreversible capacity losses for cells stored at 60ºC shifted to 35ºC and 35ºC shifted to 50ºC. Shifting the cells from a higher temperature condition to a lower one does prevent the cell from failing immediately after a four month storage period (storage at 60ºC for three months). The rate of capacity loss decreased significantly when the cell was shifted to 35ºC, but the cell degradation caused from the storage at the higher temperature conditions prompted the cell to continue to degrade and reach cell failure. The initial storage of the cells at the high temperature condition leads to increased capacity fade, but can also promote further degradation from additional phenomenon. One of the two cells (seen in Figure 20) actually experienced the same rate of degradation as if it were still being stored at the 60ºC condition. The graph depicting the reversible capacity of these cells shows once again the storage at the initial condition can have some dramatically different effects on the capacity loss and is most likely dependent on the quality of manufacturing of the cell. One of the two cells experienced heightened reversible capacity loss leading up to its failure while the other cell experienced lower reversible capacity losses during storage. This more falls in line with the prediction that when shifted to a lower storage condition the extent of capacity loss should decrease.

On the opposite end, the cells that underwent a shift from 35ºC to 50ºC experienced very predictable results. Shifting the cells to a higher temperature condition led to higher rates of irreversible capacity loss cell failure. Also, the reversible capacity of the cell continued to increase with the duration of storage, until finally the cell was no longer able to recapture the lost capacity and only experienced irreversible capacity loss and ultimately cell failure.

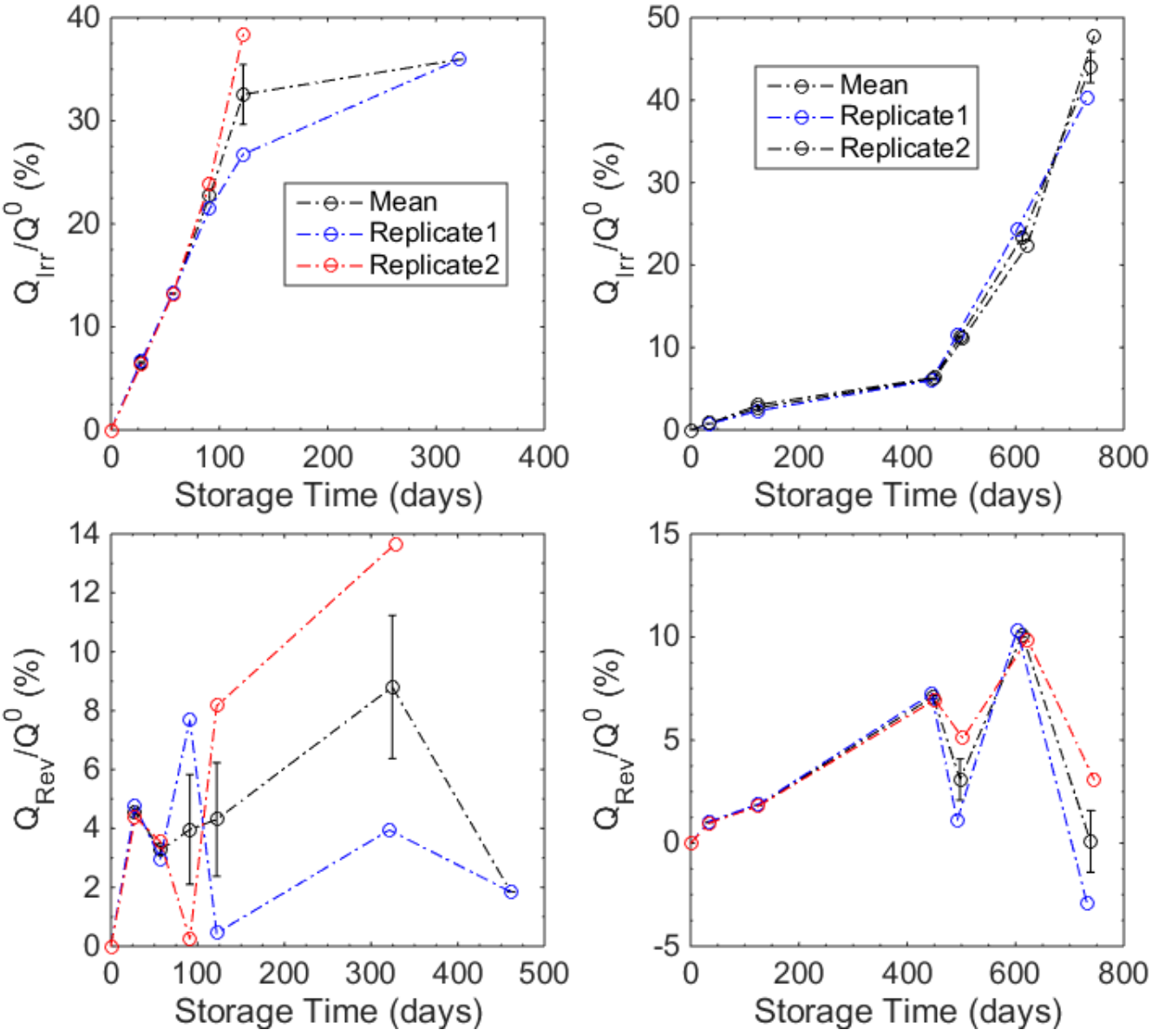

Figure 20: Irreversible capacity loss of cells stored at 60ºC shifted to 35ºC (top left), reversible capacity loss of cells stored at 60ºC shifted to 35ºC (bottom left), irreversible capacity loss of cells stored at 35ºC shifted to 50ºC (top right), reversible capacity loss of cells stored at 35ºC shifted to 50ºC (bottom right)

4.2.2 Comparison of capacity between cycles of battery tests

The storage of cells at different aging conditions prompted the loss of cyclable material and, potentially, active material loss, demonstrated through the loss of capacity in the cell. Prolonged storage at high temperatures eventually caused the cells to lose the capability to reclaim capacity lost reversibly. Thus, with repeated cycling the cell would instead lose capacity instead of regaining it. This was demonstrated in how the reversible capacity losses at each of the aging

points of the cells eventually become negative values for certain storage conditions. In order to further support this, the following section presents the final capacity values after certain cycles in the SD and RC tests.

In Figure 21 the capacities of the cells stored at 60°C and 100% SOC for the first, second, fifth, and last RC discharge are tracked over the storage periods.

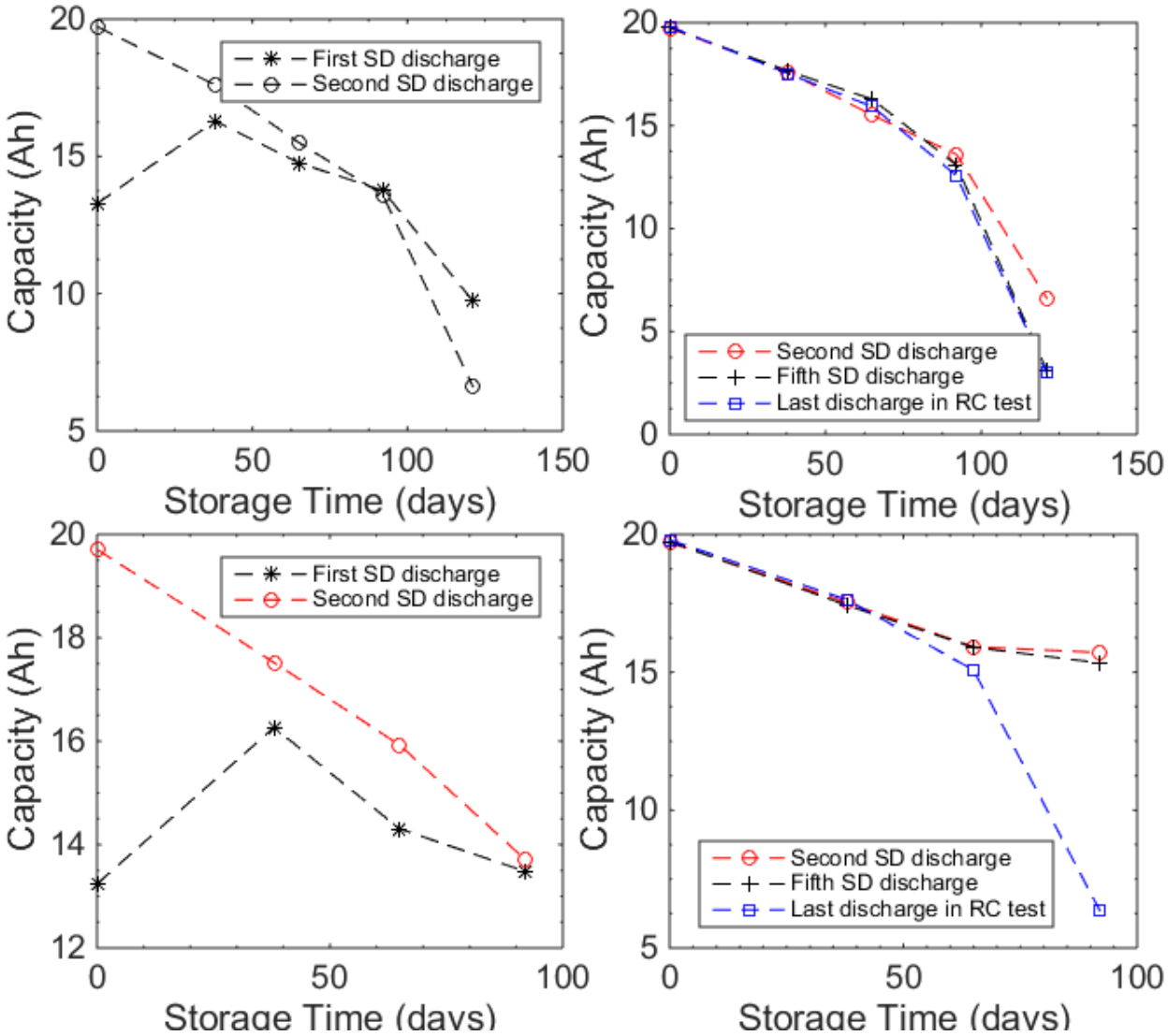

Figure 21: Loss of recapture of reversible capacity loss of cells stored at 60°C and 100% SOC

After a period of four months the cells can no longer gain capacity and undergo drastic cycling aging. At this point the cells have failed and can no longer be cycled safely. Once again, it is demonstrated that there is a possible phenomenon occurring at high temperature conditions that

is resulting in the cells losing their capability to retain or regain capacity and are instead undergoing drastic cycling aging after storage. This results in the cells reaching their EOL point at a much faster rate.

For cells stored at 35ºC and 100% SOC (Figure 22), the reversible capacity lost during storage is being reclaimed even with longer storage times at this temperature condition. The drastic degradation that occurred at 60ºC is not seen in these cells and the capacity can continue to be recaptured with cycling. As seen in the figure, though, there is a decrease in the amount of reversible capacity being gained after an extended storage period. This is most likely due to the irreversible losses in capacity occurring affecting the amount of potential reversible capacity losses that can occur.

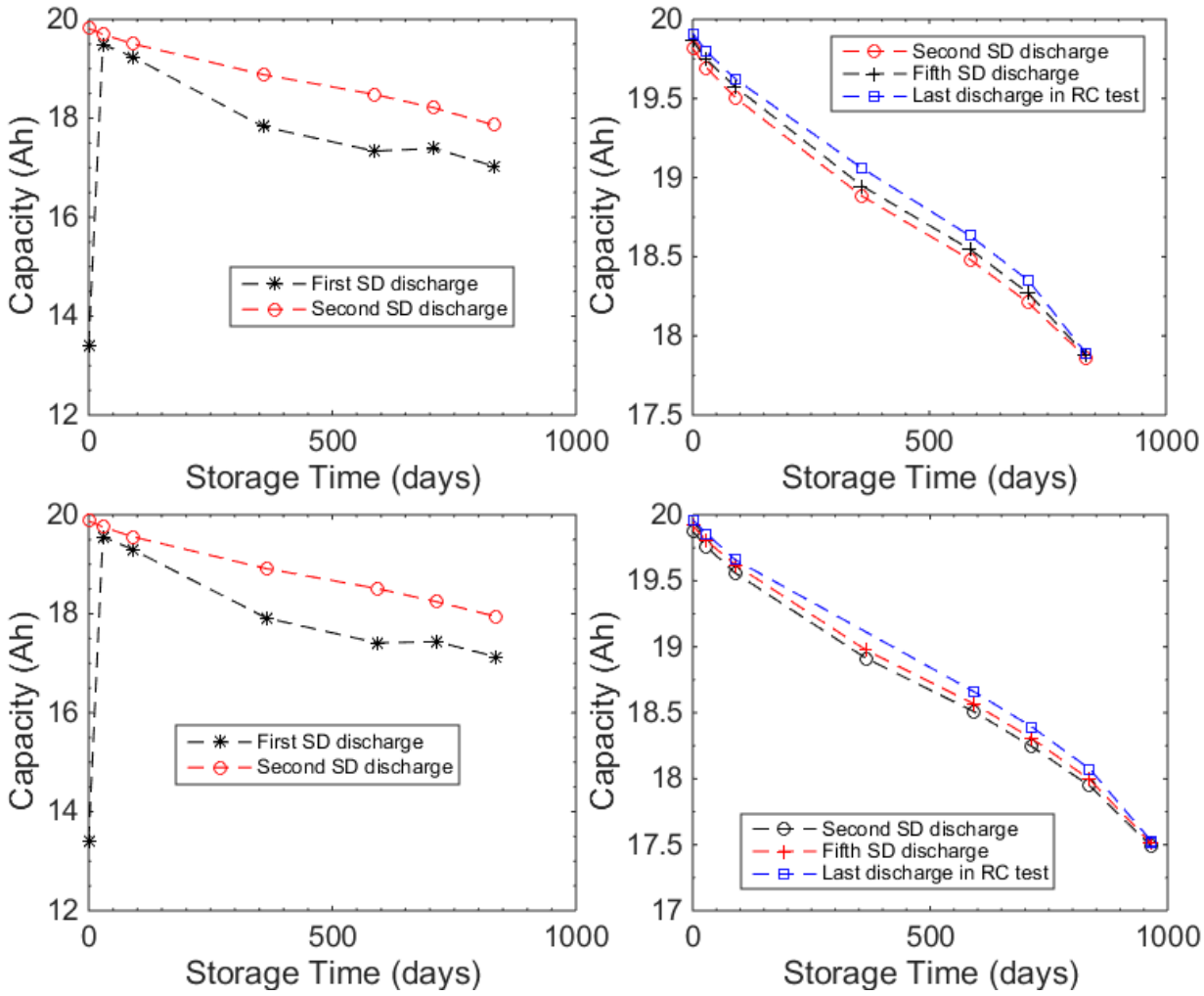

Figure 22: Gain of reversible capacity through cycling of cells, for cells stored at 35ºC and 100% SOC

Cells stored at 50ºC and 100% SOC (Figure 23) were able to recover reversible capacity loss with cycling over their entire lifespan, unlike their 60ºC counterparts. Towards the end of cycling, though, it can be seen that on the final cycle of testing, after being stored for almost 200 days, the cell started to experience capacity loss during cycling. The aging phenomena that occurred at 60ºC, may be demonstrated by this final data collection. It takes almost twice as long for it to occur, though, and the cell has already almost reached its EOL point.

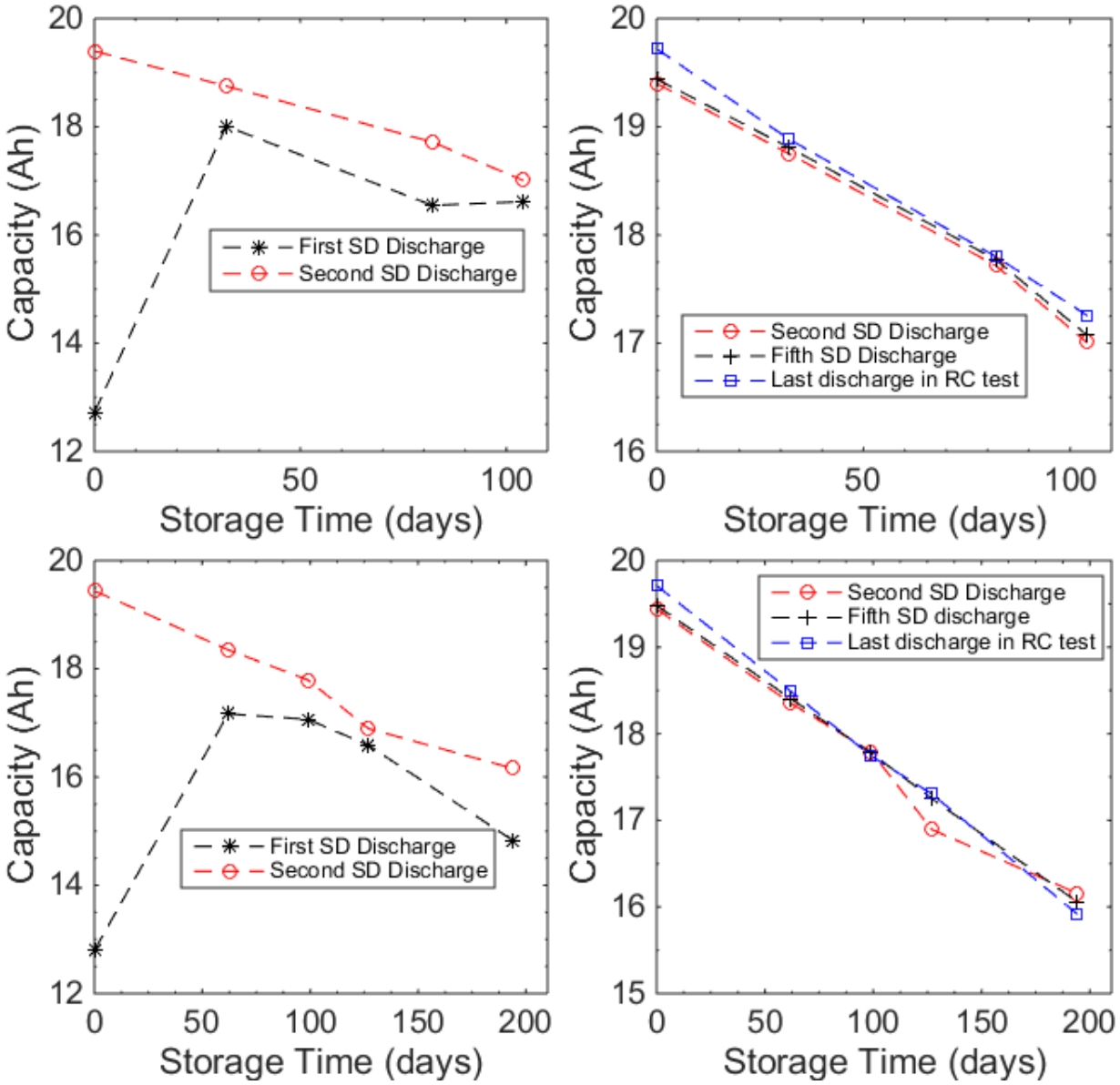

Figure 23: Gain of reversible capacity through cycling of cells, for cells stored at 50ºC and 100% SOC

Cells stored at 35ºC and 100% SOC and shifted to 50ºC and 100% SOC experienced increases in reversible capacity loss and then recapture upon cycling when shifting to 50ºC. Figure 24 depicts the capacities of the cells at these conditions, over their respective storage periods.

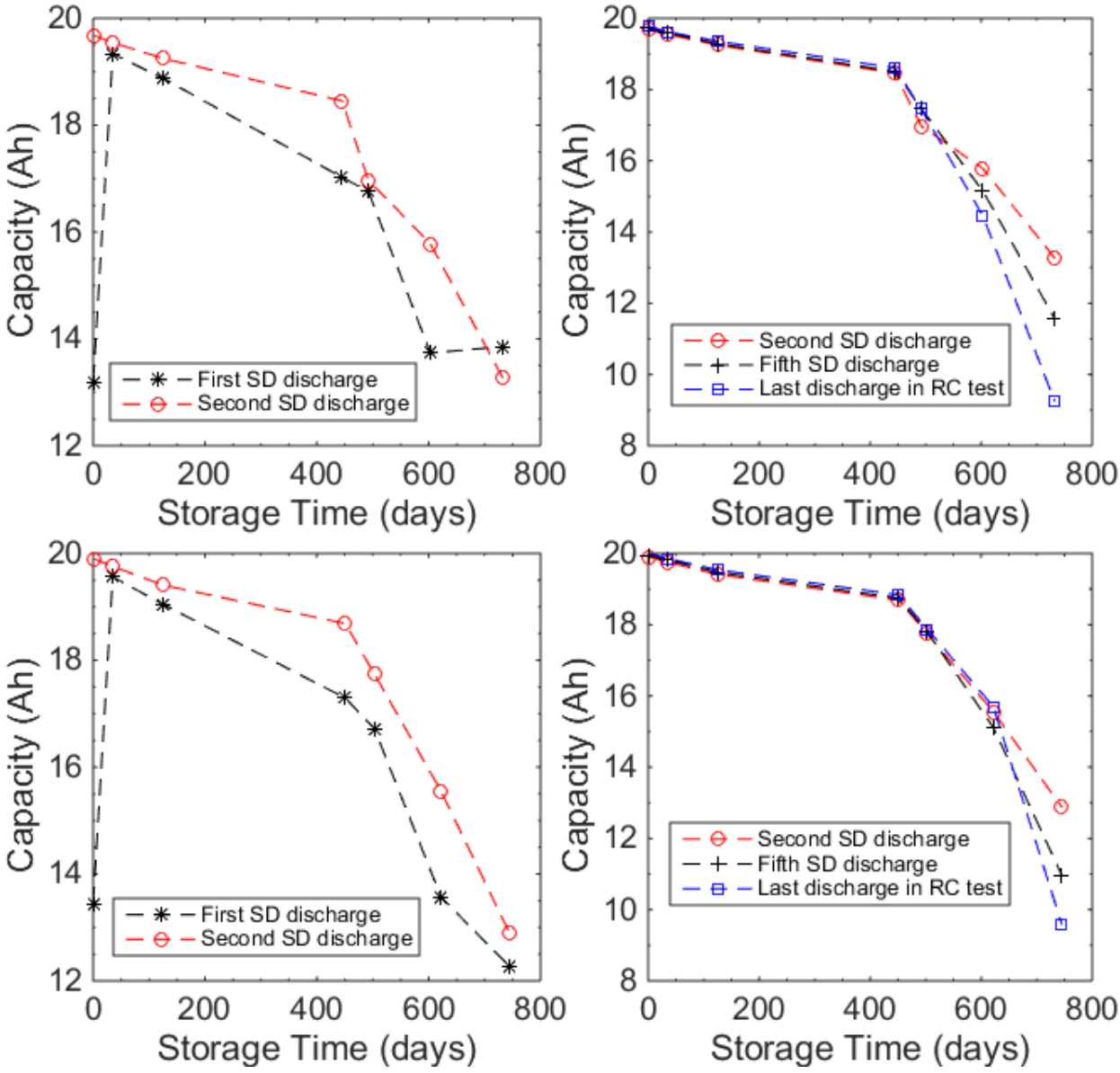

Figure 24: Decrease in recapture of reversible capacity loss of cells stored at 35ºC and 100% SOC shifted to 50ºC and 100% SOC

Continual storage at 50ºC, though, eventually led to the cells experiencing degradation in accordance with cells stored at 60ºC. Cycling of the cells after storage began to simply experience capacity fade. Up until the cells reached their EOL point they were able to gain back

some initial capacity, but further cycling ended up causing further degradation and the cell was no longer able to be cycled.

Finally analysis of the capacity for cells stored at 60ºC and 100% SOC shifted to 35ºC and 100% SOC (Figure 25) found that the cells were able to regain some capacity lost over their storage periods, but the initial storage of the cell at 60ºC had a lasting impact on the cell life.

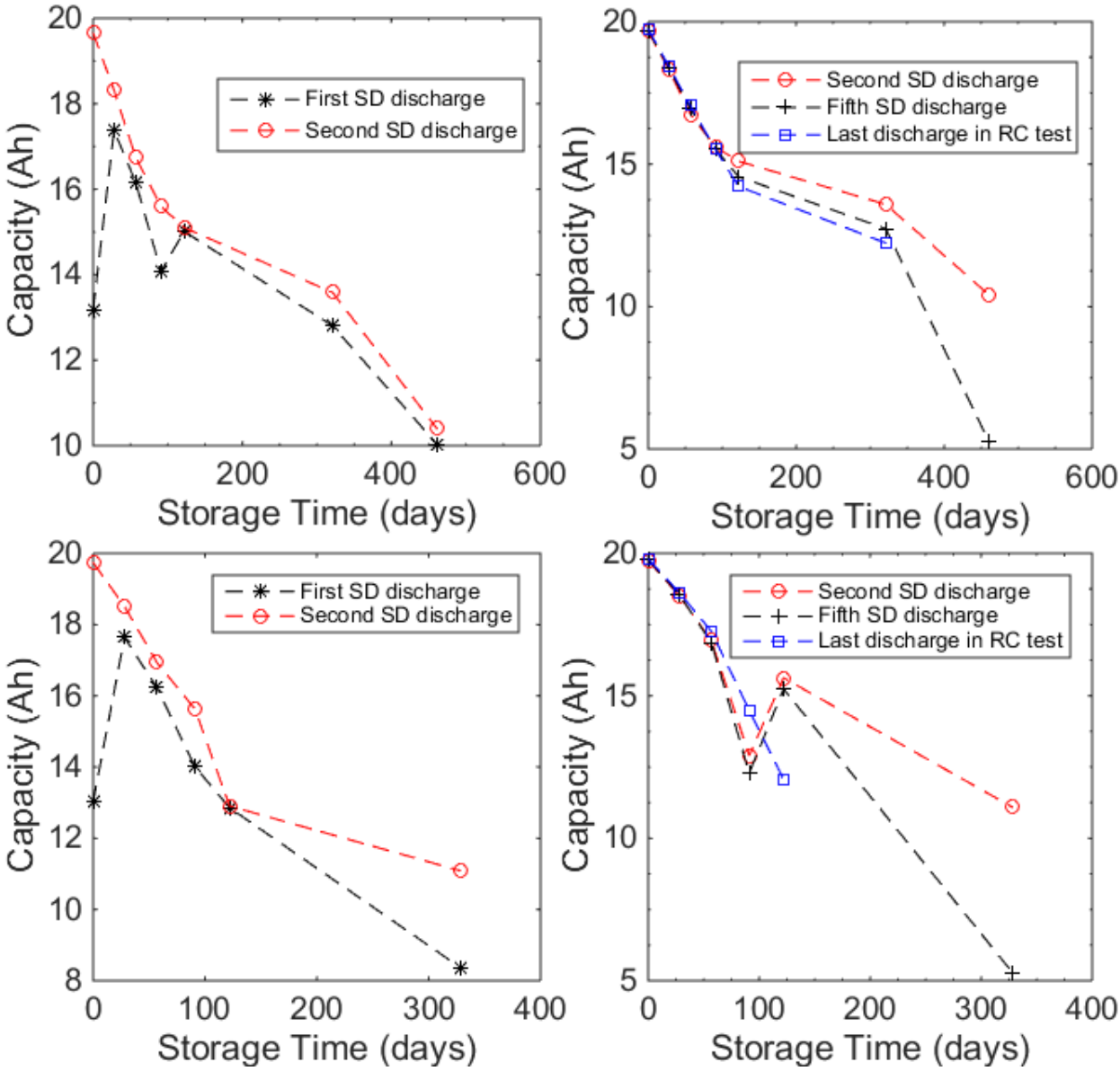

Figure 25: Loss of recapture of reversible capacity loss of cells stored at 60ºC and 100% SOC shifted to 35ºC and 100% SOC

As it can be seen in Figure 25, even after the cells have changed storage conditions (occurring at approximately 90 days) the capacity within the cells continues to decline with cycling. The degradation that has occurred within the cell has affected its continual performance, and although storing it at a less severe temperature condition can prolong its life, the cell ultimately fails.

4.2.3 Incremental Voltage Analysis, Differential Voltage Capacity Curves:

In addition to analysis of capacity fade, incremental voltage analyses of cells during aging can be completed, which involves computing the differential voltage capacity (dV/dQ) for the cells at each of their aging points. Various pieces of information regarding the degradation of the cell can be derived over the aging period. Based on previous studies performed on the aging of lithium-ion batteries, the plots of dV/dQ versus Capacity will be able to yield the degree to which the cell undergoes loss of cyclable lithium and whether or not there is the presence of active material loss occurring within the cell.

In each of the figures, the total cell capacity is divided into 3 regions (denoted as regions A, B, and C) with the corresponding capacities in each region being calculated by measuring the distance in between distinct peaks in the dV/dQ versus Capacity curve. For a fresh cell the notation is given as Q_{0A}, Q_{0B}, and Q_{0C}. Using the initial capacity in each of the regions, comparisons can be made between the capacities for these regions at all aging points over the storage life of the cell.

For the cells stored at the condition in Figure 26 there was very little change in sections B and C of the dV/dQ versus capacity curve. Q_A did undergo minor decreases with aging time, which denotes a loss of cyclable lithium content within the cell, however, since there was no visible decrease in the value of Q_B or Q_C over the aging time it can be concluded that there was not a large degree of loss of active material at the negative electrode. As this is the lowest storage temperature condition the rate of degradation is much less than that of the cells stored at higher temperatures. Thus, it is understandable that only cyclable lithium loss occurred.

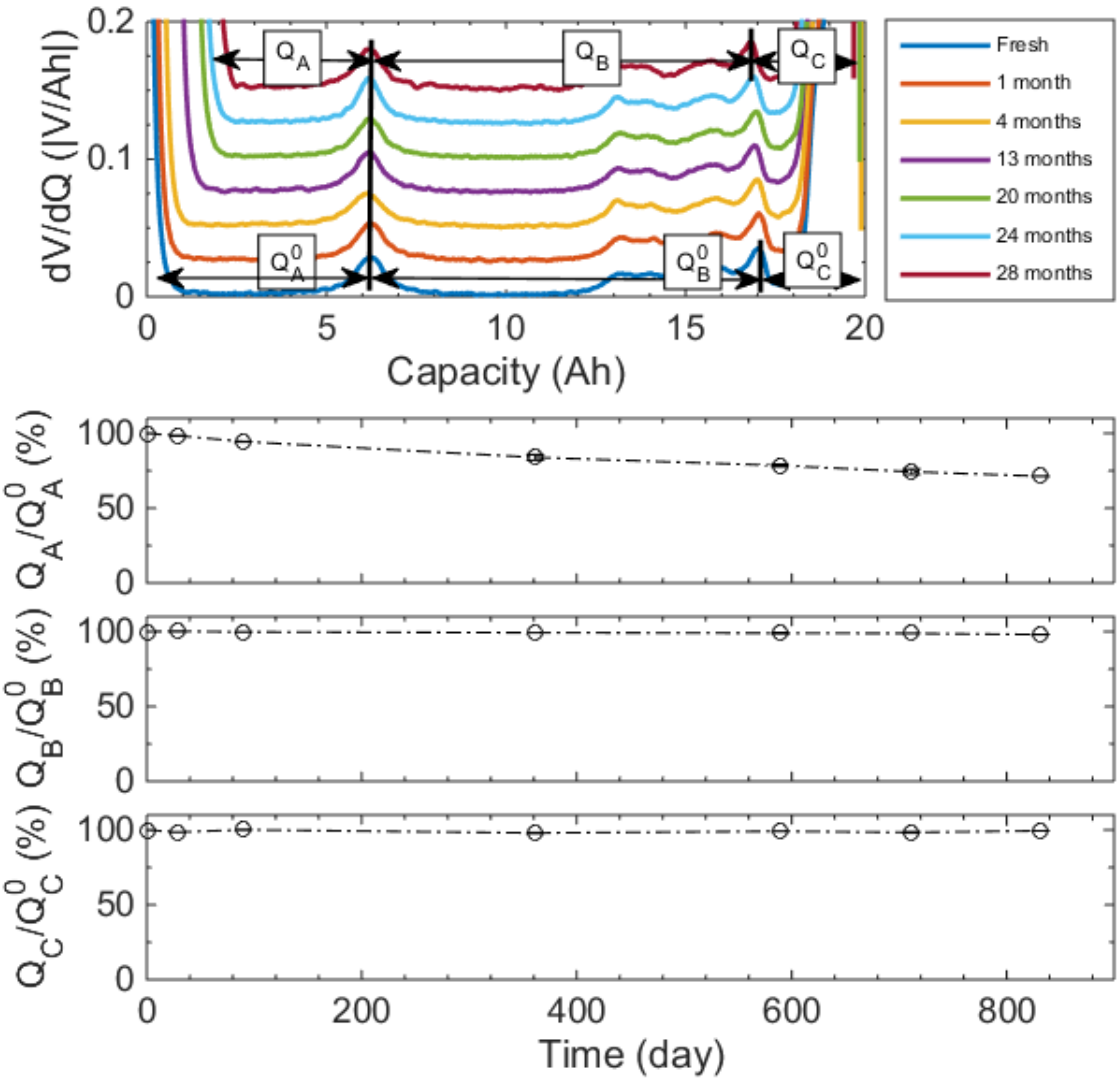

Figure 26: Discharge dV/dQ curve at a rate of C/20 for cells stored at 35ºC and 100% SOC

For the cells stored at the condition in Figure 27 the capacity in sections A and B, of the dV/dQ versus capacity curve, displayed drastic decline. The severe storage condition resulted in both the drastic loss of cyclable lithium content within the cell (seen by the decrease in Q_A) and a large degree of loss of active material at the negative electrode (seen by the decrease in Q_B). Reasons for the loss of active material can stem from possible dissolution of the active material into the electrolyte [9], or that the SEI layer had become so thick that the active material became electrochemically inactive at the carbon negative electrode. [8] After three months of storage at these conditions, the number of visible peaks dropped demonstrating that there were now fewer phase transitions in the cell.

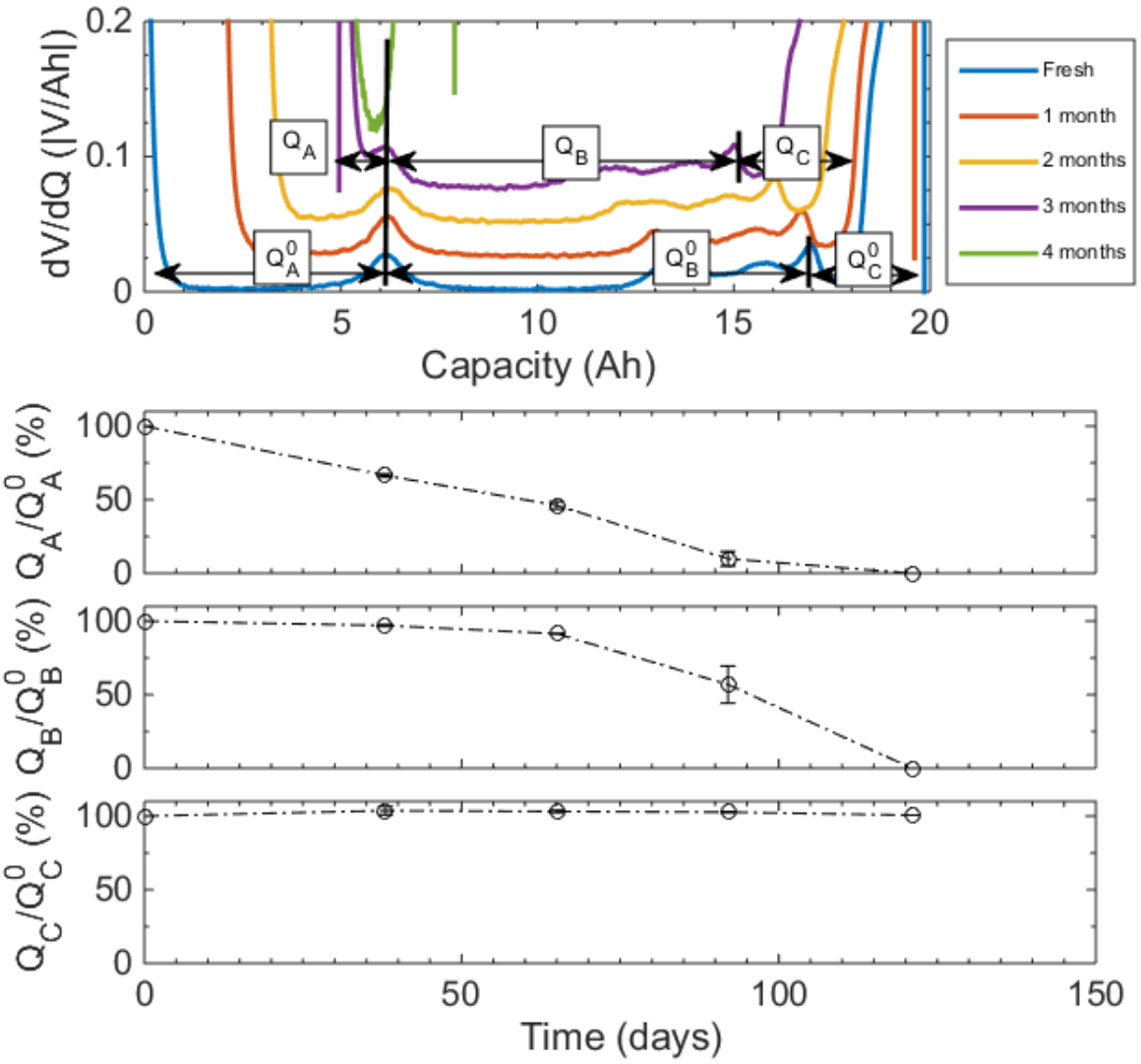

Figure 27: Discharge dV/dQ curve at a rate of C/20 for cells stored at 60ºC and 100% SOC

As this is the highest storage temperature condition the rate of degradation is increased and the presence of large concentrations of lithium intercalated into the anode increases the rate at which degradative side reactions can occur. Thus, it is not surprising to see the degree of degradation that had occurred.

Figure 28 depicts the differential voltage capacity curves for the cells stored at 50ºC and 100% SOC. After the 6 months of storage the intercalation phase transitions were still maintained in the cell. There was a decrease in Q_A and Q_B over the life of the cell depicting both a loss in cyclable lithium, as well as active material loss occurring at the anode. The losses in Q_A are much greater than the losses in Q_B, which means that the primary aging phenomena in the cell are losses of

cyclable lithium. As there is only a slight decrease in Q_B over time active material loss is not a major degradation mode at this temperature condition for this length of storage time.

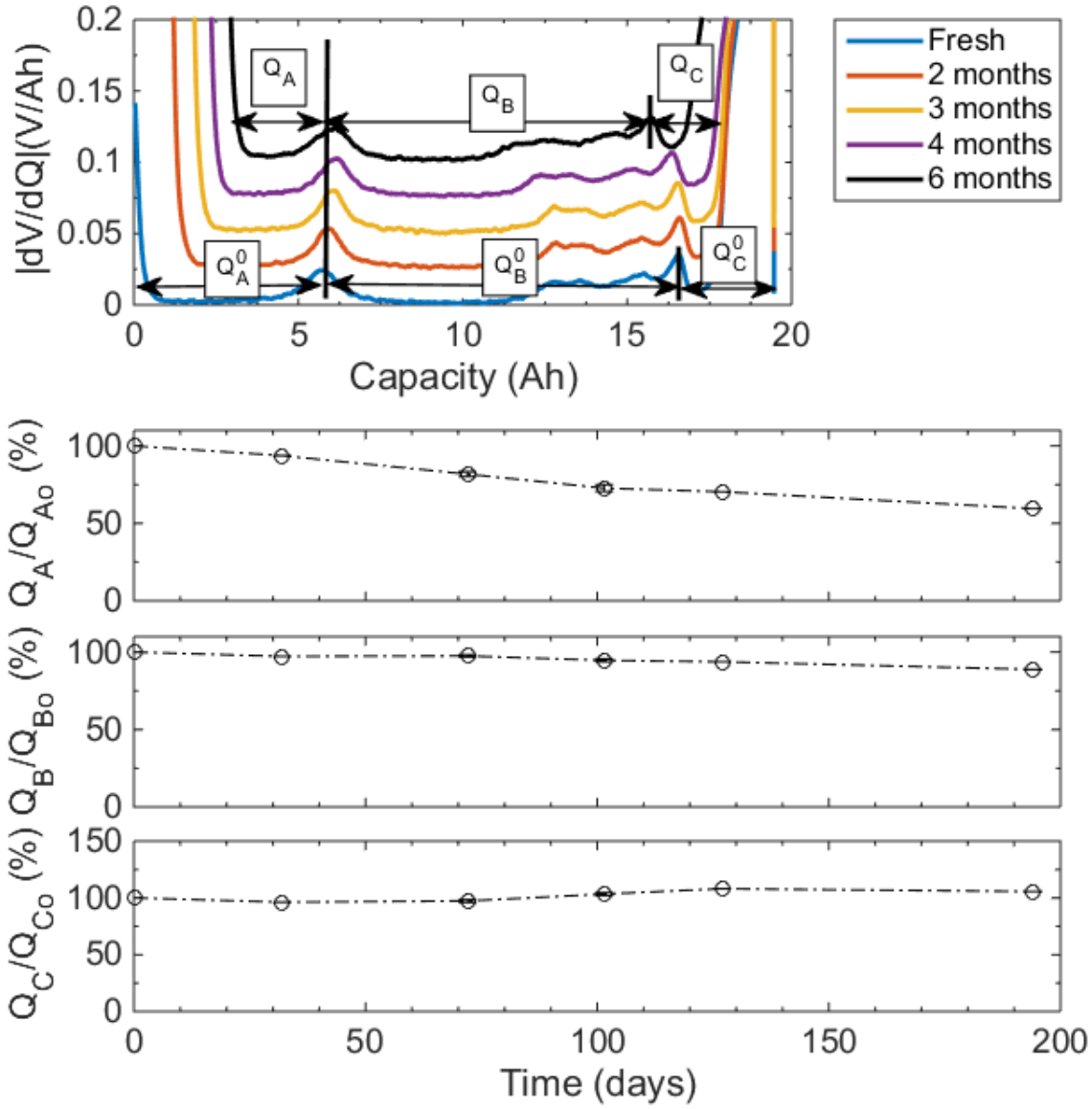

Figure 28: Discharge dV/dQ curve at a rate of C/20 for cells stored at 50ºC and 100% SOC

The active material loss was not as drastic as the losses observed by cells stored at 60ºC, but it can be postulated that this is the most likely reason for the loss in reversible capacity in these cells. The extreme active material losses occurring at the anode are causing the cells to be unable to regain capacity, and if the cells depicted in Figure 28 had continued to be stored at 50ºC they, possibly, may have demonstrated the same losses.

For the cells stored at the condition in Figure 29 the capacity in sections A and B, of the dV/dQ versus capacity curve, displayed a similar decline to that of the graphs in Figure 27. The severe storage condition resulted in both the drastic loss of cyclable lithium content within the cell (seen by the decrease in Q_A) and loss of active material at the negative electrode (seen by the decrease in Q_B). The storage of the cell at the highest storage temperature condition caused the initial decrease in Q_A and Q_B, but after the cell had shifted conditions to the lowest storage temperature the rate of degradation levelled off.

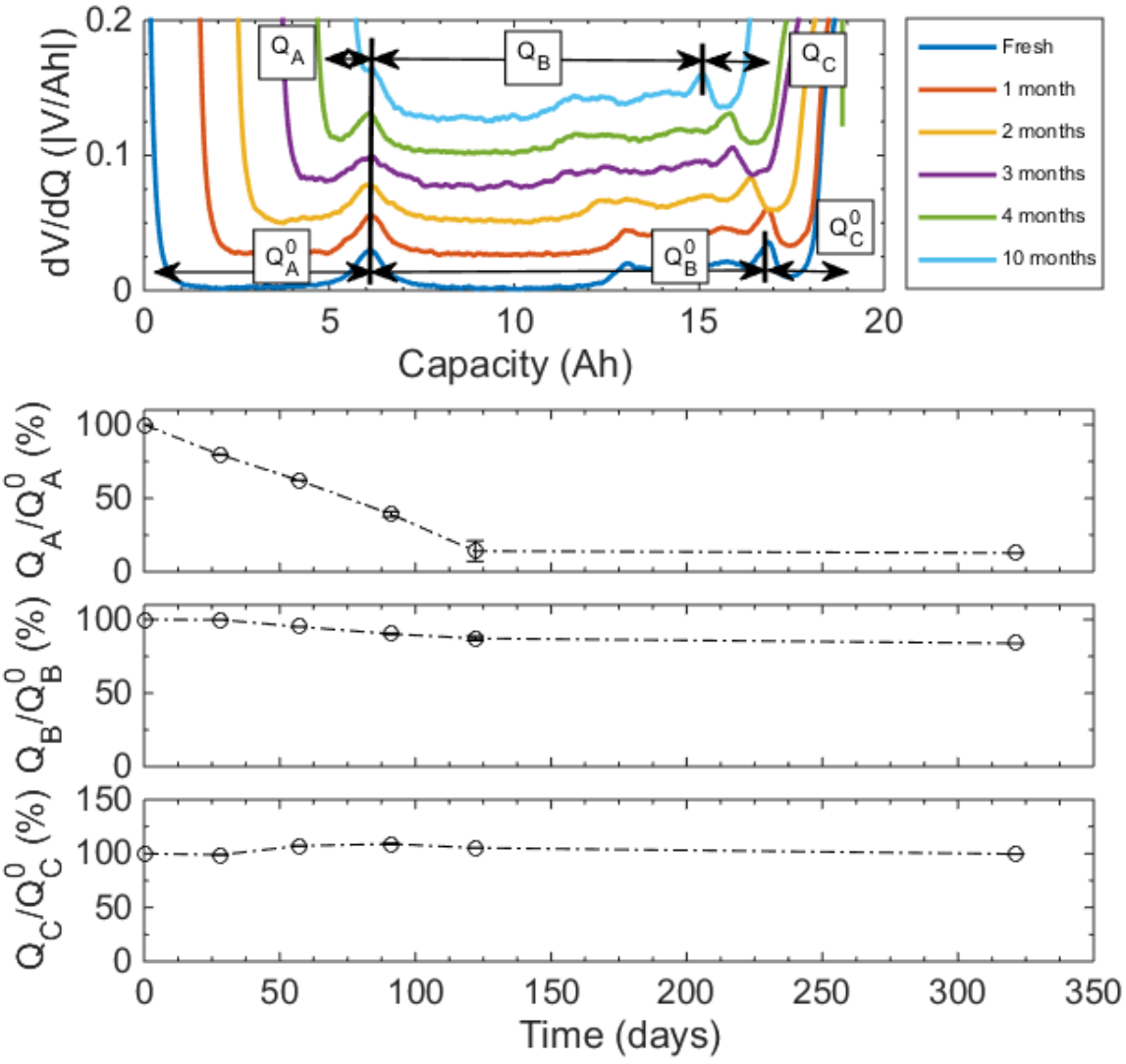

Figure 29: Discharge dV/dQ curve at a rate of C/20 for cells stored at 60ºC and 100% SOC for three months and then shifted to 35ºC and 100% SOC

For the cells stored at the condition in Figure 30 there was very little change in the capacity of sections B and C over the time the cell was stored at 35ºC and 100% SOC. Once the cell storage condition was changed to 50ºC, though, Q_B displayed a small decrease in size, demonstrating the loss of active material at higher temperatures.

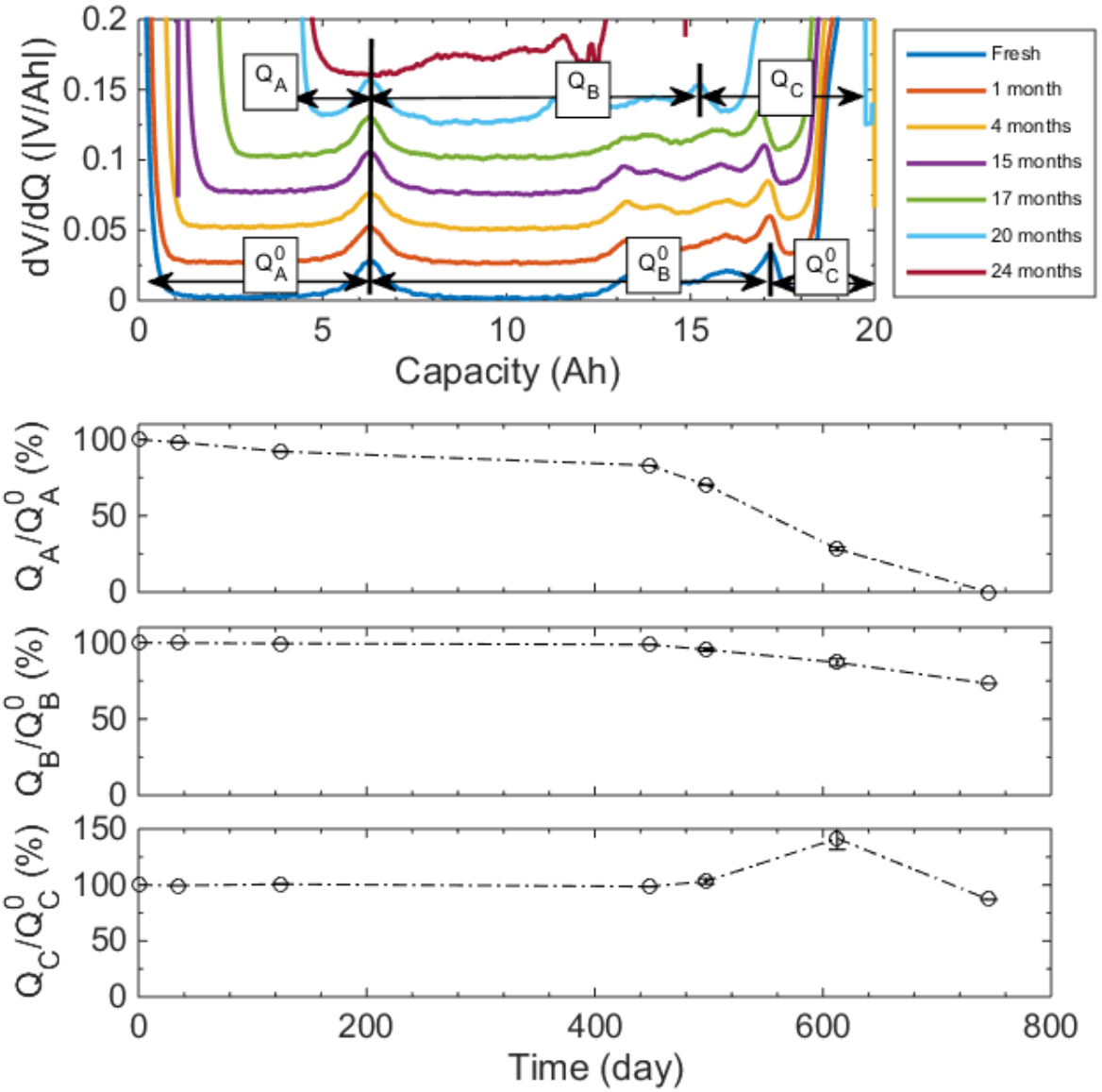

Figure 30: Discharge dV/dQ curve at a rate of C/20 for cells stored at 35ºC and 100% SOC for after 15 months of storage and then shifted to50ºC and 100% SOC

Q_A once again displayed minor changes in value at the 35ºC aging condition, but when shifted to the 50ºC storage condition there was a significant drop in the value of Q_A. Thus, the shift to

higher temperature conditions prompted a much greater degradation of the cell, resulting in larger losses of cyclable lithium. In addition, after 24 months of storage, the number of visible peaks decreased and there were now fewer phase transitions occurring within the cell. This is indicative of active material loss occurring within the cell.

4.3 Analyzing cells stored at 0% SOC at different temperatures

4.3.1 Capacity Fade:

As with the cells stored at 100% SOC, capacity losses occurring within the cells stored at fully discharged conditions (0% SOC) were tracked over their storage periods. Figure 31 shows the charge and discharge profiles of 4 different cells stored at 60°C and (a) a fully discharged state (SOC_{nom} 0%), and (b) a fully charged state (SOC_{nom} 100%) and then shifted to a fully discharged state after three months. The charge/discharge curves depicted in the figures in this section were achieved by cycling the cell at a C-rate of $C_{nom}/20$ and T = 25°C.

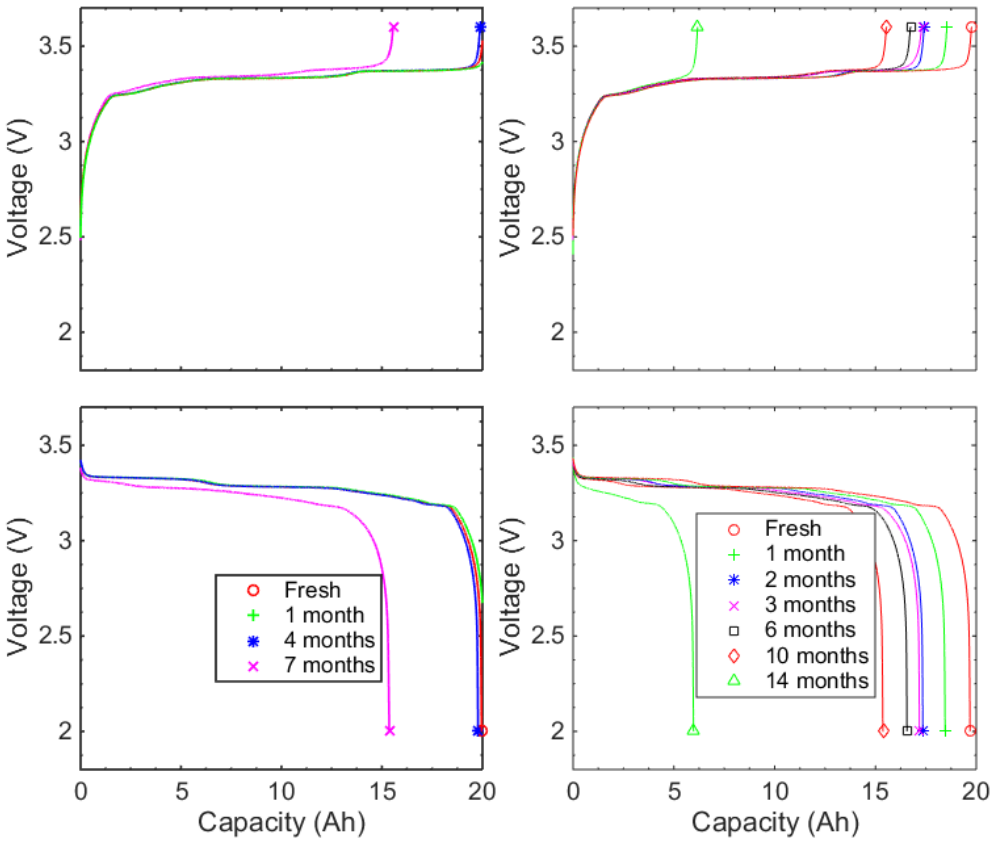

Figure 31: Charge and discharge curves over aging period for cells stored at 0% SOC and 60°C (left), and cells stored at 100% SOC 60°C, shifted to 0% SOC and 60°C after 3 months (right)

As seen with the cells stored at 100% SOC and 60ºC, there is accelerated capacity loss occurring within cells stored at 0% SOC and 60ºC. Although this loss is not as prominent as depicted in the fully charged cells, after only a small period of storage the cells had reached their EOL and could no longer be cycled safely. This severe degradation was not seen, though, in the cells initially stored at a fully charged state and then shifted to being stored at a fully discharged state. Although there is a visible decline in the capacity it is not as drastic with the cell being able to sustain storage at 60ºC for 14 months.

4.3.1.1 Percentage Capacity Loss

In terms of percent capacity loss the following graphs depict the actual calculated capacity loss for the cells at each of the conditions. Capacity loss is calculated from using the rate capability test data for the discharge C-rate of C/20.

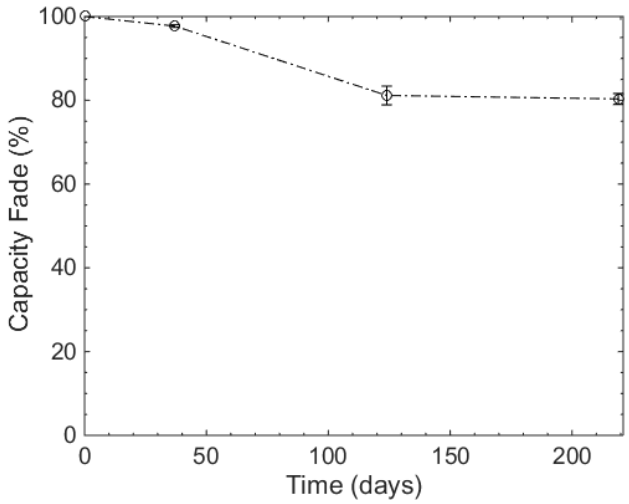

Figure 32: Percent remaining capacity of cells stored at 60ºC and 0% SOC

Figure 32 depicts the percent remaining capacity of cells stored at 60ºC and 0% SOC. After approximately seven months of storage, cells stored at discharged conditions experienced a capacity fade of approximately 20%. It should be noted, though, that only two cells stored at these conditions were able to reach the seven month storage point. A majority of the cells were unable to withstand the conditions for four months, or even one month in some cases. This is why there is a high standard error at the four month period.

Other cells, which experienced a shift in their storage conditions, were able to survive in these conditions for much longer periods. Figure 33 and Figure 34 depict remaining capacity curves for cells that experienced a change in storage conditions.

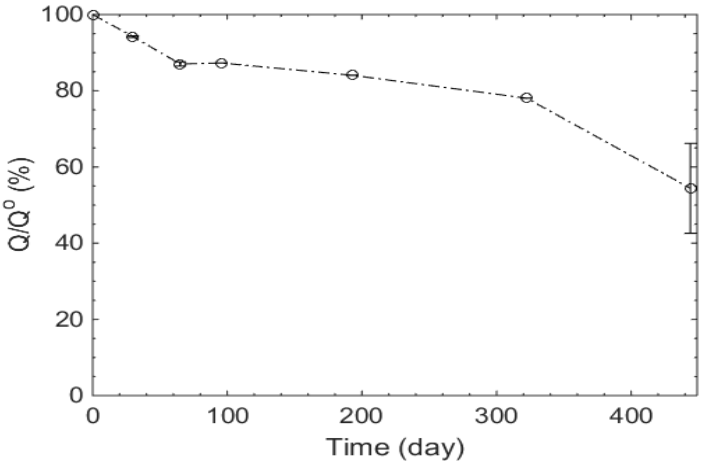

Figure 33: Percent remaining capacity of cells stored at 60ºC and 100% SOC for three months, shifted to 60ºC and 0% SOC

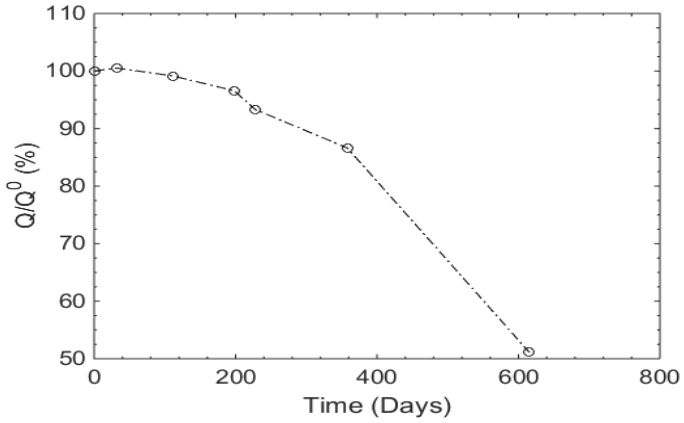

Figure 34: Percent remaining capacity of cells stored at 60ºC and 0% SOC for seven months, shifted to 35ºC and 100% SOC

Cells in Figure 33 were initially stored at 60ºC and fully charged conditions. After three months they were shifted to fully discharged conditions. This shift halted the high rate of degradation that was taking place and in the cell at fully charged conditions. The rate of decline in capacity decreased significantly and the cell did not reach its EOL point until a much later storage time point.

Cells in Figure 34 were initially stored at 60ºC and 0% SOC. After seven months they were shifted to 35ºC and 100% SOC. Based on the figure, despite the rate of degradation being slowed the cell continued to degrade quite drastically throughout its storage period. Comparing to the figures generated for cell stored only at 35ºC and 100% SOC, the rate of decline in the cells is much more gradual. Initially storing the cells at 60ºC, though, caused severe degradation to the cell that persisted throughout its storage life.

Thus, it can be seen that storing the cells at 60ºC, whether they be fully charged or discharged, results in the acceleration of aging within the cells. Shifting the cells to a lower temperature condition will prolong the cell's life, but ultimately the damage done will further increase degradation. This makes understanding the history of the cells' operation and storage very important for the study of battery degradation.

In order to better understand the proliferation of this particular aging phenomenon, testing was completed at a third storage condition for fully discharged cells. The temperature of this chamber was set to 50ºC. Since, this aging phenomena is so pronounced at the 60ºC storage condition the goal was to see if the same aging would take place at a lower storage temperature. Figure 35 displays the remaining capacity for cell stored at 50ºC and 0% SOC.

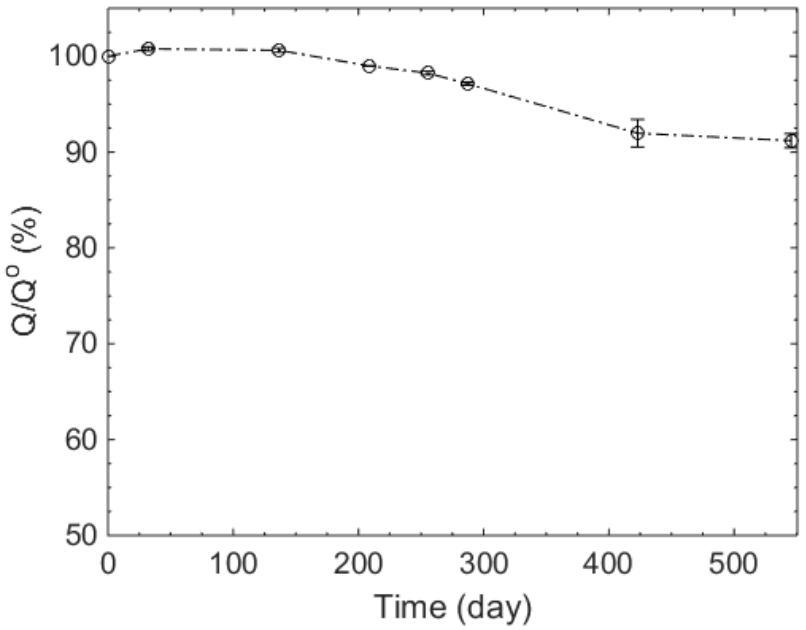

Figure 35: Remaining capacity of cells stored 50ºC and 0% SOC

At the time of writing this, cells in Figure 35 have been stored for approximately 16 months and have only lost approximately 10% of their capacity. Since they have not reached their EOL points they are still being stored under 50°C temperature conditions.

Despite the cells being stored for more than twice the amount of time than the cells stored at 60°C, the aging phenomenon seen in cells stored at 60°C was not observed. Initially, the cells showed an increase in capacity until the fourth month of storage. From there the cells experienced a steady slow loss in capacity over storage time, and not a sharp decline.

4.3.2 Incremental Voltage Analysis, Differential Voltage Capacity Curves:

The incremental capacity curve, depicted in Figure 36 presented a picture of the degradation that had occurred within the cell over its storage at 60°C and 0% SOC.

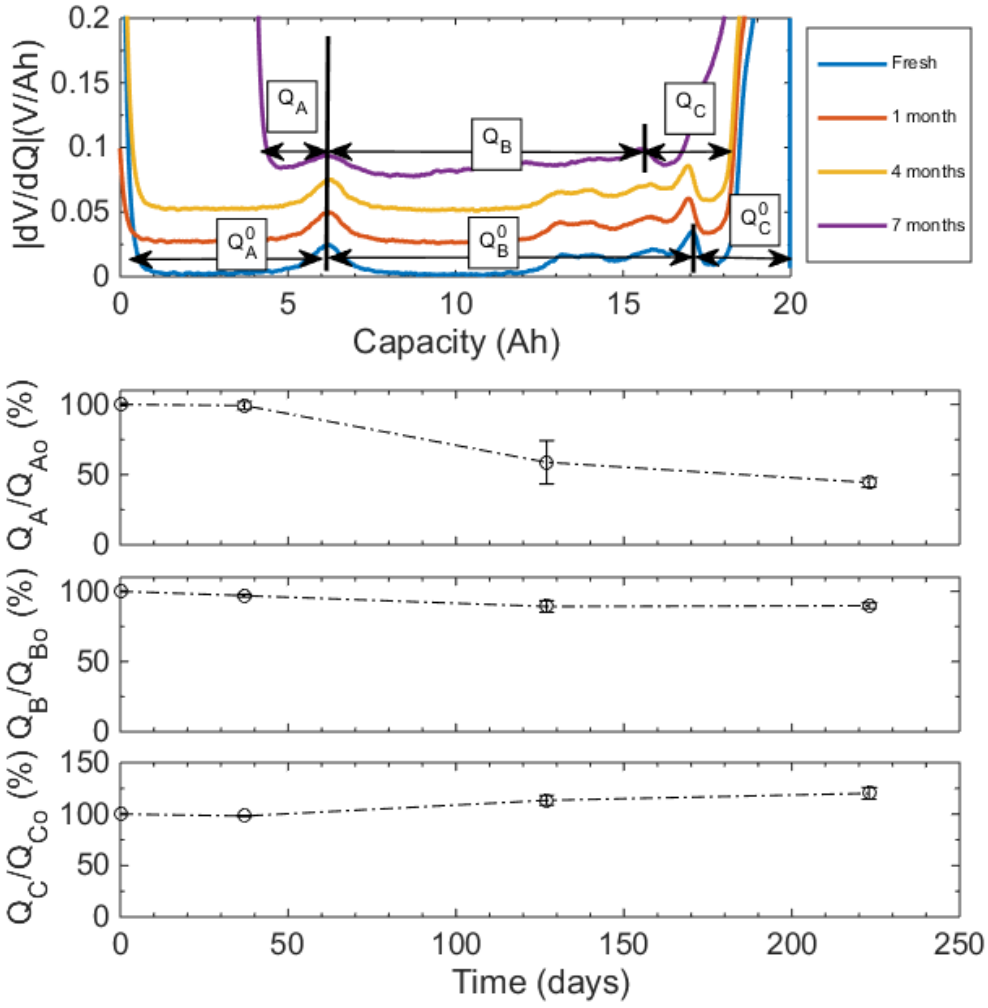

Figure 36: Discharge dV/dQ curve at a rate of C/20 for cells stored at 60°C and 0% SOC

Based on the figure, it can be noted that there was very little change in section C of the dV/dQ versus capacity curve. Q_A underwent a drastic decrease with aging time, denoting a severe loss of the cyclable lithium content within the cell. Q_B, also, experienced a decline representing a small loss of active material at the negative electrode. As there were still two peaks present, though, at the end of the testing for the cells the number of phase transitions for lithium intercalating into the graphite did not change.

The storage at 60^{o}C promotes the loss of active material within the cell at both charged and discharged conditions, and is most likely the reason for why these cells are reaching their respective EOLs prematurely. Cells stored at 50^{o}C and 0% SOC did not demonstrate this active material loss. Figure 37 displays the differential voltage capacity curves of the degradation that had occurred within the cell over its storage at 50^{o}C and 0% SOC.

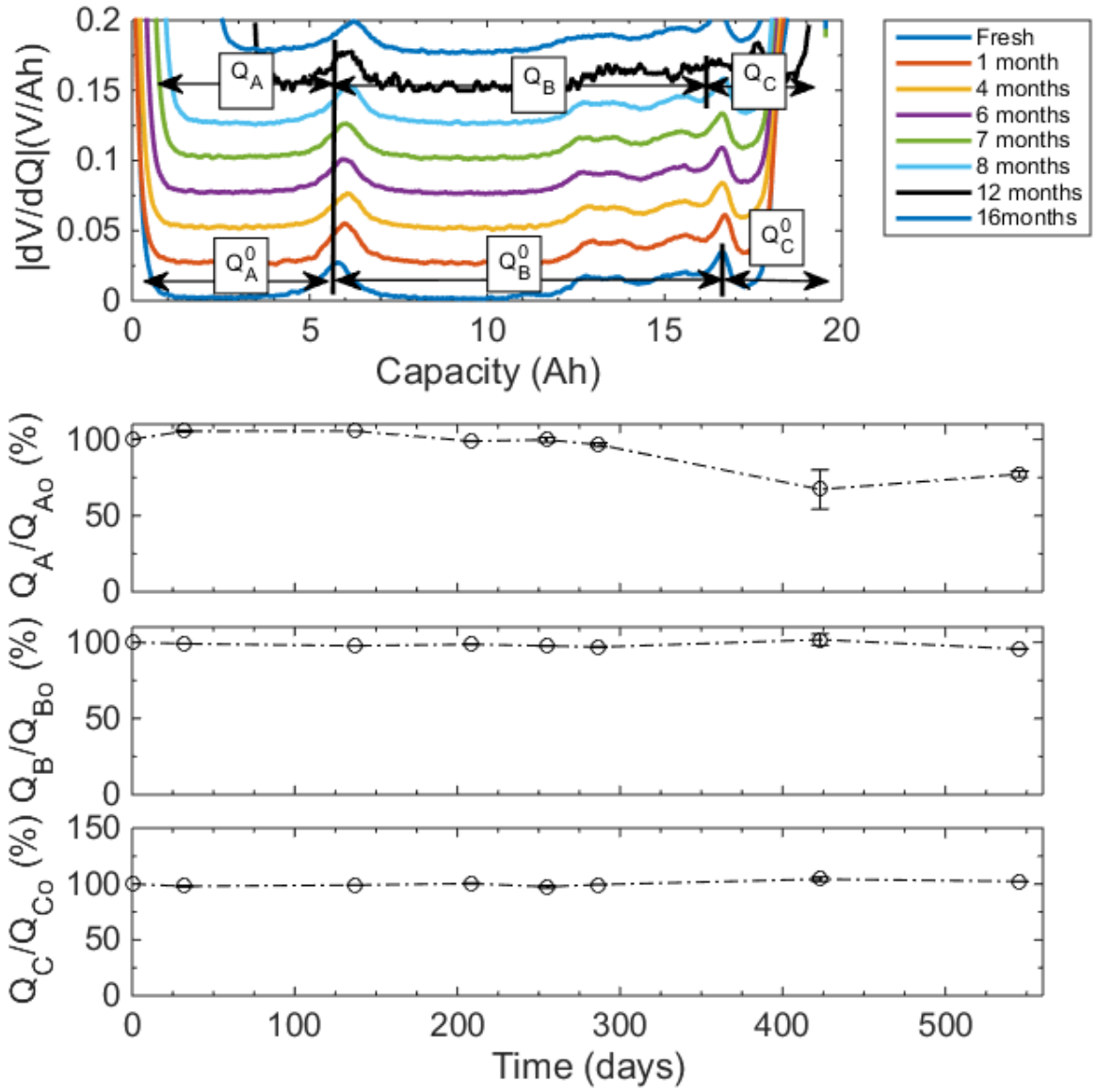

Figure 37: Discharge dV/dQ curve at a rate of C/20 for cells stored at 50ºC and 0% SOC

Despite being at only a slightly lower temperature condition, the results show that there is not a visible active material loss present in the cell. The cells stored at these conditions only experienced a loss of cyclable lithium (seen by the decrease in Q_A).

Incremental capacity curves were also generated for the cells that underwent a shift in storage conditions. Figure 38 and Figure 39 depict the results of the analysis of these cells.

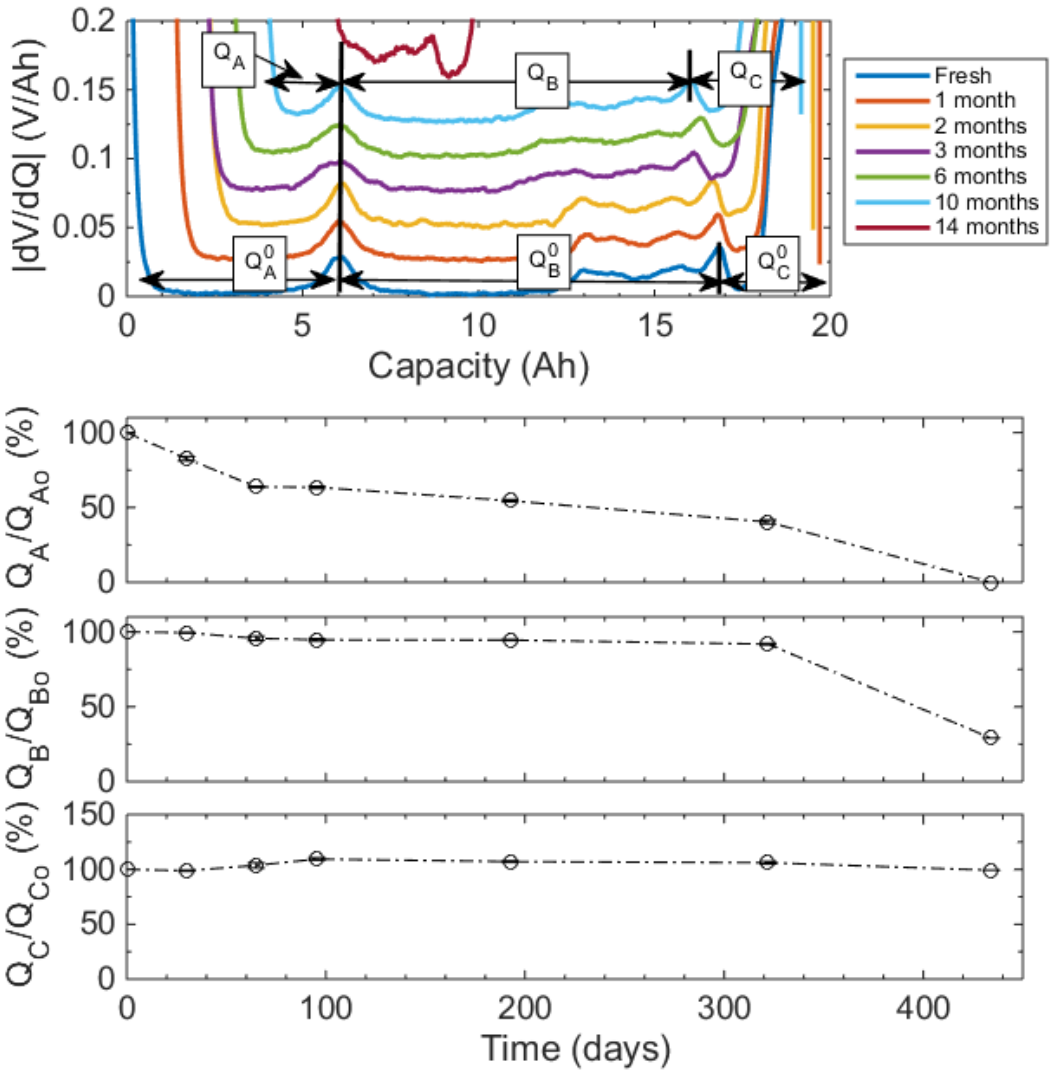

Figure 38: Discharge dV/dQ curve at a rate of C/20 for cells stored at 60ºC and 100% SOC for three months, then shifted to 60ºC and 0% SOC

Storage of the cell at fully charged conditions resulted in a swift decline of Q_A. After the change in conditions, to fully discharged, the downward slope of Q_A declined. Thus, the degree at which the loss of cyclable lithium was occurring in the cell became decreased. This is in accordance with literature as cells stored at low states of charge do not incur as high capacity fades. [9]

After the initial decline in the value of Q_B (from storage at fully charged conditions and high temperatures) the value of Q_B/ Q_{Bo} remained relatively constant until the cell finally reached its EOL. The shift to a discharged state limited the potential for severe loss of active material at the negative electrode.

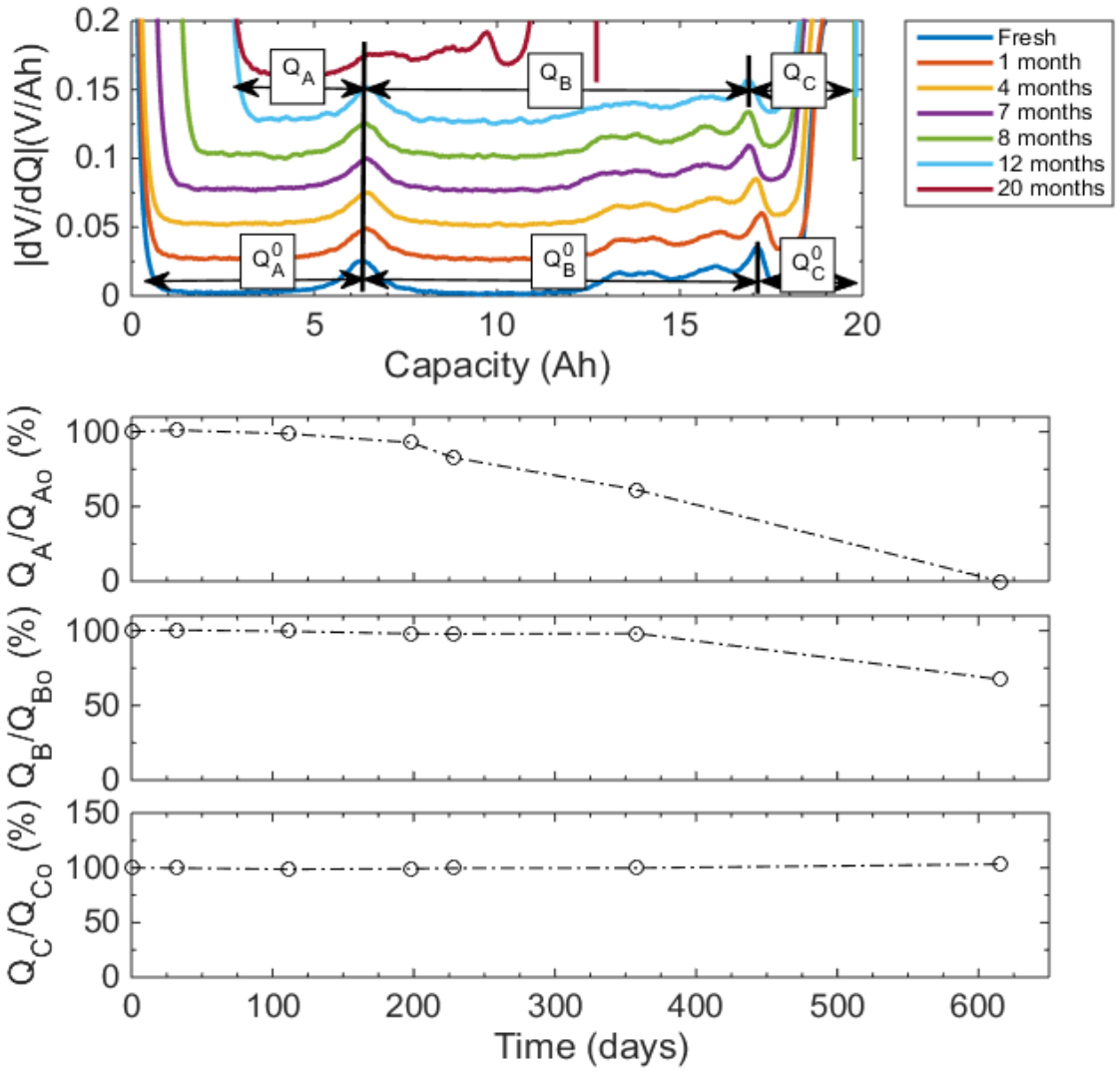

Figure 39: Discharge dV/dQ curve at a rate of C/20 for cells stored at 60ºC and 0% SOC for seven months, then shifted to 35ºC and 100% SOC

Once again, the primary losses of capacity within the cell are caused by the loss of cyclable lithium, as noted by the decrease in Q_A. After the change in conditions (to fully charged and 35ºC) the downward slope of Q_A decreased and the degree at which the loss of cyclable lithium was occurring increased. The storage of the cell at the initial conditions though, led to the cell's swift decline. The graph of Q_A/Q_{Ao} (from seven months onward) in Figure 39 does not resemble the graph of Q_A/Q_{Ao} in Figure 26, in which the cell was only stored at 35ºC and 100% SOC. Despite being in a discharged state, storage at high temperatures had dramatic consequences on $LiFePO_4$ cells even if they are shifted to a lower temperature condition. The shift can delay the cell from reaching its EOL, but ultimately the cell will fail.

The value of Q_B remained relatively constant until the cell finally reached its EOL. The shift to a lower temperature condition had a positive effect on the cell in terms of limiting the extent of degradation, from loss of active material at the negative electrode. Due to the cell initially being stored at high temperature conditions, though, continual storage, for calendar aging testing of the cell, resulted in a steady loss in capacity.

4.4 Post-Mortem Analysis

As described in the previous section, cells that have reached their EOL point are removed from storage and prepped for post-mortem analysis. The commercial cells are opened inside of an argon-filled glovebox and the aged electrode materials are sampled to undergo various analyses.

4.4.1 Qualitative Analysis of Electrode Material

Images of the post-mortem removal of the electrodes from their respective cells can be found in Appendix B: Images of post-mortem analysis of $LiFePO_4$ cells.

The first cell to undergo post-mortem analysis was a cell that had been stored under 100% SOC and 60^{o}C temperature conditions. Once the outer metal casing had been removed to expose the folded electrode sheets beneath, it was discovered that the liquid electrolyte had completely evaporated and a substance had formed onto the graphite electrode and the separator. The loss of the wetting capability of the electrolyte and the severe mechanical deformation of the entire cell, as a result of gas formation, caused the electrode materials to become very brittle and subsequently delaminate from the current collectors of both the anode and cathode. This made the possibility of performing various analyses on the electrode material to be increasingly difficult.

Similar substances that had adhered onto the graphite electrode in the cell stored at 60^{o}C and 100% SOC, were seen on the graphite electrodes of the cell stored at 60^{o}C and 0% SOC, but not as prevalently over the whole area of the electrode. The cell also showed small build-ups of material on the LFP electrode which was not seen in the previous cell.

Finally, the cell stored at 35^{o}C and 100% SOC was opened. Both electrodes did not show any signs of build-up of material on them. There was not a visible difference between these electrodes and the fresh unaged ones.

Additional analyses were then conducted on all of the cells to determine more pertinent information, such as: imaging the electrodes at high magnification (optical microscopy and scanning electron microscopy (SEM)), and composition of species on the surface of the electrode (EDX analysis and ICP).

4.4.2 Scanning Electron Microscopy (SEM)

4.4.2.1 SEM Results for Graphite Electrodes

Figure 40 through Figure 45 compares SEM micrographs of samples of fresh, unaged, graphite electrodes with the electrodes from cells after aging in storage chambers at 60 and 35 ◦C and fully charged conditions, and 60 ◦C and fully discharged conditions.

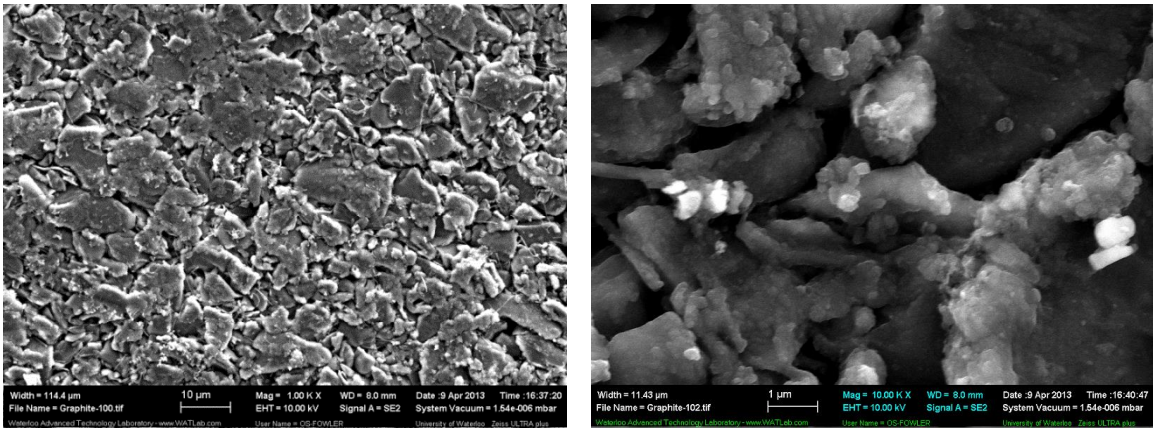

Figure 40: SEM micrographs of unaged graphite electrode at 1Kx mag. (left) and 10Kx mag. (right)

The SEM micrographs in Figure 40 depict samples of fresh graphite electrodes. As the battery has not been cycled as of yet, there is no SEI layer build-up present on the surface of the graphite grains. Grain features are clearly defined in the micrographs

Figure 41 depicts the SEM micrographs of graphite electrodes stored at 60^{o}C and 0% SOC. Based on the images, the build-up of material on the electrode is clearly its own layer adhered onto the graphite electrode. The material has not embedded itself into the bulk graphite material and is not evenly dispersed over the entire sample. In addition to the built-up of foreign material on the electrode, the surface of the bulk graphite material at high magnifications (1000-10000x) shows the SEI film forming unevenly over the graphite grains. Backscattering images in Figure 42 show that the particles within the SEI appear to be conductive materials. The particles appear brighter than the surrounding materials using this analysis technique.

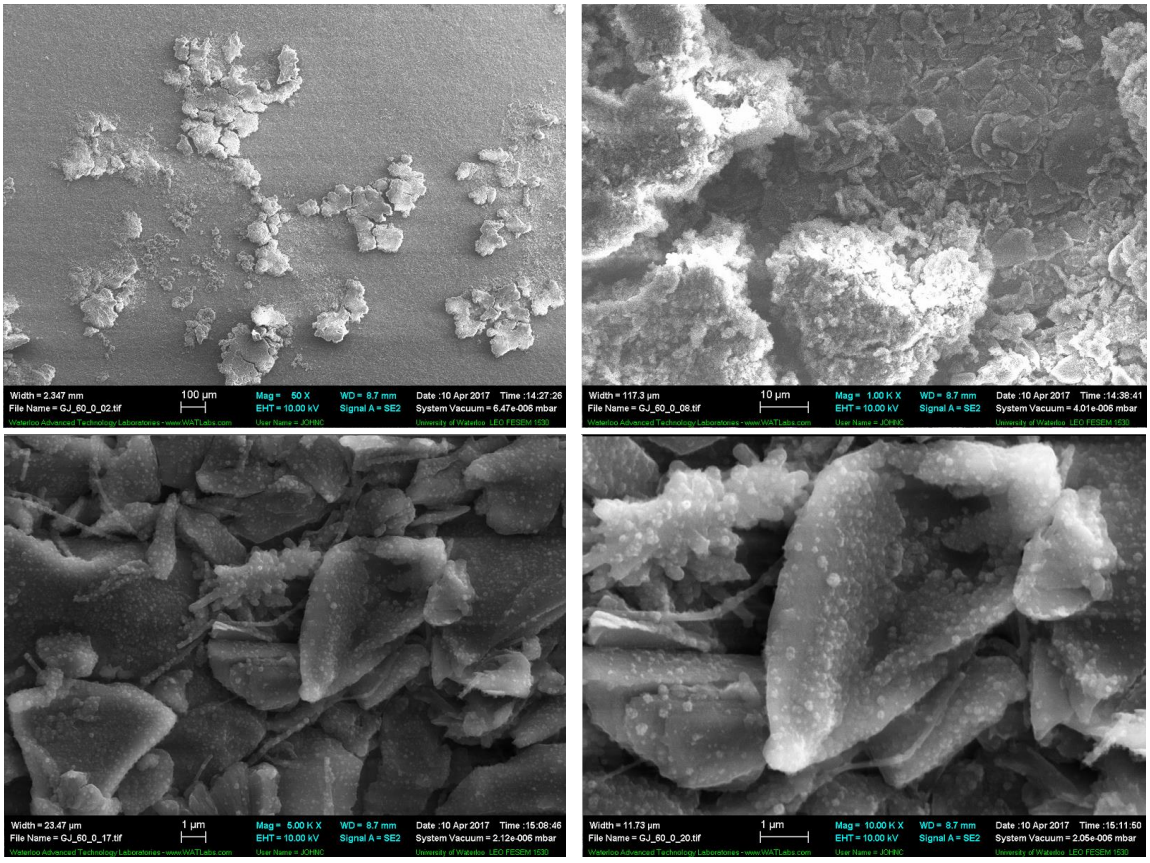

Figure 41: SEM micrographs of aged graphite electrode (60ºC and 0% SOC) at 50x magnification (top left), 1000x magnification (top right), 5000x magnification (bottom left), and 10,000x magnification (bottom right)

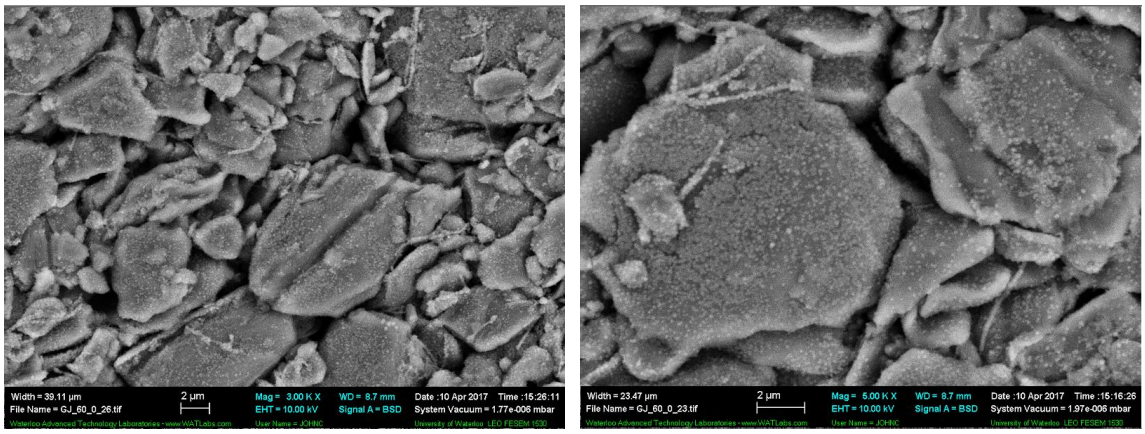

Figure 42: Back-scattering SEM micrographs of aged graphite electrode (60ºC and 0% SOC) at 3000x magnification (left), and 5000x magnification (right)

Figure 43 depicts the SEM micrographs of graphite electrodes stored at 60ºC and 100% SOC.

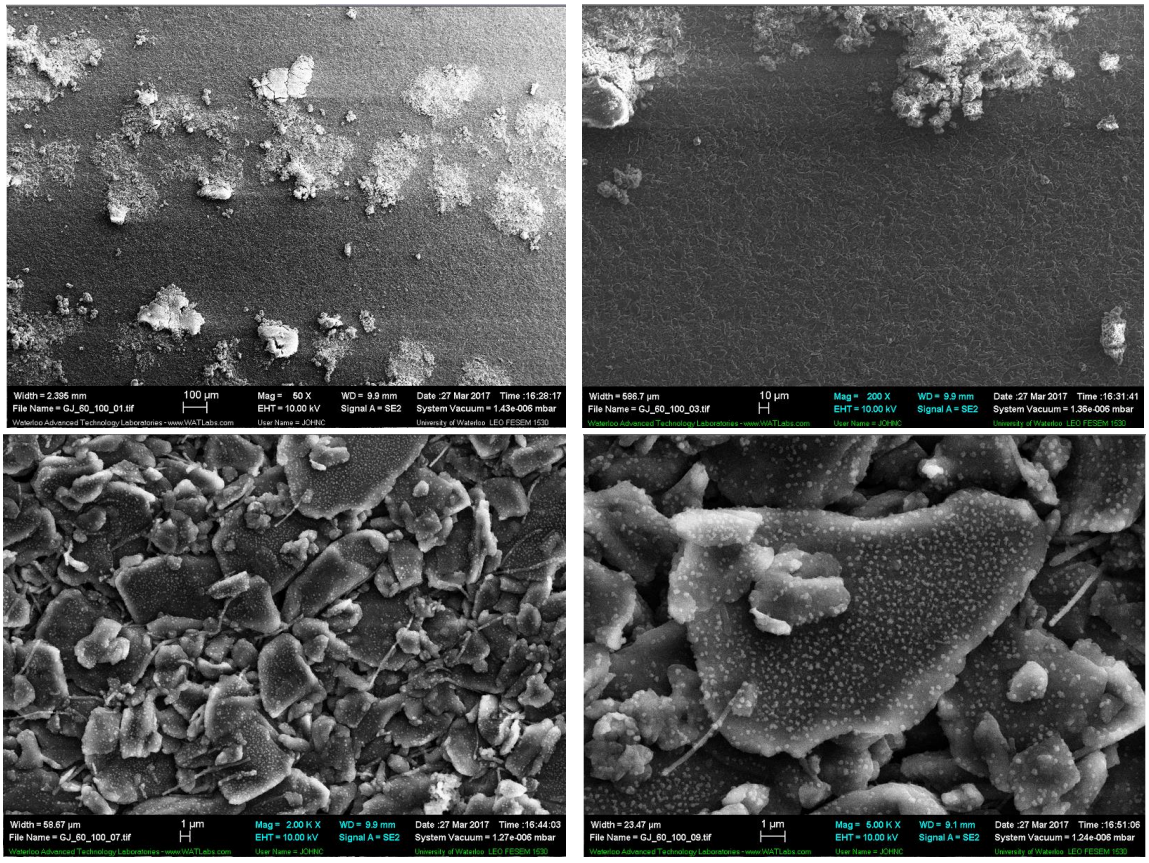

Figure 43: SEM micrographs of aged graphite electrode (60ºC and 100% SOC) at 50x magnification (top left), 200x magnification (top right), 2Kx mag. (bottom left), and 5Kx mag. (bottom right)

The SEM images showed a similar build-up of foreign material on the graphite as to that found on the graphite samples aged at discharged conditions. Once again, it can be seen that the material is its own distinct layer adhered onto the graphite electrode. Looking at the graphite grains at high magnifications, it appears that the SEI film is forming more evenly over the grains, in comparison to the previous graphite images. The edges of the grains, also, appear to be much smoother in comparison to unaged graphite, possibly owing to the formation of the SEI layer. The reason for this more even SEI development could be due to this SEI layer being much thicker than the SEI layer developed in the other cell. If this is the case the SEI layer could be more O_2 rich incorporating Li_2CO_3 and alkylcarbonates into the layer. [13]

The SEM images also appear to show very small particles that are ingrained into the layer. The electrode samples at the other conditions do not show the proliferation of these tiny particles. Analyzing these particles under a back scattering diffraction lens, the particles within the SEI appear to be conductive materials (Figure 44).

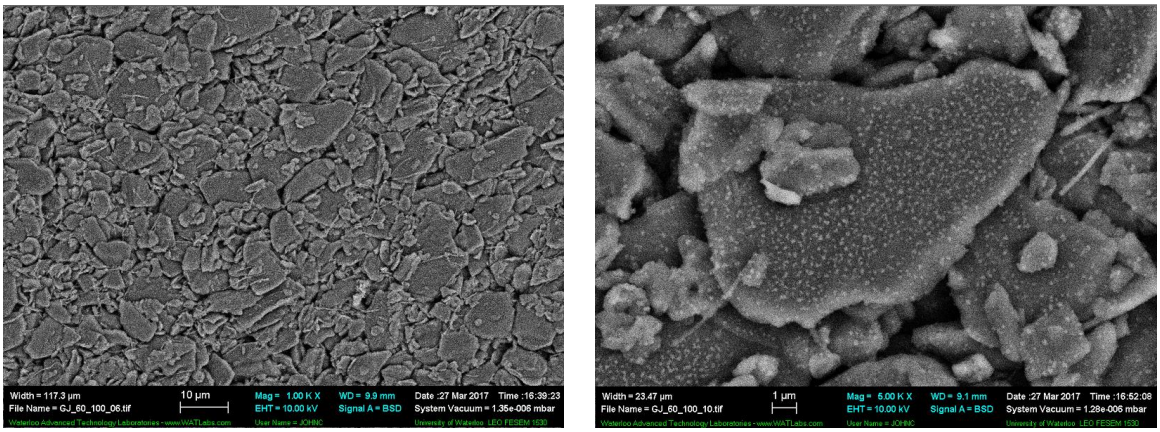

Figure 44: Back-scattering SEM micrographs of aged graphite electrode (60ºC and 100% SOC) at 1000x magnification (left), and 5000x magnification (right)

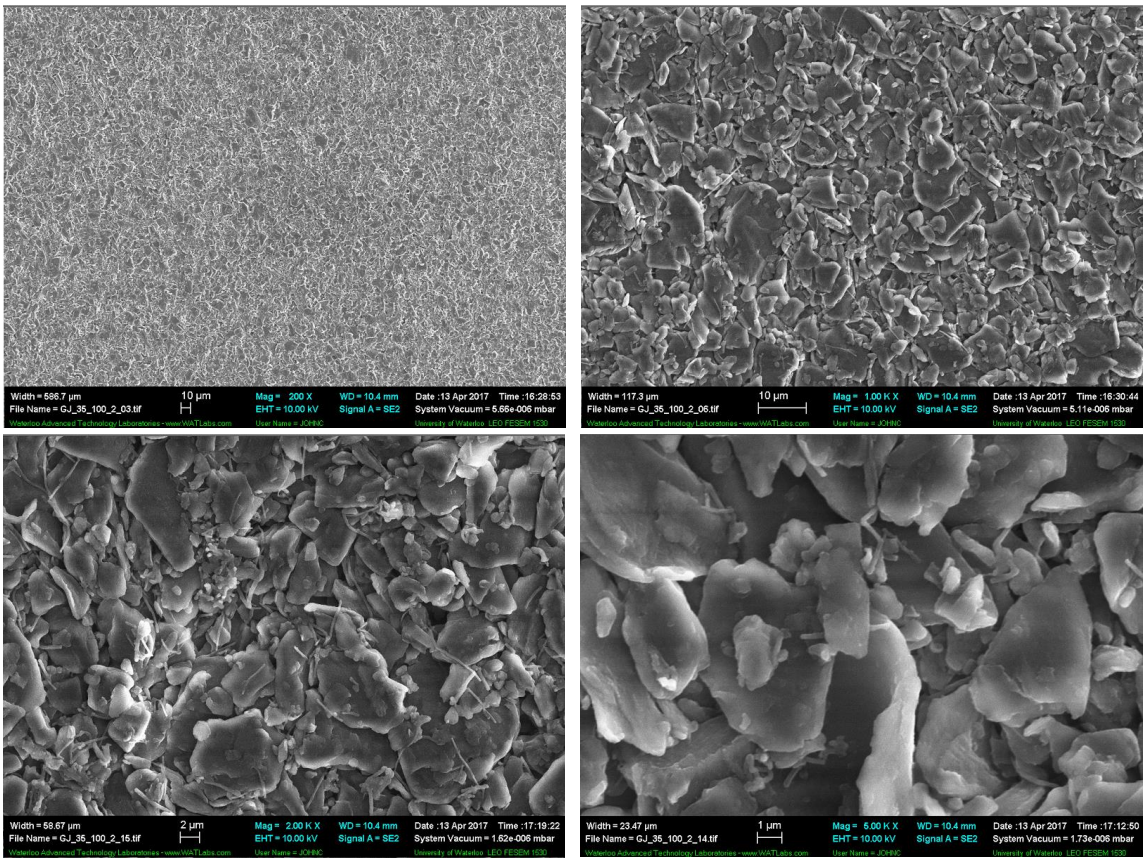

Figure 45: SEM micrographs of aged graphite electrode (35ºC and 100% SOC) at 200x magnification (top left), 1000x magnification (top right), 2000x mag. (bottom left), and 5000x mag. (bottom right)

Comparing the unaged graphite and graphite aged 35ºC and 100% SOC (Figure 40 and Figure 45), there are only small differences between the two samples in terms of the shape of the graphite. On the surface the graphite grains appear to be very similar in shape, but at the edges

the graphite appears to have become smoother during the aging period. The unaged graphite grains have very rough edges in comparison. The passivating SEI layer that forms on the graphite is the most likely reason for this difference as it is non-conductive and does not provide the same image quality if it were not present.

4.4.2.2 SEM Results for LFP Electrodes

Figure 46 through Figure 49 compares SEM micrographs of samples of fresh unaged $LiFePO_4$ with the electrodes from cells after aging in storage chambers at the same conditions as the graphite electrodes. The active material particles are the oblong shaped objects, and the degree to which the particles are conductive can be determined by the overall brightness in the image. Lighter particles contain more conductive species, such as Iron. The images also show carbon black fibers that are contained within the electrode to increase its conductivity. [78] LFP has a low conductivity and requires the addition of conductive carbon powder ("carbon black") to aid in its ability to transfer electrons. [78] The fibers appear as long filaments in the SEM micrographs.

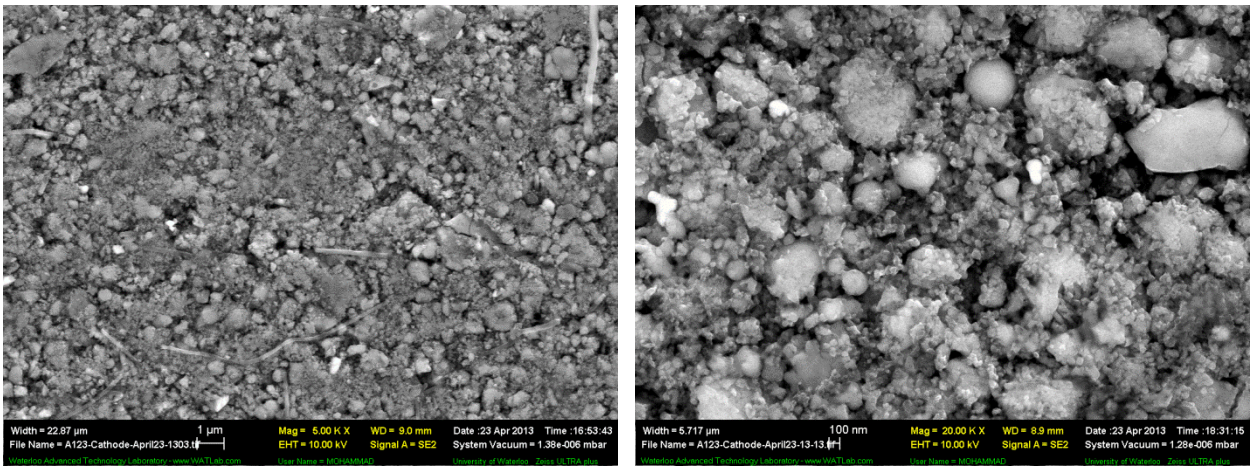

Figure 46: SEM micrographs of unaged LFP electrode at 20,000x magnification (left) and 5000x magnification (right)

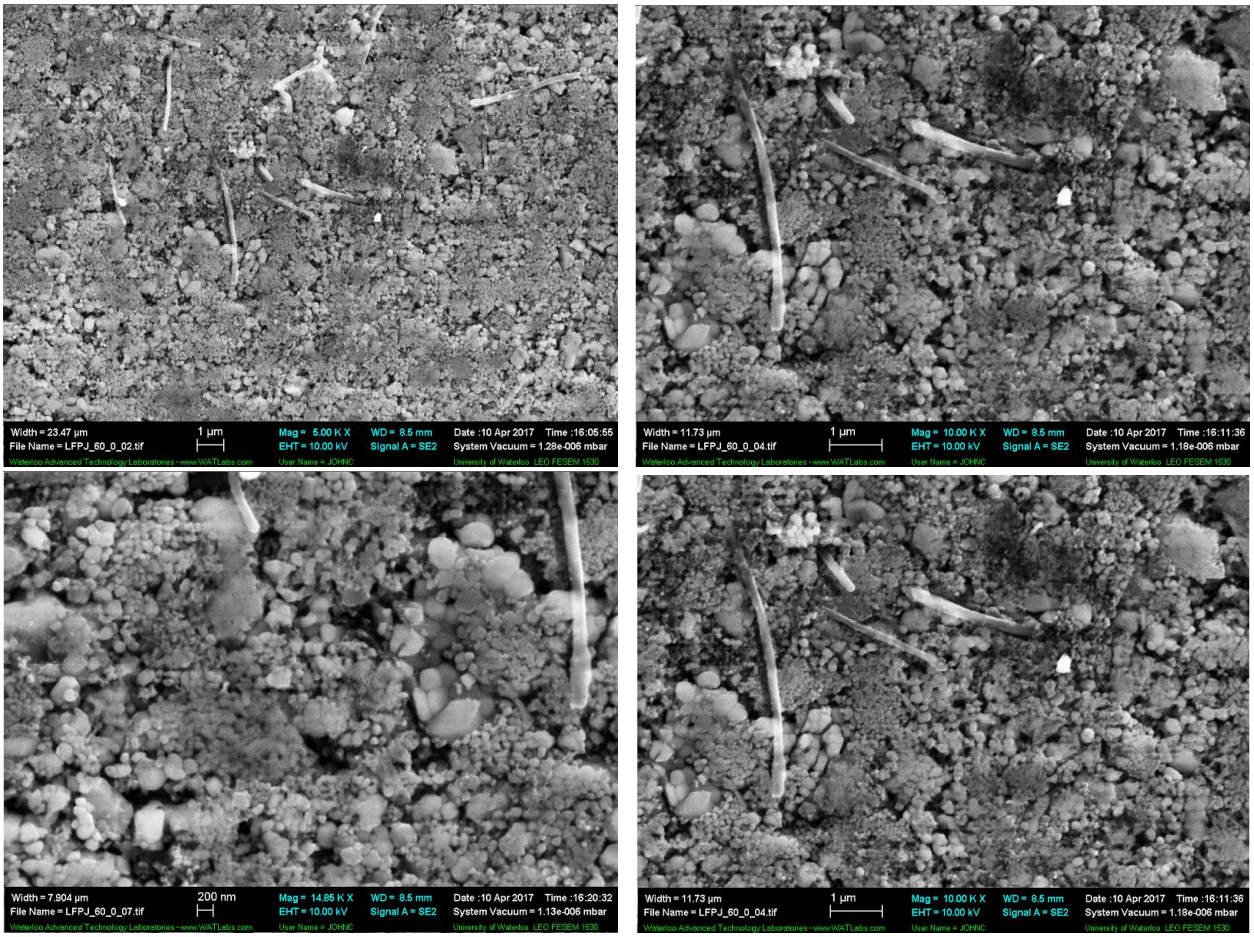

Figure 47: SEM micrographs of aged LFP electrode (60ºC and 0% SOC) at 5000x magnification (top left), 10,000x magnification (top right), 14,050x magnification (bottom left), and 10,000x magnification (bottom right)

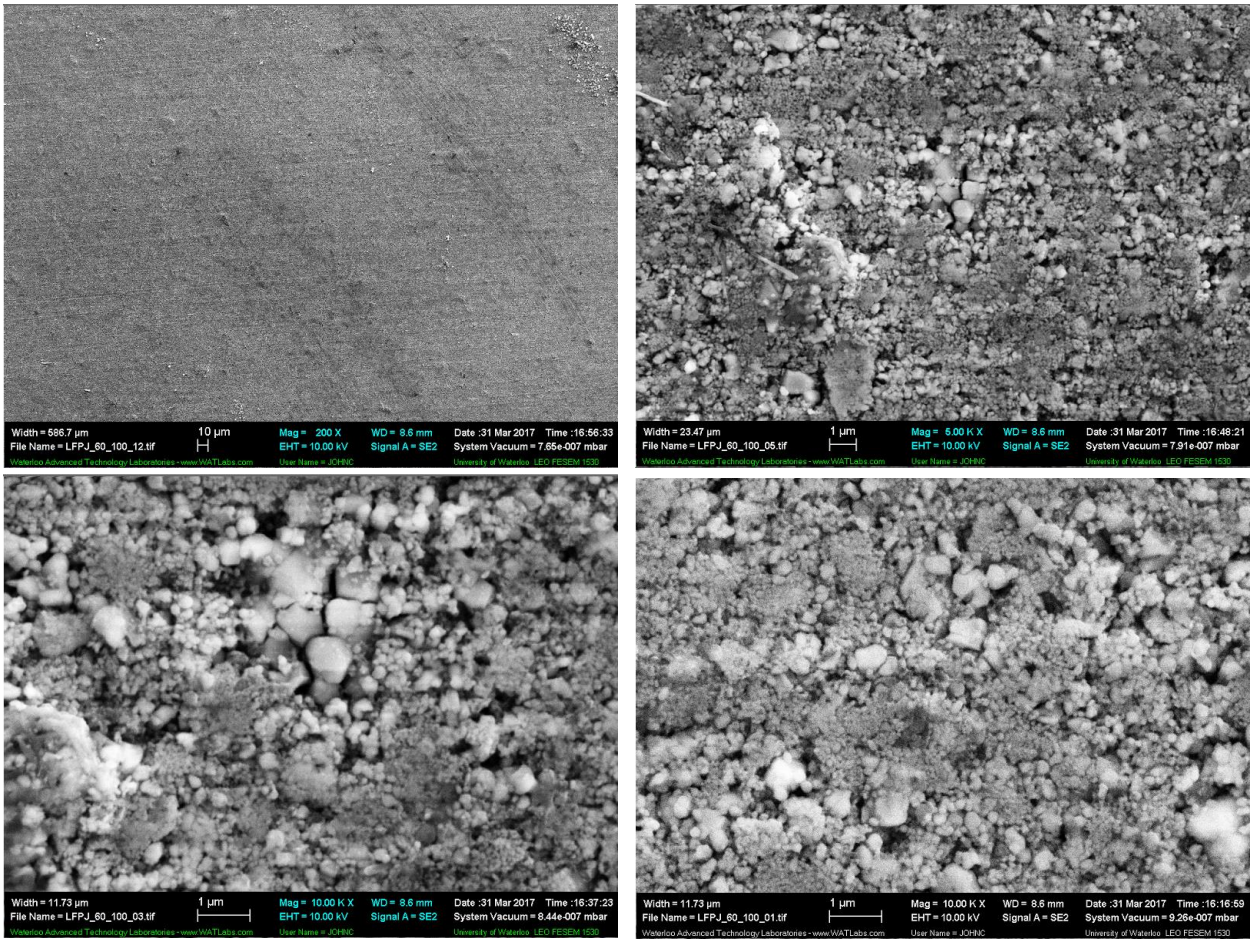

Figure 48: SEM micrographs of aged LFP (60ºC and 100% SOC) at 200x magnification (top left), 5000x magnification (top right), 10000x magnification (bottom left), and 10000x magnification (bottom right)

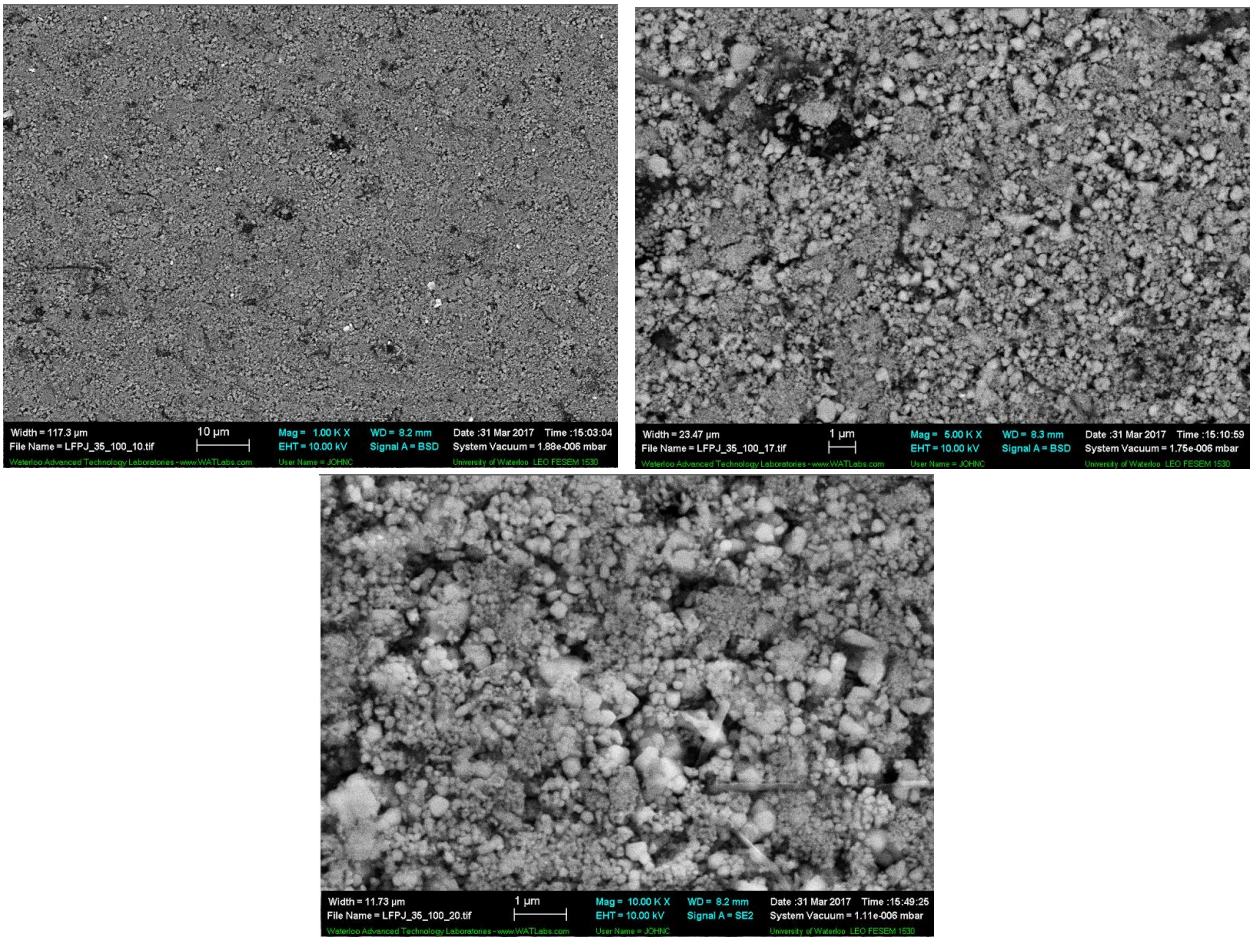

Figure 49: SEM micrographs of aged LFP (35ºC and 100% SOC) at 1000x magnification (top left), 5000x magnification (top right), 10000x magnification (bottom left), and 10000x magnification (bottom right)

Based on the SEM micrographs of the LFP electrodes, there are some particle cracks and fractures being observed for cells stored at 60ºC. It cannot, however, be definitively concluded that these fractures were caused from the storage conditions for the cells. The most likely reason for these fractures is due to the mechanical deformation of the cells due to the production of gaseous species or the intercalation stresses placed on the electrodes during cycling.

4.4.3 EDX Results

EDX studies were performed on samples of the electrodes removed from the cell in order to determine the composition and complexity of the structures being formed within the SEI on the surface of the electrode. Performing EDX analyses will also provide a potential look into species being incorporated into the SEI, including iron. If iron is present within the SEI layer of the

graphite material it will provide evidence of Fe dissolution occurring within the cell. Dissolution of Fe from the LFP electrode will denote the $LiFePO_4$ electrode becoming inactive.

Many micrograph samples, with subsequent EDX analyses, were taken of each of the electrode samples. The following results are a depiction of the general compositions of species within the samples. Table 8 describes the composition results obtained from the EDX results for each of the graphite electrode samples.

Table 8: EDX Results of Graphite Electrode samples

Sample	Fresh Graphite	Aged Graphite (35ºC and 100% SOC)	Aged Graphite (60ºC and 100% SOC)	Aged Graphite (60ºC and 0% SOC)
Species	*Atomic %*	*Atomic %*	*Atomic %*	*Atomic %*
Carbon	93.61	95.3	77.6	92.7
Oxygen	3.41	3.4	17.6	3.0
Phosphorous	-	0.04	0.7	0.2
Iron	-	0.58	0.5	<0.01
Fluorine	2.98	0.75	3.6	4.1

Based on the results in Table 8, the primary difference between the electrodes was the increase in the atomic percentage of oxygen for graphite aged at 60ºC and 100% SOC. An increase in the atomic percentage of oxygen in aged electrodes may be related with the presence of SEI compounds such as Li_2CO_3 or lithium alkylcarbonates at the particle surface that are O-rich. [13] Considering the cell was aged under the most severe conditions, and the differential voltage-capacity curve showed the presence of degradation from loss of cyclable lithium and active material loss, the presence of high atomic percentages of oxygen would correlate to the formation of new SEI layers over exposed areas. Table 9 describes the composition results obtained from the EDX analysis for each of the LFP electrode samples.

Table 9: EDX Results of LFP Electrode samples

Sample	Fresh LFP	Aged LFP (35ºC and 100% SOC)	Aged LFP (60ºC and 100% SOC)	Aged LFP (60ºC and 0% SOC)
Species	*Atomic %*	*Atomic %*	*Atomic %*	*Atomic %*
Carbon	28.6	8.92	14.7	14.5
Oxygen	46.9	55.58	49.8	54.3
Phosphorous	11.66	14.94	14.0	14.1
Iron	11.86	20.44	21.3	17.1
Fluorine	-	-	-	-

Despite undergoing aging for many months the results of the EDX analysis of the LFP electrodes show very little difference between samples. The compositions of the bulk materials remain fairly constant and there are no visible signs of a decrease in the iron content of the samples from potential active material loss.

4.4.3.1 SEM Micrographs of Adhered Materials to Electrodes

In addition to analyzing the bulk graphite materials, the different materials that have adhered onto the surface of the graphite were also analyzed. Figure 50 and Figure 51 display images of the adhered material on the aged graphite (aged at 60ºC, and fully charged and fully discharged respectively).

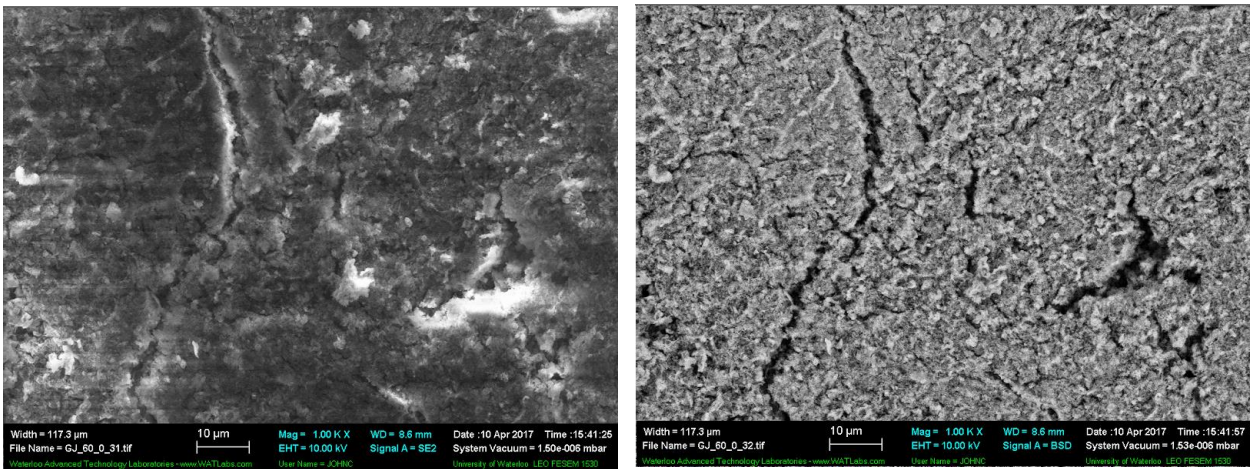

Figure 50: SEM micrographs of adhered particulate matter for graphite stored at 60ºC and 0% SOC

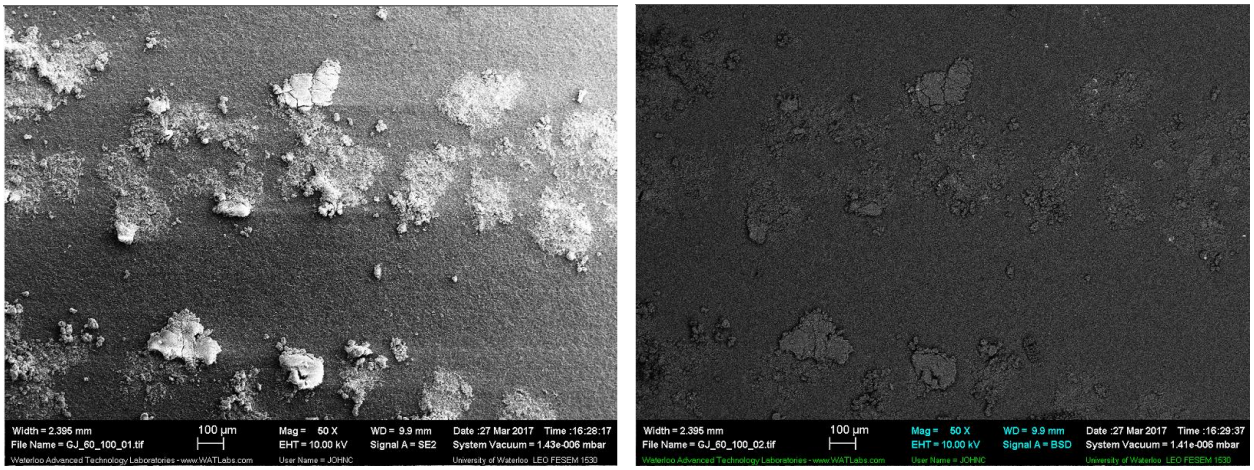

Figure 51: SEM micrographs of adhered particulate matter for graphite stored at 60ºC and 100% SOC

EDX analyses were then carried out on these materials to determine their elemental compositions. Table 10 displays the compositions for the particulate matter for the two electrodes.

Table 10: EDX analysis of particulate matter

Sample	**Aged Graphite (60°C and 100% SOC)**	**Aged Graphite (60°C and 0% SOC)**
Species	*Atomic %*	*Atomic %*
Carbon	47.5	36.7
Oxygen	26.5	51.3
Phosphorous	4.3	6.4
Iron	2.3	1.4
Fluorine	19.4	3.2

The EDX results found that the particulate matter on the cell stored at fully charged conditions was largely composed of carbon and oxygen in almost a 2:1 ratio of carbon to oxygen. The cell stored at discharged conditions, though, was the opposite. The largest atomic percentage of the species within the substance was found to be oxygen and then followed by carbon. The additional elements, Fluorine and Phosphorous, most likely come from the $LiPF_6$ salt in the electrolyte and have been combined within the substance. The presence of Iron in the samples suggests the possibility that there may be some iron dissolution occurring at the cathode, but further tests will need to be completed to confirm.

EDX results of other SEM micrographs yielded similar results to those depicted in Table 10. Sources for the carbon and oxygen in the particulate are most likely the result of contamination of the cell producing lithium carbonate, alkylcarbonates, and gaseous species. [13] These compounds are then incorporated into the material along with the salt of the electrolyte to form the particulate.

4.4.4 Optical Microscopy

Optical microscopy is a technique used to analyze materials at the micron and sub-micron level. [73] During post-mortem analysis, samples of the degraded electrodes were taken and placed under a microscope to determine from optical microscopy, defects in the electrode from the aging effects. Samples were approximately 3 cm long and 3 cm wide. These optical micrographs

were taken with an MA 200 Nikon Eclipse microscope. Figure 100 through Figure 107, in Appendix C: Optical Microscopy Images, depicts the results of the microscopy studies.

Prior to observation under the microscope, the cells had been washed in a DMC (dimethyl carbonate) solution to remove any remaining $LiPF_6$ salt that had precipitated out of the electrolyte. From the micrograph results, it was observed that cells stored under 60^{o}C conditions have a significant build-up a particulate matter. Despite the DMC wash, this particulate matter could not be removed.

Observations of all electrode samples were unable to definitively conclude that there was the presence of any cracks in the electrodes. Imaging at this magnification was not sufficient to determine this degradation condition.

4.4.5 Inductively coupled plasma (ICP) Analyses:

Inductively coupled plasma atomic emission spectroscopy (ICP-AES) is a technique used to analyze the elemental composition of electrodes. Inductively coupled plasma is used to create excited ions and atoms from a sample, which will release characteristic electromagnetic radiation in the visible range. [74] The particular wavelength of the radiation will describe the presence of a particular element and use of this method will be able to give the ratio between elements. [74] ICP is very effective and can detect the presence of elements all the way down to the ppm range. Thus, ICP-OES measurements are useful in determining if the dissolution of transition metals from the cathode is occurring, by detection of the migrated material on the anode. [13]

A drawback of this technique, however, is that ICP-OES will not give the complete sample composition. [74] Additional methods are therefore required. ICP-OES is often compared to EDX, but ICP-OES has the advantage of detecting Li.

4.4.5.1 ICP Analysis Procedure:

In the glovebox, the electrodes were removed from the cell and samples of approximately 4 (2 cm by 2 cm) to 9 (3 cm by 3 cm) cm^2 were cut using ceramic scissors. Samples were placed into vials and filled with DMC to cover the sample. The vials were shaken to thoroughly wash the sample and left overnight to dissolve any remaining salt. All of the vials were removed from the glovebox, and the samples were dried. Once dry, the active material can be scraped from the electrode. The mechanical treatment will not change the chemical composition, and is therefore

not an issue when trying to obtain pertinent composition data. The samples are then dissolved in an acid solution (digestion) to have the samples enter into solution.

4.4.5.2 ICP Analysis Results:

ICP-OES analysis was done for both electrode samples to measure the types and amounts of metallic species present for cells stored at the different conditions. Trace metal concentrations were measured to assess the migration of cathode material within the cell. Table 11 describes the results of ICP analysis.

Table 11: ICP Results of Metallic Species

	Mn (mg/kg)	Fe (mg/kg)	Ni (mg/kg)	Co (mg/kg)	Li (mg/kg)
Fresh Graphite	35.971	1662.47	203.84	83.93	7976.02
Fresh LFP	2086.60	334612.84	51.35	45.34	37799.52
Graphite Stored at 60°C/0% SOC	25.75	693.39	145.92	60.09	15765.92
LFP Stored at 60°C/0% SOC	2355.43	355028.83	140.85	143.99	34736.29
Graphite Stored at 60°C/100% SOC	38.99	1803.12	220.92	90.97	26447.30
LFP Stored at 60°C/100% SOC	1965.87	317858.88	51.26	57.41	20502.90
Graphite Stored at 35°C/100% SOC	108.11	1110.27	612.61	252.25	11193.51
LFP Stored at 35°C/100% SOC	1940.64	322254.04	94.31	41.50	35609.21

Based on the results it can be determined that there is a significant amount of lithium present on the graphite electrode. All cells stored in the glovebox, for destructive testing, are in a fully discharged state. The cyclable lithium should be intercalated into the LFP electrode. Thus, it would appear that the lithium has reacted with the electrodes in side reactions prompting its loss and subsequent incorporation into the SEI or other products. Table 12 describes the increase, or decrease, in metallic species within the electrode samples in comparison to the fresh electrode. A negative value represents a gain of that particular specie from the fresh electrode, while a positive value is a loss.

Table 12: Percentage increase or decrease of metallic species

	Mn (%)	Fe (%)	Ni (%)	Co (%)	Li (%)
LFP Stored at 35ºC/100% SOC	6.995%	3.693%	-83.662%	8.475%	5.795%
LFP Stored at 60ºC/0% SOC	-12.883%	-6.101%	-174.275%	-217.582%	8.104%
LFP Stored at 60ºC/100% SOC	5.786%	5.007%	0.176%	-26.625%	45.759%
Graphite Stored at 60ºC/0% SOC	28.412%	58.292%	28.412%	28.412%	-97.667%
Graphite Stored at 60ºC/100% SOC	-8.382%	-8.460%	-8.382%	-8.382%	-231.585%
Graphite Stored at 35ºC/100% SOC	-200.541%	33.216%	-200.541%	-200.541%	-40.340%

As determined from the differential voltage graphs, much of the lithium loss within the cell can be attributed to the loss of cyclable lithium, most likely due to the build-up of the SEI layer on the graphite electrode. The values for the lithium content in the samples correlate well to the conditions at which the cells were stored. Graphite stored at 100% SOC and 35ºC yielded the smallest increase in lithium, whereas graphite stored at 60ºC gave a much higher value. Finally, the graphite stored at discharged conditions, but at the same high temperature conditions yielded lower lithium contents in comparison to the fully charge cells. Along with temperature, the SOC of the cell greatly affects the extent of the loss of lithium.

Build-up of the SEI layer is not the only explanation for why the value of the Li content was so high for the Graphite samples. Cells stored at 60ºC experienced active material loss resulting in the electrodes being unable to allow for the intercalation and de-intercalation of Li. Also, the formation of lithium carbonate within the cell and its subsequent incorporation into the SEI layer will decrease the amount of cyclable lithium.

Finally, it was concluded that there was not a significant deposition of Fe on the anode. Cells stored at 100% SOC actually experienced a loss of iron, and graphite stored at 60ºC and 0% SOC had only a marginal increase. Looking at the cathodes, there appears to be only a marginal decrease and is not significant. Thus, dissolution of the iron from the LFP cathode cannot be concluded to have occurred during calendar aging for these storage conditions.

4.4.6 Profilometry

Profilometry is an experimental procedure to measure the topography of a sample. An optical profilometer was used for these experiments. [79] As opposed to a stylus profilometer, optical profilometers are a non-contact experimental procedure that makes use of the wave properties of light to compare the optical path difference between the sample surface and a reference surface. [79] [80]

An RTEC Instruments Optical Profilometer was used to obtain the profile readings for the electrodes. Resolution for the machine is 0.01 nm. The changes in the Z position of the optical path can then be used to digitally reconstruct the surface. The results of the average profile heights are depicted in Table 13.

Table 13: Profilometry measurements of electrodes

Storage Condition	LFP Electrode Average Profile Height (μm)	Graphite Electrode Average Profile Height (μm)
Fresh Cell (no aging)	56.0	32.4
Aged at 60ºC and 100% SOC	72.8	62.1
Aged at 60ºC and 0% SOC	92.2	44.1
Aged at 35ºC and 100% SOC	73.3	42.0

The aging of the electrodes under calendar aging conditions lead to greater electrode thicknesses, most likely attributed to the build-up of the SEI layer on the respective electrode surfaces. Increasing the storage temperature conditions leads to increased development of the SEI. SOC may also play a role in the thickening of the electrodes during aging as the electrodes stored at discharged conditions yielded much higher heights than electrodes stored at charged conditions. The opposite effect can be seen in the graphite electrodes.

It must be noted that the electrode samples taken from the cell stored at 35ºC and 100% SOC were aged for 24 months in comparison to the other cells that were only able to sustain aging at 60ºC for 4 months (100% SOC) and 7 months (0%) respectively. Thus, the higher thickness values reported for these samples is most likely attributed to the longer aging period rather than the specific aging conditions.

4.4.7 4 Point Conductivity Measurement

In order to determine the effective electronic conductivity of the electrode samples a four-probe setup was utilized. Before being able to run this experiment, the samples had to be delaminated from the current collector. For the lithium-iron phosphate electrode the samples were submerged in a 1M NaOH solution at ambient conditions. [81] The production of hydrogen at the interface, between the porous electrode and the aluminum current collector, is the principal reason for the rapid delamination of the electrode from the current collector. The aluminum reacts according to the following reaction [81]:

$$2Al + 6H_2O \rightleftharpoons 2Al(OH)_3 + 3H_2$$

$$Al(OH)_3 + NaOH \rightleftharpoons NA^+ + [Al(OH)_4]^-$$

This procedure, to remove the electrode from the current collector, will not damage the porous electrode material. [81] A similar procedure is completed on the anode to delaminate the graphite from the copper current collector, except in this case a solution of 1 M $FeCl_3$ is used instead.

The samples were then dried to remove any remaining solution. It should be noted that once removed from the current collector, all of the electrode samples became very difficult to handle. Samples from the cells stored in the highest temperature conditions were the most brittle and it was more difficult to complete the tests on those.

Once the samples were prepared the following equipment was used to complete the experiment. The probe being used in the experimental setup consists of four equally spaced metal tips with finite radii. The tips make contact with the sample along a line with electric current being carried through the two outer probes. The inner two probes are used to record the resulting voltage. The probe being utilized to complete the test is a C4S-57/1S probe which has a probe spacing of 1 mm, with 70-180 g applied force, 250 µm tip size made of Osmium metals.

In order to determine the effective electronic conductivity the following equation is used [81]:

$$\rho_{eff} = \frac{\pi}{ln2} t \left(\frac{V_{test}}{I_{test}}\right) \qquad \text{Equation 4.1}$$

Where I_{test} is the applied current, V_{test} is the measured potential, and t is the thickness of the electrode.

Using the results obtained from measuring the voltage and current values with the 4 point conductivity meter, and the thickness measurements from the profilometry studies, the effective electronic conductivity is calculated using Equation 4.1. The estimated value of the effective electronic conductivity for each of the samples is summarized in Table 14.

Table 14: Electric conductivity of LFP samples

Storage Condition	LFP Electrode Electric Conductivity (Sm)
Fresh Cell (no aging)	52.7031
Aged at 60^{o}C and 100% SOC	10.4500
Aged at 60^{o}C and 0% SOC	10.1956
Aged at 35^{o}C and 100% SOC	14.5558

Electrical conductivity is the measure of a material's ability to allow the transport of an electric charge. Having good electrical conductivity is very important when selecting materials for cathodes and anodes of cells. [81] All of the aged electrodes reported a loss of electronic conductivity, with the samples from the higher storage temperature conditions experiencing the most significant losses. SOC did not appear to play a factor in loss of conductivity as samples of LFP electrodes from cells stored at discharged and charged conditions obtained similar values.

4.5 Summary of Calendar Aging of $LiFePO_4$ Cells

In this chapter, results for non-destructive and destructive testing of $LiFePO_4$ cells were completed to determine the extent of aging occurring within the cells and to attempt to determine which degradative phenomena were arising. Storage of the cells at different aging conditions promoted the loss of capacity in a number of ways and, depending on the storage conditions, resulted in the cells reaching their EOL points much sooner than they would have if stored at ambient temperature conditions.

The highest capacity loss was observed in cells stored at high temperature and fully charged conditions. This was demonstrated by tracking irreversible capacity loss over storage time and was observed in the ICP analysis (cells stored at 60^{o}C and 100% SOC had the highest Li content within the bulk graphite). Utilizing differential voltage capacity curves, it was found that the modes of degradation resulting in the capacity loss were the result of the loss of cyclable lithium and a loss of active material at the anode. This is in accordance with what the literature states

would occur, as the increased temperatures and high concentrations of lithium at the anode promote the proliferation of degradative side reactions to occur. [8] [18] Post-mortem analysis (SEM and optical microscopy images of the electrode samples) of these cells found that there was a build-up of a secondary layer of material on the anode, although it did not cover the entire area. The formation of this material over the anode is most likely correlated to the loss of active material as the build-up of this material may be preventing Li ions from being able to intercalate within the active graphite material. In literature, it has been found that with continual build-up of the SEI layer at the anode areas of the active graphite material can become inactive, preventing further intercalation of lithium ions. [8] It can be suggested that a similar phenomenon is being observed here.

Temperature played the most significant role in the degradation of the cell. As depicted in the capacity loss curves for cells stored at 0% SOC and 60^{o}C and 50^{o}C, despite the cells being stored at a lower state of charge, storage at the 60^{o}C temperature condition led to much higher capacity losses compared to the 50^{o}C storage condition. These losses were not as high if the cell had been stored under fully charged conditions, but the cell storage temperature played the most distinct role in the degradation of the capacity of the cell. During post-mortem analysis, SEM micrographs displayed the presence of a material that had adhered onto the surface of the graphite that was similar in composition to that of the material found on the graphite samples for cells that had been fully charged. The high temperature storage conditions are likely promoting the proliferation of the side reactions that form this material and is a likely reason for the active material loss that is being observed to be occurring within the cell as it ages (observed through differential voltage capacity curves). The SOC at which the cell was stored at then determined the extent of the loss of the active material. Similar results were seen when comparing cells stored at 50^{o}C and charged and discharged conditions respectively, although the losses were not as severe at this temperature condition.

Finally, a “history” effect could be observed from cells that were stored at initially high temperature conditions and then shifted to less severe ones. Storage of $LiFePO_4$ batteries at high temperatures had a pronounced effect on the rate of degradation, even after the cells had been switched to new, less severe storage conditions. Based on the capacity fade results, depicting the irreversible capacity losses in cells that underwent a shift in temperature conditions (from a

higher temperature to a lower one), there will be a decrease in the rate of degradation observed. The storage of the cells at the initial, much higher, temperature condition, however, promoted continual and increased degradation throughout the storage life of the cell. The differential voltage capacity curves demonstrated that the active material losses would continue to increase despite the shift. Had the cell been stored at much less severe conditions over its entire lifespan, the degradation would have been a steady and much smaller decrease with time and would be more likely caused only by a loss of cyclable lithium. These results lead to the observation that the history of storage for a cell will have a dramatic impact on its continual usage.

4.6 Failure of $LiFePO_4$ Cells due to Cycling and Calendar aging conditions

4.6.1 Failure of cells stored under OCP conditions

$LiFePO_4$ cells were stored under different conditions to determine the degradation reactions that were occurring. By storing the cells at much higher temperature conditions than would normally be experienced, degradation phenomena that would not be observed for long periods of time at ambient conditions can be studied.

The two most prevalent modes of degradation occurring within the cell were the loss of cyclable lithium and active material losses. Both forms of degradation were observed, very distinctly, in cells stored at over 50^{o}C (based on differential voltage-capacity curves created). Eventually the capacity within the cells had dropped so far that they could no longer be safely stored within the environmental chambers and were removed.

In addition, the severe degradation caused from storage at these temperatures also promoted the production of gases within the cell. After a cell was removed from storage, cycling of the cell to determine the degradation was performed at ambient conditions and the cells in question did not show any visible signs of swelling during this process. Gas production within the cell was observed only after the cycling procedure was completed and the cell was placed back into storage. For some cells the resulting gas expansion within the cell was quite drastic. From then on, due to safety concerns, the cells were then segregated from testing equipment and were not cycled again.

Cells were stored for a period of 1 to 2 years under ambient conditions. In some cases, the cells retained their respective volumes. Figure 52 displays the extent of swelling experienced by the cells. For cells tested at a temperature of 60^{o}C and 100% SOC.

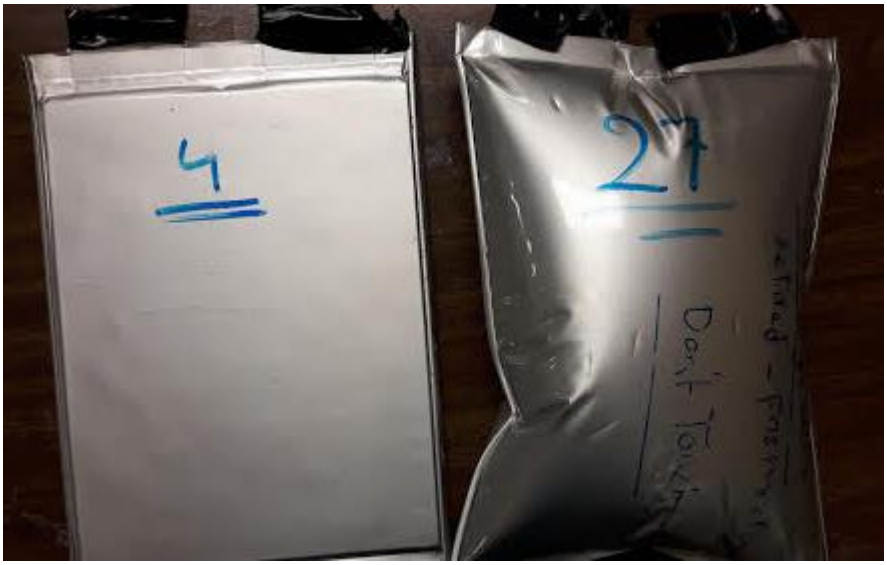

Figure 52: Extent of swelling of aged cell (right) compared to fresh cell (left)

Some cells, however, experienced a volume reduction, in comparison to their initial volumes when first removed from the thermal chamber. These cells were primarily cells stored at 60^{o}C and 0% SOC. When comparing these cells with the ones under discharged conditions, but at the same temperature, the amount of gas produced in the discharged cells was significantly less than those stored under charged conditions. Figure 53 displays the comparison of cells tested under 60^{o}C temperatures at 0% SOC (left) and 100% SOC (right).

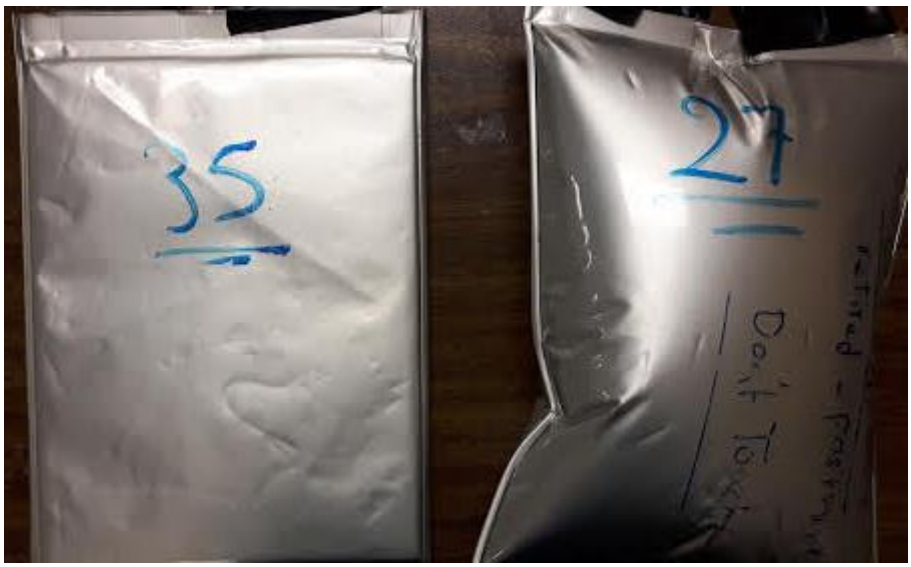

Figure 53: Swelling Observed between Aged cells stored at 0% SOC (left) and 100% SOC (right)

In an article published in 2016, by D.J. Xiong, et al., gas production in vacuum sealed Li-ion cells (NMC/graphite electrode cells) were studied under OCP storage conditions. [82] Full pouch cells were combined with electrolyte and stored at 60^{o}C conditions and 100% SOC. Others were first separated into their individual electrode components, washed with DMC, and the individual electrodes were combined inside pouch bags with electrolyte, before being placed inside thermal chambers. The electrodes contained within the respective bags were fully lithiated graphite and delithiated NMC to match the stored Li-ion pouch cells. [82]

From the results of the article, it was found that there the productions of gases within the pouch bags, with the delithiated NMC, was much greater than the gas production in all of the other tests. [82] Pouch bags stored with lithiated graphite electrodes experienced negligible gas production, while the pouch cells that had not been dismantled at all experienced some gas production but not as significantly as the pouch bags. The conclusion was that the graphite electrode within the cell plays a role in limiting the production of gaseous species. Additional studies of this phenomenon determined that within the pouch cell that the primary gaseous specie produced is carbon dioxide (produced at the cathode). Carbon dioxide in a pouch cell migrates to the anode where it is reduced decreasing the amount of gas within the cell. [82]

This phenomenon was also seen during the calendar aging experiments completed for this research. Cells stored at 60ºC and 0% SOC, showed much greater volumes of gas production during storage when first removed (as described previously), but over the yearlong storage at ambient conditions the volume decreased. As these were full cells and not half-cell electrodes, the loss of gas over time was most likely promoted by the graphite electrode. As the active material of the graphite electrode had not fully degraded (based on the voltage capacity differential curves) it is logical that the remaining active material would allow for the reduction of the gaseous species.

This assessment is also supported by the cells stored at 60ºC and 100% SOC. The most likely reason why the cell volumes stayed relatively the same is because the extent of aging led to severe degradation of the active material at the anode (as seen in differential voltage capacity curves). With the active material lost from the anode electrode the gaseous species within the cell cannot be reduced and the gas within the cell does not decrease.

4.6.1.1 Calendar Aging of LiBs and Influence on Battery Pack Design

Prolonged storage of batteries at extreme conditions has already shown that severe degradation will take place resulting in a high degree of capacity failure and large quantities of gases produced from side reactions occurring within the cell. Figure 52 displays the extent of swelling from storing the cell at 60ºC and 100% SOC. The cells have ballooned outward in a very dramatic way, and if this were to have occurred in a battery pack, there would be insufficient space to accommodate the increase in volume and the cell would subsequently burst. Bursting of the cell will cause exposure of the electrolyte to the air can have very damaging results on the battery pack, resulting in the potential for thermal runaway to occur and fire.

This is an unfortunate failure mode of LiBs as the space between cells cannot be increased. The increase would expand the footprint of the battery pack within the vehicle, resulting in the potential decrease in the range of the vehicle (with removal of cells) and increase in the weight of the battery pack in the vehicle. To protect the battery module or battery pack from catastrophic failure, though, cell vents or tear-away tabs are built into the cells to allow the safe release of gas if excessive pressure builds up. [72] The gas is then expelled from the battery pack by means of a built-in vent, which connects the internal surroundings of the battery pack to those external to the vehicle.

The cell can then be disconnected from the battery through the use of integrated circuitry module so as to prevent further damage to the battery pack and fuses can be used in the battery to prevent electrical fire, spark, and shock hazard. Additional safety features can also be added to detect the presence of flammable gases within the battery enclosure and if the concentration is rising. A signal can then be sent to the controller to increase airflow out of the battery pack case or have vehicle enter into emergency shutdown conditions. Further design considerations for the battery pack include: using self-extinguishing materials inside the battery case, and installing a firewall between battery case and driver and passenger spaces to protect the consumers.

4.6.2 Case study of Safety of cycling $LiFePO_4$ Cells at high and low temperatures

The cycling procedure for these cells was to first perform a characterization test of each cell consisting of a charge, discharge and then a charge to fifty percent of the capacity of the cell. This was then followed by an HPPC test to obtain the resistance at that particular point of the cell's life. This characterization test was completed at four different temperatures (-30^{o}C, 0 ^{o}C, 25 ^{o}C, 60 ^{o}C) using a climate chamber to maintain constant temperature. After the characterization the cell was removed from the climate chamber and cycled for 50 cycles at room temperature.

After 50 cycles of the battery at CCCV cycling, the cell was beginning to experience signs of swelling. After 100 cycles the swelling continued to increase within the cell, but it was only during the characterization following that the cell underwent a catastrophic failure. The characterizations at -30^{o}C, 0 ^{o}C, and 25 ^{o}C had been completed, but during the 60^{o}C characterization the cell experienced an internal short circuit causing the cell to undergo thermal runaway.

Once the cell had reached the upper limits of the test conditions, the equipment entered emergency shutdown conditions and ceased cycling. The cell, though, continued to climb in temperature reaching temperatures over 300^{o}C. Figure 54 depicts the extent of the damage that the cell incurred after the thermal runaway.

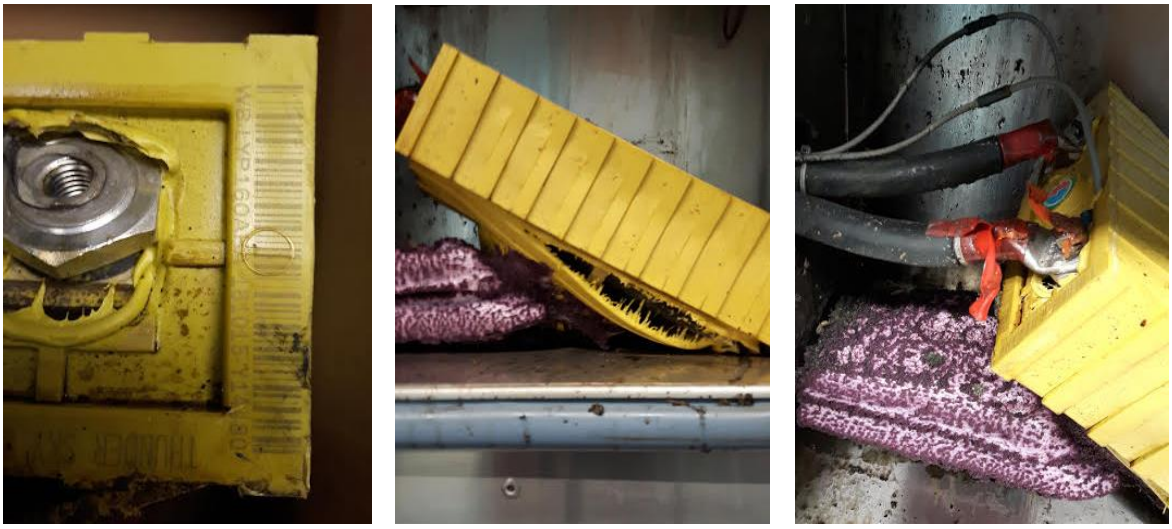

Figure 54: $LiFePO_4$ cell thermal runaway aftermath

The cell was removed from the climate chamber for post-mortem analysis. The reason for the failure was, most likely, due to the fact that the cell was cycled at sub-zero temperatures at $1C_{nom}$. Charging at sub-zero temperatures can result in the plating of lithium onto the negative electrode (anode). If dendrites form and puncture the separator it can lead to a short circuit.

Post-mortem analysis of the battery has revealed severe degradation of the battery has occurred. On the exterior casing the battery had been severely damaged showing significant melting at the contacts and on the side of the cell that was leaning up against the support blocks (Figure 55).

Figure 55: Post-mortem analysis first assessment of thermal runaway

On the interior, the electrodes had become extremely brittle, having dried out from the extreme temperatures experienced during the thermal runaway. The coated LFP and graphite coatings

from the positive and negative electrodes were delaminating from their respective current collectors. Many of the electrodes had actually fused together and required excessive force to separate the layers.

An internal short-circuit is the most likely cause of the thermal runaway, resulting from electrodes within the cell coming in contact with each other to cause the short. A cell is composed of two electrodes, electrolyte, and a separator. If the two electrodes make contact with each other a short can be created. When cycling at low temperatures, there is the risk of deposition of solid lithium metal on the anode of the cell, causing the loss of cyclable lithium. If enough lithium becomes plated onto the electrode it can puncture through the separator and contact the cathode electrode causing an internal short circuit. [83] Lithium plating can also be caused from: cycling the cell at high rates and due to the presence of microscopic metal particles making contact with other parts of the cell. [37]

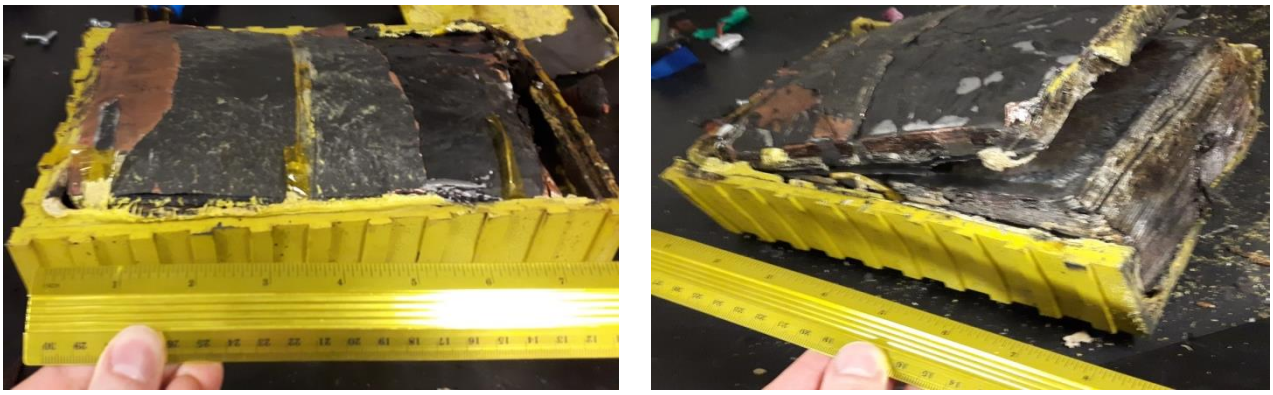

Figure 56: Extent of damage to anodes and cathodes

4.6.3 Thermal Runaway Conditions

When an internal short has been created, the cell discharges through it creating a hot-spot. Active materials will undergo exothermic reactions and given the right conditions (amount of heat generation and insufficient heat removal from the hotspot and the cell) thermal runaway occurs As the cell heats up the separator will begin to melt causing other internal short-circuits to occur, referred to as secondary internal short circuits, and increasing the possibility for the cell to undergo thermal runaway. [83]

In addition to the lithium plating, the swelling of the cell created additional pressure on the electrodes. Forcing electrodes closer together can aid in instigating the internal short-circuit. Gas formation within the cell is believed to have been caused by a number of factors. Based on previous work, gas formation has been found to occur due to the partial reduction of many compounds within the electrolyte. At elevated temperatures and high SOC, oxidation of the electrolyte components can occur at the positive electrode interface resulting in the production of CO_2 and ethylene gas. [69].

In order to remove the excess gas from the cell, a pressure valve installed on the cell will allow small amounts of gas to escape as the pressure in the cell increases. Based on the analysis of the destroyed cell, though, it appears as if the plastic surrounding the pressure relief valve melted sealing the area. Gas was then unable to escape as the pressure rose with the thermal runaway overheat. When the pressure became too great for the casing to endure the thermally damaged casing exploded outward releasing the electrolyte.

Cycling the cell at sub-zero temperatures became the initial catalyst for the destruction of the lithium-ion cell. Combining the lithium plating that occurred with the rigorous cycling at higher than normal temperature conditions aided in furthering the degradation (with the formation of gaseous compounds). After only approximately 100 cycles, the cell eventually lead to the short circuit seen in the figures and underwent thermal runaway. Although, the system was able to shutdown safely and cease cycling the damaged cell it is not able to ultimately protect against an internal short-circuit.

4.6.4 Preventative Measures

As previously discussed, there are a variety of standard safety related technologies to guard against abuse of the Li-ion batteries (external short-circuits, overcharging, etc.). [33] Internal short circuits are particularly hard to prevent from occurring within a cell as they cannot be prevented from adding additional circuit protection. [32] [34] To prevent internal short circuits, lithium-ion cells rely on the use of chemical means to supress the short from occurring.

An overheating cell can cause the separators to distort or melt, which can cause contact between the electrodes and a short circuit to occur. [32] To prevent this much stronger separators or

separators with different physical properties can be utilized. For instance: rigid separators, flexible ceramic powder coated plastic, or shutdown separators. [36]

Rigid separators do not distort even under extreme temperature conditions, but do not prevent against impurities within the cell. [36] [84] A flexible ceramic powder coated plastic, though, prevents contact between the electrodes, resists penetration by impurities, and does not shrink at high temperatures. All of these properties aid in preventing the propagation of a short circuit across the separator, Finally, a shutdown separator contains plastic that melts closing up the pores to avoid a short circuit. Unfortunately, for shutdown separators, when the pores close the cell will no longer function.

If an internal short were to occur, though, its occurrence can be detected by a drop in cell voltage, triggering isolation of the battery from charger or load. [15] [36] This will not prevent the short, but the mitigation will prevent further damage to neighbouring cells and the pack.

Another method for protecting the battery pack from a potential thermal runaway event due to an internal short is by relying on the battery management system. A battery pack has to be equipped with a BMS system to ensure that the cells within the pack do not operate outside of their voltage and temperature thresholds during cycling. In addition, a BMS can isolate a cell in the battery pack if an internal short occurs. This can be detected by a drop in cell voltage, triggering isolation of the battery from charger or load. Once again, the short cannot be prevented, but the mitigation will prevent further damage to neighbouring cells and the pack.

4.6.5 Summary of Degradation Case Study

As previously stated, in the world of battery systems the lithium-ion battery has become the foremost energy storage technology for electric vehicles. [76] Ensuring the proper safety measures are in place to prevent damage to personnel and components are paramount, when running a battery system, whether it is in a laboratory setting or in a battery pack within a vehicle. The reactions occurring under adverse conditions will promote degradation of the cell that can cause Li-ion batteries to potentially fail in a very hazardous manner.

$LiFePO_4$ cells from two different manufacturers were subjected to calendar testing and cycling testing respectively under different temperature conditions. Cells subjected to high temperatures under OCP conditions experienced gas formation, with the highest degree of swelling occurring

at the conditions of 60^{o}C and 100% SOC. If left at the increased temperatures the cells may have potentially undergone thermal runaway damaging the other cells in the chamber. The cells undergoing cycling aging at low and high temperatures promoted both gas formation and lithium deposition. This ultimately led to the cell undergoing thermal runaway. With the cell in an enclosed space minimal damage was done and the program was able to stop itself, but if in a battery pack system external circuits and a BMS could have prevented the cell from being cycled at temperatures below and above it operating points.

Unfortunately, the safety concerns regarding violent failure of the LIB system are a major obstacle to overcome in order for there to be higher consumer appeal of EDV technologies. The cycling of $LiFePO_4$ cells can be very dangerous if operating outside of the operating thresholds of that particular cell. It is crucial that all the necessary safety systems are effectively tested and correctly validated.

4.7 Battery Pack Design for EcoCar 3 Competition

UWAFT has had a long tradition of competing in Advanced Vehicle Technology Competitions (AVTCs). The team has now embarked on participating in the EcoCAR 3 competition, sponsored by the US Department of Energy and General Motors. The task for the university students participating in the challenge is to complete the entire development process, from design to integration, completely re-engineering a stock V6 Camaro into a hybrid-electric vehicle. [41] This will not be the first time UWAFT has designed and built a hybrid-electric vehicle. The team has significant experience in performing the design and building of battery pack systems gained from participating in: the EcoCAR 2 competition, EcoCAR: the Next Challenge and Challenge X which focused on the design and building of FCEVs.

The goals of this challenge are: to improve fuel economy, reduce emissions, and maintain performance of the vehicle. [41] The competition runs over a four-year period, with various milestones having to be completed annually, and, at the end, the teams pursue the goal of having a full operational hybrid-electric vehicle.

4.7.1 UWAFT Procedure for Developing a Battery Pack Design:

UWAFT is currently participating in the EcoCAR 3 competition, the most recent Advanced Vehicle Technology Competition (AVTC) (2014 – 2018), challenging participating universities across North America to re-design a 2016 Chevrolet Camaro. The goal of the competition is to design a vehicle which reduces the environmental footprint of the stock vehicle while maintaining design aspects including safety and consumer acceptability.

Determination of the chosen architecture, in Year One, required developing the requirements set by the team and the competition. These requirements are found in Appendix D: Vehicle Technical Specifications. Teams then use software and model-based design to generate a variety of hybrid vehicle concepts/architectures that attempt to meet the requirements and would be innovative to build in the following three years of the competition. Based on the assessments, which used tools such as MATLAB/Simulink, Autonomie, and Unigraphics NX, UWAFT selected a split-parallel architecture for construction. The selected architecture is unique in the fact that the vehicle can run in series, parallel, or split operation depending on the SOC of the battery and the torque demanded by the driver.

In accordance with choosing the architecture, a selection of the battery pack modules (number and configuration) was completed. Utilizing battery module data provided by the competition, through two suppliers, UWAFT was able to decide upon a module design that met the desired vehicle technical specifications (VTS). Table 15 outlines the module designs that UWAFT could select from.

Table 15: Battery pack options for EcoCAR3 competition

Manufacturer	Model	Capacity (kWh)	Peak Current (A)	Continuous Current (A)	Nominal Voltage (V)
A123	6x15S2P	10.8	350	115	292
A123	7x15S2P	12.6	350	115	340
A123	6x15S3P	16.2	520	175	292
A123	7x15S3P	18.9	520	175	340
Enerdel	PE 350-394	12.1	105	70	317
Enerdel	PP 320-394	11.2	320	125	317

The battery chosen for the vehicle is a 16.2 kWh A123 pack, which uses six 15S3P modules, which are connected in a series configuration. Based on the analyses and simulations performed,

this pack configuration is able to provide the user with approximately 70 km of all-electric range, meeting the daily driving range of North Americans of 40.55 km. [85] Based on the specifications outline in Table 15, the pack can run at a nominal voltage of 292 V, and can provide a peak current of 400 A to the two electric motors. Figure 57 displays the battery pack configuration and equipment provided by A123.

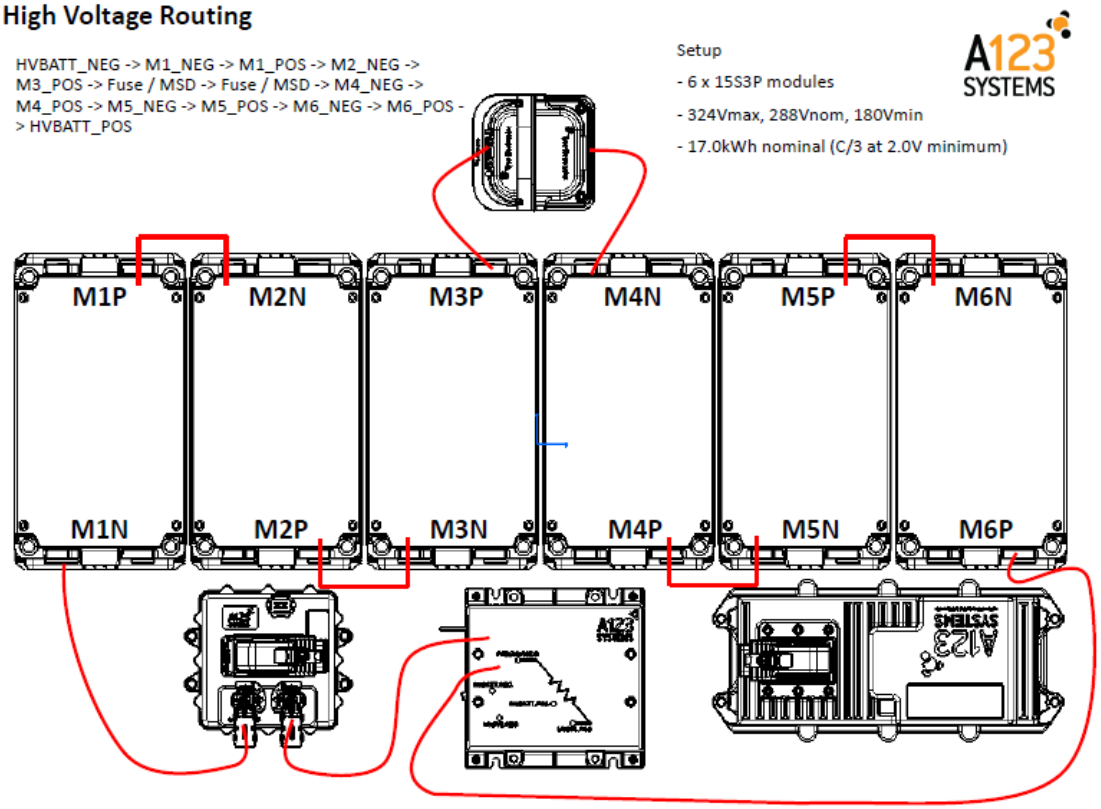

Figure 57: High Voltage Routing for A123 Battery Modules in a 6x15S3P Arrangement [86]

Equipment provided by A123, to construct the battery pack, includes: the battery modules, the Current Sense Module, the BMS, and the battery contactors. [86] From this initial stage, UWAFT then designs and builds the battery pack enclosure and pack configuration to surround the system, providing it protection and safeguarding consumers from the high voltage connections, in accordance with EcoCAR3 Safety requirements. [41]

4.7.2 Construction and Design Criteria

The vehicle supplied by GM is a stock 2016 Camaro with all of the stock vehicle components. [41] Utilizing the stock structure, the team must determine how to modify the vehicle to accommodate the components of the new architecture. The team must not, however, make any major structural modifications. [41]

When considering the design of the battery pack, there are several criteria which need to be considered. First and foremost, as required by the competition, the vehicle has to have a curb mass of 1860 kg. [41] As the battery modules are one of the heaviest components being integrated into the vehicle significant work must be done to keep the mass of the design low, while being able to meet load requirements. In addition, being able to lower the mass of the vehicle will aid in meeting the performance and fuel economy. Also, it is important to consider the ease of fabrication of the mounts. If the design is very complicated it will be time-consuming to construct as it may require specific equipment and costly. [87] Finally, as high voltage is a very dangerous hazard present in the vehicle, with the incorporation of a battery pack system, significant design work has been performed to ensure safety of the component and that it conforms to competition and vehicle standards. [41] [86]

4.7.2.1 Placement

When considering the placement of the battery pack for installation in the vehicle, the size of the components and their general safety have a dominant impact on determining its location. To protect the battery pack in the case of a crash, the battery pack cannot be located in any of the crash zones of the vehicle, eliminating select areas in the engine bay and trunk as they are designed to crush in the event of a collision. [41] Thus, the decision was made to situate the battery pack in the front of the vehicle's trunk. The trunk is the only location with the area to accommodate the modules and fulfills the necessary requirements for the rules of the competition. Based on the designs, the battery pack enclosure can be built into the trunk to optimize both passenger and cargo capacity. With the remaining trunk area, additional powertrain components, required for the hybrid retrofit, can be installed as well.

4.7.2.2 Load Cases for ESS Mounting Structure

Battery pack assembly is crucial to ensuring the safe-guarding of the batteries within the battery modules and protecting consumers from high voltage and fire hazards (if punctured Li-ion cells

will explode). A battery pack enclosure needs to be finger-proof so as to protect from the battery's lethal electrical potential, and the battery frame must be designed from durable materials and be able to sustain loading conditions endured during operation of the vehicle. [41] If the battery pack modules were to become dislodged and slide out of alignment they could become severely damaged resulting in potential harm to the consumer. In order to properly hold the battery modules in place, the battery frame is to be designed to withstand the following loading conditions from the competition [41]:

- 20g Loading in the Front – Rear Longitudinal Direction;
- 20g Loading in the Left – Right Lateral Direction; and,
- 8g Loading in the Up – Down Vertical Direction.

4.7.2.3 Space Claim:

Due to the limited space, and requirements of the competition to maintain cargo capacity, a space claim analysis for the trunk space was completed. By maneuvering the modules in different arrays inside the trunk area, the team could find the best fit. [87] The following images, Figure 58, Figure 59, and Figure 60, show three of the preliminary module configurations that were considered for placement within the vehicle's trunk. The vehicle CAD has been removed due to confidentiality reasons.

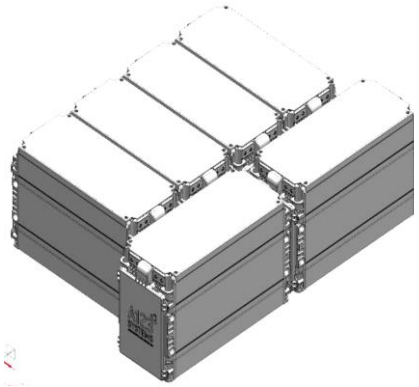

Figure 58: Module Design 1

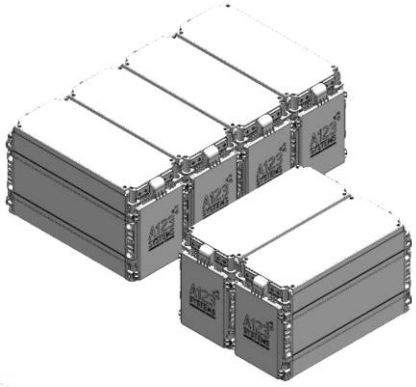

Figure 59: Module Design 2

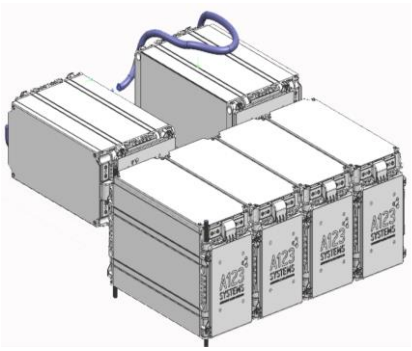

Figure 60: Module Design 3

The module configuration determines how the mounting structure will be designed to hold the modules. After the space claim analysis, Figure 60 was chosen based on its smaller volume, height, and weight considerations. [87]

4.7.2.4 Mounting Structure:

Module placement determines how the mounting structure will be designed to hold the components. The mounting structure of battery pack is comprised of two sections: a lower and upper section. In the upper section, this mount will hold two of the six modules, with the modules lying on their side to decrease the overall height of the battery pack in accordance with the space claim. The lower section will houses the remaining four modules, standing upright, side by side. The mounting structure was then developed from many iterations of design optimization. This was completed using the team's CAD software. All design work is completed using Siemens Unigraphics NX 9 software.

In order to maintain structural stability and reduce the overall weight of the vehicle the battery mount will be constructed out of 6061 aluminum. 6061 aluminum is approximately three times lighter compared to the 4130 steel used to make up the EcoCAR 2 battery pack. For the preliminary design of the battery pack, the enclosure shall be constructed out of aluminum, but subsequent designs will be constructed from carbon fibre. The carbon fibre construction will further aid in the weight reduction of the vehicle and work towards the team's goal of achieving a 47/53 weight ratio.

4.7.2.5 Structural Considerations: Structural FEA

Structural Finite Element Analysis (FEA) is used in structural mechanics to develop a numerical solution as to the structural integrity and durability of complex systems. [87] The technique is completed on the final design of the structure, to ensure that it can withstand the loading conditions, with a safety factor of 1.5. These loading conditions are the same as those used during the optimization, and are placed at the center of gravity of each battery module. All optimization/FEA is completed using Altair Hyperworks 13. Iterations are made on the exact design of the frame based on FEA results. The results of the FEA analysis show areas where the frame can become damaged under load and require further design iterations if they do not meet the requirements. After subsequent iterations UWAFT submitted a design that passed the Preliminary Design Review for the EcoCAR 3 competition and are now integrated into the vehicle.

4.7.2.5.1 Meshing

In order to be able to perform the FEA analysis the mounting structures need to have a meshing system applied to both. The battery pack is initially set up in NX and then the geometry is

imported to Hypermesh, The Hypermesh program allows the user to create two-dimensional shell elements and three-dimensional solid elements in the imported object to calculate the stress and strain over the entire geometry. The designer initially sets up the design and non-design spaces where the optimization solver can and cannot place material to meet the loading conditions. The battery assembly is primarily made up of shell elements, simulating the aluminum tubing and plate which the structure is made up of. Shell elements are used as they best represent the bending that may occur in the thin frame members.

Figure 61 and Figure 62 show the completed meshing of the upper and lower sections of the battery frame. To achieve the proper meshing of the elements, 5 mm CQUAD4 and CTRIA3 first order shell elements were utilized. To model the effect of having the modules placed onto the mounts and to distribute the loads at the boltholes spokes were created using RBE2 rigid elements from the center of the bolt hole to the edge of the bolt hole. These RBE2 elements were then connected together to represent the center of gravity of each battery module.

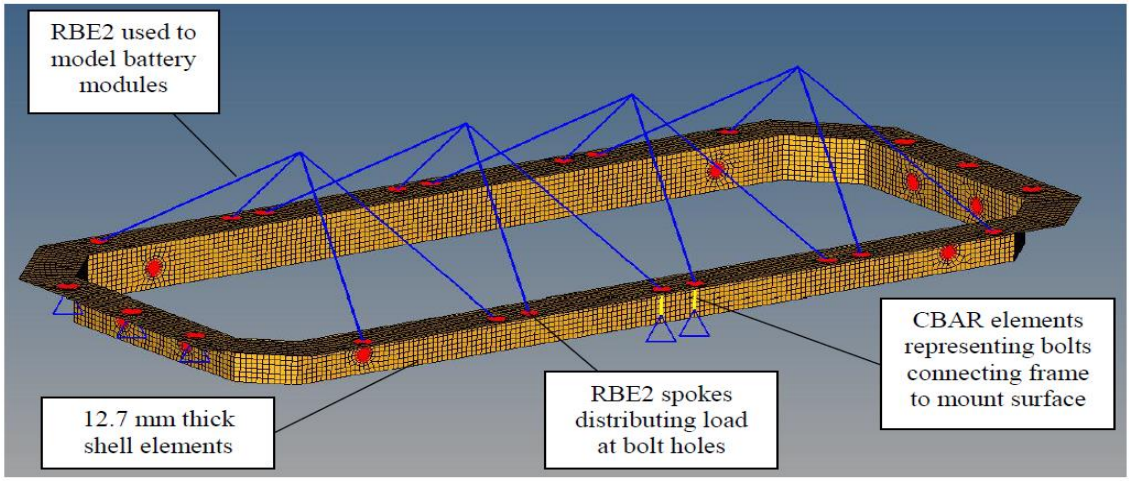

Figure 61: Meshing of lower battery mount

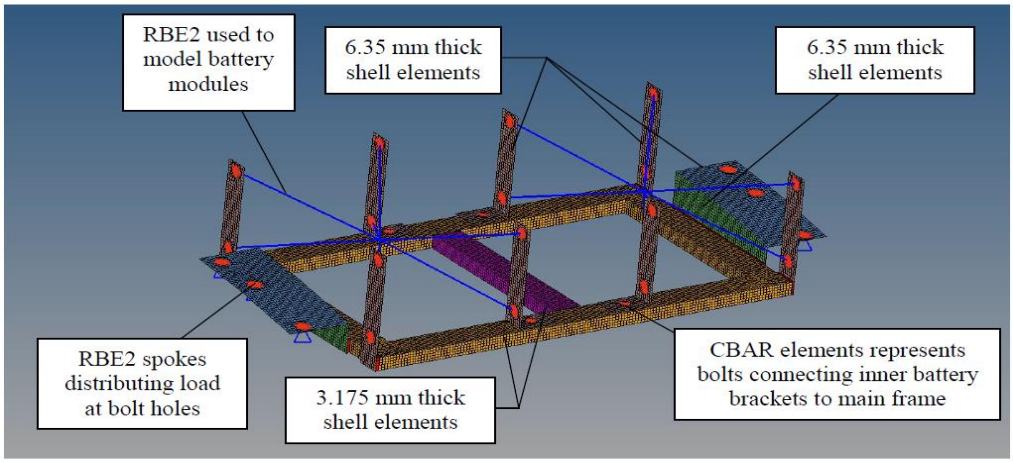

Figure 62: Meshing of upper battery mount

All six degrees of freedom are fixed at the mounting holes of the battery frame. The load and constraint locations are shown in Figure 63.

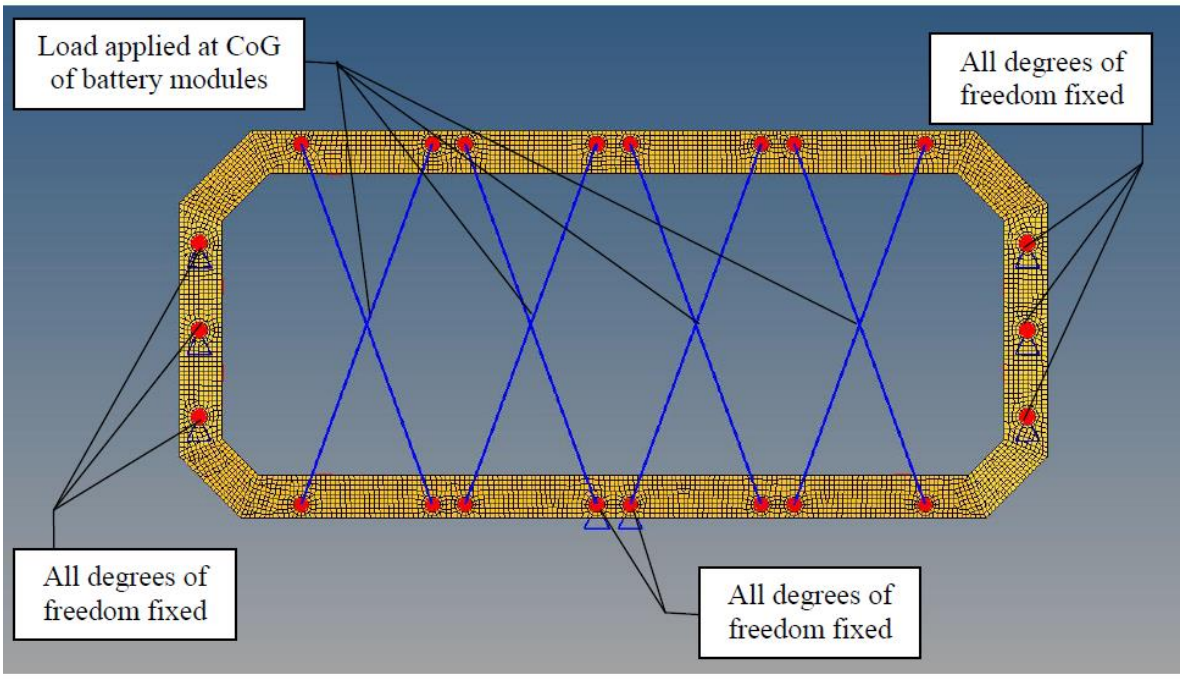

Figure 63: Load and constraint location for upper battery frame

The loads for the load cases were applied to the center of gravity of each of the battery modules. All six degrees of freedom are fixed at the mounting holes of the battery frame. The load and constraint locations are shown in Figure 64.

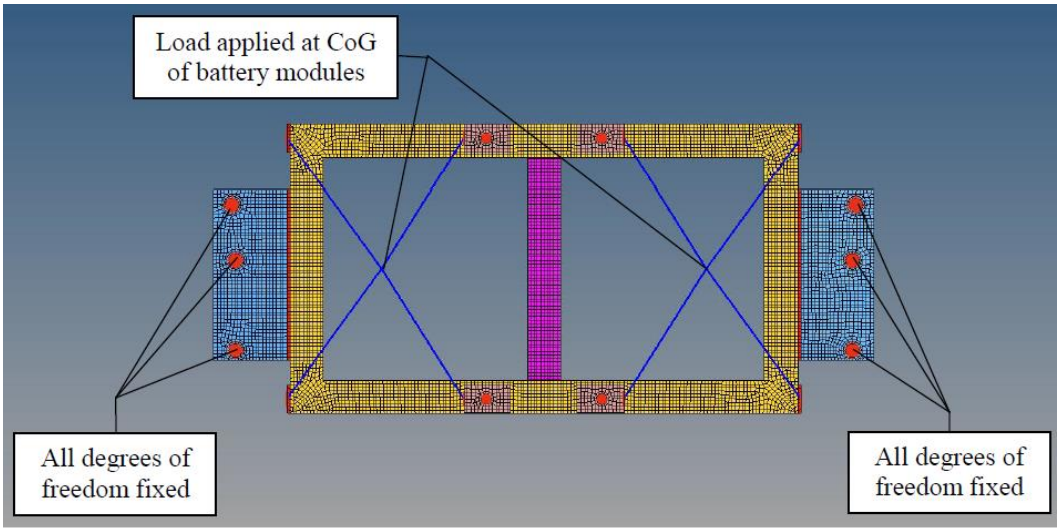

Figure 64: Load and constraint location for upper battery frame

4.7.2.5.2 Upper Frame Finite Element Analysis

As the battery mount is split into two sections, the FEA can be split into two separate analyses. The loading conditions are the same as those used during the optimization, and are placed at the COG of each battery module. Starting with the upper battery mount, Figure 65 through Figure 67 display the FEA analysis completed for each of the loading cases for the upper mounting section. Table 16 also describes the results of the FEA analysis.

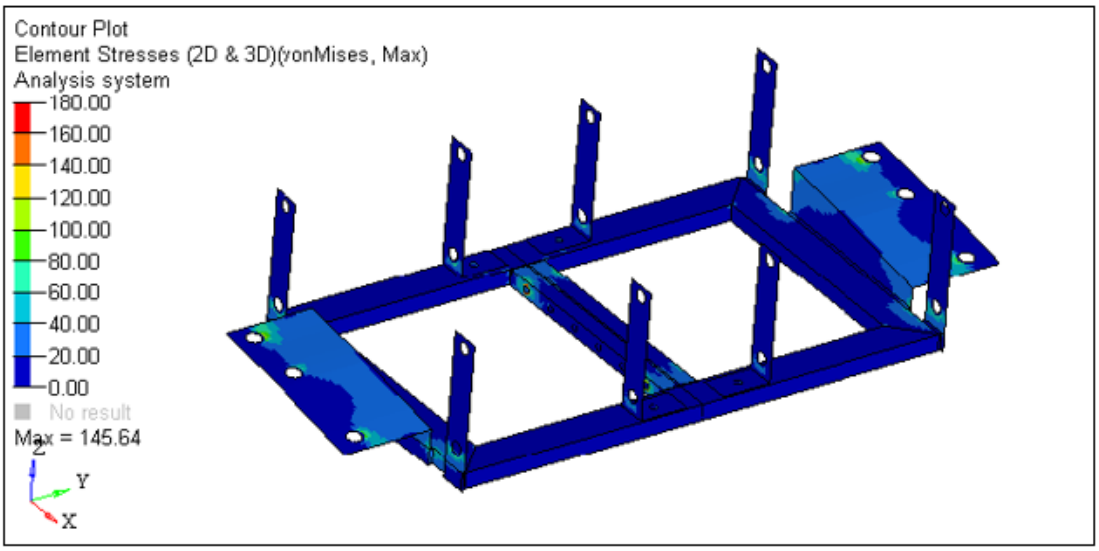

Figure 65: Upper frame design von Mises stress contour for 20g longitudinal load case

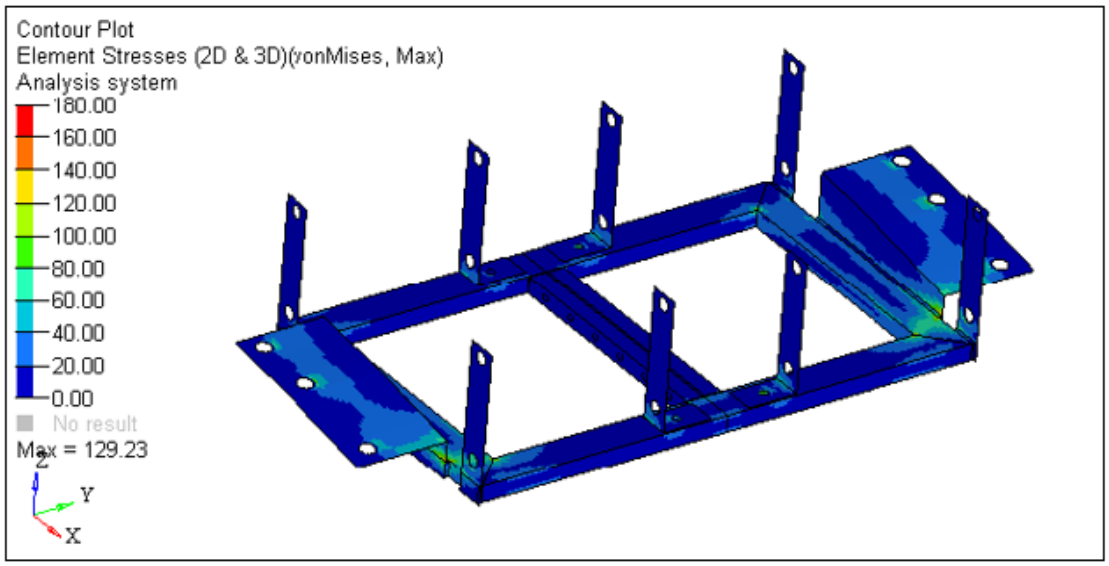

Figure 66: Upper battery frame design von Mises stress contour for 20g lateral load case

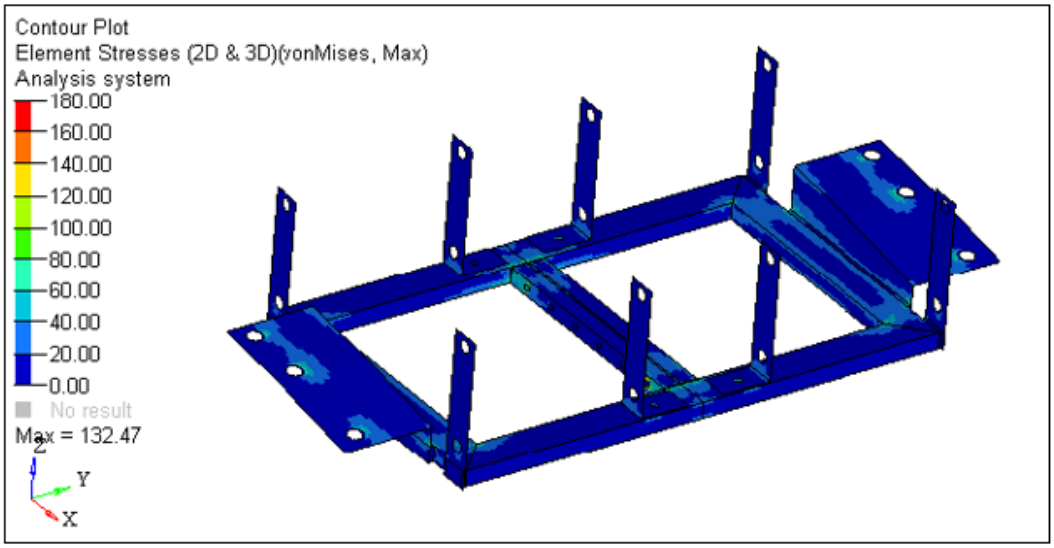

Figure 67: Upper battery frame design von Mises stress contour for 8g vertical load case

The areas indicated in blue in the figures, show that the depicted areas endure minimal loading in most areas. In all of the figures, there are no areas that endure very high stress (depicted in "red"), and the areas that are depicted in "green" are within tolerance levels for what the mount can endure, as the safety factors calculated (shown in Table 16) exceed the 1.5 safety factor required by the competition.

Table 16: Upper Battery Frame FEA Results

Load Case	Maximum Stress [MPa]	Safety Factor	Contour Plot
20g Longitudinal	145.64	1.7	Figure 65
20g Lateral	129.23	1.9	Figure 66
8g Vertical	132.47	1.8	Figure 67

Based on the FEA analysis done for the upper section, the design will meet the load specifications and not plastically deform under static conditions. Under all of the loading conditions the safety factor for the mount was found to be in excess of the 1.5 factor as set by the competition, resulting in the frame being appropriate for construction.

4.7.2.5.3 Lower Frame Finite Element Analysis

The figures depicting the FEA analyses of the three different loading cases are shown in Figure 68 to Figure 70. Table 17 also describes the FEA analysis of the ESS lower section.

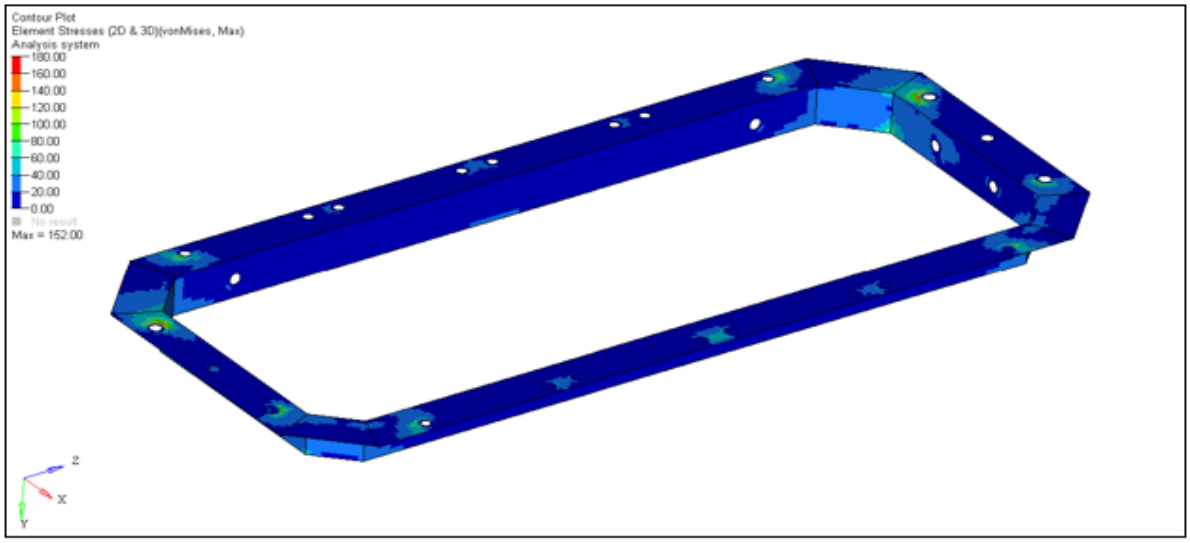

Figure 68: Lower frame von Mises stress contour plot for 20g longitudinal load case

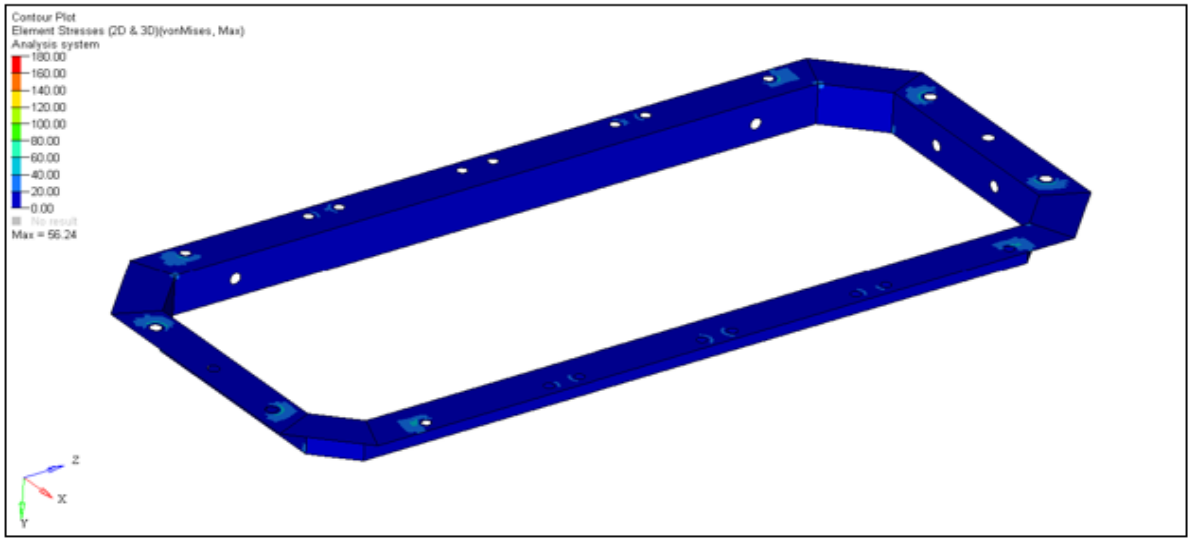

Figure 69: Lower frame von Mises stress contour plot for 20g lateral load case

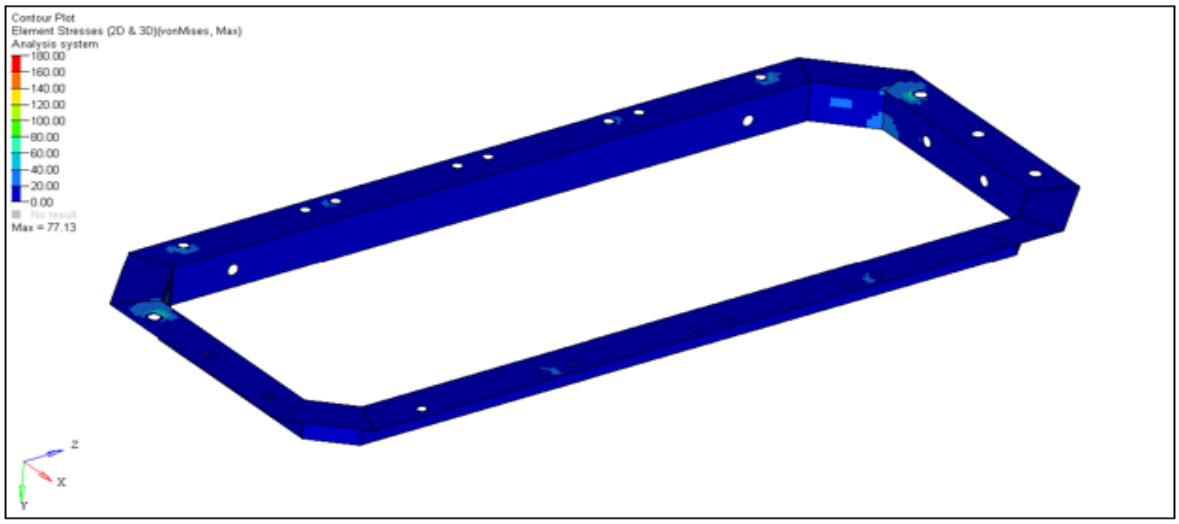

Figure 70: Lower frame von Mises stress contour plot for 8g vertical load case

Once again, it was found that the areas endure minimal loading in most areas. In all of the figures, there are no areas that endure very high stress (depicted in “red”), and the areas that are depicted in “green” are within tolerance levels for what the mount can endure, as the safety factors calculated (shown in Table 17) exceed those required by the competition.

Table 17: Lower Battery Frame FEA Results

Load Case	Maximum Stress [MPa]	Safety Factor	Contour Plot
20g Longitudinal	152.00	1.6	Figure 68
20g Lateral	56.24	4.3	Figure 69
8g Vertical	77.13	3.1	Figure 70

As the design was able to meet all of the load conditions, Figure 71 and Figure 72 became the resulting design for the battery pack for the Camaro. The figures are the CAD images of the battery mounting structure.

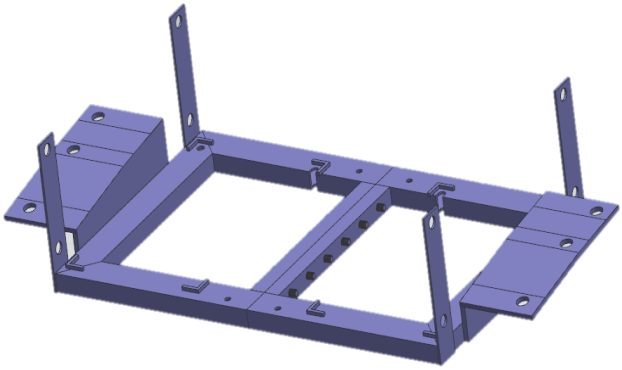

Figure 71: Upper mounting Structure of ESS

Figure 72: Lower Mounting Section of ESS

4.7.3 Additional Requirements

4.7.3.1 High Voltage Interlock Loop

As the ESS operates at high voltages, it is required that the system have a high-voltage interlock loop (HVIL) installed. An HVIL circuit consists of a series of switches that will disconnect the battery from the other HV sources. [88] In the event that someone attempts to tamper with a system connected to the HVIL circuit, the circuit will disconnect and result in the system being de-energized, rendering the system safe to repair, service, or install. [88] In accordance with competition rules and electric vehicle regulations [89], the team has installed the circuit indicated in Figure 73 into the ESS system.

The HVIL circuit in question combines the Manual Service Disconnect, inertial switch, and both emergency stop switches into the circuit. If any of these pieces of equipment are triggered the circuit will open and prevent current from flowing from the battery.

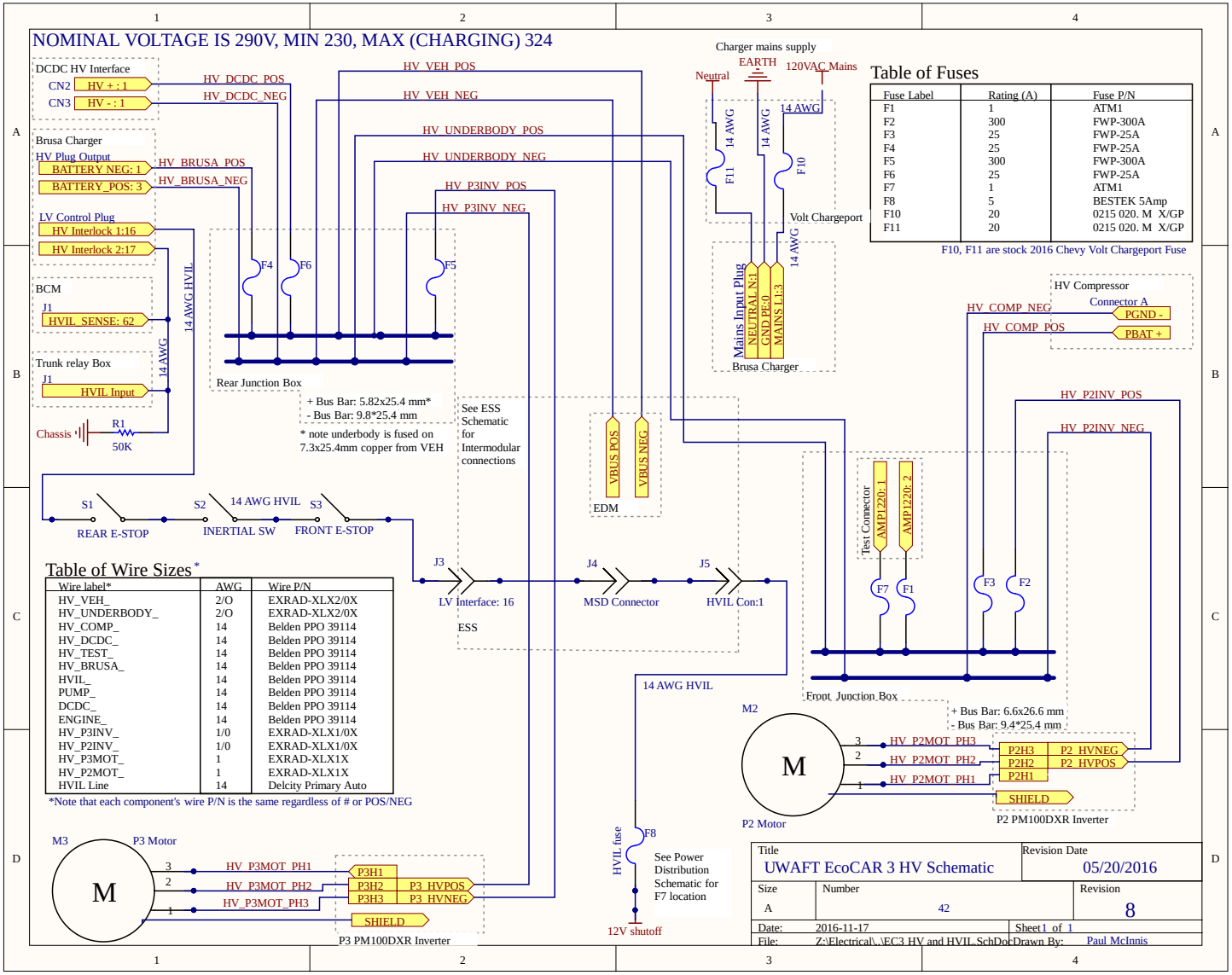

Figure 73: High Voltage Schematic for UWAFT Team

4.7.3.2 Venting

As previously described, gases can build-up in cells and be released within the battery pack enclosure. In order to prevent the continual build-up of gases within the enclosure, a built-in vent, connecting the internal surroundings of the battery pack to those external to the vehicle, aids in the expulsion of the gases. The vent needs to have adequate flow to avoid excess pressure buildup of gases, should the cells within the battery pack fail.

Requirements for placement of the vent on the battery pack are that the vent on the pack side should be located as high as possible and must be above the expected vehicle water line to prevent water intrusion. For routing the vent gas line connection to the external surroundings, there should be at least one bend (angle greater than 45 degrees), to prevent splash from entering the pack, and the vent path must have no areas where water can accumulate. Also the connection should slope towards the output to allow any water in the vent line to drain.

In accordance with these requirements UWAFT has provided the following vent location in the battery pack (Figure 74), which has easy access to connect the hose to the passenger side rear wheel well vent.

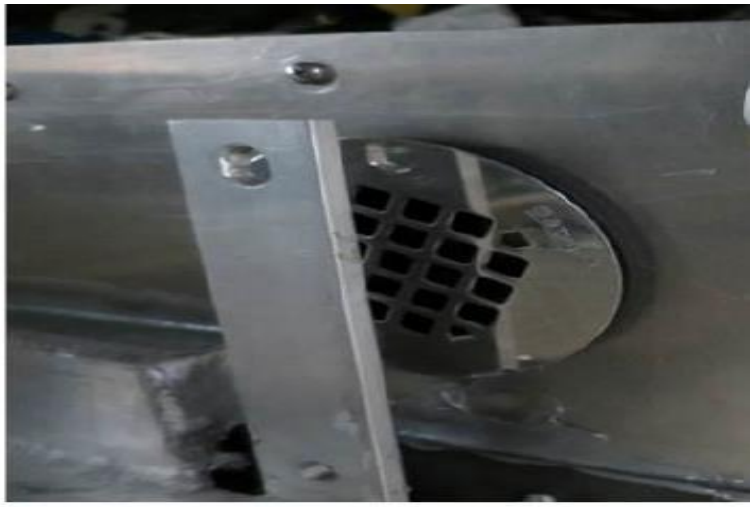

Figure 74: Battery Pack Vent

4.7.3.3 Manual Service Disconnect (MSD)

Battery packs built for the EcoCAR3 competition must incorporate a manual service disconnect (MSD) into the battery pack configuration. Its role is to disconnect and de-energize the ESS HV

electrical system while service is performed on the vehicle. [88] The MSD also acts as a vital part of the HVIL system, preventing an external short circuit and “breaking” the connection in the middle of the pack to split the pack potential in half. [88]

4.7.3.4 Battery Management System

In order to ensure that the battery in an electric vehicle is able to sustain life for the duration that it is required by consumers, a comprehensive controls sequence is utilized to limit battery degradation. [32] The battery management system (BMS) measures the overall SOH of the battery pack and controls the current, voltage, temperature, and other parameters of the system when in operation. [45] For lithium-ion batteries safe-operating windows are very strict and exceeding these restrictions will lead to rapid degradation and even result in safety complications [15].

5 Warranty Simulation Lifespan Analysis of a $LiFePO_4$ Battery Pack

Long term studies of the life of a product (many years in duration) must be performed using a simulation. The long-term nature of the project would create heavy costs to track the various parameters associated with a product at each of the stages, from initial construction to eventual end-of-life (80% of remaining capacity within battery pack). Using the model described in Section 2.8.3, a life cycle model can be developed to analyse the battery pack capacity over a long-term lifespan. As the criterion for an EV battery pack is at least 10 years of life, simulations of the battery pack life cycle will be completed over this duration. In doing so, an assessment of the amount of degradation, as a result of cycling aging, can be compared to that of the total calendar aging degradation.

5.1 Modeling degradation

The two degradation modes that need to be modeled are cycling and calendar aging. Each degradation mode relies on different parameters in order to calculate the extent to which the cells will degrade within a battery pack.

5.2 Calendar Aging

Based on the research completed by Ecker et al., they were able to develop a semi-empirical model for the calendar aging of lithium-ion batteries, utilizing the parameters of: temperature, aging period, and potential which is related to the SOC of the cell. The equations can be found under Section 2.8.3.

5.3 Cycling Aging

For the cycling aging model, the work done by Wang et al. was selected to represent the degradation of cells due to cycling. Results from testing of $LiFePO_4$ cells aged by Wang et al. found that the capacity fade is primarily caused from the loss of active lithium, mostly associated with degradation at the anode. The team analyzed the effects of: time, temperature, depth of discharge, and rate of discharge. From their work, the following semi-empirical model was developed (Equation 5.1):

$$Q_{loss} = Bexp\left[\frac{-31500}{RT}\right](Ah)^{0.55} \quad \text{Equation 5.1}$$

Where Q_{loss} is the capacity lost within the cell over the duration of cycling, B is the pre-exponential constant, R is the universal gas constant, T is the temperature in Kelvin, and Ah is the number of amp-hours that flow through the battery. Fitting of the parameters for the above equation is determined, once again, through a regression analysis. It should be noted that the parameters for the above equation are fitted for the $LiFePO_4$ chemistry and cannot be used for other battery chemistries without completing the same testing and fitting the model.

5.4 Model Parameters' Identification Method

Long term studies of the life of a product (many years in duration) must be performed using a simulation. The long-term nature of the project would create heavy costs to track the various parameters associated with a product at each of the stages, from initial construction to eventual end-of-life (80% of remaining capacity within battery pack). Using the model described in Section 5.2, a life cycle model can be developed to analyse the battery pack capacity over a long-term lifespan. As the criterion for an EV battery pack is at least 10 years of life, simulations of the battery pack life cycle will be completed over this duration. In doing so, an assessment of the amount of degradation, as a result of cycling aging, can be compared to that of the total calendar aging degradation.

5.5 Simulation Assumptions

Certain assumptions will be taken into account in this life cycle model to simplify the system. All of the cells in the battery pack will be considered to have the same chemistries and physical parameters. Thus, the aging processes will be similar in each cell over the ten year simulation. As an extension, the battery pack itself will be considered as an entire system, with temperatures assumed to be constant (35^{o}C) during cycling, as controlled by the on-board BMS. During points when the vehicle is in the "off" condition the battery will be susceptible to the surrounding temperature conditions (daily temperature data, for the Waterloo area, for the weather conditions outside of the vehicle), with the degree of degradation being dependent on those conditions. Transients of the temperature depletion from "on" state to "off" state will be removed as the total time duration in the "off" condition is much greater than the time it takes to reach the temperature outside of the vehicle.

Assessing the aging at each individual time step of the simulation will be too small to create significant loss in the battery thus, the aging time is summed until the system reaches a point where the vehicle is activated and the system will begin to run. As the effects of the drive cycle need to be captured in the simulation a one second time step is selected. The total number of amp-hours being fed through the battery then has to be calculated over the time period to assess the cycling degradation.

In order to simulate the vehicle being driven each day for the ten year span, a drive cycle was developed for a typical consumer to drive each day for a morning commute to work, go into engine-off storage conditions for an eight hour work day, and then have a drive cycle for the commute back home. The assumption for this vehicle is that it will only be used to drive to and from work to simplify the analysis. Weekend driving is also included to account for the driver completing additional tasks, but will follow the same driving pattern for simplicity. The vehicle is charged overnight and the cycle repeats.

5.6 Vehicle Model

5.6.1 Proposed Architecture:

The vehicle architecture selected for this study is a fully electric vehicle, or a Battery Electric Vehicle (BEV). As the name describes, the primary energy source is a battery pack. This electrical source can be charged from the grid and recharged during driving using regenerative braking. To provide propulsion, DC electrical energy from the battery is converted into AC to provide power to the motor. The motor converts the electrical energy into mechanical energy and transmits it through the vehicle's transmission, axles, and finally to the wheels to meet the road load. Figure 75 displays the architecture described for a typical BEV. (Iqbal Husain, Electric and Hybrid Electric Vehicles Design Fundamentals, Second Edition)

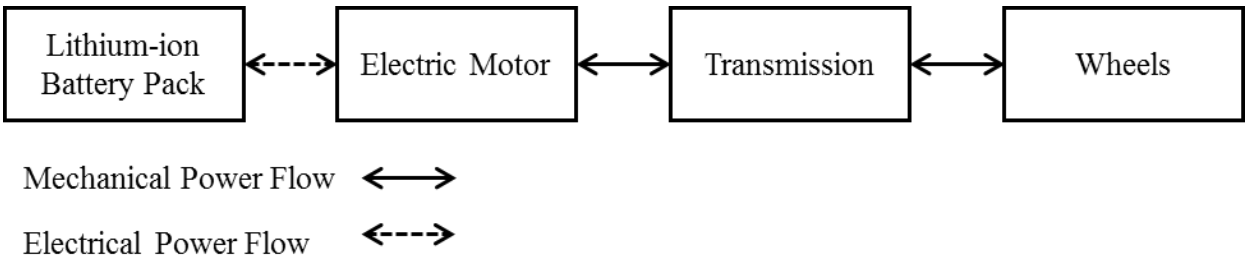

Figure 75: Vehicle Architecture

For batteries in pure electric vehicles the conditions become much more simplistic. When the vehicle is moving, other than a little braking regeneration, the batteries are mainly undergoing discharge [90]. When the vehicle is being charged in a charging station, their batteries are in a charge state. If the system is not being charged or discharged, the vehicle is in open circuit conditions.

The vehicle being utilized in this study for simulation of the degradation is a 2016 Camaro. The Camaro has been retrofitted into a plug-in hybrid electric vehicle (PHEV) by the UWAFT team to participate in the EcoCAR3 competition. Since the work is analyzing the degradation of the batteries within the vehicle, the assumption of this work is that the vehicle will only be driven as an electric vehicle and will not utilize the engine satisfying the vehicle architecture in Figure 75.

The battery pack currently in the vehicle is composed of six LiFePO4 battery modules arranged in series. This yields a total nominal voltage and nominal capacity of 292 V and 58.8 Ah respectively. The battery modules are provided by A123 Systems and the configuration within each module is that there are three strings of fifteen cells (15s3p). From simulations of the powertrain, using the Autonomie software, the vehicle was able to attain over 70 km of range simply using the battery pack and charge depleting from 90% SOC to 10% SOC. The electrified range is well within the limits of the simulation which will require approximately 59 km of range (not taking into account the battery receiving energy from regenerative braking).

5.7 Fitting the Data and Model Verification

The data obtained from the cell degradation was used to fit the parameters of the Ecker et al. equation using the built-in "nlinfit" function within Matlab. The resulting values of the parameters are displayed in Table 18.

Table 18: Fitted parameters of calendar aging model

c_A	c_T	c_V
9.40349505079611e-05	5.1901857057731	1.08931697767615

Due to time constraints, parameter identification for the cycling aging model was done using the manufacturer's data. In another researcher's future work, a cycling aging battery model will be developed, but it is currently beyond the scope of this work.

5.7.1 Model Verification

In order to verify the model being generated from the non-linear fit operation, a subset of the data collected was selected. The parameters for these data points were used in the model to generate comparison results. It is important to note that results with capacities lower than 15 Ah (25% or greater capacity loss within the cell) were omitted as the extent of degradation includes both the loss of cyclable lithium and active material loss. Since the study is mainly focusing on the loss of cyclable lithium over time in the battery pack, considering the data from cells that experienced such severe degradation would not yield a representable model. The loss of active material will lead to issues when operating with a BMS and may cause a complete cell failure. Therefore, such data points will not be included for the purpose of the creation of the model or its validation.

The capacity loss determined from the model was compared to the data from the experiment using the root mean squared error formula.

$$RMSE = \sqrt{\frac{1}{n}\sum_{i=1}^{n}\left(y_i - f(x_i)\right)^2} \qquad \text{Equation 5.2}$$

Where y_i is the actual value and $f(x_i)$ is the predicted value, and n is the number of data points. Validation of the model was completed by taking 10 random data points from the collected data, omitting them from the non-linear regression model, and then utilizing them to generate a predicted value based on the calculated model parameters. The RMSE value was then calculated.

The RMSE was determined to be 0.025. This shows that the difference between calculated capacity loss and the data measured from experiments is very small, which shows that the model fits well with the experimental data.

5.8 Battery Control System of Simulation

In order to ensure that the battery in an electric vehicle is able to sustain cell life for the duration that it is required by consumers, a battery management system (BMS) implements various strategies to limit battery degradation and ensure safety constraints are met. To ensure the strategy is effective, and to ensure that cell health is adequate for function, the BMS measures the overall cell SOH and manages the operation parameters of the system to keep them within safe bounds. In lithium-ion batteries, cell SOH is important as safe-operating windows are very

strict and improper management leads to rapid degradation and this can develop safety complications [15]. Specific ways the BMS can minimize degradation and safety hazards are: managing charge/discharge voltage and current, and by monitoring cell temperature.

When charging or discharging, it is critical that the cell voltages are maintained within the operating range (2.0V and 3.65V for Lithium-Iron Phosphate) [16]. As voltage is not being tracked in the model, capacity thresholds shall be utilized instead. The vehicle shall be discharged to 10% SOC and charged to 90% SOC. Charging to a full 100% SOC and discharging all the way to 0% SOC greatly increases the cell degradation that can occur.

Temperature conditions of the $LiFePO_4$ cells cannot go below -30^{o}C or above 55^{o}C during cycling. The BMS measures each individual cell to ensure that the temperature does not exceed these thresholds. Many BMS systems will actually prevent a user from operating the battery pack or optimize the temperature of the battery pack. In Tesla's electric vehicles, if the temperature of the battery pack falls below freezing, the car will not permit charging, as this will damage the cells [91] [92]. This is very beneficial in maintaining the life of the battery pack, but in the short term, until the battery pack warms up, regenerative braking is lost. Protocols in the simulation will dictate that during charging and discharging that the cell will only be able to be charged and discharged at 25^{o}C.

5.9 Simulation Results

The simulation was run for a period of ten years. Each day the drive cycle was run twice and the battery was charged at the end of the day. As the system being analyzed is specifically the lithium-ion battery pack, the drive cycle was converted from a vehicle speed demand value to a realistic current demand value for an HEV. The values of current for each time step in the drive cycles were determined by utilizing Autonomie and analyzing current output from the battery pack. The current profile is depicted in Figure 76.

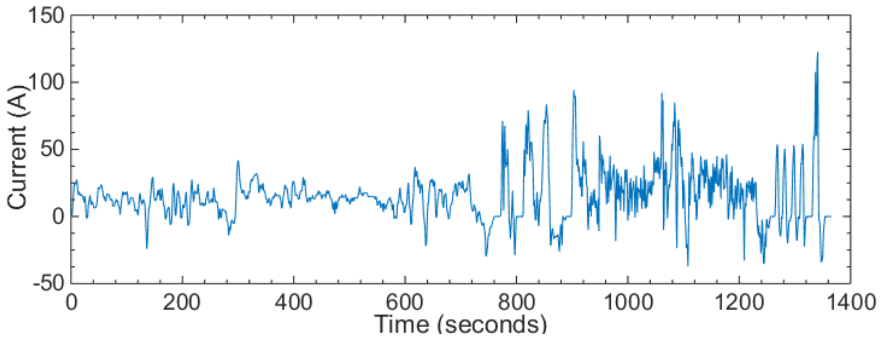

Figure 76: Current profile of drive cycle for battery pack

Using this profile to cycle the battery, the aging of the battery pack can be investigated under realistic operation conditions.

5.10 Temperature:

Figure 77 through Figure 80 display random samples of the temperature conditions that the battery pack experiences on a given day within a particular time of year, going from winter to fall. The first two figures are for temperature conditions in the Waterloo area, and the second two figures are for temperature conditions in Tampa, Florida. As the duration of the simulation is going to be for ten years and the vehicle is only operational for a short period of time throughout the day, transient temperature fluctuations have been removed from the system. Also, in this system it is assumed that the operating temperature of the battery pack can be maintained as a constant value.

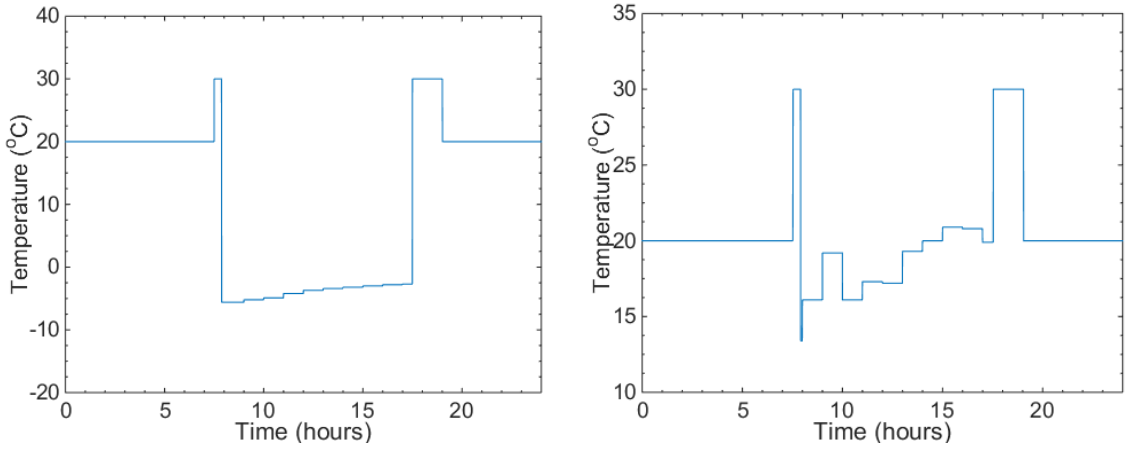

Figure 77: Temperature samples for a random day in the Waterloo data for winter (left) and spring (right)

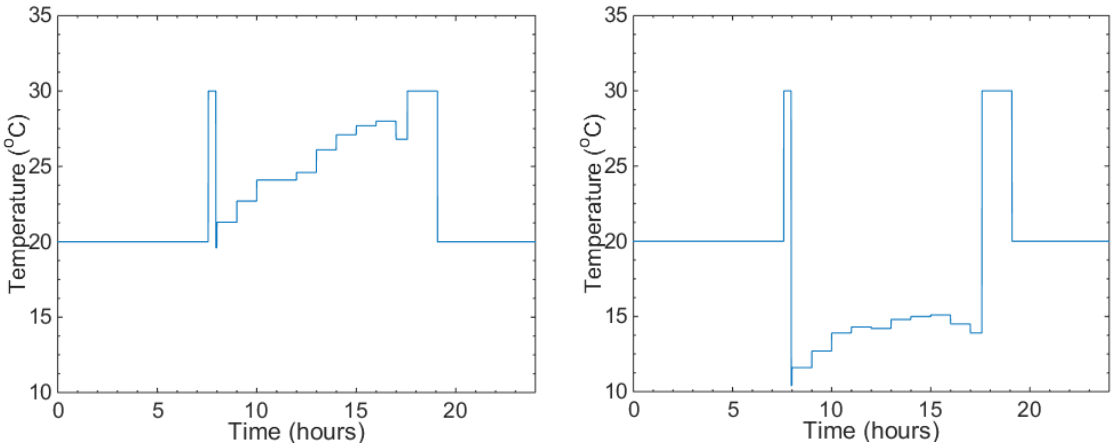

Figure 78: Temperature samples for a random day in the Waterloo data for summer (left) and fall (right)

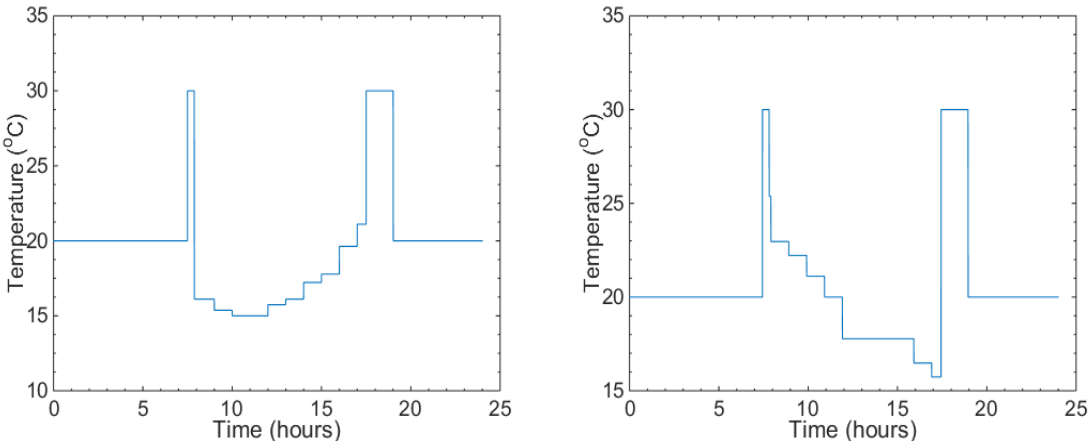

Figure 79: Temperature samples for a random day in the Tampa data for winter (left) and spring (right)

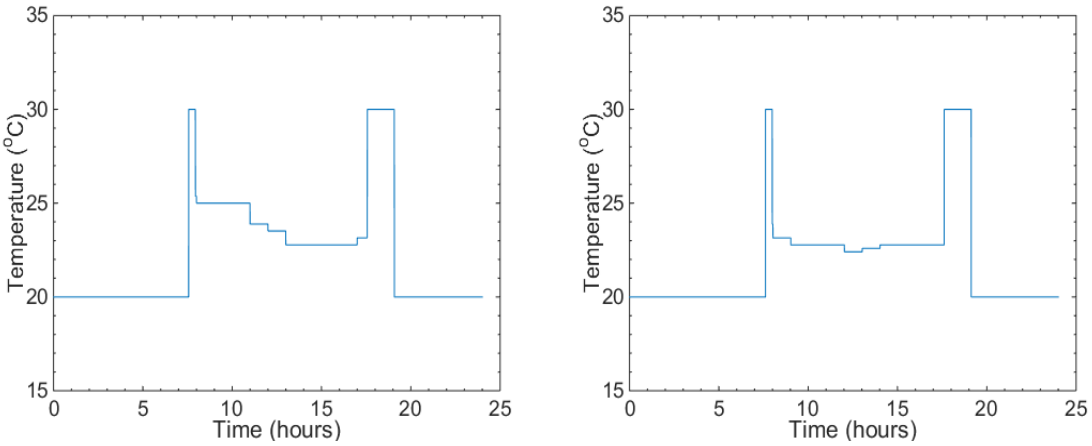

Figure 80: Temperature samples for a random day in the Tampa temperature data for summer (left) and fall (right)

The temperatures for the year are used for each year of the simulation. The temperature data is real-world hourly temperature data taken for ambient temperatures in Waterloo, Ontario, Canada [93], and in Tampa, Florida, United States. Thus, the battery pack will go through similar fluctuations as to those described in the figures each year, as if a person was driving in the Waterloo or Tampa area.

5.11 Daily Cycling Schedule

The battery packs were cycled at 30ºC from 10% DOD all the way down to 90% DOD as a maximum. Thus, the change in SOC is at most 80% and the vehicle will require recharging or must rely on a secondary source of power to continue to operate. Figure 81 displays a capture of the capacity changes that the battery pack undergoes each day.

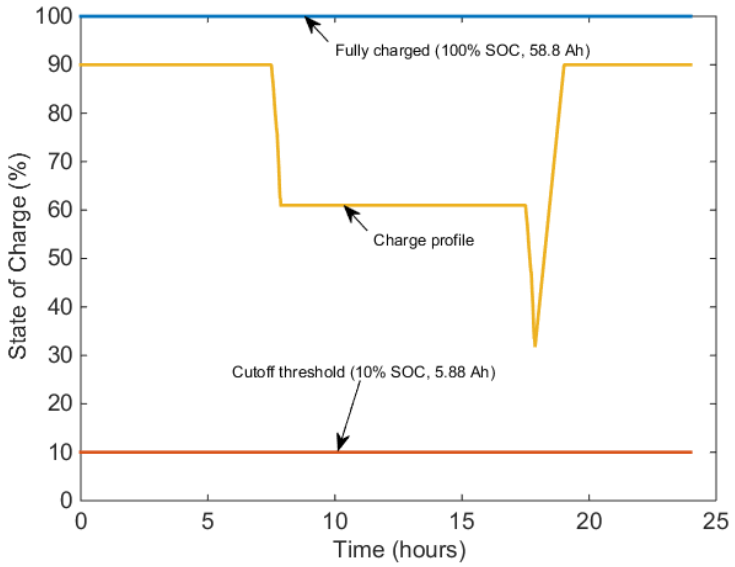

Figure 81: Capacity profile of vehicle given as SOC change over 1 day of usage

The vehicle begins with charge depletion of the cell as the vehicle operates over the drive cycle. Once the drive cycle ends there is a period of OCP conditions, followed by another drive cycle and the vehicle finally being charged to its maximum capacity (90% SOC). The vehicle is once again under OCP conditions until the following morning when it is to be used again, repeating the cycle. After each day, though, the total capacity that the vehicle can be potentially fully charged to begins to decrease as the cell has sustained a certain amount of degradation in that time.

5.12 Capacity Fade Results after 1 year duration

The primary parameters being monitored in the simulation is the capacity and the capacity fade that is occurring within the battery pack. Results for both conditions of the vehicle being driven in Waterloo and Tampa were tabulated and comparisons drawn from the data.

Figure 82 shows simulation results for capacity fade endured by the cell if the electric vehicle were operating in Waterloo. The figure depicts three different data sets, one for the results of calendar aging alone (marked by the red line), cycling aging alone (marked by the blue line), and the total capacity fade (marked by the yellow line). Despite the battery pack being in OCP conditions for an estimated 92% of its life, after one year the primary capacity fade mechanism is in fact cycling aging.

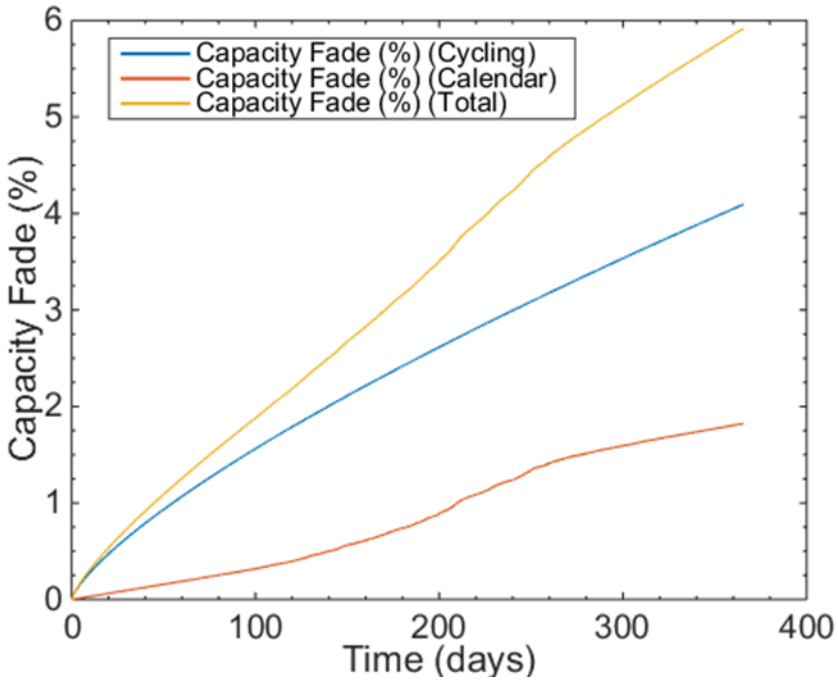

Figure 82: Total, Calendar, and Cycling aging losses after 1 year of simulation in Waterloo area

At the end of 1 year, the battery pack had endured approximately 1.8 % aging from calendar aging and 4% from cycling aging. This yields a total aging for the cell of almost 6%. As calendar aging is directly related to the SOC and temperature of the battery during storage, it can be seen in the figure the effect of increasing ambient temperature conditions. With higher temperatures, there is a noted increase in capacity fade due to calendar aging. As the temperatures begin to decline, the changes in capacity fade decreases and returns to a similar rate as seen in the

beginning of the year. Overall, though, the losses from cycling aging play a much greater role in the decline of capacity when simulating a vehicle in the Waterloo climate.

Figure 83 shows simulation results for capacity fade endured by the cell if the electric vehicle were operating in Tampa for one year. Once again, the degradation due to cycling aging played a greater role in the loss of capacity within the battery pack for this first year of operation. The total loss due to cycling was approximately 4% (no difference in driving patterns or battery operation temperature, so degradation due to cycling will be similar between simulations). One major difference between the two simulations, though, is the extent of degradation from calendar aging. The values for calendar aging are much greater in this simulation, due to the temperatures in the Tampa area being much greater over the entire year.

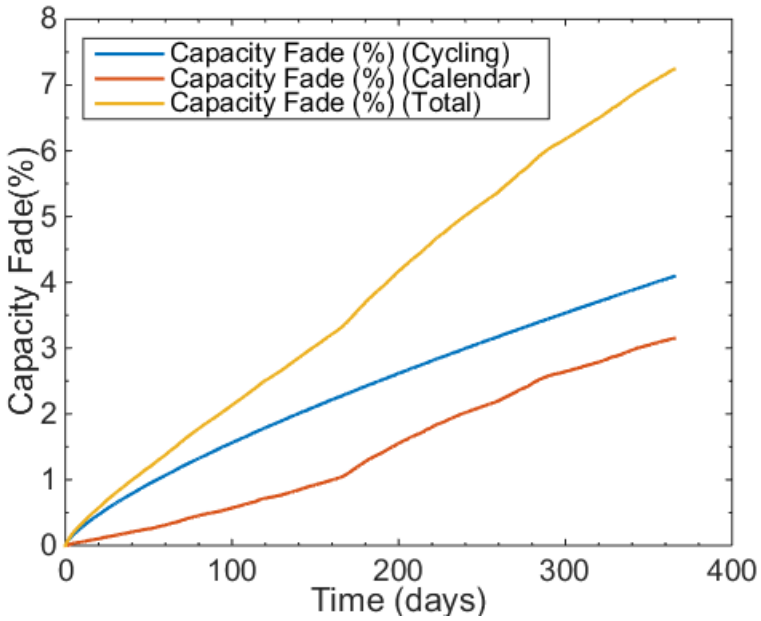

Figure 83: Total, Calendar, and Cycling aging losses after 1 year of simulation in Tampa area

Figure 84 displays the actual loss in capacity over the one year simulation for the vehicle battery pack in both geographical areas. In terms of capacity, this is a loss of approximately 3.53 Ah for the simulation run for Waterloo and 4.26 Ah for the simulation run for Tampa. In the first year of operation the battery pack has lost an additional 0.73 Ah just because of the geographic location in which the vehicle was simulated.

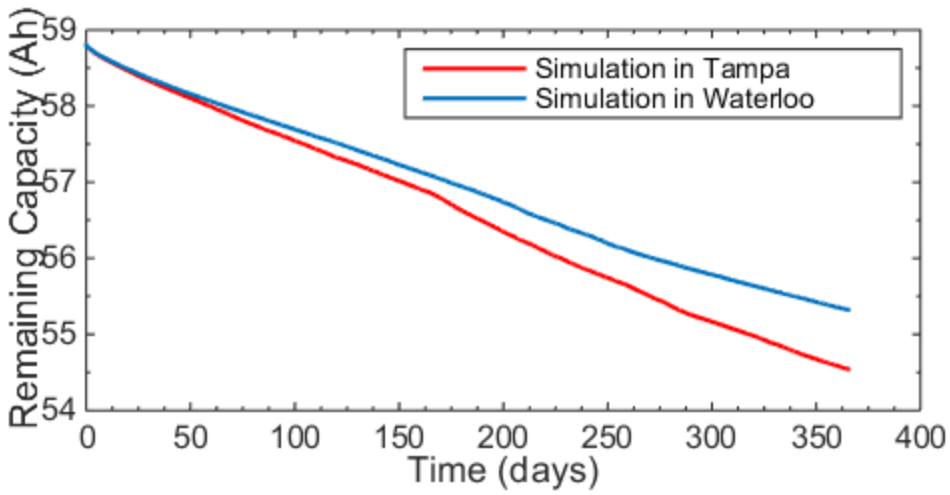

Figure 84: Actual capacity fade of battery pack over one year

5.13 Extent of degradation after ten years

The simulation was run for a whole ten years, for both geographical areas, with the end capacity fade for each year being monitored. The vehicle was either being used (undergoing charge depletion) or charging for only 8% of its life. The other 92%, the battery pack was under OCP conditions. Figure 85 depicts the cycling, calendar, and total capacity fade for the vehicle simulated in the Waterloo area.

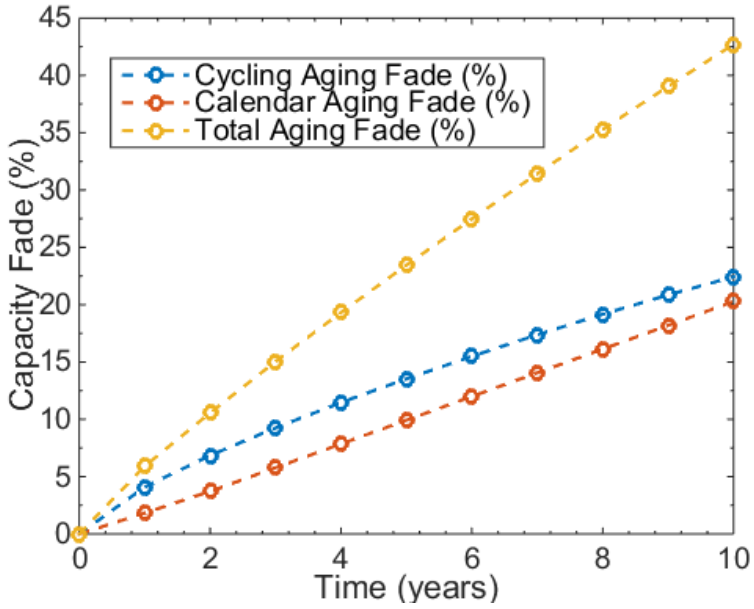

Figure 85: Capacity fade from calendar and cycling aging using simulations of temperature in the Waterloo area

After only five years the total capacity fade within the battery pack had exceeded the 20% EOL condition and the battery pack would be considered no longer viable. This EOL is much less than the consumer requirement of 10 years. After only five years the battery pack endured approximately 9.923% of capacity fade from calendar aging and an additional 13.53% from cycling aging. In order to track the total possible degradation that can occur, the full ten years of simulations were completed. After ten years, the battery pack endured approximately 20% of capacity fade from calendar aging alone and another 22% capacity fade from cycling aging.

Ultimately, the aging incurred by calendar aging did not exceed that of cycling aging. There is a significant gap in the amount of aging with respect to calendar aging and cycling aging at the EOL point (five years). Despite the battery pack being in OCP conditions for much of its life, the extent of calendar aging was not as severe as the cycling aging that had occurred. Even after the full ten years of simulations were completed, cycling aging still exceeded the total calendar aging. It can be noted, though, that the difference between the values for capacity fade from the two different aging phenomena is decreasing.

Now making a comparison to the vehicle being simulated as driving in the Tampa area, Figure 86 depicts the cycling, calendar, and total capacity fade that the battery pack endured for ten years of simulation.

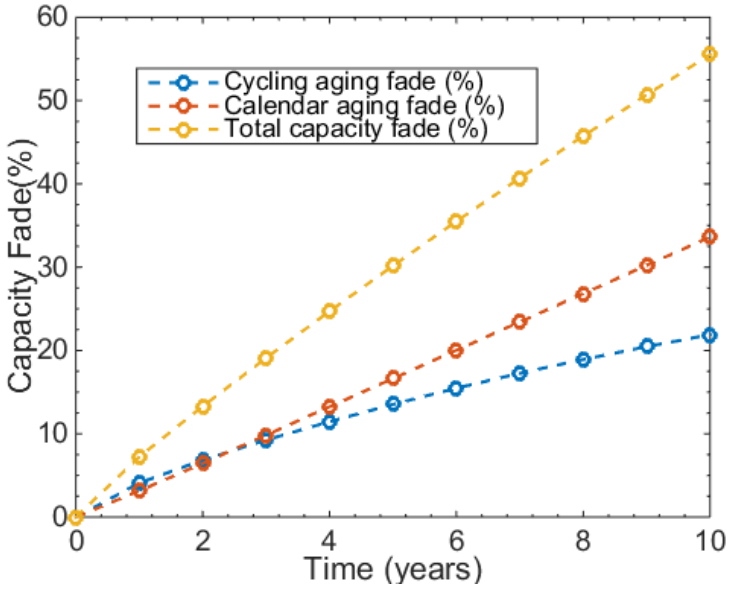

Figure 86: Capacity fade from calendar and cycling aging using simulations of temperature in the Tampa area

This time after only four years the total capacity fade within the battery pack had exceeded the 20% EOL condition and the battery pack would be considered no longer viable. At the fourth year of the simulation the battery pack had endured approximately 13.25% of capacity fade from calendar aging and an additional 11.46% from cycling aging. In order to track the total possible degradation that can occur, the full ten years of simulations were completed. After ten years the battery pack endured approximately 34% of capacity fade from calendar aging alone and another 22% capacity fade from cycling aging.

The increased temperature conditions that the battery pack has to endure throughout the year increase the capacity fade due to calendar aging. Within two years of operation the capacity fade due to calendar aging has actually surpassed the cycling aging. This trend continues onward for the entire ten year simulation with a final capacity loss differential between the two types of aging being 12%.

Ultimately, the aging incurred by calendar aging is highly dependent on the temperature at which the battery pack is exposed to. If the surrounding conditions are quite high throughout the year, the battery pack will incur more capacity fade due to calendar aging and will become the dominant aging mechanism in the cell.

5.14 Summary of Lifetime Prediction Modelling

In this work a simulation model was presented to predict lifetime of a high power lithium-ion battery under realistic operation conditions in two different geographic areas and the impact of the various aging phenomena that can occur within the cell. A $LiFePO_4$ battery module with a nominal voltage of 292 V and a nominal capacity of 58.8 Ah, currently being used in the UWAFT prototype vehicle for the EcoCAR3 competition, is researched. Ten year simulations were completed for both scenarios and the cycling and calendar aging was determined based on degradation models. It has to be kept in mind that the findings presented here are only valid for the specific cell considered in this work.

The two different geographic locations had dramatically different effects on the degree of calendar aging that the vehicle endured. Despite the vehicle being under OCP conditions for much of its lifespan (approximately 92%) exposure to the ambient conditions for the vehicle

being simulated in the Waterloo area resulted in the calendar aging being less than the cycling aging. After ten years cycling aging was still the most dominant aging mechanism.

This changes, though, if the vehicle is placed in a warmer climate. The degree to which calendar aging takes place in the vehicle is much greater if the ambient temperature conditions are also more severe. Over ten years the extent of calendar aging far exceeded the amount of cycling aging that occurred within the battery pack. As a result of this new climate exposure, the battery pack reached its EOL point a full year ahead of the other simulated pack.

In both scenarios, the effect of calendar aging does have a distinct effect on overall battery lifetime. Both vehicles experienced greatly depleted ranges over a short period of time and reached their EOL point much sooner than the ten year consumer requirement. Thus, when considering battery lifetime, it is very important to take both cycling aging and calendar aging into consideration for losses of capacity in lithium-ion batteries in an electric vehicle. Calendar aging does play a significant role in the loss of capacity within the battery pack, due to the battery pack not being utilized on a constant basis in the vehicle, and incorporating it into the analysis resulted in the battery pack reaching its EOL much sooner than the consumer requirement.

In future work the relation between calendar and cycle life has to be investigated in more detail to account for this effect. Also, with more testing capabilities a cycle life model will be further developed by being able to model degradation with drive cycles.

6 Second-Use of Vehicle Batteries

As previously described, a lithium-ion battery pack used in a BEV application must be able to sustain life for approximately 10 years in order to meet consumer requirements [8], but the EOL for vehicle applications is defined as being when the remaining capacity of the battery pack reaches 80% of its original capacity. [94] These depleted batteries are then sent off to be recycled to re-use the materials and re-gain some of the investment. Recycling batteries may not be economical in the future, though, as a larger number of battery chemistries are being changed to iron and manganese presenting a diminishing recycled end-of-life value, especially as lithium-ion batteries have a high manufacture cost. [94] EOL EV batteries still have an estimated 80% of their remaining capacity and the remaining capacity can be utilized in other applications. [95] This will delay the battery from being recycled and increase the economic viability of the battery pack. [94] One method of utilizing this investment past the initial vehicle use phase of the battery's lifecycle is through repurposing. In a battery repurposing scheme a Li-Ion battery pack can be implemented in a stationary setup to offset energy use in the application after it has been used in a vehicle.

Through the increased use of Hybrid-Electric Vehicles (HEVs), Plug-In Hybrid-Electric Vehicles (PHEVs) and EVs, the utility grid system will experience an increased strain [96]. The use of these vehicles, in coordination with the increased development of renewable energy sources which fluctuate with weather patterns, is adding to this strain issue [96]. By using a repurposed battery pack, loads on the grid are able to be shifted to more opportune times. The benefits of this load-shifting as part of future 'smart-grid' developments have been shown to have economic benefits for the consumer at its end use [97].

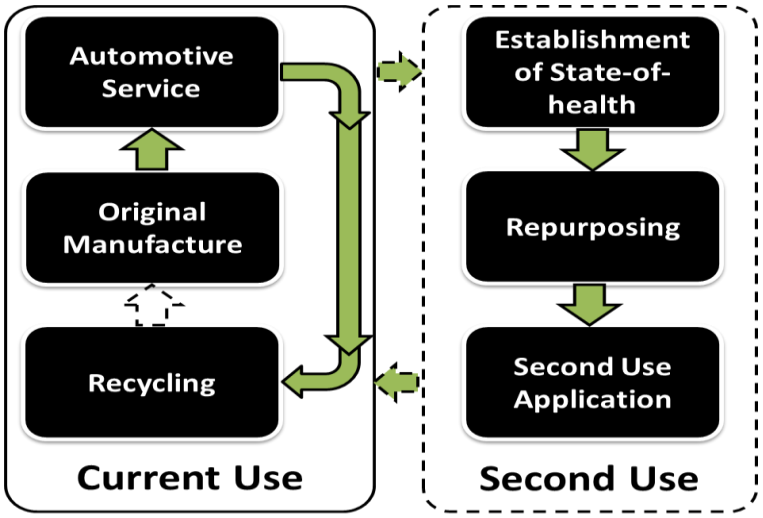

Figure 87: Vehicle Battery Life Cycle [98]

In Ahmadi et al. the lifecycle of Li-ion batteries was explored with the focus on making comparisons of current practices to looking at second-use potential, as described in Figure 87 [99]. It was found that repurposing the battery, for stationary grid storage, resulted in significant potential emissions reduction of 56% (24 t CO_2e) over the total eighteen year lifetime [99]. The sources of CO_2 reduction primarily came from the proliferation of PHEVs over ICEs and the subsequent re-use of the batteries for grid storage.

6.1 Canada's Energy Market and the Need for Repurposed Batteries

Figure 88 displays the Average Household Annual Energy Usage in Canada for various fuel types. Each year an average Canadian household uses approximately 4.3×10^4 kJ of electricity (117.73 kJ/day), per the energy mix shown in Figure 3 [100]. This electricity can be supplied, or offset at least, throughout the day by renewable and surplus energy stored within a repurposed battery pack.

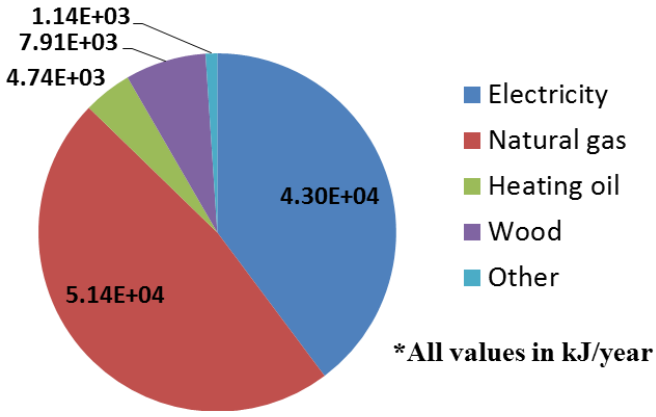

Figure 88: Average Household Annual Energy Usage 2009 [100]

In order to supply electricity to the millions of households, business, and industries in Canada, a wide variety of energy sources are utilized. Figure 89 details Canada's electricity generations mix.

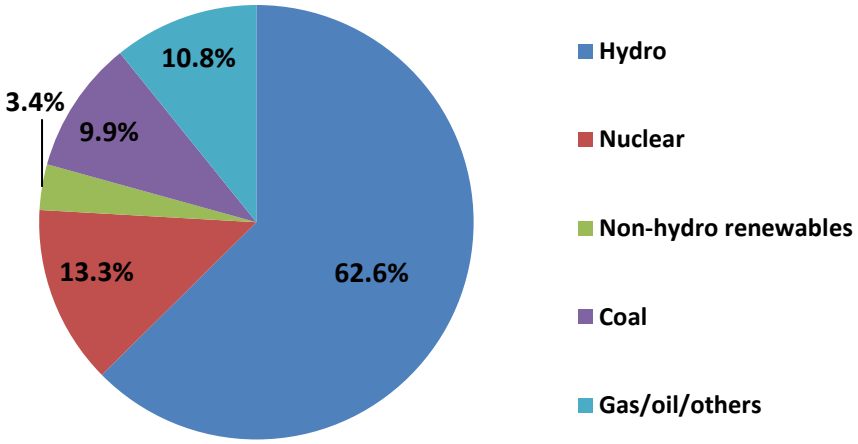

Figure 89: Canada's Energy Mix for Electricity Generation 2014 [101]

Electricity generation in Canada is largely provided by hydroelectric and nuclear power [101]. Although, hydroelectricity supply can be somewhat increased and decreased depending on electricity demands, nuclear only provides a base load of power and cannot simply be ramped up or down depending on electricity demand transients. To account for these fluctuations, non-renewable energy sources are utilized during points of increased demand, but these sources typically produce greenhouse gases. Non-hydro renewable energy sources would be an excellent method of providing energy during transient demand conditions, but one of their greatest disadvantages is that supply and demand mismatches can occur. A mismatch in this context

refers to the time that electricity is generated (supplied) not aligning with the time that the energy is demanded. This energy can then not be effectively utilized in Canada's energy grid.

The benefit of having a dedicated stationary battery pack is that it can aid in the smoothing of these grid transients. By charging the battery pack during the "off-peak" times of the day, the stored energy can be supplied when it is actually required and the need for additional energy sources to supply the power would then be deemed unnecessary. In addition, these re-purposed battery packs can also aid in decreasing the mismatch problem of renewable energy sources by being able to transfer the energy supplied at the time that it is generated to the battery to be stored for later use (when it is actually demanded). Excess energy in Ontario is currently being exported at a lower cost, causing huge losses. From January to October 2013 Ontario exported 14,983,776 MWh at a rate of 2.54 cents per kWh. This resulted in a $1.2 billion loss causing the rates for Ontario to increase. [102]

Industry leaders are beginning to see the benefits of dedicated home battery packs for smoothing grid demands and have released their own products in the market. In April 2015, for example, Tesla announced the Powerwall, a 6.4 kWh battery pack that can be installed in a residence for daily cycle applications [103]. One useful application is to charge the Powerwall battery pack with zero-emission electricity from solar panels. After Tesla's release of the Powerwall, Nissan released a design for vehicle-to-grid technology called xStorage [104]. Unlike other energy storage systems, xStorage differentiates itself by utilizing repurposed batteries from Nissan's electric fleet. As a result of the roll out of xStorage, Nissan has made a design change to their battery packs making them more modular so that they are easier to remove by technicians and be transferred over to second-life applications.

6.2 Controlling Battery Degradation in Electric Vehicles

In order to ensure that the battery in an electric vehicle is able to sustain cell life for the duration that it is required by consumers, battery management system (BMS) implements strategies to limit battery degradation and ensure safety constraints are met. To ensure the strategy is effective, and to ensure that cell health is adequate for function, the BMS measures the overall cell SOH and manages the operation parameters of the system to keep them within safe bounds. In lithium-ion batteries, cell SOH is important as safe-operating windows are very strict and improper management leads to rapid degradation and this can develop safety complications [15]. Specific

ways the BMS can minimize degradation and safety hazards are: managing charge/discharge voltage and current, and by monitoring the cell temperature,

When charging or discharging, it is critical that the cell voltages are maintained within the operating range (3.0V and 4.2V for Lithium-Colbalt Oxide) [16]. This is accomplished through the use of many analog voltage measurement channels within the BMS that read per-cell voltage [15]. Because the BMS manages charging and discharging, it is possible to limit or halt current flow to ensure that these voltage limits are respected.

In terms of discharge current, protection against cell damage takes place in a similar manner to that of discharge voltage protection - halting or limiting current flow in case of over-consumption from cells [15]. Note that it is also possible to limit battery consumption to a percentage based upon the battery SOC, increasing the lifespan of the cells [105].

The BMS is also capable of elongating cell life and ensuring safe performance with the use of cell-level, or module-level temperature measurements [15]. The operating temperatures of Li-ion batteries is dependent on their cell chemistry but, generally speaking, the range of temperatures within which Li-ion batteries can be safely operated (charged and discharged safely) is 0^{o}C to 45^{o}C [16]. Outside of this safe range, the BMS can prevent further use of the battery through opening contactors or performing an emergency stop of the system. Within this range however, there is also the capability to limit cell discharge as a function of cell temperature to ensure the (usually significant) thermal mass of the battery does not exit the safe operating range by accumulating heat during strenuous or lengthy discharge cycles [40] [32].

In addition to limiting battery degradation, the BMS provides the necessary SOH information to characterize the cells after they have reached their EOL point (80% remaining SOC) Once the ESS has reached its limitations for use in vehicle applications, the information provided by the BMS will be necessary for determining the extent of degradation experienced by the battery over its lifetime [18]. This information is pertinent to determining whether or not the battery pack can be utilized for secondary applications, detailing the history of state of charge (SOC) or depth of discharge (DOD), and the state of health (SOH) of the battery pack [15].

6.3 Barriers to Adoption

Although Li-Ion batteries have tremendous potential for stationary energy storage applications, there are technical and regulatory barriers to their use. For example, Li-Ion batteries are classified as “Dangerous Goods” by Transport Canada [106], due to their high voltage, risk of exposure of reactive materials and fire risk. In addition to the risk involved in transporting EV batteries, there is risk associated with the performance of the battery in its second life.

After a battery pack has gone through many cycles (approximately 1000 or more to meet consumer requirements [18]) it can no longer be used to power an EV. Several degradative mechanisms occur within the cells of the battery pack, reducing capacity and increasing the risk of failure of one or more of the cells. Although it is difficult to ensure the safety of an EV battery pack for re-purposing, due to the risks involved in installing, servicing, and using it, there has been an increase in insurance codes and standards.

6.3.1 Insurance Codes and Liability Standards

Insurance costs, or premiums, are calculated based on the risks of a failure occurring to a given object and is further refined with the accumulation of statistics which consider cost of repair, frequency of claims, and severity of injuries over time [107]. With a higher risk of failure there is a higher premium, and with lower risk there is a lower premium.

As using repurposed EV batteries for energy storage is an innovation, there are no previous statistics to aid in properly assessing the coverage for the unit within a home or business. An insurance company can consider potential risks such as power surge protection, liability for damage to the local power grid, or the risk of fire from a burning or exploding battery; however, with a lack of available standards and certifications, insurance companies are unsure of how such a system will influence coverage and are unsure of how to guide consumers. The unfamiliarity of the technology may cause disruptions to the insurance market with no comprehensive assessment being capable for the systems now [108]. It should be noted though, under CA PUC Tariff Rule 21, that all equipment must be certified (either through UL or another Nationally Recognized Testing Laboratory (NRTL)) when attempting to connect new components to the grid, which requires standards for the certification testing. The development of appropriate standards and statistics on repurposed battery packs will come with time, but is not available yet.

Liability and ownership of an EV battery at its end-of-life (EOL) is an important concern Defects in an EV battery can cause leaks, explosions or fires which may, result in harm to people or property [109]. When a defect within a battery results in damages to people or property, the owner of the battery is liable for some portion, if not all, of the cost of damages [109]. An Original Equipment Manufacturer (OEM) will make a battery and insure its use for the vehicle application that the OEM intends. The OEM may not anticipate, though, that the vehicle owner will allow the battery to be repurposed by a third party. If the second-life uses of the battery result in damages, then the automotive manufacturers may be liable as current regulations and standards are unclear. Because of this lack of clarity around their liability, OEMs are hesitant to allow their EV batteries to be repurposed for grid storage applications and will, most likely end up being recycled or sent to a wrecking yard [109].

6.3.2 Lack of data on degradation of battery packs

For an EV battery pack to be repurposed, its State-of-Health (SOH) must be determined so that it may be properly classified. The condition of an EOL EV battery pack varies widely based on the vehicle it was in, how aggressively it was cycled, and the environment in which it was operated. With these varying conditions battery packs, will degrade at different rates and have varying SOHs.

In industry, there is uncertainty about how to define the SOH of a battery and how it should be evaluated [90]. Currently, the SOH parameter is a unitless percentage which measures the current condition of a battery cell, module, or system, compared to its ideal conditions. [90]. In the automotive industry, it is generally accepted that if the battery capacity drops below 80% of its initial value, the SOH is also considered less than 80%, and the batteries should be removed and replaced in the vehicle [99].

The capacity of a Li-Ion battery decreases over time, due to the degradation of the battery increasing the cell's internal resistance. This degradation occurs in every cell in a battery module over time in addition to the degradation from operating the battery, resulting in a decline in the SOH of the battery module. The aging of the cells can be evaluated using battery aging models, but these models cannot characterize all the influences on SOH, such as battery damage caused by vehicle collision or battery short circuits [90].

This is a concern for automotive recyclers as storing and managing EOL EV batteries creates uncertainty and increases the risk of a hazard occurring with the battery pack. This risk is increased especially as most automotive recyclers lack the specialized knowledge that the OEM and its dealer network have with safe servicing practices of the system. Additionally, many recyclers do not understand how to properly test the battery, nor have access to testing equipment, nor understand its SOH after coming out of the vehicle. [110] These drawbacks create problems in attempting to repurpose batteries for a second life application and can result in a significant environment and safety risk for automotive recyclers. To combat these concerns re-manufacturing firms may need to test batteries for degradation and quality to establish baselines for each pack, after acquiring them. These assessments of the EOL EV battery may include fade mechanisms associated with capacity, and power as well as the testing for cells which have catastrophically failed [110].

Currently, only vehicle manufacturers and dealers can check the diagnostic codes displayed by the packs to check their SOH. Establishing a classification system for deciding on how repurposed battery packs would be best utilized is needed for repurposing EV batteries.

6.3.3 Availability and Variability

As electrification of the vehicle market is a recent undertaking, there are a limited number of EVs on Canadian roads today. The current fleet stands at just over 18,000 vehicles (10,034 (54%) of are BEVs while the balance, 8,417 (46%), are PHEVs), [111] and in 2010 less than 1,000 EVs were sold in Canada. [112] The number of EVs being sold is climbing, as illustrated in Figure 90, but, currently there is not a significant supply of depleted EV battery packs. In accordance with consumer requirements, EVs are expected to have their batteries last at least 10 years for BEVs and 15 for HEVs [18]. Thus, with almost 7000 EV sales in 2015 [111], it will not be until at least 2025 until these batteries may be available for repurposing.

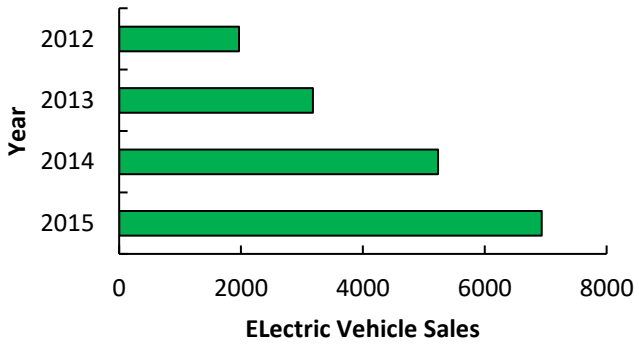

Figure 90: EV sales in Canada over the past four years

When these batteries are available for repurposing, it is not known how many of them will have an SOH that will be useful. With the small current supply of EVs in Canada, there is a limit on the potentially available EV batteries with an adequate SOH for repurposing. In addition to the lack of availability, the variability of battery designs between companies is a barrier to creating uniform procedures for construction of repurposed battery packs. Table 19 details the various battery types and designs utilized by a few of the many EV manufacturers.

Table 19: List of Battery Types and Designs

Make and Model	Design
Chevrolet Bolt, 60 kWh (2016) [21]	Prismatic/Pouch
Tesla S 85, 90kWh (2015) [113]	18650
Nissan Leaf, 30kWh (2016) [20]	Pouch/Prismatic
Toyota Prius 4.4 kWh (2016) [2]	Prismatic

Repurposing each of these different types of batteries will require reassembling each of the different types of cells into different configurations, as well as developing the control system, which will also be dependent on the application and type of battery. This can be an arduous task with each battery type requiring a unique design, controls logic set, and manufacturing process [114]. Also, based on research done by SEED, it was determined that unless the batteries of the battery pack were modular it would be too risky and costly to break apart the packs.

6.3.4 Installation into Residences

As the repurposed battery pack is a depleted high voltage battery, installation inside a household or small commercial area comes with a set of requirements. For example, Tesla provides owners of their Powerwall with requirements that must be adhered to, to safely operate the system [115].

Tesla specifies that the Powerwall must be installed:

- At a height that prevents damage from flooding;
- In an area that is not exposed to ambient temperatures above 60^{o}C or below -30^{o}C;
- And in conditions where it is not susceptible to high humidifies or near any water sources.

Installation of a battery pack system would require that these specifications be met before final placement of the equipment. These specifications may limit placement options for homeowners and business owners.

6.4 Current Applicable Design Codes

To determine the safety measures needed for repurposing an EV battery, an analysis of the applicable codes is completed. As in-home energy storage using Li-ion batteries – both new and repurposed – is a new technology it is not explicitly referred to in many published codes. Design specifications for the battery pack are thus drawn from similar codes for lead-acid stationary storage applications.

A report by the *Pacific Northwest National Laboratory* outlines the codes and standards in the United States for energy storage systems [108]. In Table 20 and Table 21, the codes applicable to the design of repurposed packs, outlined in this report, are displayed. Table 20 focuses on codes which are specific to the battery pack used in the stationary assembly, while Table 21 focuses on codes which outline design considerations for the repurposed pack assembly.

Table 20: Applicable Codes for Repurposed Li-ion Battery Packs in a Stationary Application

Code Category	Code Title	Connection to Repurposed Packs
Battery Pack	IEC 61960 Ed 3: Secondary lithium cells and batteries for portable applications	Covers criteria for the selection of secondary lithium cells for remanufacturing
	IEC 62485-2: Safety requirements for secondary batteries and battery installations – Part 2: Stationary batteries	Covers protections from hazards with stationary battery packs with nominal voltages less than 1500 V
	IEC CD 62619: Secondary cells and batteries containing alkaline or other non-acid electrolytes. Safety requirements for secondary lithium cells and batteries, for use in industrial applications.	Under development, covers requirements on all aspects of stationary application use of Li-ion batteries including erection, use, inspection, maintenance, and disposal of cells
	IEC CDV 62620: Secondary cells and batteries containing alkaline or other non-acid electrolytes – Secondary lithium cells and batteries for use in industrial applications	Covers tests and requirements for Li-ion cells to be used in a stationary application
	IEC 62620 Ed 1: Large format secondary lithium cells and batteries for use in industrial applications	Covers specifications for cells in secondary industrial applications
	IEEE 1660: Guide for Application and Management of Stationary Batteries Used in Cycling Service	Covers battery management strategies, with changes relative to cycling for stationary applications
	UL 1642: Lithium Batteries	Covers requirements for lithium batteries in stationary applications for safety of technicians, users, and other design features

Table 21: Applicable Codes for the Repurposed Battery Pack Assembly

Code Category	Code Title	Connection to Repurposed Packs
Entire Assembly	ANSI C84.1: Electric Power Systems and Equipment – Voltage Ratings (60 Hertz)	Standard covers nominal voltage ratings and operating conditions for 60-hertz systems above 100 volts
	IEC 62257-9-2: Recommendations for small renewable energy and hybrid systems for rural electrification – Microgrids	Standard covers requirements for how microgrids can be maintained and safety upheld
	IEC 62897: Stationary energy storage systems with lithium batteries – Safety requirements (under development)	Covers hazards that need to be mitigated for the use of a stationary pack with Li-ion cells
	IEEE 1375: Guide for the protection of stationary battery systems	Covers guidelines for options of protecting stationary battery systems
	NFPA 111-2013: Standard on stored electrical energy emergency and standby power systems	Covers safe operation of stationary energy storage systems with the grid in the event of service disruptions
	UL 9540: Outline for investigation for safety for energy storage systems and equipment	Covers safety for all energy storage systems, being charged and discharged at a later point in time to shift demand

The Canadian Electrical Code, or CSA C22.1, is published by the CSA to address the installation and maintenance of electrical equipment in Canada [116]. The repurposed battery packs contain electrical components that can obtain and feed electrical energy into the electrical grid. Incorporation of a stationary energy storage repurposed battery pack into a residential home or a

small commercial installation requires that all equipment be installed per the Canadian Electrical regulations. Current applicable design codes for installation of a repurposed battery pack are described in Table 22.

Table 22: Applicable Codes for Repurposed Li-ion Battery Canadian Electrical Codes

Code	Description
CEC 26-544	Batteries with exposed live parts shall be kept in a room or enclosure accessible only to authorized personnel.
CEC 26-546	Storage batteries shall not be subjected to ambient temperatures greater than 45°C or less than the freezing point of the electrolyte.
CEC 26-550	- Battery trays, racks, and other surfaces on which batteries are mounted shall be a) Level b) Protected against corrosion from the battery electrolyte; c) except as permitted in Subrule (5), covered with an insulating material having a dielectric strength of at least 1500 V; d) of sufficient strength to carry the weight of the battery; and e) designed to withstand vibration and sway where appropriate. - Battery cells shall be spaced a minimum of 10 mm apart. - Battery cells having conductive containers shall be installed on non-conductive surfaces. - Sealed cells and multi-compartment sealed batteries having conductive containers shall have an insulating support if a voltage is present between the container and ground. - Cells and multi-compartment vented storage batteries, with covers sealed to containers of non-conductive, heat-resistant material, shall not require additional insulating support. - Batteries having a nominal voltage greater than 150 V and with cells in rubber or composition containers shall be sectionalized into groups of 150 V or less.
CEC 64-800	Storage batteries for dwelling units shall have the cells connected so as to operate at less than 50 V nominal.
CEC 64-812	Equipment shall be provided to control the charging process of the battery.

The codes culminate in the following design specifications:

- The batteries must be stored on level ground, with sufficient storage to protect personnel;
- This storage must also be secure, and only accessible by authorized personnel to reduce the risk of injury and death;
- For the batteries themselves, it is noted that they must be sectionalized into smaller groups if connected as a large installation with nominal voltages greater than 150V.
- A storage battery installed in a dwelling unit shall have the cells connected so as to operate at less than 50 V nominal.
- Equipment shall be provided to control the charging process of the battery [116].

Using these standards to design the repurposed battery pack, the following design features were deemed as most pertinent to the preliminary bench test design. To prevent a hazard from occurring, a controller must be installed to ensure proper operation of the system and mitigation of faults.

The nominal voltage of the pack must be designed to be less than 50V. Also, the battery pack itself must be secured and enclosed in a protective case only accessible to the appropriate personnel.

In a separate code, IEEE 484, regulations are stated for the design and installation of vented lead-acid batteries. The code states that the battery pack must be stored in an area with an ambient temperature of approximately 25°C. The area must also be protected, and isolated from vibration which can lead to disconnects and damage to the interior components of the battery pack casing [108].

This specification is also found in Tesla's Powerwall installation manual. Putting a limit on the temperature around the battery creates some limitations on the system's placement, especially as Canada has a much colder climate. To maintain proper operating temperatures for the battery, a thermal control system needs to be installed either in the pack or additional insulation and heating units need to be supplied in the garage. Both solutions to the temperature mitigation of the repurposed battery will add cost to the installation of the unit.

A recently approved standard for international distribution by the International Electrotechnical Commission (IEC), IEC 62619 Ed. 1.0 [108] focuses on the safety requirements for secondary lithium cells for use in industrial applications. To be approved for use, the cells and entire battery systems must pass a series of tests ensuring that the cells will not undergo thermal runaway and that the battery management system (BMS) is able to control the battery system and prevent overcharging and overheating [117].

As the repurposed pack is going to be installed in a new system, in application outside of its original intended use, a new controls structure imbedded in the BMS must be tested once again. It must be ensured that there are no circumstances where a fault can occur which risks damage to the owner or to the system.

6.5 Failure Analysis

To determine the most probable failure modes and associated risks with the design of a stationary repurposed battery pack, two failure analyses are conducted. The first analysis tool is the Failure Modes and Effects Analysis (FMEA) which begins with the function of a specific part, and breaks down its potential failure modes to effects and causes. Each risk is evaluated by its Risk Priority Number (RPN), which ranks their relative severity and probability, with larger RPN risks being

targeted for mitigation. The RPN is calculated from the risk severity (SEV), probability of occurrence (OCC), and ability to detect (DET). SEV, OCC, and DET are rated on a 1-10 scale, with 10 reflecting the highest probability of failure. The calculation for RPN is as follows:

$$RPN = SEV * OCC * DET \qquad \text{Equation 6.1}$$

6.5.1 Severity

The severity value in the RPN calculation is a measure of the extent which a failure can damage a system or component. Table 23 shows how severity is classified and the associated rank that is used in the RPN calculation.

Table 23: Severity RPN Ranking

Rank	Severity Criteria	Severity of Effect
10	Hazardous without warning	Compromises safety without warning
9	Hazardous with warning	Compromises safety with warning
8	Very High	Loss of Functionality
7	High	Reduced Functionality
6	Moderate	Customer experiences discomfort.
5	Low	Customer experiences some dissatisfaction.
4	Very Low	Defect noticed by most customers.
3	Minor	Defect noticed by average customer.
2	Very Minor	Defect noticed by discriminating customer.
1	None	No effect.

6.5.2 Occurrence

The occurrence variable is the probability of the failure occurring within the life cycle of the analysis. Table 24 shows how occurrence criteria are associated with each rank.

Table 24: Occurrence RPN Ranking

Rank	Occurrence Criteria	Description
10	Inevitable	≥ 1 in 2
9	Almost Inevitable	1 in 3
8	Very High	1 in 8
7	High	1 in 20
6	Moderate	1 in 80
5	Low	1 in 400
4	Very Low	1 in 2000
3	Remote	1 in 15,000
2	Very Remote	1 in 150,000
1	Negligible	1 in 1,500,000

6.5.3 Detection

Detection refers to the extent to which a failure mode can be determined. This variable has a direct relation to its impact on the system. The RPN system for qualifying a detection system is shown in Table 25 .

Table 25: Detection RPN Ranking

Rank	Detection Criteria	Description
10	Absolute Uncertainty	Controller cannot detect failure (or no controller)
9	Very Remote	Controller has a very remote chance of detecting failure mode
8	Remote	Controller has a remote chance of detecting failure mode
7	Very Low	Controller has a very low chance of detecting failure mode
6	Low	Controller has a low chance of detecting failure mode
5	Moderate	Controller has a moderate chance of detecting failure mode
4	Moderately High	Controller has a moderately high chance of detecting failure mode
3	High	Controller has a high chance of detecting failure mode
2	Very High	Controller has a very high chance of detecting failure mode
1	Almost Certain	Controller is almost certain to detect failure mode

6.5.4 Results of Analysis

The risks in the FMEA conducted for the repurposed battery pack are divided based on the components in the assembly (charger, inverter, battery pack, controller, and battery pack casing).

Table 26: Highest Risks of Design

Rank	Item/Function	Potential Failure	RPN
1	The charger/inverter shall convert power to charge/discharge the battery pack.	Overheating	180
2	The battery pack shall store and deliver energy	Overheating	180
3	The controller shall direct pack components (charger/inverter)	Overheating	180
4	The cell is a single unit within the battery pack and shall store and deliver energy.	Thermal runaway	180

Through the FMEA, it is determined that the two largest risks to the end user could occur due to overheating and overcharge/overdischarge.

Overheating, with a RPN of 180, can damage the assembly, thus rendering the pack incapable of charging or discharging, as well as personnel injury, such as burns. The main failure mechanisms

leading to overheating are loss of control input to the charger/inverter or a power surge to the unit. It is believed that this risk can be mitigated in the design by implementing a redundant controls system, which has multiple voltage and current sensors to monitor the pack's operation.

Thermal runaway of a cell, also with a RPN of 180, can lead to catastrophic failure of the entire battery pack and potentially damage its surroundings. The unit would be rendered completely inoperable in this case. Thermal runaway can be caused by a variety of issues including: thermal, mechanical, or electrical abuse, as well as an internal cell fault likely caused from the degradation. To mitigate the risk, a thorough controls structure must be designed to monitor pack operation and prevent potential abuses, as well as equipping the system with electronic circuit protection. These controls and pieces of hardware can be tested through controls simulation prior to the implementation with the pack. A Hardware-in-the-Loop (HIL) simulation will allow faults to be inserted in the control code and mitigate any potential errors.

6.5.5 Fault Tree Analysis

The second failure analysis conducted is a Fault Tree Analysis (FTA). A FTA works from the opposite direction of a FMEA, breaking down a potential safety risk to its root failure [118]. Five main safety risks are identified with the repurposed battery pack including: electrocution, slip/fall, inhalation, cut/scrape, and burn/explosion. The FTA utilizes AND and OR gates which connect the safety risks as they are broken down [118]. An example FTA analysis for Burns/Explosions is described in Figure 91. The most prevalent root causes are determined based on a probability analysis of the FTA figure which suggests that the more "OR" gate branches (with fewer "AND" gates) a particular circuit has the higher the probability of this circuit leading to the top fault condition [118].

The most prevalent root causes of burns/explosions in the repurposed pack arise from installation issues, improper preventative maintenance, and catastrophic failure of the battery pack. As the packs will have to be manually created (as battery packs from different vehicles have different configurations and cell types [99] [94] [25]) and serviced it is very difficult to achieve precision and repeatability using manual assembly techniques [40] [32]. Also, during the removal and construction process of the battery pack there is the possibility that cells can endure handling damage. These manufacturing problems can easily lead to the short-circuiting of a cell within the battery pack and a hot cell condition occurring [40] [32].

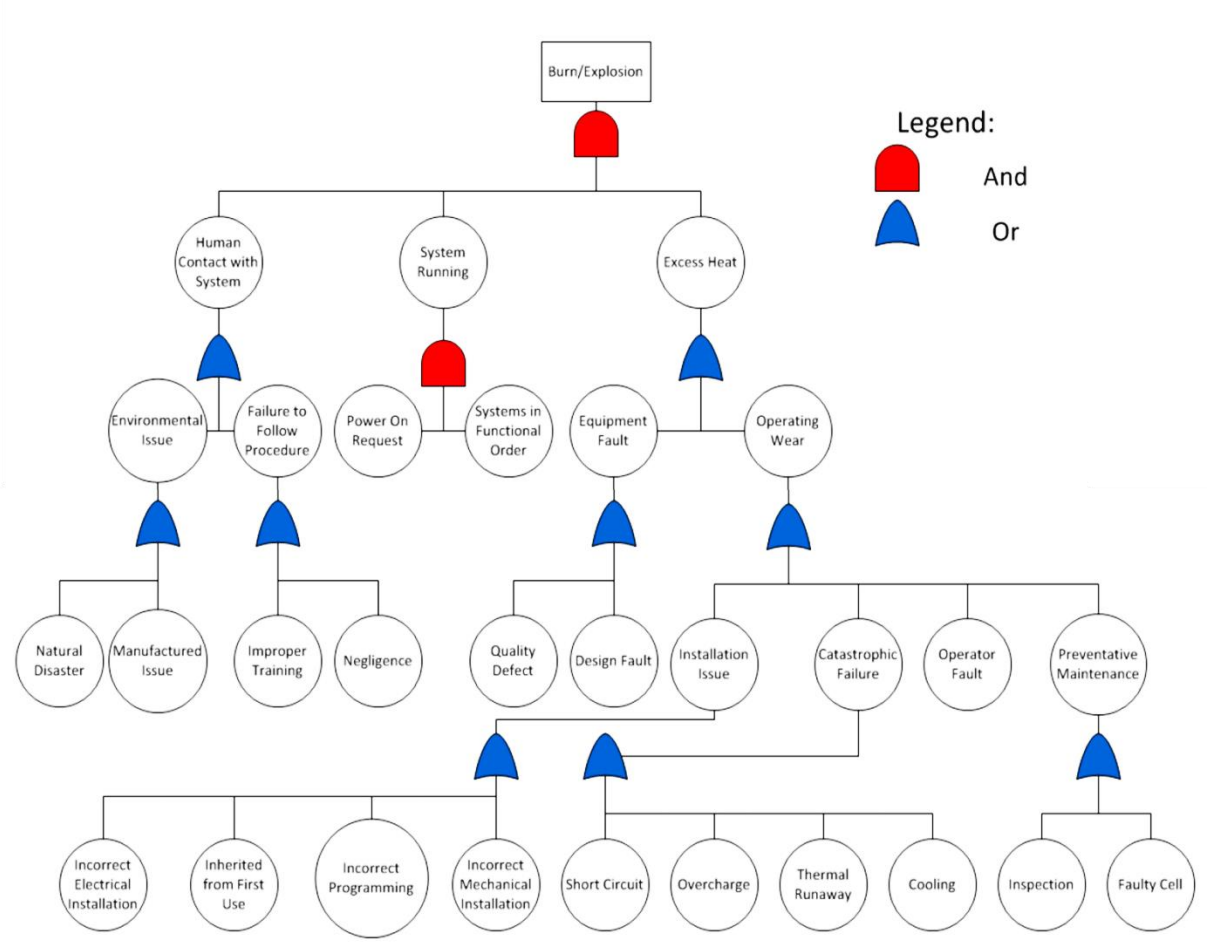

Figure 91: Fault Tree Analysis Example for Burns/Explosions

6.6 Degradation Classification

To provide a proper assessment of battery packs for repurposing, a 5-level system is proposed. This system categorizes how packs should be repurposed based on their SOH after the vehicle use phase. Batteries can be sorted based on a diagnostic process completed by the vehicle manufacturer or dealer and decisions on the battery's future can be made with the level categories shown below in Table 27.

Table 27: Repurposed Battery Pack Classification

Level	Description
Level 1	Little or no degradation
Level 2	Some degradation, vehicle re-use
Level 3	Some degradation, stationary repurposing
Level 4	Significant degradation, material recycling
Level 5	Catastrophic failure/damage, material recycling

Level One and Level Two batteries have experienced minimal degradation during the vehicle use phase, with more than 80% of the battery pack's capacity remaining [119]. Batteries that are classified into these two categories can potentially be used in the vehicle before being taken out for use in a repurposed application. Level Three batteries have degraded to below the 80% threshold for capacity remaining, but still have enough life to be used in a repurposed application. In this scenario, a second battery could be installed in the vehicle to extend its life and the original battery can be taken out for stationary storage. The Level Four and Five categories are for batteries which have been significantly degraded or suffered catastrophic damage. In this state, the batteries are unable to provide energy for either the vehicle or stationary use, and should be recycled. Utilizing this level classification system, after their use within vehicles, EV batteries can be properly sorted based on their SOH.

6.7 Summary of Second-Use of Vehicle Grade Battery Packs

In summary, the authors investigate the current barriers to adopting the repurposing of EV batteries for stationary energy storage and how battery pack designs and battery management systems may be affected. A design process is proposed which should be followed in the application of a repurposed battery pack in a stationary energy storage situation. Repurposed packs offer an alternative to more expensive energy storage solutions, which require new packs or specific infrastructure such as pumped hydro. There are many areas of research which still need to be sorted, in order to develop supply chains which can distribute used batteries to a re-manufacturer. The exact supply of vehicle batteries nearing end of life is still uncertain, as Li-ion technology is new to the market. Also, legislation needs to be drafted in order to properly regulate this market.

To encourage the adoption of EV batteries for stationary applications it is important to prove that the battery packs are safe. The safety risks identified by the failure mode analysis and fault tree assessments display the need for additional safeguards to be in place to protect consumers from harm. As the repurposed EV batteries have been depleted, there is a higher risk of failure occurring. Thus, the employment of safeguards, such as those developed in the FMEA Action Plan, is crucial, along with ensuring that recyclers and remanufacturers have knowledge of the SOH of the battery and its past usage. A system similar to the SOH classification system described in this work, along with associated testing, needs to be implemented in order to further the technology's development.

7 Conclusions and Recommendations

7.1 Conclusions

The objective of this thesis is to explore the degradation phenomenon occurring within commercial $LiFePO_4$, with a primary focus on calendar aging of the battery. Calendar aging experiments were carried out at various temperatures and states of charge (SOC) to determine the extent of degradation. For each set of conditions, two cells were tested in order to have reproducibility between the results, including the cells that underwent a change in storage conditions. The conditions of 60^{o}C and 0% SOC, though, required that more cells be tested due to the high degree of cell failure that was being observed. In total, 32 A123 20AH cells underwent calendar aging tests. The conclusions from this investigation are summarized as follows:

1) **Highest capacity loss was observed in cells stored at high temperature and fully charged conditions.** This was demonstrated by tracking irreversible capacity loss as a function of storage time and was also observed in the ICP analysis (cells stored at 60^{o}C and 100% SOC had the highest Li content within the bulk graphite). The capacity losses were the result of the loss of cyclable lithium and a loss of active material at the anode. This is in accordance with what the literature states would occur, as the increased temperatures and high concentrations of lithium at the anode promote the proliferation of degradative side reactions to occur. [8] [18] Post-mortem analysis (SEM and optical microscopy images of the electrode samples) of these cells revealed that there was a build-up of a secondary layer of material on the anode, although it did not cover the entire area. The formation of this material over the anode is most likely correlated to the loss of active material as the build-up of this material may prevent Li ions from being able to intercalate within the active graphite material.
2) **Temperature played the most significant role in the degradation of the cell.** As depicted in the capacity loss curves for cells stored at 0% SOC and 60^{o}C and 50^{o}C, despite the cells being stored at a lower state of charge, storage at the 60^{o}C temperature condition led to much higher capacity losses compared to the 50^{o}C storage condition. The high temperature storage conditions are likely promoting the proliferation of the side

reactions that form a material that adheres onto the graphite, decreasing the available area for lithium to intercalate into the graphite.

3) **A "history" effect could be observed from cells that were stored at initially high temperature conditions and then shifted to less severe ones.** Storage of $LiFePO_4$ batteries at high temperatures had a pronounced effect on the rate of degradation, even after the cells had been switched to new, less severe storage conditions. Shifting cells from a higher temperature storage condition to a lower one will decrease the rate of capacity loss observed at the previous storage condition. The storage of the cells at this initial high-temperature condition, though, promotes increased degradation throughout the storage life of the cell. Had the cell been stored at much less severe conditions over its entire lifespan, the loss in capacity would have been a much smaller decrease with time.

The results of this investigation influenced the following…

1) **A lifetime prediction model was developed for a battery pack, within an electric vehicle, using the calendar aging data obtained from the aging experiments.** The effect of calendar aging has a distinct effect on overall battery lifetime. Both vehicles experienced greatly depleted ranges after a short period of time and reached their end of life (EOL) point much sooner than the ten year consumer requirement target. Thus, when considering battery lifetime it is very important to take both cycling aging and calendar aging into consideration for losses of capacity in lithium-ion batteries in an electric vehicle. However, it must be noted that the simulation results presented in this work are limited to the A123 AMP20 batteries selected for testing and modeling. The model generated for the battery requires semi-empirically-fit models for both calendar and cycling aging. Also, the cycling aging model relies on the use of manufacturer data rather than experimentally collected data. Regardless of these limitations, the results support the need for further investigation into the effect of calendar aging on battery lifetime.
2) **A process for the formation of a battery pack using repurposed vehicle batteries was proposed.** The design process outlines the process of formation of a battery pack based on current applicable standards, failure analysis of repurposed batteries, and market analysis of in-vehicle batteries. This analysis also helped to identify current barriers to the adoption of repurposed batteries for energy storage. Following this, the design process

was applied to build a bench test setup of the finalized design to prove functionality of the system.

3) **A process for classifying battery pack states of health has been created. To encourage the adoption of EV batteries for stationary applications, it is important to prove that the battery packs are safe.** As the repurposed EV batteries have been depleted, there is a higher risk of failure occurring. Thus, the employment of safeguards, such as those developed in the FMEA Action Plan, is crucial, along with ensuring that recyclers and remanufacturers have knowledge of the SOH of the battery and its past usage. A similar system to the state of health (SOH) classification system described in this work needs to be developed for large scale implementation.

7.2 Recommendations

The following recommendations outline areas of focus for future work in the testing of $LiFePO_4$ batteries and potential methods to improve the accuracy of the simulations presented in this work.

Completion of an in-depth analysis of the effect of "storage history" on the lithium-ion batteries. During testing it was found that initially storing cells at high temperature conditions led to them experiencing increased degradation throughout their lifetimes despite undergoing a change of conditions. Research should be completed in determining the reaction pathway for this increased degradation within the cells.

Continue with post-mortem analyses of EOL cells. Many cells were utilized in the calendar aging experiments. Only four of these cells were utilized in the post-mortem analysis for the conditions: 35^{o}C and 100% SOC, 60^{o}C and 100% SOC, 60^{o}C and 0% SOC, and an unaged cell. There are still a number of cells that require post-mortem analysis, including cells stored at the temperature condition of 50^{o}C. It will be interesting to observe if there are similar degradation species present in the 50^{o}C samples as there were on the 60^{o}C samples.

Proceed with the development of a more advanced lifetime model. In future work the relation between calendar and cycle life has to be investigated in more detail to account for this effect.

Also, with more testing capabilities the cycle life model will be further enhanced by being able to model degradation with drive cycles over many cycles.

In order to better understand SOH for potential repurposed battery packs, as Li-ion powered electric and hybrid vehicles reach their EOL, degradation studies should be completed to verify estimates in SOH. A further study of the degradation of full battery packs is required to better understand how degradation is occurring within the cells. These studies will provide insight into how SOH can be assessed in a full battery pack, as they are introduced in repurposed applications. As a result, companies repurposing batteries will be better equipped to assess the SOH of incoming battery packs and be able to classify them, potentially using the standard described in this text.

8 References

[1] M. Bellis, "Who Invented the Car," 1 July 2016. [Online]. Available: http://inventors.about.com/od/famousinventions/fl/Who-Invented-the-Car.htm. [Accessed 17 October 2015].

[2] Toyota, 2013. [Online]. Available: http://www.toyotapriusbattery.com/.

[3] K. Smith, M. Earleywine, E. Wood, J. Neubauer and A. Pesaran, "Comparison of Plug-In Hybrid Electric Vehicle Battery Life Across Geographies and Drive Cycles," in *2012 SAE World Congress and*, Detroit, Michigan, 2012.

[4] H. Cars, "History of Hybrid Vehicles," 27 March 2006. [Online]. Available: http://web.archive.org/web/20090208230718/http:/www.hybridcars.com/history/history-of-hybrid-vehicles.html. [Accessed 17 October 2015].

[5] A. Boulanger, A. Chu, S. Maxx and D. Waltz, "Vehicle Electrification: Status and Issues," World Team Now, Malibu, 2011.

[6] A. Barré, B. Deguilhem, S. Grolleau and M. Gérard, "A review on lithium-ion battery ageing mechanisms and estimations for automotive applications," *Journal of Power Sources*, vol. 241, pp. 680-689, 2013.

[7] M. Kassem, J. Bernard, R. Revel, S. Pélissier, F. Duclaud and C. Delacourt, "Calendar aging of a graphite/LiFePO4 cell," *Journal of Power Sources*, vol. 208, p. 296–305, 2012.

[8] S. Grolleau, A. Delaille, H. Gualous, P. Gyan, R. Revel, J. Bernard, E. Redondo-Iglesias and J. Peter, "Calendar aging of commercial graphite/LiFePO4 cell - Predicting capacity fade under time dependent storage conditions," *Journal of Power Sources*, vol. 255, pp. 450-458, 2014.

[9] M. Kassem, J. Bernard, R. Revel, S. Pélissier, F. Duclaudd and C. Delacourt, "Calendar aging of a graphite/LiFePO4 cell," *Journal of Power Sources*, vol. 208, pp. 296-305, 2012.

[10] M. Turcotte, "Commuting to work," Statistics Canada, 2011. [Online]. Available: https://www12.statcan.gc.ca/nhs-enm/2011/as-sa/99-012-x/99-012-x2011003_1-eng.cfm. [Accessed 8 July 2016].

[11] M. Ecker, J. B. Gerschler, J. Vogel, S. Käbitz, F. Hust, P. Dechent and and, "Development of a lifetime prediction model for lithium-ion batteries based on extended accelerated aging test data," *Journal of Power Sources,* vol. 215, pp. 248-257, 2012.

[12] E. Wood, "Battery End-of-Life Considerations for Plug-in Hybrid Electric Vehicles," Colorado State University, Fort Collins, Colorado, 2011.

[13] M. Kassem and C. Delacourt, "Postmortem analysis of calendar-aged graphite/LiFePO4 cells," *Journal of Power Sources,* vol. 235, pp. 159-171, 2013.

[14] M. Safari and C. Delacourt, "Aging of a Commercial Graphite/LiFePO4 Cell," *Journal of The Electrochemical Society,* vol. 158, no. 10, pp. A1123-A1135, 2011.

[15] L. Lu, X. Ha, J. Li, J. Hua and M. Ouyang, "A review on the key issues for lithium-ion battery management in electric vehicles," *Journal of Power Sources,* vol. 226, pp. 272-288, 2013.

[16] D. Linden and T. B. Reddy, "Chapter 1 Basic Concepts," in *Handbook of Batteries*, New York, McGraw-Hill, 2002, pp. 19-34.

[17] I. Husain, in *Electric and Hybrid Vehicles: Design Fundamentals, Second Edition*, CRC Publisher, 2010.

[18] J. Vetter, P. Novak, M. Wagner, C. Veit, K. Moller and J. Besenhard, "Ageing mechanisms in lithium-ion batteries," *Journal of Power Sources,* vol. 147, pp. 269-281, 2005.

[19] K. Young, C. Wang, L. Y. Wang and a. K. Strunz, Electric Vehicle Integration into Modern Power Networks, R. Garcia-Valle and J. A. P. Lopes, Eds., New York: Springer Science+Business Media, 2013, pp. 15-56.

[20] Nissan, 2010. [Online]. Available: http://www.nissanusa.com/leaf-electric-car/.

[21] General Motors, "2016 CHEVROLET VOLT BATTERY SYSTEM," General Motors, 2016. [Online]. Available: https://media.gm.com/content/dam/Media/microsites/product/Volt_2016/doc/VOLT_BATTERY.pdf. [Accessed 3 July 2016].

[22] P. Simon and Y. Gogotsi, "Materials for electrochemical capacitors," *Nature Materials,* vol. 7, pp. 845-854, 2008.

[23] C. Lin, A. Tang, H. Mu, WenweiWang and C. Wang, "Aging Mechanisms of Electrode Materials in Lithium-Ion Batteries for Electric Vehicles," *Journal of Chemistry,* vol. 2015, pp. 1-11, 2015.

[24] A. Barré, B. Deguilhem, S. Grolleau, M. Gérard, F. Suard and D. Riu, "A review on lithium-ion battery ageing mechanisms and estimations for automotive applications," *Journal of Power Sources,* vol. 241, pp. 680-689, 2013.

[25] L. Ahmadi, M. Fowler, S. Young, R. Fraser, B. Gaffney and S. Walker, "Energy efficiency of Li-ion battery packs re-used in stationary power applications," *Sustainable Energy Technologies and Assessments,* vol. 8, pp. 9-17, December 2014.

[26] D. Finley, "Battery Degradation Modeling for Vehicle Applications," University of Waterloo, Waterloo, Ontario, 2014.

[27] U. S. D. o. Energy, "Battery Testing, Analysis and Design," United States Department of Energy, Washington D.C., 2013.

[28] P. Ramadass, B. Haran, R. White and B. Popov, "Capacity fade of Sony 18650 cells cycled at elevated temperatures: Part I. Cycling performance," *Journal of Power Sources,* vol. 606, p. 112, 2002.

[29] J. Tarascon and M. Armand, "Issues and challenges facing rechargeable lithium batteries," *Nature,* vol. 414, pp. 359-367, 2001.

[30] C. Mikolajczak, M. Kahn, K. White and R. Thomas Long, "Lithium-Ion Batteries Hazard and Use Assessment," The Fire Protection Research Foundation, Qunicy, Massachusettes, 2011.

[31] I. Buchmann, "Pouch Cell - Small but not Trouble Free," Battery University, 2011. [Online]. Available: http://batteryuniversity.com/learn/archive/pouch_cell_small_but_not_trouble_free. [Accessed 22 January 2016].

[32] C. Hendricks, N. Williard, S. Mathew and M. Pecht, "A failure modes, mechanisms, and effects analysis (FMMEA) of lithium-ion batteries," *Journal of Power Sources,* vol. 297, pp. 113-120, 2015.

[33] A123 Energy Solutions, "Battery Pack Design, Validation, and Assembly Guide using A123 Systems AMP20m1HD-A Nanophosphate Cells," A123 Energy Solutions, Livonia, Michigan, 2014.

[34] Battery University, "Lithium-ion Safety Concerns," Cadex, 2010. [Online]. Available: http://batteryuniversity.com/learn/archive/lithium_ion_safety_concerns. [Accessed 11 June 2016].

[35] I. Buchmann, "BU-305: Building a Lithium-ion Pack," Battery University, 2016. [Online]. Available: http://batteryuniversity.com/learn/article/building_a_lithium_ion_pack. [Accessed 23 January 2016].

[36] Electropedia, "Battery Safety," Woodbank Communications Ltd, 2005. [Online]. Available: http://www.mpoweruk.com/safety.htm. [Accessed 11 June 2016].

[37] UL LLC, "Safety Issues for Lithium-Ion Batteries," UL LLC, 2013.

[38] U. Irfan, "How Lithium Ion Batteries Grounded the Dreamliner," Scientific America, 18 December 2014. [Online]. Available: https://www.scientificamerican.com/article/how-lithium-ion-batteries-grounded-the-dreamliner/. [Accessed 1 February 2017].

[39] Natural Resources Canada, "Developing Electrical Safety Standards to Introduce Electric Vehicles into Canada," 2016. [Online]. Available: http://www.nrcan.gc.ca/energy/funding/current-funding-programs/eii/16104. [Accessed 10 June 2016].

[40] Woodbank Communications Ltd, 2005. [Online]. Available: http://www.mpoweruk.com/failure_modes.htm. [Accessed 22 February 2017].

[41] Argonne National Laboratory, "Non-Year-Specific Rules - Revision: G," Argonne National Laboratory, 2016.

[42] J. Kessen, "Beyond Chemistry: Robust Battery Pack Design Key to EV Safety," A123, 22 May 2012. [Online]. Available: http://www.a123systems.com/Beyond-Chemistry-Robust-Battery-Pack-Design-Key-to-EV-Safety.htm. [Accessed 10 June 2016].

[43] K. W. E. Cheng, S. Cheng, B. P. Divakar, H. Wu, K. Ding and a. H. F. Ho, "Battery-Management System (BMS) and SOC Development for Electrical Vehicles," *IEEE TRANSACTIONS ON VEHICULAR TECHNOLOGY,* vol. 60, no. 1, pp. 1-13, 2011.

[44] H. Rahimi-Eichi, F. B. Unnati Ojha and M.-Y. Chow, "Battery Management System An Overview of its Application in the Smart Grid and Electric Vehicles," *IEEE industrial electronics magazine,* pp. 4-16, 2013.

[45] I. Buchmann, "BU-908: Battery Management System (BMS)," Cadex, 29 01 2016. [Online]. Available: http://batteryuniversity.com/learn/article/how_to_monitor_a_battery. [Accessed 15 June 2016].

[46] K. Smith, E. Wood, S. Santhanagopalan, G.-H. Kim, J. Neubauer and A. Pesaran, "Models for Battery Reliability and Lifetime," in *Battery Congress 2013*, Ann Arbor, Michigan, 2013.

[47] J. Christophersen, I. Bloom, E. Thomas and V. Battaglia, "Battery Life Estimator Manual Linear Modeling and Simulation," Idaho National Laboratory, Idaho Falls, Idaho, 2009.

[48] A. Moshirvaziri, "LITHIUM-ION BATTERY MODELING for ELECTRIC VEHICLES and REGENERATIVE CELL TESTING PLATFORM," University of Toronto, Toronto, Ontario, 2013.

[49] Q. Badey, G. Cherouvrier, Y. Reynier, J.-M. Duffault and S. Franger, "Ageing forecast of lithium-ion batteries for electric and hybrid vehicles," *Current Topics in Electrochemistry*, vol. 16, pp. 65-79, 2011.

[50] X. Hua, S. Li and H. Peng, "A comparative study of equivalent circuit models for Li-ion batteries," *Journal of Power Sources*, vol. 198, pp. 359-367, 2012.

[51] H. He, R. Xiong and J. Fan, "Evaluation of Lithium-Ion Battery Equivalent Circuit Models for State of Charge Estimation by an Experimental Approach," *Energies*, vol. 4, pp. 582-598, 2011.

[52] V. Ramadesigan, P. W. C. Northrop, S. De, S. Santhanagopalan, R. D. Braatz and a. V. R. Subramaniana, "Modeling and Simulation of Lithium-Ion Batteries from a Systems Engineering Perspective," *Journal of The Electrochemical Society*, vol. 159, no. 3, pp. 31-45, 2012.

[53] R. Nicolas, "The different driving cycles," 5 January 2013. [Online]. Available: http://www.car-engineer.com/the-different-driving-cycles/. [Accessed 03 January 2016].

[54] US Environmental Protection Agency, "Dynamometer Drive Schedules," 27 April 2016. [Online]. Available: https://www.epa.gov/vehicle-and-fuel-emissions-testing/dynamometer-drive-schedules. [Accessed 29 June 2016].

[55] N. A. CHATURVEDI, R. KLEIN, J. CHRISTENSEN, J. AHMED and A. KOJIC, "Algorithms for Advanced Battery-Management Systems," *IEEE CONTROL SYSTEMS MAGAZINE*, pp. 49-68, 2010.

[56] B. Xu, "Degradation-limiting Optimization of Battery Energy Storage Systems Operation," Federal Institute of Technology Zurich (ETH Zurich), Zurich, 2013.

[57] P. Keil, S. F. Schuster, J. Wilhelm, J. Travi and A. Hauser, "Calendar Aging of Lithium-Ion Batteries I. Impact of the Graphite Anode on Capacity Fade," *Journal of The Electrochemical Society,* vol. 163, no. 9, pp. 1872-1880, 2016.

[58] A. K. Padhi, K. Nanjundaswamy and J. B. Goodenough, "Phospho-olivines as Positive-Electrode Materials for Rechargeable Lithium Batteries," *J. Electrochem. Soc.*, vol. 144, no. 4, pp. 1188-1194, April 1997.

[59] E. Wang, D. Ofer, W. Bowden, N. Iltchev, R. Moses and K. Brandt, "Stability of Lithium Ion Spinel Cells III. Improved Life of Charged Cells," *Journal of The Electrochemical Society,* vol. 147, no. 11, pp. 4023-4028, 2000.

[60] A. H. Zimmerman, "Self-Discharge Losses in Lithium-Ion Cells," *IEEE AESS Systems Magazine,* pp. 19-24, 2004.

[61] K. Ohue, T. Utsunomiya, O. Hatozaki, N. Yoshimotoa, M. Egashira and M. Morita, "Self-discharge behavior of polyacenic semiconductor and graphite negative electrodes for lithium-ion batteries," *Journal of Power Sources,* vol. 196, p. 3604–3610, 2011.

[62] M. Koltypin, D. Aurbach, L. Nazar and B. Ellis, "More on the performance of LiFePO4 electrodes—The effect of synthesis route, solution composition, aging, and temperature," *Journal of Power Sources,* vol. 174, p. 1241–1250, 2007.

[63] S. J. Harris, A. Timmons, D. R. Baker and C. Monroe, "Direct in situ measurements of Li transport in Li-ion battery negative electrodes," *Chemical Physics Letters,* vol. 485, p. 265–274, 2010.

[64] Q. Badey, G. Cherouvrier, Y. Reynier, J.-M. Duffault and S. Franger, "Ageing forecast of lithium-ion batteries for," *Current Topics in Electrochemistry,* vol. 16, 2011.

[65] A. H. Zimmerman and M. V. Quinzio, "Lithium Plating in Lithium-Ion Cells," in *NASA Battery Workshop*, Huntsville, AL, 2010.

[66] S. Bourlot, P. Blanchard and S. Robert, "Investigation of aging mechanisms of high power Li-ion cells used for hybrid electric vehicles," *Journal of Power Sources,* vol. 196, p. 6841–6846, 2011.

[67] A. W. Golubkov, D. Fuchs, J. Wagner, H. Wiltsche, C. Stangl, G. Fauler, G. Voitic, A. Thaler and V. Hacker, "Thermal-runaway experiments on consumer Li-ion batteries with metal-oxides and olivin-type cathodes," *RSC Adv.*, vol. 4, pp. 3633-3642, 2014.

[68] K. Kumai, H. Miyashiro, Y. Kobayashi, K. Takei and R. Ishikawa, "Gas generation mechanism due to electrolyte decomposition in commercial lithium-ion cell," *Journal of Power Sources,* Vols. 81-82, p. 715–719, 1999.

[69] C. Mikolajczak, M. Kahn, K. White and R. T. Long, "Lithium-Ion Batteries Hazard and Use Assessment," Quincy, 2011.

[70] K. S. Ng, C. S. Moo, Y. P. Chen and Y. C. Hsieh, "Enhanced coulomb counting method for estimating state-of-charge and state-of-health of lithium-ion batteries," *Applied Energy,* vol. 86, pp. 1506-1511, 2009.

[71] A123 Systems, "20Ah Prismatic Pouch Cell," 2017. [Online]. Available: www.a123systems.com. [Accessed 31 October 2015].

[72] E. R. D. Doughty, "A General Discussion of Li Ion Battery Safety," *The Electrochemical Society Interface,* vol. 2, no. 37-44, p. 21, 2012.

[73] M. W. Davidson and M. Abramowitz, "OPTICAL MICROSCOPY," The Florida State University, Tallahassee, Florida, 1999.

[74] T. Waldmann, A. Iturrondobeitia, M. Kasper, N. Ghanbari, F. Aguesse, E. Bekaert, L. Daniel, S. Genies, I. J. Gordon, M. W. Loble, E. D. Vito and a. M. Wohlfahrt-Mehrensa, "Review—Post-Mortem Analysis of Aged Lithium-Ion Batteries: Disassembly Methodology and Physico-Chemical Analysis Techniques," *Journal of The Electrochemical Society,* vol. 163, no. 10, pp. 2149-2164, 2016.

[75] M. Heb, *Kinetics and stage transitions of graphite for lithium-ion batteries,* Zurich: Otto-von-Guericke University Magdeburg, 1983.

[76] L. Boulet-Roblin, M. E. Kazzi, P. Novak and C. Villevieillez, "Surface/Interface Study on Full xLi2MnO3·(1 − x)LiMO2 (M = Ni, Mn, Co)/Graphite Cells," *Journal of The Electrochemical Society,* vol. 162, no. 7, pp. 1297-1300, 2015.

[77] J. Goldstein, D. Newbury, D. Joy, C. Lyman, P. Echlin, E. Lifshin, L. Sawyer and J. Michael, Scanning Electron Microscopy and X-ray Microanalysis, 3rd ed., New York: Spinger US, 2003.

[78] S. Bewlay, K. Konstantinov, G. Wang, S. Dou and H. Liu, "Conductivity improvements to spray-produced LiFePO4 by addition of a carbon source," *Materials Letters,* vol. 58, pp. 1788-1791, 2004.

[79] E. C. Teague, F. E. Scire, S. M. Baker and S. W. Jensen, "THREE-DIMENSIONAL STYLUS PROFILOMETRY," *Wear,* vol. 83, pp. 1-12, 1982.

[80] J. C. WYANT, C. L. KOLIOPOULOS, B. BHUSHAN and O. E. GEORGE, "An Optical Profilometer for Surface Characterization of Magnetic Media," *ASLE Transacations,* vol. 27, no. 2, pp. 101-113, 1984.

[81] Z. Mao, M. Farkhondeh, M. Pritzker, M. Fowler and Z. Chen, "Multi-Particle Model for a Commercial Blended Lithium-Ion Electrode," *Journal of The Electrochemical Society,* vol. 163, no. 3, pp. 458-469, 2016.

[82] D. J. Xiong, L. D. Ellis, K. J. Nelson, T. Hynes, R. Petibon and a. J. R. Dahn, "Rapid Impedance Growth and Gas Production at the Li-Ion Cell Positive Electrode in the Absence of a Negative Electrode," *Journal of The Electrochemical Society,* vol. 163, no. 14, pp. A3069-A3077, 2016.

[83] M. Keyser, D. Long, J. Ireland, Y. Jung, K.-J. Lee, K. Smith and S. Santhanagopalan, "Numerical and Experimental Investigation of Internal Short Circuits in a Li-ion Cell," 2011. [Online]. Available: https://energy.gov/sites/prod/files/2014/03/f10/es109_kim_2011_p.pdf. [Accessed 12 1 2017].

[84] M. Armand and J.-M. Tarascon, "Building better batteries," *Nature Publishing Group,* vol. 451, pp. 652-657, 2008.

[85] S. C. Davis, S. W. Diegel and a. R. G. Boundy, "Transportation Energy Data Book Edition 33," U.S. Department of Energy, Wahington, 2014.

[86] A123 Systems, "EcoCAR2 Energy Storage System (ESS) Deepdive," EcoCAR2 Competition, Washington, 2011.

[87] J. Tham, "ME 599 Hybrid Vehicles (Fall 2015) Final Design Report Design and Finite Element Analysis of Battery Module Mounting Structure," University of Waterloo Alternative Fuels Team (ME 599), Waterloo, 2015.

[88] G. Pistoia, Lithium-Ion Batteries: Advances and Applications, Amsterdam: Elsevier, 2014.

[89] National Electrical Manufacturers Association, "ANSI/IEC 60529-2004 Degrees of Protection Provided by Enclosures," National Electrical Manufacturers Association, Rosslyn, Virginia, 2004.

[90] L. Lu, X. Han, J. Li, J. Hua and M. Ouyang, "A review on the key issues for lithium-ion battery management in electric vehicles," *Journal of Power Sources,* vol. 226, pp. 272-288, 2013.

[91] Tesla Motors, "Cold Weather Driving," Tesla Motors Club, 15 1 2015. [Online]. Available: https://teslamotorsclub.com/tmc/threads/cold-weather-driving.64591/. [Accessed 21 4 2017].

[92] Tesla Motors, "Slow supercharging in cold weather," Tesla Motors Company, 13 2 2015. [Online]. Available: https://forums.tesla.com/en_CA/forum/forums/slow-supercharging-cold-weather. [Accessed 21 4 2017].

[93] Government of Canada, "Historical Climate Data," 2017. [Online]. Available: http://climate.weather.gc.ca/historical_data/search_historic_data_e.html. [Accessed 15 1 2017].

[94] L. Ahmadi, S. B. Young, M. Fowler, R. A. Fraser and M. A. Achachlouei, "A cascaded life cycle: reuse of electric vehicle lithium-ion battery packs in energy storage systems," *International Journal of Life Cycle Assessment,* vol. 22, no. 1, pp. 111-124, April 2017.

[95] E. Cready, J. Lippert, J. Pihl, I. Weinstoc, P. S. and R. Jungst, "Final Report: Technical and Economic Feasibility of Applying Used EV Batteries in Stationary Applications," Sandia National Laboratories, Albuquerque, New Mexico, 2003.

[96] S. W. Hadley and A. A. Tsvetkova, "Potential Impacts of Plug-in Hybrid Electric Vehicles on Regional Power Generation," *The Electricity Journal,* vol. 22, no. 10, pp. 56-68, 2009.

[97] N. Jiao and S. Evans, "Business models for sustainability: the case of second-life electric vehicle batteries," *Procedia CIRP,* vol. 40, pp. 250-255, 2016.

[98] National Renewable Energy Laboratory, "Battery Second Use for Plug-In Electric Vehicles," National Renewable Energy Laboratory, 26 June 2015. [Online]. Available: http://www.nrel.gov/transportation/energystorage/use.html?print. [Accessed 5 August 2016].

[99] L. Ahmadi, A. Yip, M. Fowler, S. B. Young and R. A. Fraser, "Environmental feasibility of re-use of electric vehicle batteries," *Sustainable Energy Technologies and Assessments*, vol. 6, no. 64-74, 2014.

[100] Natural Resources Canada - Office of Energy Efficiency, "Energy Efficiency Trends in Canada, 1990 to 2009," Natural Resources Canada, 09 July 2012. [Online]. Available: http://oee.rncan.gc.ca/publications/statistics/trends11/appendix-1.cfm?graph=14&attr=0. [Accessed 17 August 2016].

[101] Natural Resources Canada, "Energy Fact Book 2015-2016," Ottawa, 2015.

[102] P. Gallant, "Ontario's Power Trip: Province lost $1.2-billion this year exporting power," Financial Post, 02 12 2013. [Online]. Available: http://business.financialpost.com/2013/12/02/ontarios-power-trip-province-lost-1-2-billion-this-year-exporting-power/. [Accessed 12 12 2016].

[103] J. Russel, "Tesla's $3,000 Powerwall Will Let Households Run Entirely On Solar Energy," Tech Crunch, 30 April 2015. [Online]. Available: https://techcrunch.com/2015/04/30/tesla-powerwall-home-battery/#.uayvgx:LhV8. [Accessed 29 July 2016].

[104] Nissan Great Britain, "Nissan and Eaton make home energy storage reliable and affordable to everyone with 'xStorage'," 10 May 2016. [Online]. Available: http://www.newsroom.nissan-europe.com/uk/en-gb/Media/Media.aspx?mediaid=145249. [Accessed 10 August 2016].

[105] P. Ellsworth, W. Scott, M. Fowler, R. Fraser, B. Gaffney and D. V. Lanen, "Internal Resistance Optimization Utilizing "Just in Time" Control," in *SAE 2015 World Congress Exhibition*, Detroit, Michigan, 2015.

[106] Government of Canada - Transport Canada, "Did you know that Lithium Batteries are Dangerous Goods?," March 2016. [Online]. Available: https://www.tc.gc.ca/eng/tdg/lithium-batteries-are-dangerous-goods-1162.html. [Accessed 27 July 2016].

[107] J. Will, "Will buying a 'green' vehicle increase my insurance rates?," The Globe and Mail, 10 September 2012. [Online]. Available: http://www.theglobeandmail.com/globe-drive/culture/commuting/will-buying-a-green-vehicle-increase-my-insurance-rates/article626015/. [Accessed 29 July 2016].

[108] D. Conover, "Inventory of Safety-related Codes and Standards for Energy Storage Systems," Department of Energy, Oak Ridge, Tennessee, September 2014.

[109] UCLA BerkeleyLaw, "Reuse and Repower, How to Save Money and Clean the Grid with Second-Life Electric Vehicle Batteries," UCLA, California, 2014.

[110] D. S. B. O. K. B. A. L. A. Cimprich, "Responsible Stewardship of Electrified Vehicles," University of Waterloo, Waterloo, Ontario, 2015.

[111] M. Stevens, "Electric Vehicle Sales in Canada: 2015 Final Numbers," Fleetcarma, 9 February 2016. [Online]. Available: http://www.fleetcarma.com/ev-sales-canada-2015/. [Accessed 4 August 2016].

[112] J. Cocking and D. v. Lanen, "Design of an Energy Hub with Energy Storage for a Commercial Building," Waterloo Engineering, Waterloo, 2014.

[113] Tesla Motors, "Impacts of Battery Charging Rates of Plug-in Electric Vehicle on Smart Grid Distribution Systems," 2010. [Online]. Available: http://www.teslamotors.com/.

[114] M. Foster, P. Isely, C. R. Standridge and M. M. Hasan, "Feasibility assessment of remanufacturing, repurposing, and recycling of end of vehicle application lithium-ion batteries," *Journal of Industrial Engineering Management*, vol. 7, no. 3, pp. 698-715, 2014.

[115] Tesla, "Powerwall Support," 2016. [Online]. Available: https://www.tesla.com/en_CA/support/powerwall?redirect=no. [Accessed 4 August 2016].

[116] Canadian Standards Association, "Canadian Electrical Code, Part 1," Canadian Standards Association, Missisauga, Ontario, 2016.

[117] International Electrotechnical Commission, "IEC 62619 Ed1 NP Secondary Cells and Batteries Containing Alkaline or Other Non-Acid Electrolytes Safety Requirements for Secondary Lithium Cells and Batteries, for use in Industrial Applications," IEC, Rosslyn, Virginia, 2015.

[118] R. K. Wood, K. G. Stephens and B. O. Barker, "FAULT TREE ANALYSIS: AN EMERGING METHODOLOGY FOR INSTRUCTIONAL SCIENCE," *Instructional Science*, vol. 8, pp. 1-22, 1979.

[119] N. Omar, M. A. Monem, Y. Firouz, J. Salminen, J. Smekens, O. Hegazy, H. Gaulous, G. Mulder, P. V. d. Bossche, T. Coosemans and J. V. Mierlo, "Lithium iron phosphate based

battery – Assessment of the aging parameters and development of cycle life model," *Applied Energy,* vol. 113, pp. 1575-1585, 2014.

[120] J. Vetter, P. Novák, M. Wagner, C. Veit, K.-C. Möller, J. O. Besenhard, M. Winter, M. Wohlfahrt-Mehrens, C. Vogler and A. Hammouche, "Ageing mechanisms in lithium-ion batteries," *Journal of Power Sources,* vol. 147, pp. 269-281, 2005.

[121] M. Safari, M. Morcrette, A. Teyssot and C. Delacourt, "Multimodal physics-based aging model for life prediction of Li-ion batteries," *Journal of The Electrochemical Society,* vol. 156, no. 3, pp. A145-A153, 2009.

[122] J. Lo, "Effect of temperature on lithium-iron phosphate battery performance and plug-in hybrid electric vehicle range," University of Waterloo, Waterloo, Ontario, 2013.

[123] J. Tarascon and M. Armand, "Issues and challenges facing rechargeable lithium batteries," *Nature,* vol. 414, pp. 359-367, 2001.

[124] D. White, "Safety and Preventing Thermal Run Away in Large Li-Ion Batteries," Battery Power, June 2012. [Online]. Available: http://www.batterypoweronline.com/main/markets/testingservices/safety-and-preventing-thermal-run-away-in-large-li-ion-batteries/. [Accessed 17 July 2016].

[125] D. Conover, "Overview of Development and Deployment of Codes, Standards and Regulations Affecting Energy Storage System Safety in the United States," U.S. Department of Energy, Richland, 2014.

[126] Allstate, "Car Insurance for Your Electric Vehicle," Allstate, April 2014. [Online]. Available: https://www.allstate.com/tools-and-resources/car-insurance/electric-vehicle.aspx. [Accessed 4 August 2016].

[127] CSA Group, "CAN/CSA-E62133:13," CSA Group, 2013. [Online]. Available: http://shop.csa.ca/en/restofworld/component-standards/cancsa-e6213313/invt/27035982013. [Accessed 15 August 2016].

[128] W. Burr, "Electric Vehicle Charging Stations," Electrical Industry Canada, 2016. [Online]. Available: http://electricalindustry.ca/latest-news/364-electric-vehicle-charging-systems. [Accessed 16 August 2016].

[129] P. Gowalecki, Interviewee, *personal communication.* [Interview]. 18 August 2016.

[130] P. Gevorkian, Solar Power in Building Design: The Engineer's Complete Design Resource, New York: McGraw-Hill Education, 2008.

[131] CSA Group, February 2017. [Online]. Available: http://www.csagroup.org/services/codes-and-standards/standards-development/how-standards-are-developed/. [Accessed 21 February 2017].

[132] National Fire Protection Agency, February 2017. [Online]. Available: http://www.nfpa.org/news-and-research/news-and-media/press-room/reporters-guide-to-fire-and-nfpa/about-codes-and-standards. [Accessed 21 February 2017].

[133] U. S. D. o. T. -. F. H. Administration, "Average Annual Miles per Driver by Age Group," United States Department of Transportation - Federal Highway Administration, 13 July 2016. [Online]. Available: https://www.fhwa.dot.gov/ohim/onh00/bar8.htm. [Accessed 25 October 2016].

[134] K. Takei, K. Kumai, Y. Kobayashi, H. Miyashiro, N. Terada, T. Iwahori and T. Tanaka, "Cycle life estimation of lithium secondary battery by extrapolation method and accelerated aging test," *Journal of Power Sources,* Vols. 97-98, pp. 697-701, 2001.

[135] M. Safari and C. Delacourta, "Simulation-Based Analysis of Aging Phenomena in a Commercial Graphite/LiFePO4 Cell," *Journal of The Electrochemical Society,* vol. 158, no. 12, pp. A1436-A1447, 2011.

[136] N. A. Chaturvedi, R. Klein, J. Christensen, J. Ahmed and A. Kojic, "Algorithms for Advanced Battery-Management Systems," *IEEE CONTROL SYSTEMS MAGAZINE,* pp. 49-69, June 2010.

[137] N. Lohmann, M. Fischnaller, J. Melbert, T. Musch, P. Lamp, S. Scharner and a. V. Liebau, "Cycle Life Investigations on Different Li-ion Cell Chemistries for PHEV Applications Based on Real Life Conditions," *SAE International,* 2012.

Appendix A: Regulation Test Criteria

Table 28: Regulation Testing Criteria

Test Criteria/Standard	Description	Pass Criteria
External short circuit	Creates a connection between anode and cathode terminals of a cell to determine how cell can withstand maximum current flow.	Cell does not explode or cause a fire.
Abnormal charge/ Overcharge	Applies over-charging current rate and charging time to determine if sample can withstand stress.	Cell does not explode or cause a fire.
Forced discharge/ Overdischarge	Discharged cell connected in series with a specific number of charged cells of same type. The imbalanced pack is then short-circuited.	Cell does not explode or cause a fire.
Crush	Determines ability to withstand a specified crushing force (13 kN).	Cell does not explode or cause a fire.
Impact (cell)	Determines cell's ability to withstand an impact. Impact is applied to a cylindrical steel rod placed across the cell.	Cell does not explode or cause a fire.
Shock	Cell or battery is secured to testing machine calibrated to apply a specified average and peak acceleration for duration of test.	Sample may not explode, ignite, leak or vent.
Vibration	Applies simple harmonic motion to a sample, at specified amplitude, with variable frequency and time.	Sample may not explode, ignite, leak or vent.
Heating (cell)	Cell is exposed to an elevated temperature condition for a period of time.	Sample may not explode or ignite.
Temperature cycling	Subjects each sample to a specific temperature above and below room temperature for a certain number of cycles.	Sample may not explode, ignite, leak or vent.
Low pressure (altitude)	Sample is exposed to pressure less than standard atmospheric	Sample may not explode, ignite, leak or vent.
Projectile/External fire	Cell sample exposed to a flame on a wire mesh structure.	If flame causes an explosion or ignition of the cell, no part of cell sample can penetrate or protrude through wire mesh test cage.
Drop	Cell/battery is exposed to a specific number of free falls to a hard surface.	Sample may not explode or ignite.
Molded casing heating test	Plastic encased batteries are subjected to a specific elevated temperature for a specific time.	Internal cells may not show any evidence of mechanical damage.
Insulation or isolation resistance	Sample is subjected to a resistance measurement between each battery terminal and the accessible metal parts of the battery pack.	Measured resistance must exceed the specified minimum value.
Internal short circuit test or propagation test	JIS C8714, SBA S1101 and IEC 62133 second edition – internal short circuit by disassembling a charged cell sample casing and placing a specified nickel particle under the cell winding construction.	Sample may not explode or ignite.

Appendix B: Images of post-mortem analysis of $LiFePO_4$ cells

Figure 92: Graphite electrode aged 60ºC 100% SOC

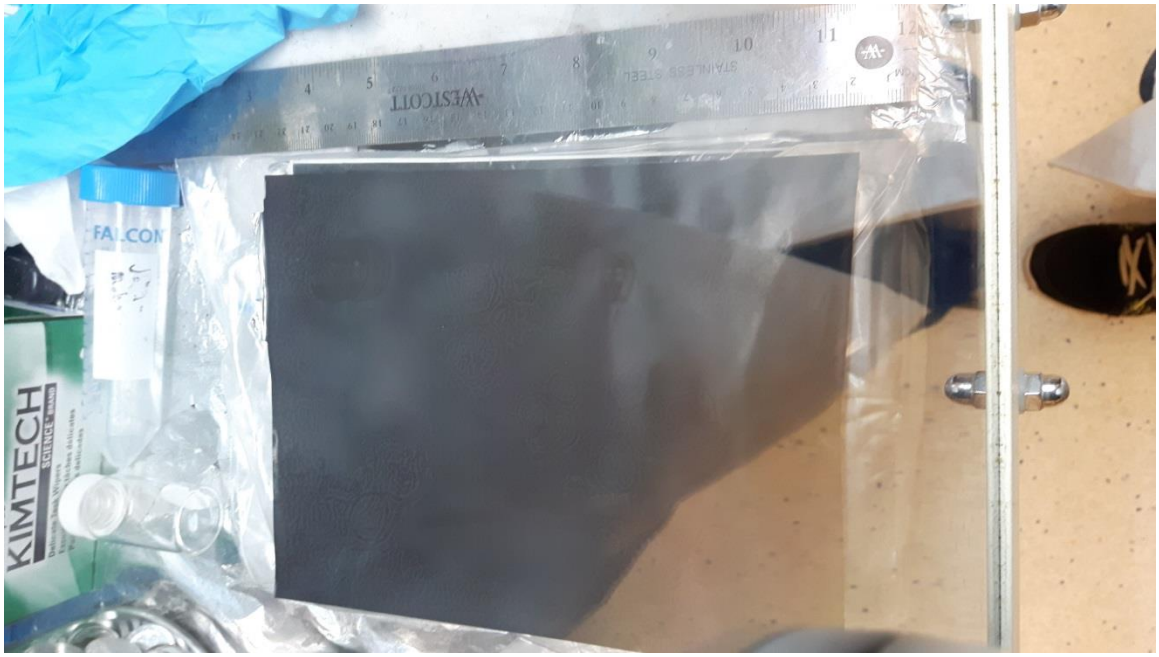

Figure 93: LFP electrode aged 60ºC 100% SOC

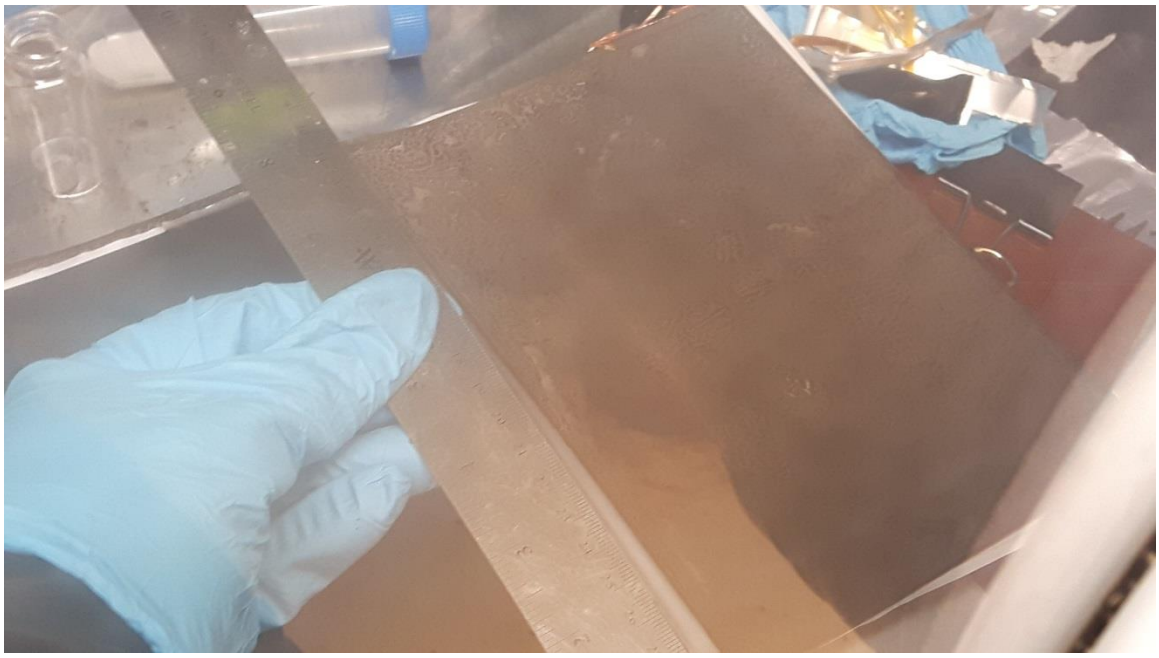

Figure 94: Graphite electrode aged 60ºC 0% SOC

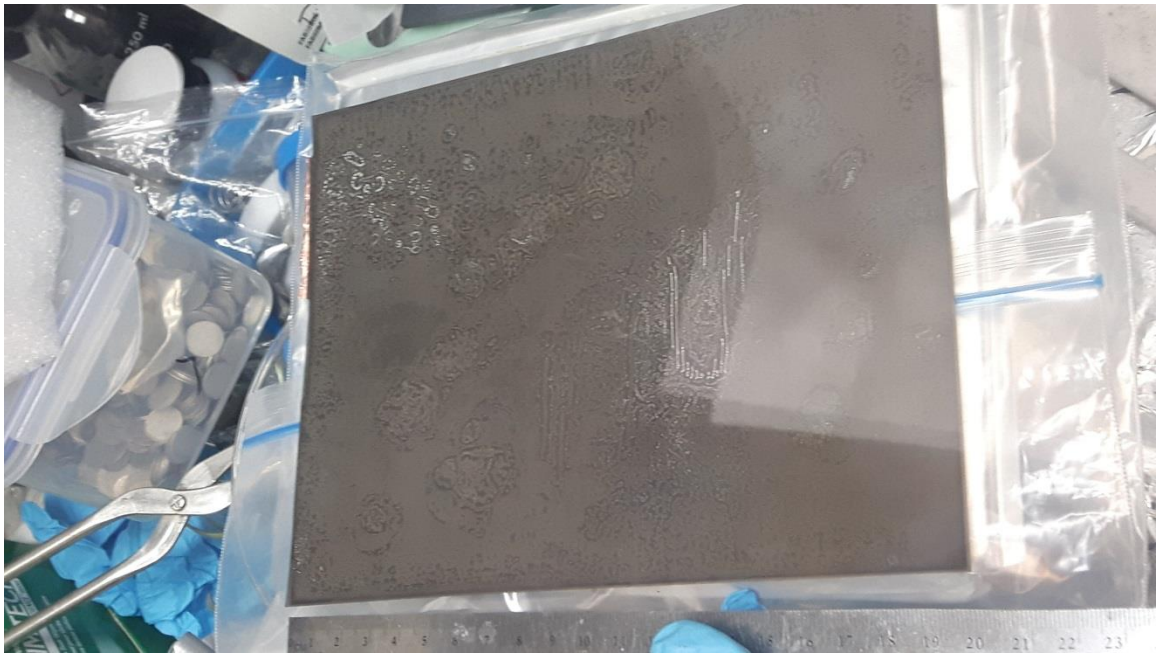

Figure 95: LFP electrode aged 60ºC 0% SOC

Figure 96: Graphite electrode aged 35ºC 100% SOC

Figure 97: LFP electrode aged 35ºC 100% SOC

Figure 98: Fresh Graphite electrode

Figure 99: Fresh LFP electrode

Appendix C: Optical Microscopy Images

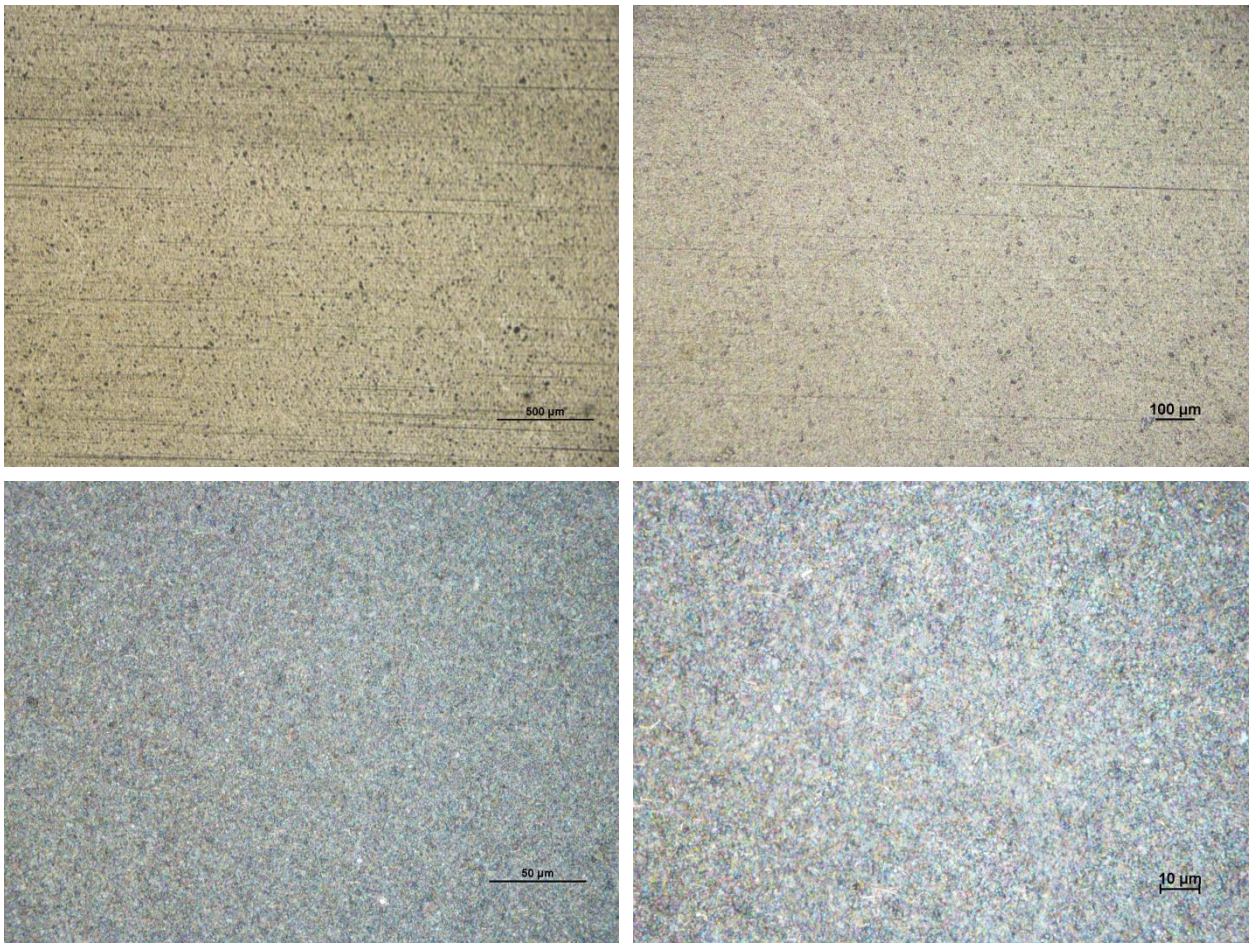

Figure 100: Fresh LFP (upper left: 5x magnification, upper right: 10x magnification, bottom left: 50x magnification, bottom right: 100x magnification)

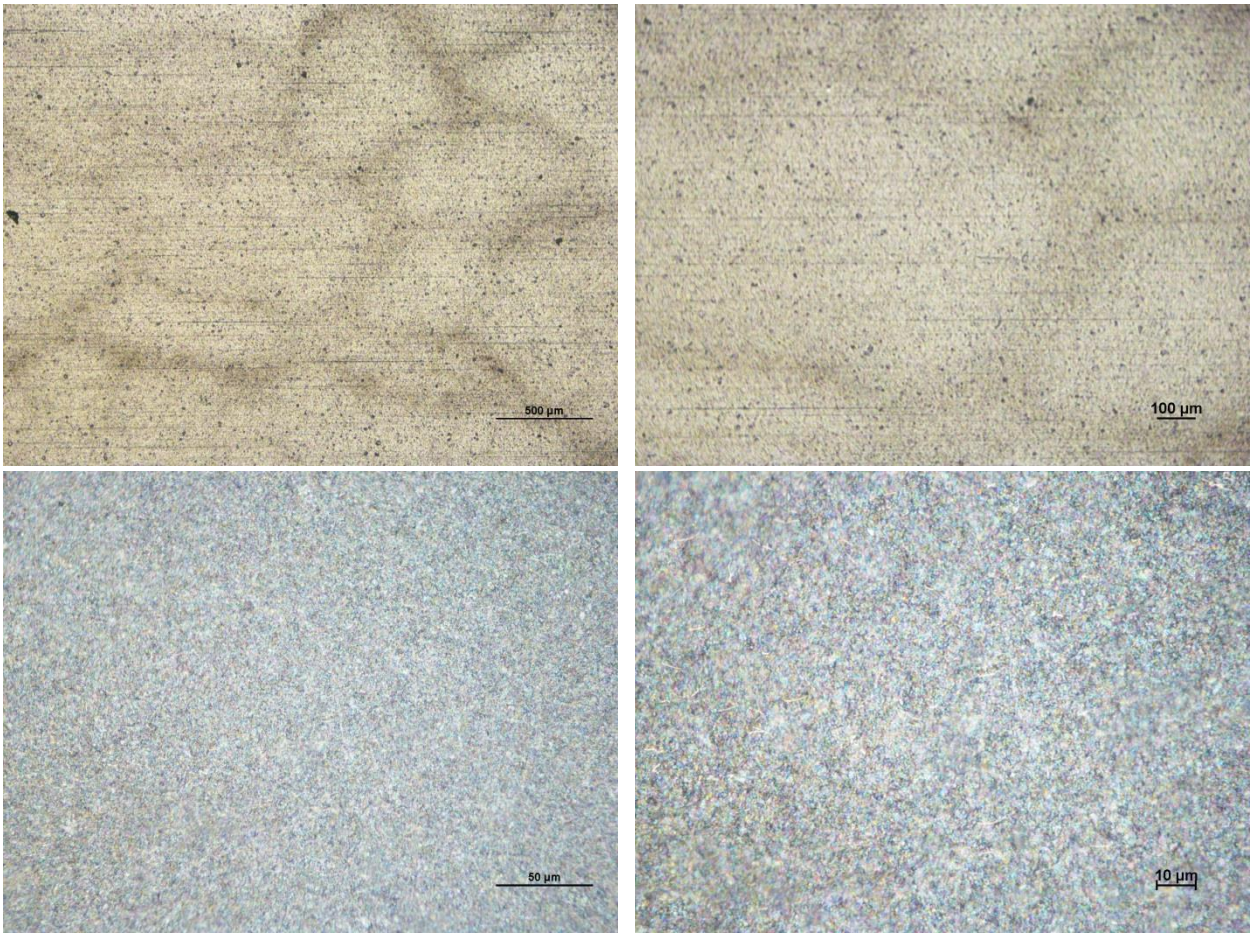

Figure 101: LFP aged 60ºC and 0% SOC (upper left: 5x magnification, upper right: 10x magnification, bottom left: 50x magnification, bottom right: 100x magnification)

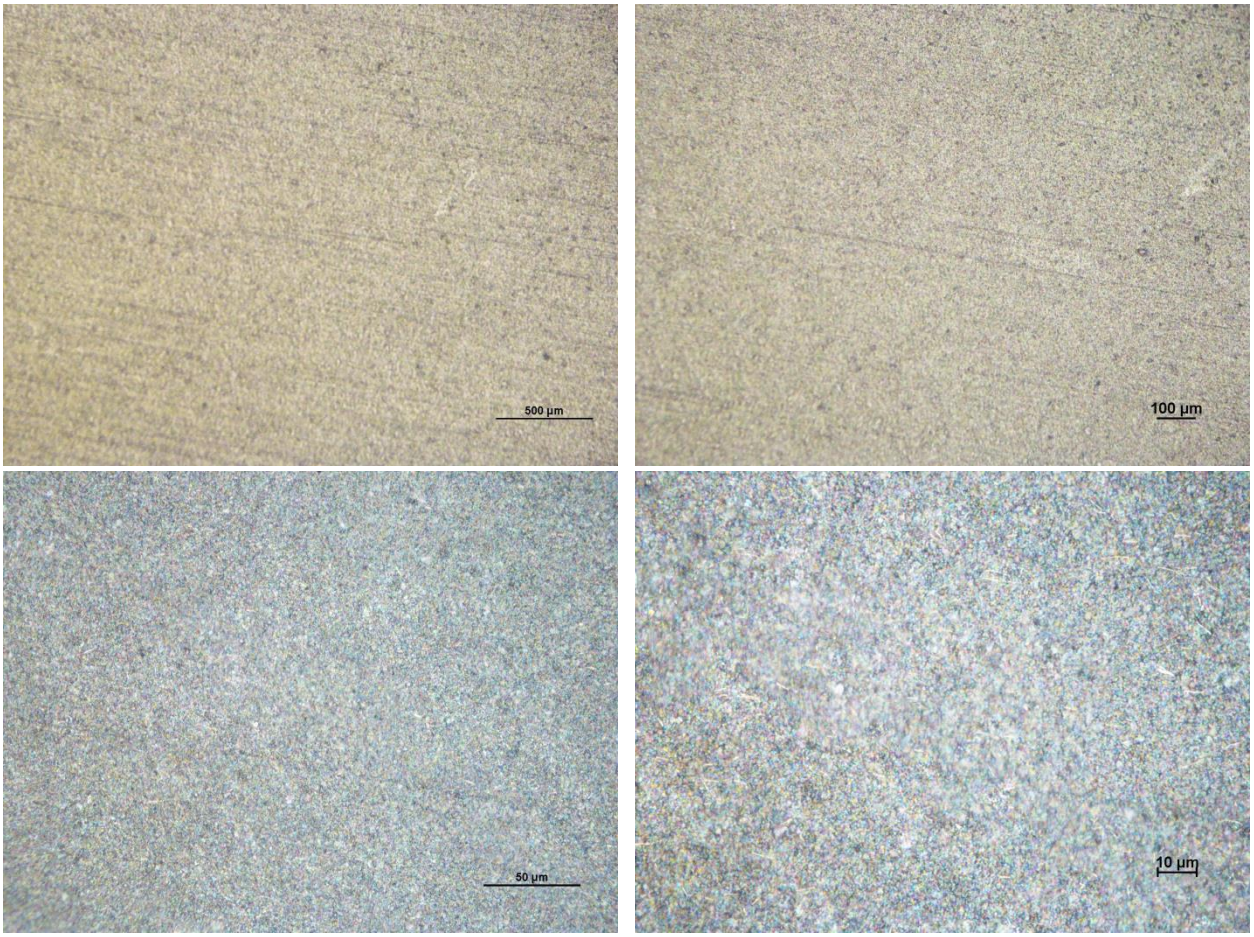

Figure 102: LFP aged 35ºC and 100% SOC (upper left: 5x magnification, upper right: 10x magnification, bottom left: 50x magnification, bottom right: 100x magnification)

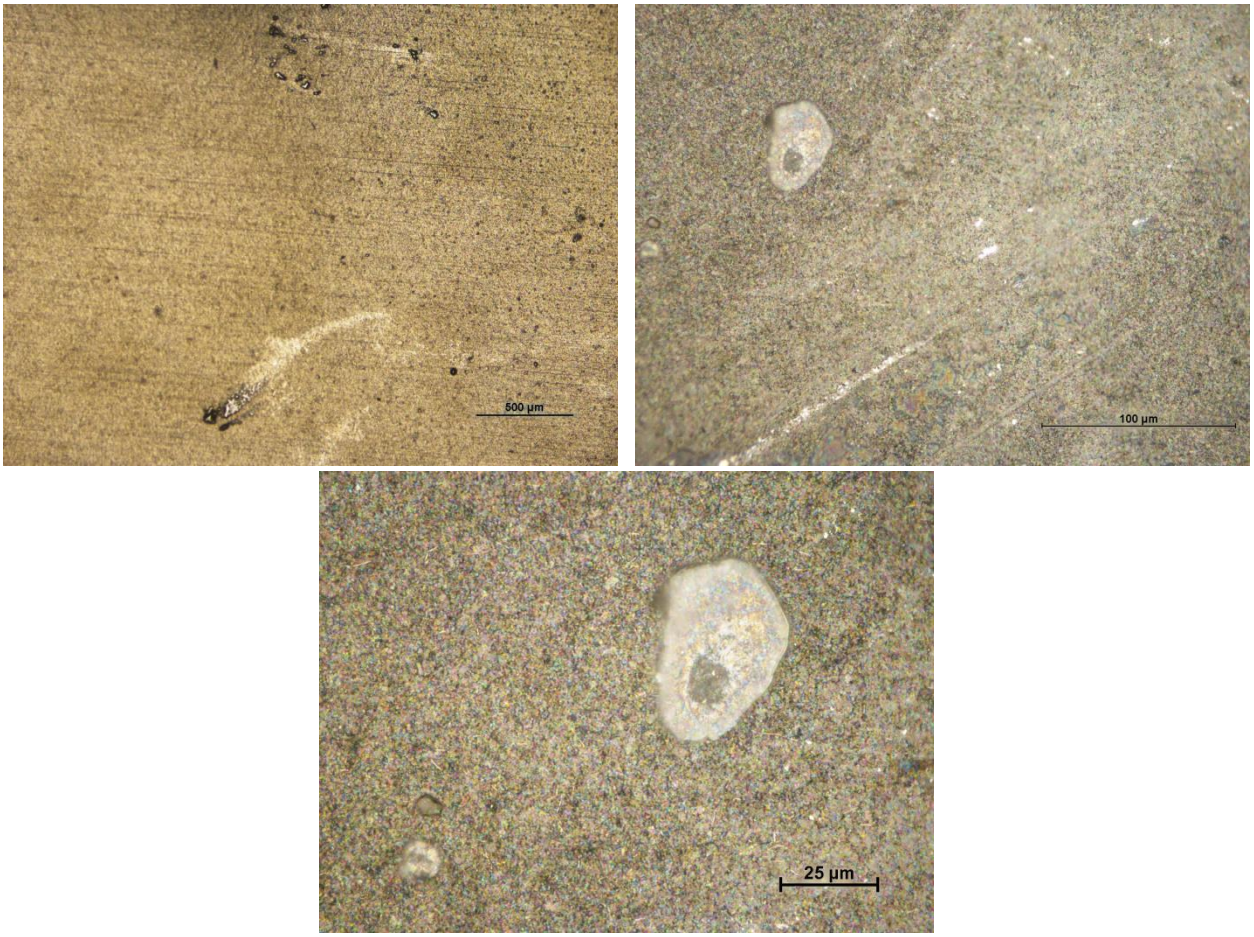

Figure 103: LFP aged 60ºC and 100% SOC (upper left: 5x magnification, upper right: 50x magnification, bottom: 100x magnification)

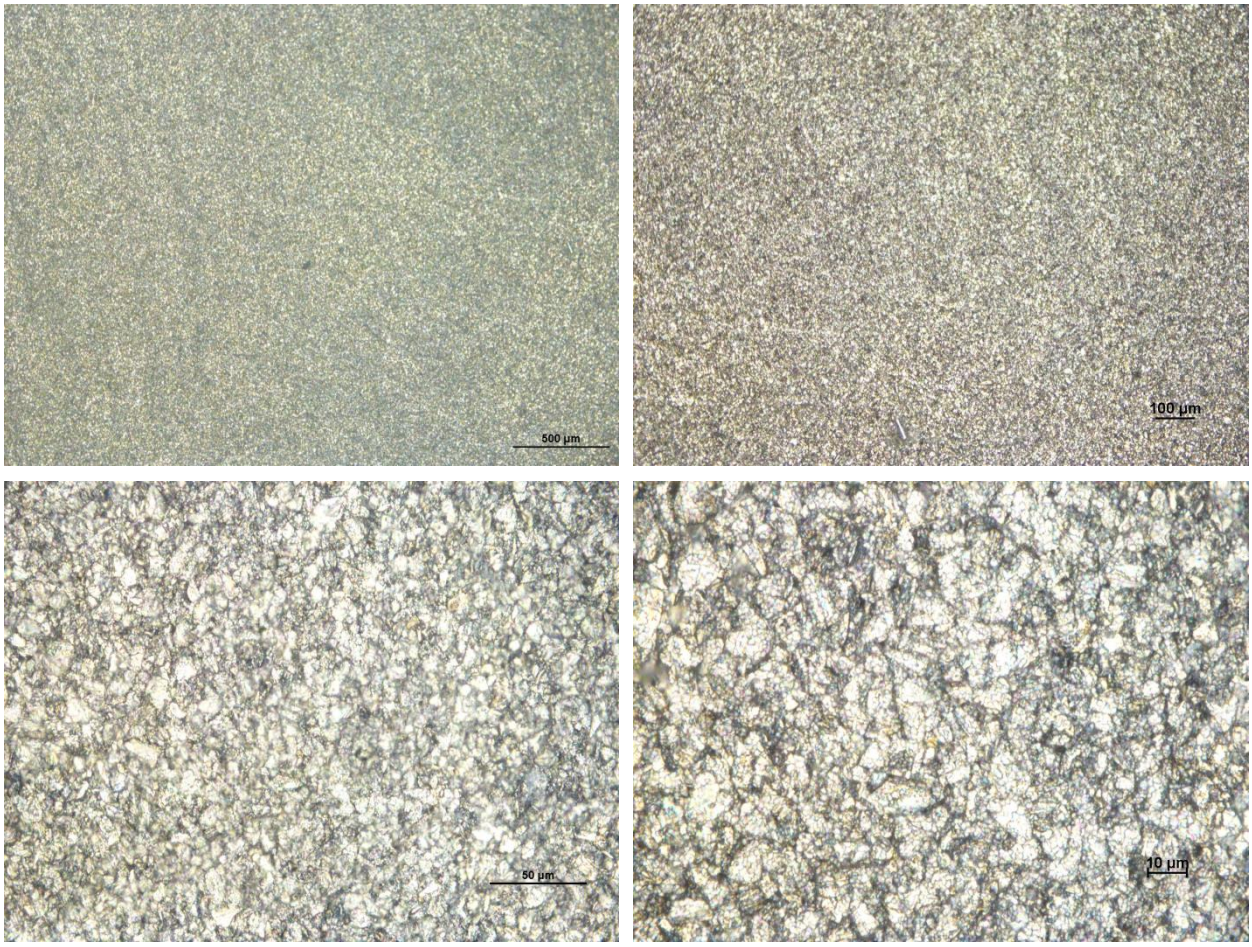

Figure 104: Fresh graphtite (upper left: 5x magnification, upper right: 10x magnification, bottom left: 50x magnification, bottom right: 100x magnification)

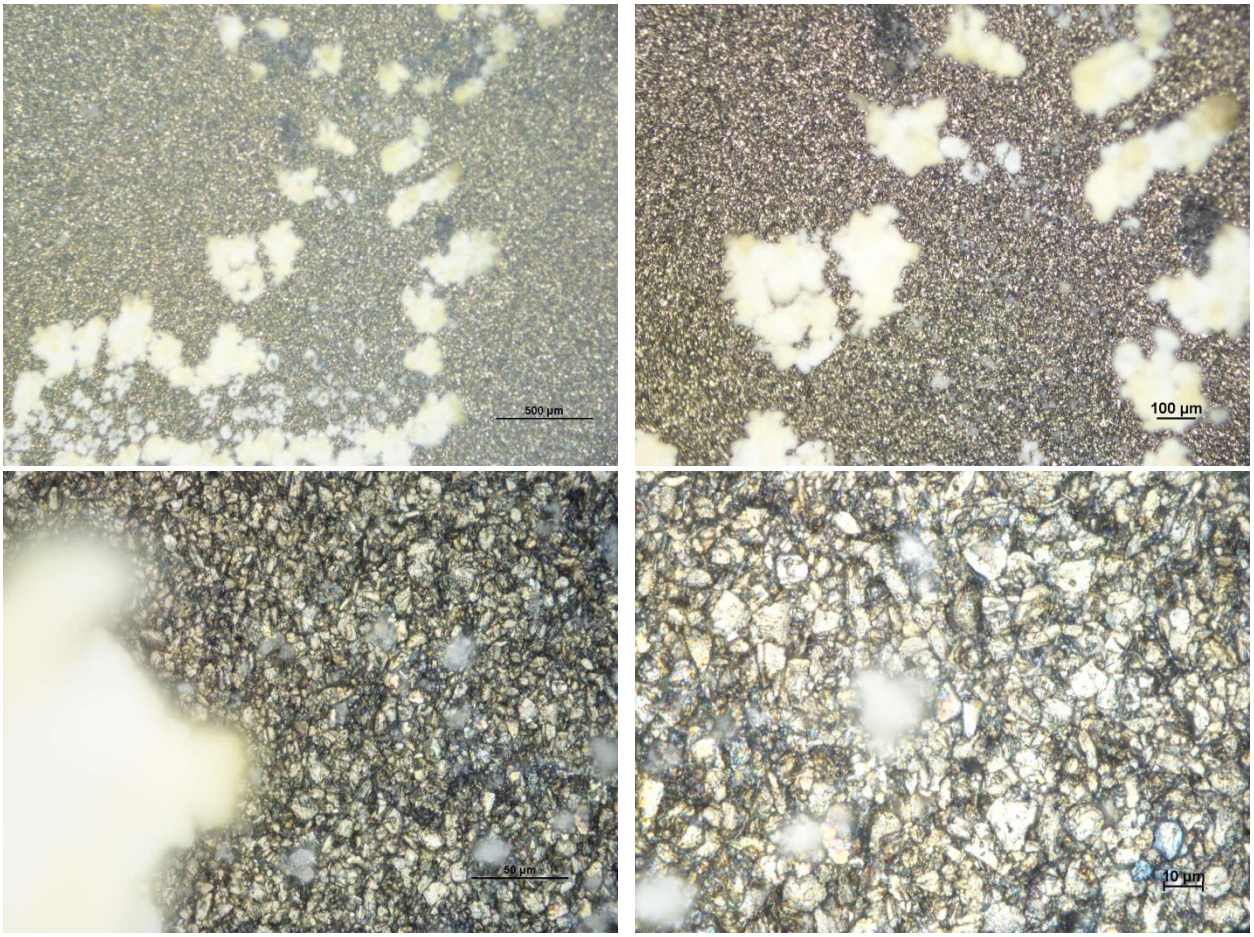

Figure 105: Graphite aged 60ºC and 0% SOC (upper left: 5x magnification, upper right: 10x magnification, bottom left: 50x magnification, bottom right: 100x magnification)

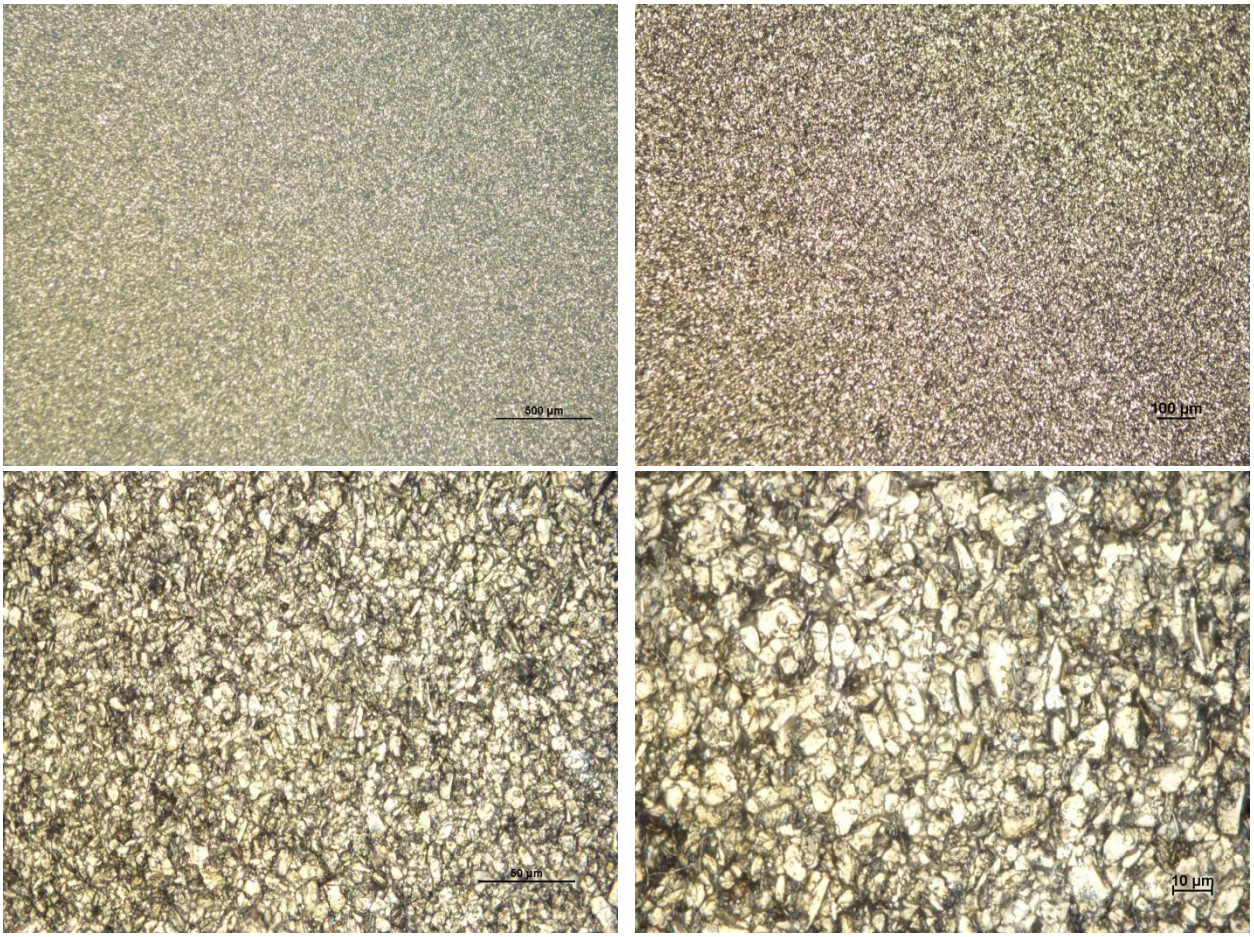

Figure 106: Graphite aged 35ºC and 100% SOC (upper left: 5x magnification, upper right: 10x magnification, bottom left: 50x magnification, bottom right: 100x magnification)

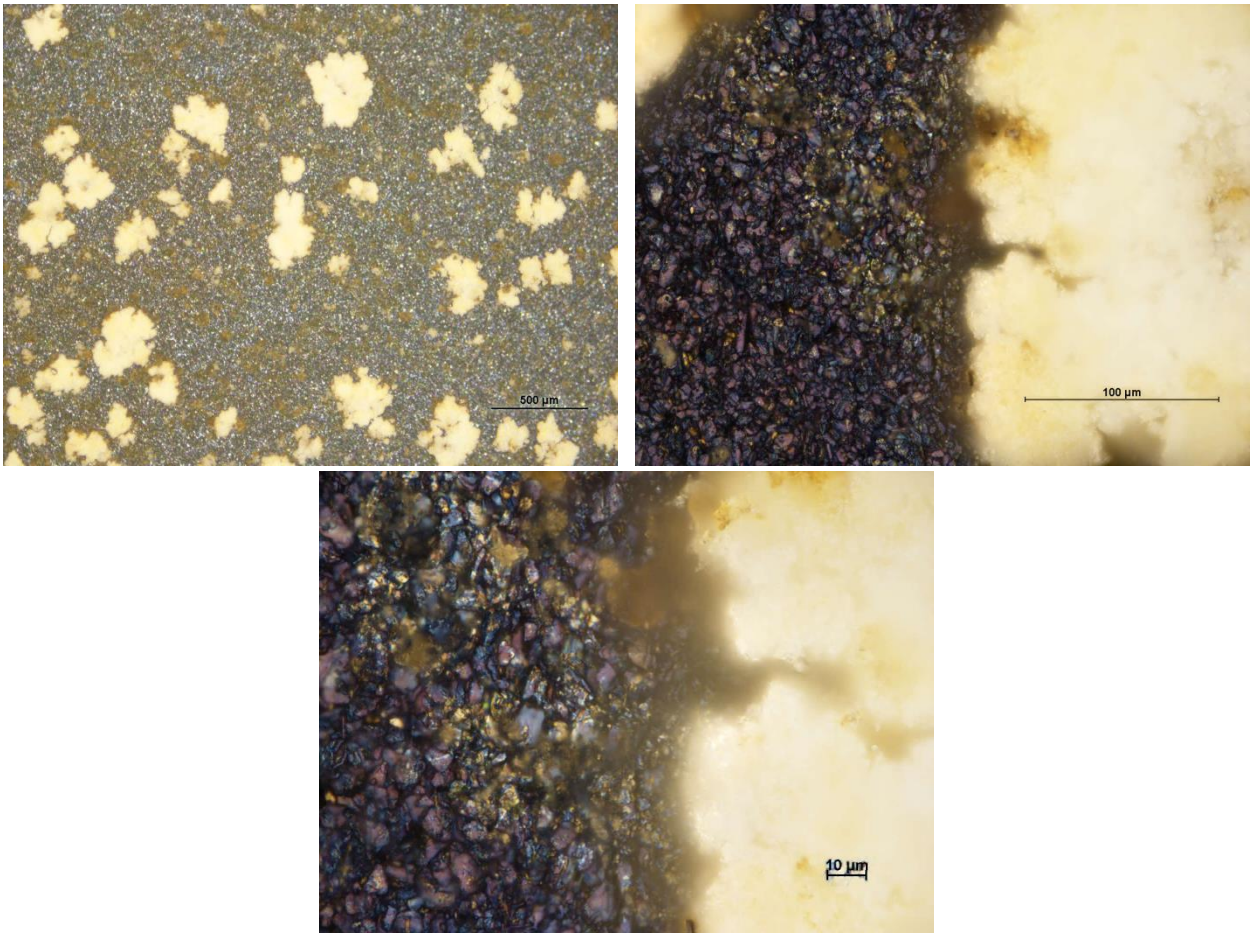

Figure 107: Graphite aged 60ºC and 100% SOC (upper left: 5x magnification, upper right: 50x magnification, bottom: 100x magnification)

Appendix D: Vehicle Technical Specifications

Table 29: Vehicle Technical Specifications

Specification	Target	Requirement	UWAFT	As Designed
Acceleration, IVM-60mph [s]	5.9	7.9	5.82	5.6
Acceleration, 50-70mph (Passing) [s]	7.3	9.9	6.6	3.2
Braking, 60-0mph [ft]	128	135	121.4	121
Acceleration Events Torque Split (Fr/Rr)	0/100	49/51	0/100	0/100
Lateral Acceleration, 300ft. Skid Pad [G]	0.85	0.80	0.84	N/A
Double Lane Change [mph]	55	52	54.4	N/A
Highway Grade ability, @60 mph for 20 mins	6%	6%	6%	7%
Cargo Capacity [ft^3]	2.4	2.4	2.4	2.4
Passenger Capacity	4	2	4	4
Curb Mass [kg greater than stock]	**	<314	275	98
Starting Time [s]	2	15	5	N/A
Total Vehicle Range [km]	**	226	301	396
CD Mode Range [km]	**	N/A	36	69
CD Mode Total Energy Consumption [Wh/km]	**	N/A	267.8	193
CS Mode Fuel Consumption [mpgge]	**	N/A	30	62
UF-Weighted Fuel Energy Consumption [Wh/km]	**	N/A	736.3	183
UF-Weighted AC Electric Energy Consumption [Wh/km]	**	N/A	238	105
UF-Weighted Total Energy Consumption [Wh/km]	700	840	758	287
UF-Weighted WTW Petroleum Energy Use [Wh PE/km]	420	750	621	54
UF-Weighted WTW Greenhouse Gas Emissions [g GHG/km]	225	250	222.6	96
UF-Weighted Criteria Emissions [g/km]	TBD	TBD	2.64	0.40